Hub ratio of horizontal axis wind turbine rotors for optimal performance

by

Howard Tennyson Fawkes

Thesis submitted in fulfilment of the requirements for the degree

Doctor of Engineering in Mechanical Engineering

Faculty of Engineering and the Built Environment
Cape Peninsula University of Technology

Supervisor: Prof G Oliver

Bellville, Cape Town
July 2023

Declaration

I, Howard Tennyson Fawkes, declare that the contents of this thesis represent my own unaided work, and that the thesis has not previously been submitted for academic examination towards any qualification. Furthermore, it represents my own opinions and not necessarily those of the Cape Peninsula University of Technology.

5 July 2023

Abstract

Manufacturers of large horizontal axis wind turbines (HAWTs) have produced wind turbines with hub ratios ranging mostly from 1.5% to 3.5%, but some exceed 9% and prototypes have been tested with hub ratios over 18%. The hub ratios of wind turbines below 100 kW range from 1% to 12%. This study investigates the effect of hub ratio on the peak performance of ideal HAWT rotors.

The performance of two sets of rotors (standard design vs. adapted design) with varying hub ratios (10%, 15%, 20% and 25%) were compared against the performance of a 5% hub ratio rotor of standard design. Computational fluid dynamics (CFD) simulation and physical testing produced performance data. Size of models (ϕ280 mm rotor) necessitated physical testing and simulation within a laminar flow regime. Testing utilised vertical relative velocity of rotors into a stationary body of water. A similar CFD simulation case study of a 30 m diameter HAWT rotor in air provides further results - applicable to a fully turbulent flow regime.

The Blade Element Momentum Method (BEMM) in its standard form, as well as with an adaption, was used to predict performance of the rotors and to generate blade chord and pitch angles for creation of virtual models for CFD simulation and 3D-printed models for physical testing of the ϕ280 mm rotors. A large hub in a HAWT rotor accelerates the air close to the hub. If this effect is included in the rotor design then performance is enhanced. The classical BEMM does not take this effect into account and an adaption to the BEMM was created so that the performance benefit of a larger hub could be included in the 'adapted' rotor designs. The adaption uses potential flow theory to predict an axial velocity gradient along the span of the blade in the rotor plane. This axial velocity gradient replaces the uniform axial velocity that is assumed across the entire rotor plane in the classical BEMM. The adaption also takes rotor 'spillage' losses into account.

The adapted BEMM was found to be a better performance predictor than the standard BEMM for the ϕ280 mm 10% and 15% hub ratio rotors and for all of the ϕ30 m rotors. Results show that when blade designs were customised to the size of the hub, peak rotor power occurred at a hub ratio close to 10%, with power improvements of 0.35% (CFD, ϕ280 mm), 0.44% (testing, ϕ280 mm) and 0.27% (CFD, 30 m case study) compared to the 5% hub ratio baseline rotors. In contrast, if the standard BEMM is used in the design and performance prediction, no benefit is predicted for hub ratios greater than the 5% rotor. The 280 mm 10% hub ratio rotor, designed using the adapted BEMM, produced power improvement of 0.29% (CFD) and 0.90% (testing), compared to the equivalent rotor designed with the standard BEMM. The CFD simulations, of both the 280 mm and the 30 m rotors show that a custom-designed rotor up to a hub ratio of 15% produces at least as much power as a 5% hub ratio rotor.

Acknowledgements

I wish to thank Graeme Oliver for his supervision and I appreciate the assistance of Daniel Barnard, Michael Petersen, Vuyani Moni, and Simphiwe Nqabisa, as well as the support from Ashleigh McGugan and Holly and Ella Fawkes.

The financial assistance for this research was received from the CPUT University Research Fund.

Contents

List of Figures

List of Tables

List of Symbols

Symbol	Chapter 1	Units
a'	angular induction factor	-
A	area of rotor	m^2
A_1	upstream area of stream tube	m^2
A_2	downstream area of stream tube	m^2
c	chord	m
C_D	coefficient of drag	-
C_L	coefficient of lift	-
C_P	power coefficient	-
r_{hub}	hub radius	m
R	rotor radius	m
v	fluid axial velocity at rotor plane	$m \cdot s^{-1}$
v_1	free stream fluid axial velocity	$m \cdot s^{-1}$
v_2	fluid axial velocity far downstream	$m \cdot s^{-1}$
V_r	relative velocity	$m \cdot s^{-1}$
μ	dynamic viscosity	$kg \cdot m^{-1}s^{-1}$
ω	angular velocity of wake	$rad \cdot s^{-1}$
Ω	angular velocity of rotor	$rad \cdot s^{-1}$
ρ	density	$kg \cdot m^{-3}$
	Chapter 3 – Section 3.1	
a	axial induction factor	-
B	number of blades	-
C_n	normal coefficient of wind force	-
C_t	tangential coefficient of wind force	-
C_θ	tangential velocity of wake	$rad \cdot s^{-1}$
dP	power from element or annulus	W
D	drag	N
dM	torque on element or annulus	N·m
dr	thickness of annular element	m
dT	thrust on element or annulus	N
F	Prandtl overall loss factor	-
F_{hub}	Prandtl hub loss factor	-
F_{tip}	Prandtl tip loss factor	-
L	lift	N
N	number of annular elements	-
p_0	static pressure	Pa
p_N	wind force normal to rotor plane	N
p_T	wind force tangential to rotor plane	N
P	power of rotor	W
r	element radius	m
T	thrust	N
u	fluid axial velocity at rotor plane	$m \cdot s^{-1}$
u_1	fluid axial velocity far downstream	$m \cdot s^{-1}$
V_0	free stream fluid velocity	$m \cdot s^{-1}$
V_{rel}	relative velocity	$m \cdot s^{-1}$
λ_r	local speed ratio	-

α	angle of attack	degrees
Δp	pressure change	Pa
ϕ	relative wind angle	degrees
ϖ	angular velocity of wake	rad·s^{-1}
ω	angular velocity of rotor	rad·s^{-1}
σ	local solidity	-
θ	local pitch angle	degrees
	Chapter 3 – Section 3.2	
	Rankine half-body potential flow theory (Kersalé)	
a	half-width	m
m	source strength	kg/s
U	uniform flow velocity	m·s^{-1}
U_z	velocity component in axial direction	m·s^{-1}
Ψ	stream function	m^{2}s^{-1}
	Airship potential flow theory (Kennard)	
a	length of line sink	m
A	thickness ratio	-
b	size factor	-
v_x	velocity component in axial direction	m·s^{-1}
	BEMM adaption procedure	
P	power	W
U	fluid velocity	m·s^{-1}
A	cross-sectional area of fluid stream	m^2
$P_{5\%}$	power of the 5% baseline rotor	W
U_{pf}/U	air velocity ratio from potential flow analysis	-
U_{rel}	corrected wind relative velocity	m·s^{-1}
V_0'	imaginary non-uniform upstream wind velocity	m·s^{-1}
	Chapter 4	
d	diameter	m
l	length	m
T	torque	N·m
	Chapter 5	
A	amplitude constant for exponential decay	-
k	decay rate constant	-
Y	exponential decay value	-
Y_0	asymptote value	-

Glossary

HAWT	horizontal axis wind turbine
BEMM	blade element momentum method
CFD	computational fluid dynamics
TSR	tip-speed ratio
STD	standard
ADP	adapted
hub	the central component of a rotor, that provides an attachment point for rotor blades and which transmits torque to the driveshaft of the gearbox or generator
rotor	a rotating assembly of rotor blades attached to a hub at the centre of rotation, for the purpose of converting wind into mechanical rotational power
profile	the planar cross section through a rotor blade
chord	the length of a blade profile measured from the leading to the trailing edge
spinner	a lightweight aerodynamically shaped shell structure that is attached to, and fits over, the mechanical hub
near-hub region	the area surrounding the space occupied by the hub – usually referring to a region of flow through the rotor or the location on the rotor blades
pitch bearing	the bearing on the hub that blades are attached to, which allow the pitch of blades to be adjusted during operation (usually only on large turbines)
root	the end of the blade that attaches to the hub or pitch bearing
power coefficient	the ratio of power absorbed by the rotor divided by power available in the wind
blade root cut-outs	when the aerofoil surface of a rotor blade is fully or partially terminated before reaching the hub, usually due to space limitations around a small hub
vortex	a rotating region of fluid
wake	region of fluid that has interacted with the rotor, characterised by vortices and turbulence downstream of the rotor
axial induction	the fractional decrease in fluid velocity between the free stream and the rotor plane
angular induction	a ratio of the rotation speed imparted to the wake and the rotation speed of the rotor
shrouded HAWT	when the rotor is contained within a short, shaped duct that increases flow through the turbine
nacelle	the housing (immediately behind the hub) that contains all the electro-mechanical generation machinery for a wind turbine
drag	the component (parallel to the free stream) of the force exerted by a flowing fluid on an object
lift	the component (perpendicular to the free stream) of the force exerted by a flowing fluid on an object
streamline	a line that is everywhere parallel to the flow velocity, representing the path of a particle in a flowing fluid
boundary layer	region of fluid close to the surface of an object where the flow is slowed down by shearing forces between the fluid and the surface
thrust	the force, perpendicular to the rotor plane, that is exerted by the wind on the rotor
blockage ratio	the extent to which the object in a wind tunnel blocks the cross-sectional area of the test section of the wind tunnel, and which is a source of error in wind tunnel testing
rotational periodicity	the solving of a geometrically symmetrical CFD mesh by considering only one of the repeated portions of the mesh

potential flow	a fluid flow modelling method that uses potential line and streamline functions to model simple flows or more complex flows through superposition of potential functions

CHAPTER ONE

Background, literature review and hypothesis

This research investigates the effect of rotor hub ratio on the aerodynamic performance of ideal, horizontal axis wind turbine (HAWT) rotors. ‘Ideal’ in this context means rotor design that adheres to accepted theory, and avoidance, where possible, of design compromise for the purpose of manufacturing. In particular, this research attempts to determine:

1) if there is an improved peak performance for a larger-than-negligible hub ratio.
2) the optimum hub ratio.
3) the gain in output power that can be achieved if an optimum hub ratio is chosen instead of a minimum hub ratio.
4) the limit to hub ratio, beyond which there is no performance benefit over a minimal hub.

To achieve these objectives, the peak power of a rotor, designed with a minimal hub ratio was compared to that of other rotors that were designed with larger hub ratios. The Blade Element Momentum Method (BEMM), was used for rotor design and initial performance prediction. The BEMM does not include the significant aerodynamic effect of accelerated airflow around a large hub and therefore, this research also required the development of an adaption to the BEMM that was used in the design of the rotors that were customised to their hub ratio.

In this research, hub ratio is defined as the aerodynamic hub diameter (in the plane of the rotor) divided by the rotor diameter (see Figure 1.1).

$$\text{hub ratio} = \frac{d}{D}$$

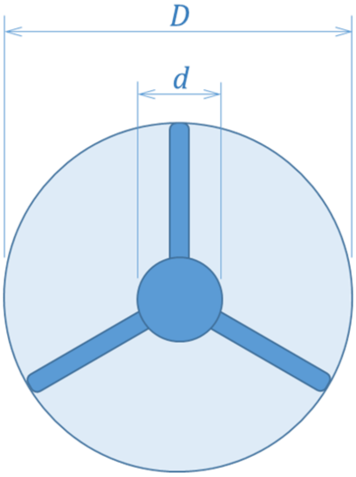

Figure 1.1: Hub ratio of a horizontal axis wind turbine

In mechanical terms, the hub is the component that serves as the attachment point of the blades to the driveshaft. In this study, the term 'hub' will be used when describing the effective aerodynamic diameter, at the centre of a HAWT rotor, which excludes the passage of air and deflects it onto the rotor. In many cases this is achieved by the nose cone (also called the *spinner*) – a lightweight aerodynamically shaped shell structure that is attached to and fits over the mechanical hub (see Figure 1.2).

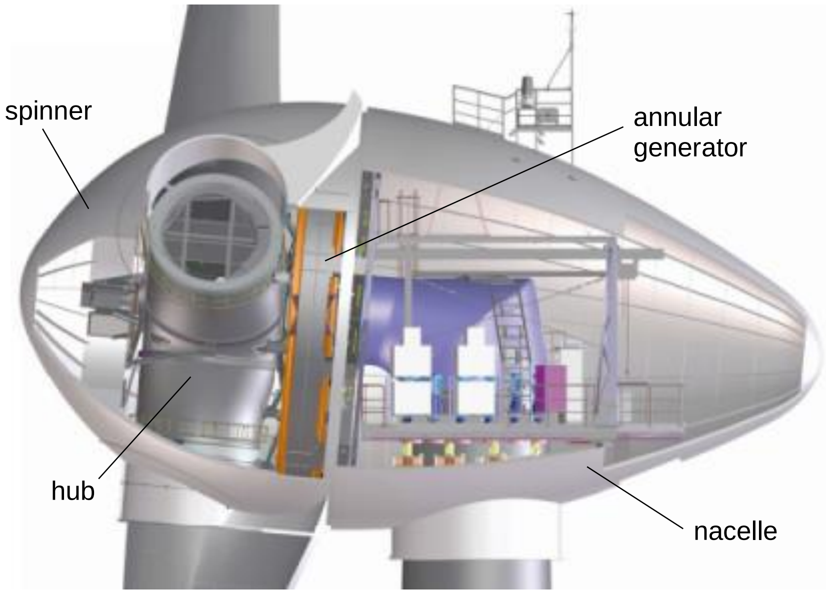

Figure 1.2: Cutaway of Enercon E126 nacelle

Source: Ruiz-Jarabo, 2010.

A pilot study (see Appendix A) was conducted from June 2017 to June 2018 to determine the range of hub ratios that have been, and are being used by HAWT manufacturers. The results (see Figure 1.3) show that most large turbines (>1 MW) have a hub ratio between 1.5% and 3.5%, but for some production models, the range extends beyond 9% and large prototypes have had hub ratios exceeding 18%. Smaller HAWTS (<1 MW) have a broad range between 1% and 13%.

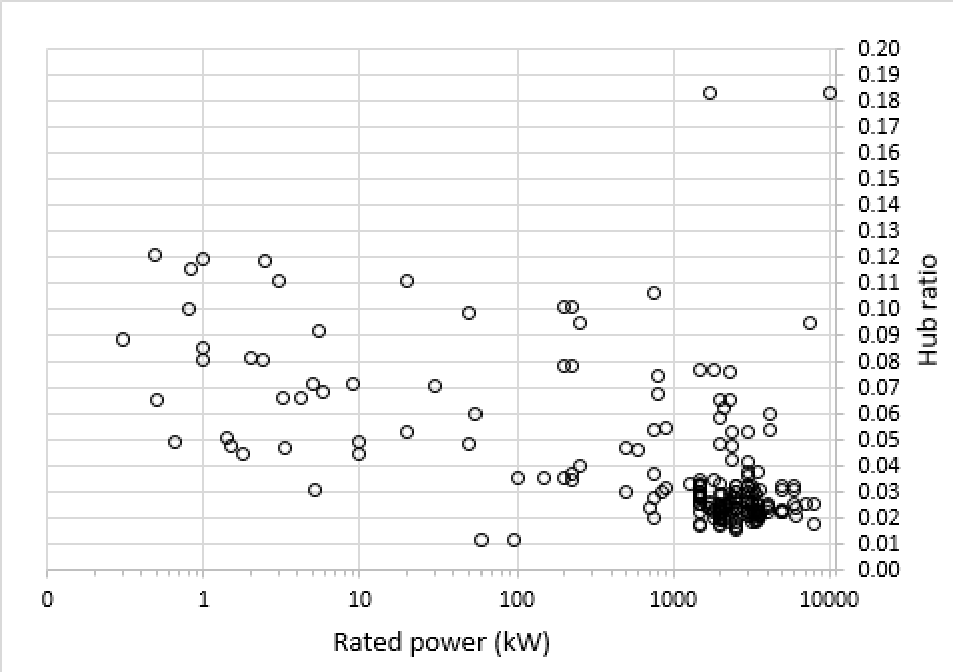

Figure 1.3: Hub ratios of HAWT models from pilot study (2017-2018)

For manufacturers of large wind turbines the choice of generator type - annular (without gearbox) or conventional (with gearbox) has been the biggest determinant for hub ratio. *Enercon*, a leading manufacturer of large wind turbines, chose to use the annular generator (see Figures 1.2 and 1.4). Annular generators have much larger diameters than equivalent conventional generators and the annular generator system results in the need for a large diameter nacelle and spinner to accommodate the annular generator if streamlining of the nacelle is a design objective.

Figure 1.4: Annular generator manufacturing at Enercon, Magdeburg, Germany

(Source: Astroman Magazine, 2011)

1.1 Hub ratio and the near-hub region: Lessons from industry and research

In 2007, *Enercon* installed the first E-126 turbine in Emden, Germany. At the time, it was the most powerful wind turbine in the world. The 2007 model was rated at 6 MW, and this was upgraded to 7.58 MW in 2011 (Enercon E-126, 2022). The E-126 had a hub ratio of 9.44% (Van Agt, 2011) which was larger than any other large turbine at that time. One of the reasons for the large hub ratio was the need to accommodate the diameter of the annular generator – technology pioneered by Enercon, which allowed for a low-maintenance, gearless drive system.

Enercon's machines were reported to have power coefficients (C_P) in the region of 50% and higher (Libii, 2013) The Betz theoretical maximum achievable power coefficient is 59.3% (Hansen, 2008) and nearest competitors (with small-hub turbines) were achieving power coefficient percentages in the mid-40's (Ruiz-Jarabo, 2010). The main reason for such a high power coefficient, according to Enercon, was the attention given to the near-hub aerodynamic profile of the rotor blades, and ensuring that maximum use was made of air flowing around the large hub. This was in contrast to the industry standard of completely circular near-hub blade profiles which only achieved a profile of aerodynamic value much further outward along the span of the blade (see Figure 1.5).

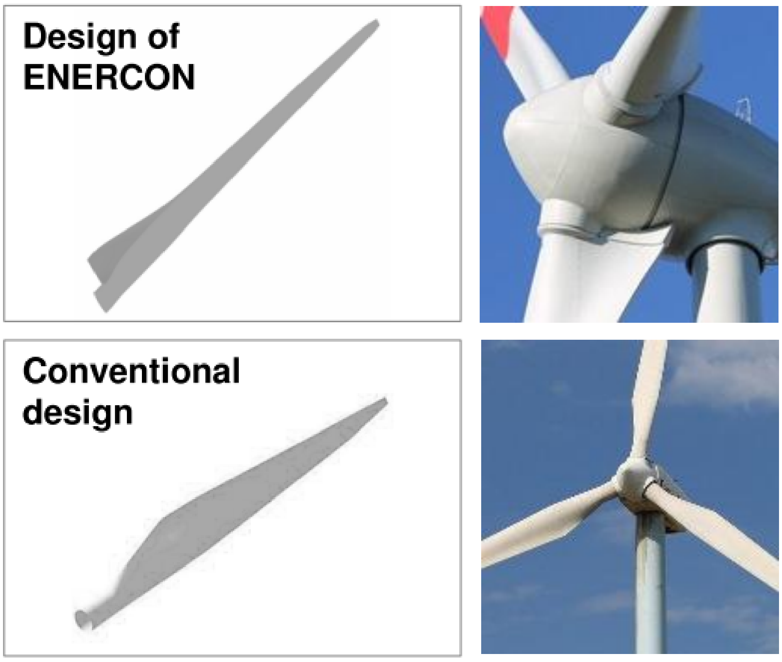

Figure 1.5: Near-hub blade design of Enercon vs. conventional blades (left, top and bottom). Near hub region of Enercon blades (right top) and conventional blades (right bottom)

(Sources: (left, top and bottom) Ruiz-Jarabo, 2010, (top right) Wind-turbine-models.com, 2017 (bottom right): Wind-turbine-models.com, 2020)

Circular near-hub blade profiles were, and still are, seen as a necessary feature for structural integrity of composite blades in an industry that has been racing to produce larger diameter machines. Enercon overcame this design barrier by manufacturing the near-hub region of the blade from steel (see Figure 1.6) and attaching a composite blade to this steel blade stub. The steel blade stub allowed for a smaller diameter pitch bearing at the hub, and a far superior aerofoil profile at the root of the blade. The Enercon turbines with their large hub ratios achieved the highest power coefficients among manufacturers through careful use of the near-hub wind energy.

Figure 1.6: Steel blade stubs attached to hub of Enercon E-126

(Source: Juwi,AG, n.d.)

In June 2015, *Windpower Monthly* (Weston, 2015) reported that *General Electric* (GE) had installed an 18m diameter aluminium dome onto the front of a 100 m diameter rotor of a 1.7 MW wind turbine (the GE 1.7-100). The assembled prototype was named the ecoROTR and is shown in Figure 1.7.

Figure 1.7: Two views of the GE ecoROTR

(Source: GE, 2015a)

GE reported (GE, 2015b) that wind tunnel tests of a model suggested a 3% improvement in performance might be possible with this design adaption. To date, the results of the full size prototype are unpublished and the ecoROTR did not move beyond prototype development. The ecoROTR project showed that a leader in the wind industry recognised the loss of energy that was occurring in the aerodynamically compromised near-hub region of one of their largest turbines and deemed the loss to be sizeable enough to justify a radical and costly attempt to reduce this loss by diverting the lost air 18% of the way outward along the blade length to where the aerodynamics of the blade were more efficient. Criticism of this project (Weston, 2015) included that the full potential for power gain was unlikely to be achieved without tailoring of the blades (particularly pitch optimization) to allow for the changed airflow through the rotor.

1.2 Efficiency challenges in the near-hub region of rotors with minimal hub ratio

For rotors with minimal hub ratio, the near-hub region presents some challenges to efficient flow through the rotor and blade aerodynamic efficiency. These include low relative velocity in the near-hub region, the need for attachment of the blade root to a circular pitch bearing, structural requirements for long blades, radial flow exacerbated by blade root ‘cut-outs’ and a root vortex that intensifies exponentially as the axis of the rotor is approached. Each of these challenges will now be discussed in turn.

<u>Low relative velocity of near hub region reduces aerodynamic performance</u>

Figure 1.8 shows how the aerodynamic performance of any blade profile is directly related to the lift-drag ratio (C_L/C_D) (Manwell, 2009).

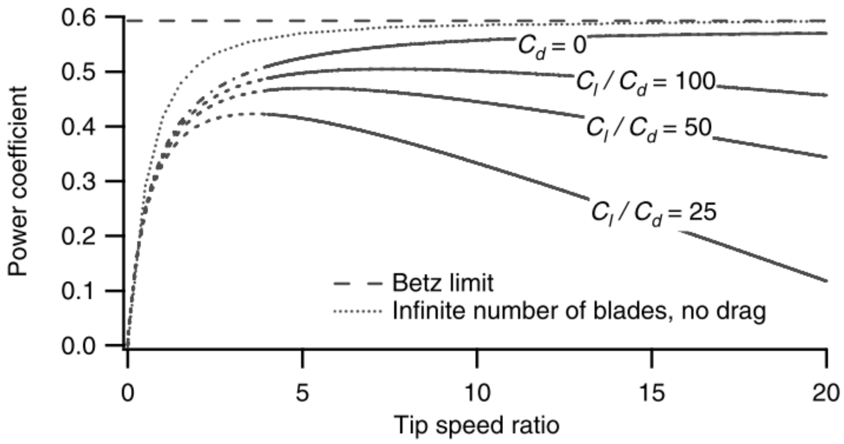

Figure 1.8: Power coefficient vs. Tip speed ratio for a three-bladed optimum rotor as a function of the lift to drag ratio

(Source: Manwell, 2009)

The lift-drag ratio is directly proportional to Reynolds number. For a particular fluid density (ρ) and viscosity (μ), Reynolds number for the blade profile is directly proportional to relative velocity (V_r) and profile chord (c), and can be expressed as in (1.1).

$$Re = \frac{\rho V_r c}{\mu} \tag{1.1}$$

At a particular rotor angular velocity, blade velocity at any point is proportional to radius. The relative velocity (assuming no radial flow) of wind over the blade is created from tangential and axial components and the tangential component is generated from blade velocity. The small radii of the near-hub region, of rotors with minimal hub ratio, result in a very low blade (and relative) velocity, low Reynolds number and poor aerodynamic performance.

Conversely, HAWTS with large hub ratio enjoy higher Reynolds numbers in the near-hub region due to larger radius (of the near-hub region) and higher blade velocity. It is therefore theoretically easier to achieve higher Reynolds numbers and lift-drag coefficients from large hub-ratio rotors, than from rotors with minimal hub ratios. The relationship between Reynolds number and lift-drag ratio is shown in Figure 1.9.

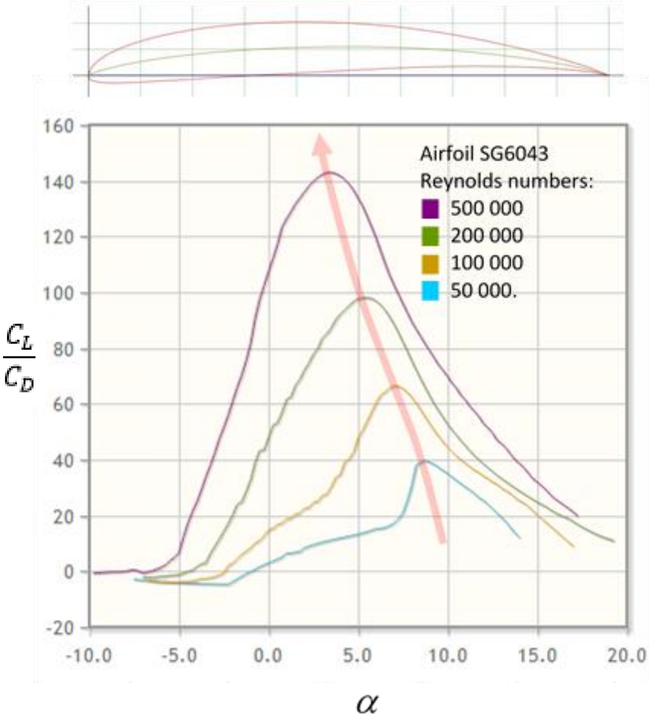

Figure 1.9: Benefit of larger hub ratio: Reynolds number and C_L/C_D for an uncompromised aerofoil increase with radius

(Adapted from Airfoiltools.com)

Circular attachment to pitch bearing, structural demands of long blades and short chord compromise the near-hub blade profile

Structural requirements and the need to attach to a circular pitch bearing, result in blades of minimal hub-ratio rotors having large circular roots and compromised transitional aerofoils, with much greater thickness, in the hub region (see Figure 1.10).

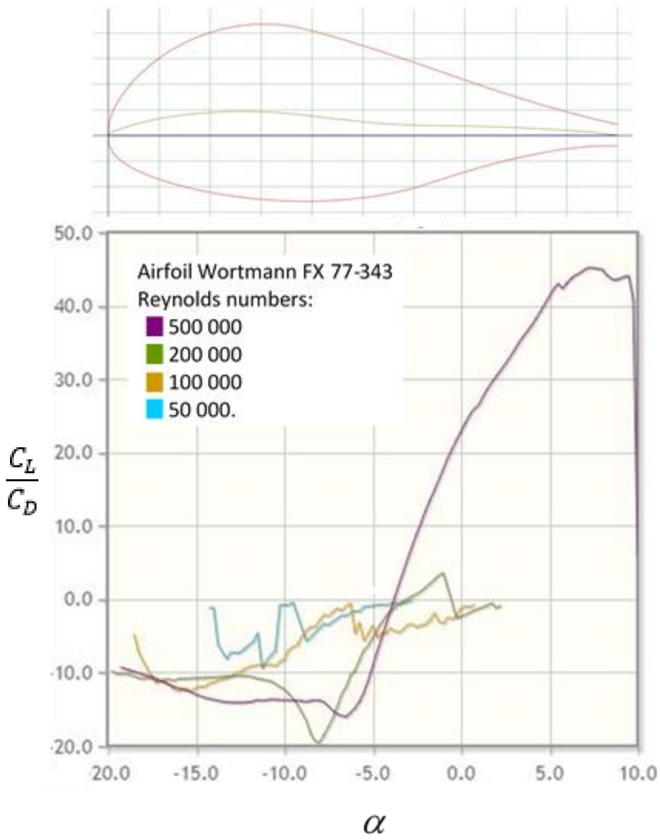

Figure 1.10: Benefit of larger hub ratio: Typical thick near-hub profile has a low C_L/C_D , even at higher Reynolds number (C_L/C_D should be compared with Figure 1.8)

(Adapted from Airfoiltools.com)

The near-hub region is where the structural demands of a blade are highest. Most large HAWT blades are hollow, constructed from glass-reinforced plastic (epoxy and/or polyester), with carbon-fibre used in areas requiring greater stiffness and core material within the skin and stiffening panels as a sandwich construction. (Lee et al, 2012).

A rotor with large hub ratio has shorter blades than a rotor of the same diameter with a minimal hub ratio. Therefore a HAWT with large hub ratio has potentially lower loading at the blade root. This reduced structural requirement allows for reduction of the diameter of the circular attachment to the pitch bearing, and when use is made of alternative blade materials, can allow for a less-compromised near-hub blade profile (see Figure 1.11).

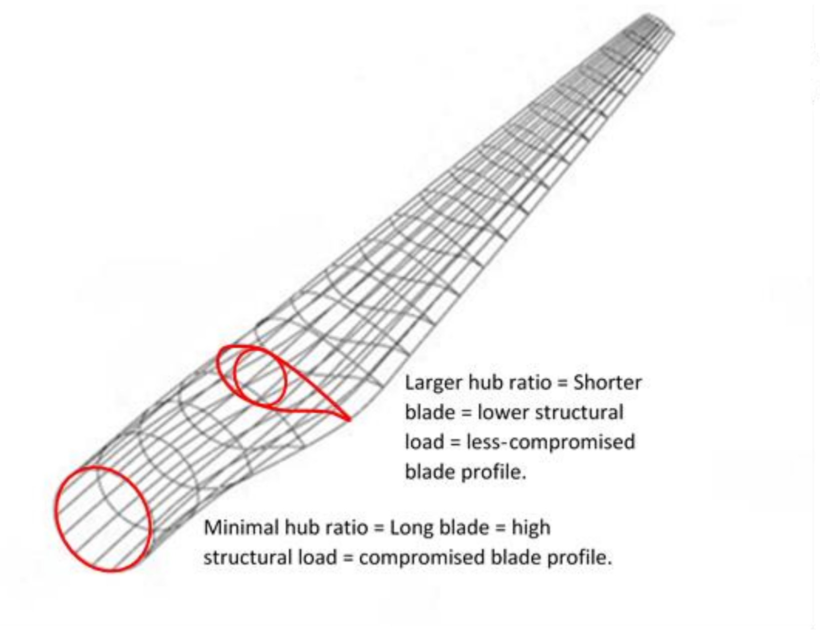

Figure 1.11: Benefit of larger hub ratio: Reduced blade length allows for a less-compromised root profile

(Adapted from Lee et al, 2012)

The reduced blade root diameter and use of steel blade stubs of the Enercon E126 (as seen in Figure 1.6) is an example of the practical achievement of this potential benefit.

At small hub also provides insufficient space for large chord lengths at the hub-blade interface, and the problem of already-low Reynolds numbers in the near-hub region is therefore exacerbated. Aerofoils like the Wortmann 77-343 (Figure 1.10), designed for low Reynolds number and for the transition from a circular blade root, are usually used in the near-hub region of rotors with minimal hub ratios.

<u>Blade root cut-outs exacerbate radial flow</u>

Small hubs cannot accommodate large blade root profiles and blade chords are radically reduced near the hub as a 'cut-out'. Blade root cut-outs allow flow over the inner 'end' of rotor blades – providing a source of radial flow along the blades. A radial velocity component in the flow over a blade reduces blade aerodynamic efficiency because radial flow (and radial force) cannot contribute to the delivery of torque to the blade or contribute to peak power. Herraez (2014) did however show, using CFD simulation, that close to the stall condition, when significant separation from the low-pressure blade surface occurs, radial flow along the blade in the separated zone can be beneficial in delaying separation. This thesis however, compares peak power generation - which occurs at angles of attack much lower than the stall angle, and therefore, radial flow in this thesis (and in rotors operating at optimum design conditions) is an efficiency reducer. The effect of blade root cut-outs can be seen in Figure 1.12.

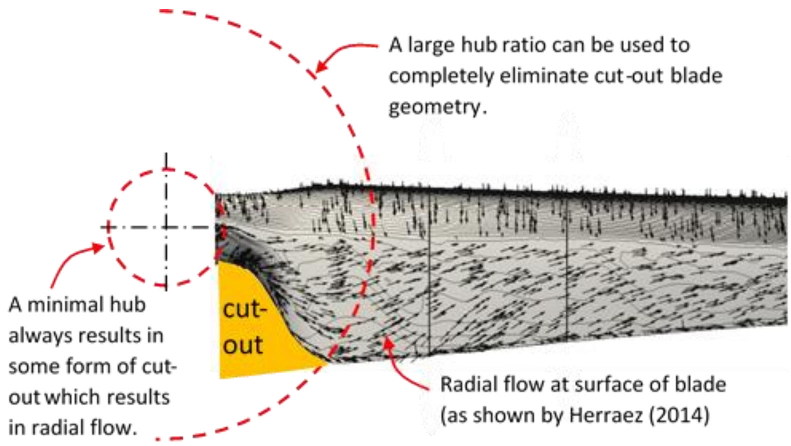

Figure 1.12: Benefit of larger hub ratio: Blade root cut-outs can be eliminated

(Adapted from Herraez, 2014)

Blade root cut-outs are generated through the need to accommodate the juncture of blades to a minimal hub and for providing a circular root for attachment to the pitch bearing. Larger hubs provide enough hub surface area to accommodate an ideal chord and the larger hub can eliminate the need for the near-hub 'cut-out' if the diameter of the pitch bearing is small enough to be contained within the boundaries of the aerofoil (as shown in Figure 1.11).

<u>The root vortex, which intensifies closer to the rotor axis, is a source of energy loss</u>

The wake of a wind turbine rotates in the opposite direction to the rotor rotation. In Figure 1.13, wake rotation, as quantified by the angular induction factor *a*', can be seen to intensify rapidly from the radius ratio of 0.2 towards the rotor axis.

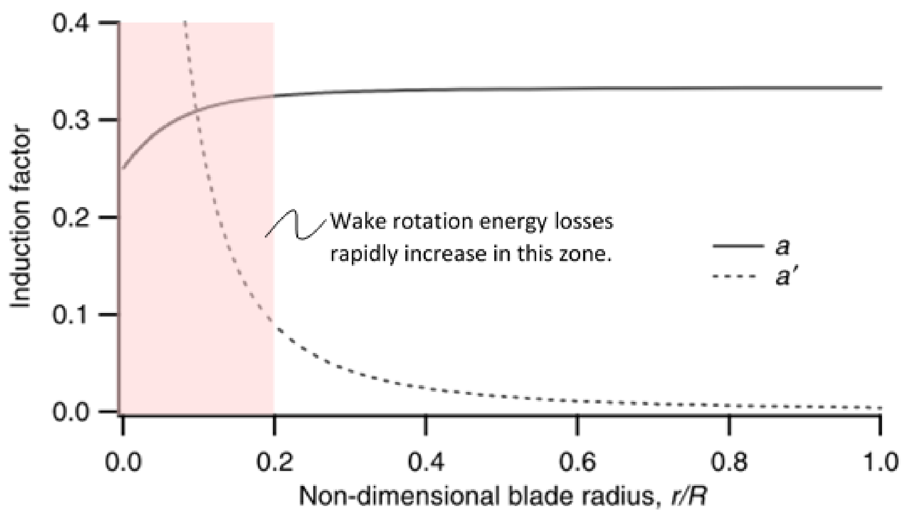

Figure 1.13: Axial induction factor *a* and angular induction factor *a*' for an ideal wind turbine, λ = 7.5, with wake rotation

(Adapted from Manwell, 2009)

The angular induction factor *a*' is defined as,

$$a' = \omega / 2\Omega \tag{1.2}$$

where ω is the angular velocity of the wake, and Ω is the angular velocity of the rotor.

The transformation of available wind energy into rotational kinetic energy in the wake results in less energy being available for extraction by the rotor. The zone from radius ratio 0.2 towards the rotor axis is where the wake rotation intensifies rapidly to form the *root vortex*. Sorenson et al (2015) used numerical simulation to show the form of the wake of a HAWT. Two distinct vortex zones can be seen – the spiralling vortex created by flow over the tips of the rotor blades and the root vortex generated by the increasing wake rotation towards the axis of the rotor. The images of the wake from Sorenson's work can be seen in Figure 1.14.

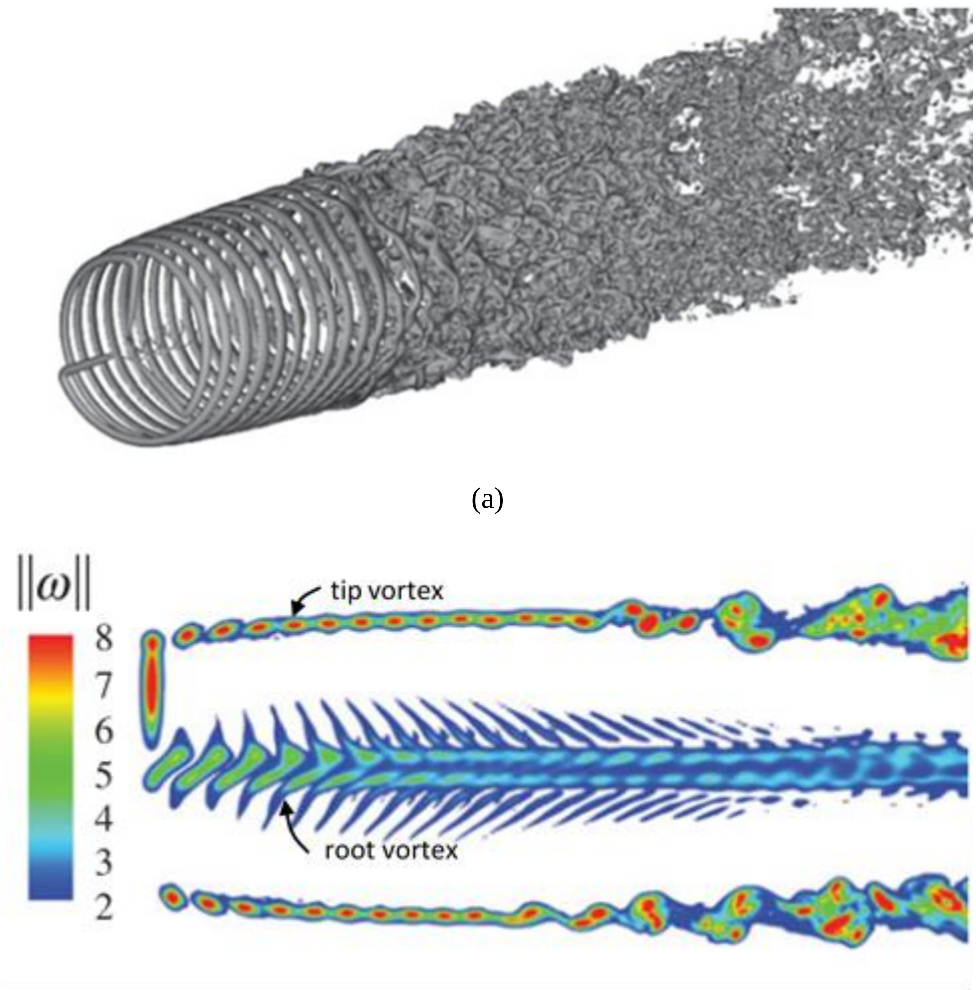

(a)

(b)

Figure 1.14: Vortices in a HAWT wake: (a) Isosurfaces of vorticity magnitude ($\|\omega\|$ = 6) showing the spiralling tip vortices and root vortex. (b) Cross-section through the wake showing range of vorticity intensity and location of root and tip vortices

(Source: Sorensen et al (2015), labels added)

The intensity of the root vortex can be significantly reduced if a large hub ratio is used to divert flow to the part of the blade that has a lower angular induction factor.

This discussion has shown that rotors with large hub ratios have the potential for higher performance than rotors with minimal hub ratios.

1.3 Existing published research on optimum hub ratio for a HAWT

Hub ratio has been studied in shrouded HAWTs and in gas turbines within ducts, but the impact of hub ratio on 'open' HAWTs has received little attention.

Hub ratio of shrouded HAWTs was investigated by Ohya et al (2008) and Ohya and Karasudani (2010). Setoguchi et al (2001) and Thakker et al (2003) studied hub ratio of impulse gas turbines (within a duct) for wave power generation. Ying et al (2015) investigated hub ratio of an impulse rotor for application as a small wind turbine within a duct.

For an 'open' HAWT, Kanya and Visser (2010) compared performance of rotors of various geometries using CFD simulation of a 'flat' blade versus NACA4421 and SG6043 profiles for hub ratios ranging from 0.05 (5%) to 1 (100%). As can be seen in Figures 1.15, 1.16 and 1.17, all but one of the power coefficient (C_P) versus hub ratio graphs trended consistently downward as hub ratio was increased from 5% - indicating no advantage in increased hub ratio beyond 5%. Kanya and Visser conclude that:

> "...a lower hub area results in a more efficient design, as might be expected…" [and]
> "... a hub ratio 0.1 (10%) should not be exceeded to maximise C_P, at least for the NACA 4421 and the SG6043."

Kanya and Visser used mRotor – rotor design software that uses the BEMM - to design the rotor blades, and this study does not describe any measures taken to optimise the blade design for the larger hub ratio.

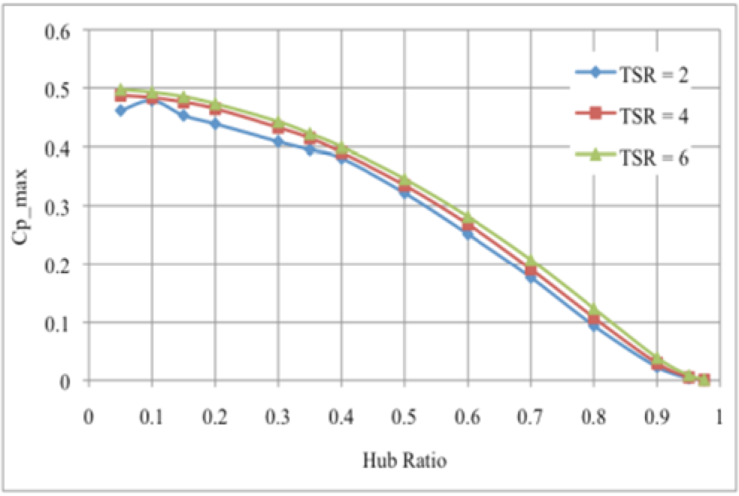

Figure 1.15: Kanya and Visser results: C_{PMax} vs. hub ratio for the SG6043

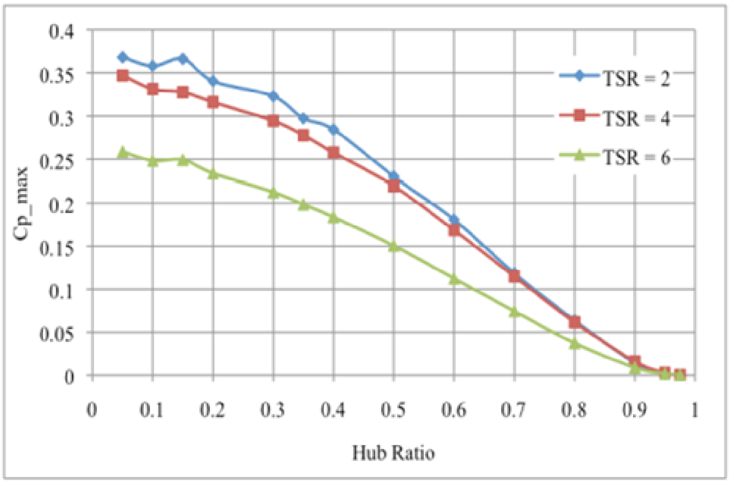

Figure 1.16: Kanya and Visser results: C_{PMax} vs. hub ratio for the flat plate

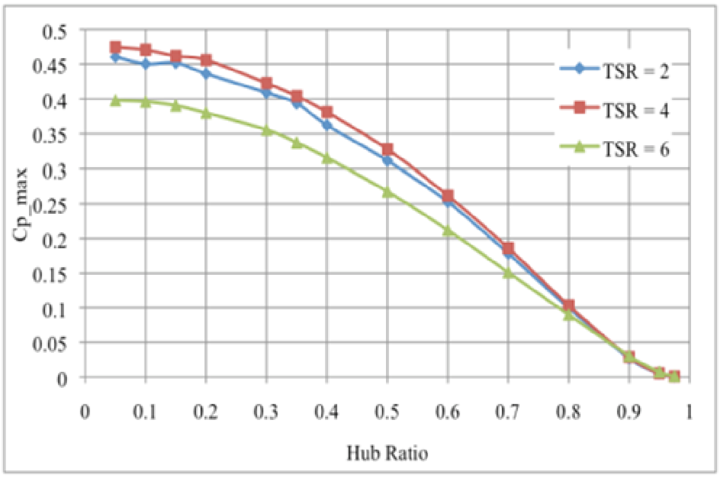

Figure 1.17: Kanya and Visser results: C_{PMax} vs. hub ratio for the NACA 4421

(Source: Kanya and Visser, 2010)

In 2019, the value of a large hub ratio in the design of a large HAWT was considered in a National Renewable Energy Laboratory (NREL) report, titled *Investigation of Innovative Rotor Concepts for the Big Adaptive Rotor Project* (Johnson et al, 2019). The objective of the Big Adaptive Rotor project was:

"*...to identify and develop the necessary technology to enable the development of a land-based 5-megawatt turbine with a 200-m rotor designed for International Electrotechnical Commission Class III A conditions*."

NREL reported the benefits and challenges of a large hub ratio as summarised in Table 1.1.

Table 1.1: Benefits and challenges of large hub ratio concept

Benefits	Challenges
Reduces blade length for a given rotor diameter – thereby easing transport constraints.	Increased drag on the rotor due to drag over the surface of the hub – causing torque reduction.
Allows for increase of rotor swept area (repowering).for the same blade length	Increased rotor thrust due to larger nose cone – which would increase demands on the tower.
Pitch systems would carry a lower pitching moment for the same rotor diameter – which would improve responsiveness and reduce costs.	Pitch system placement further outboard would add complexity, could increase operations and maintenance costs and could introduce reliability issues.
Allows for lower maximum chord at hub-blade interface*, and smaller size reduces cost of transport.	
Overall energy production for the rotor would be increased.	

* Note that ideal chord calculation using the Schmitz equation in Manwell (2002) produces a chord that only starts reducing beyond a hub ratio of approximately 14%

(Source: Johnson et al, 2019)

Cost and performance metrics as well as science challenges were evaluated in a workshop setting of industry and academic participants who were asked to rate their perceived impact of the various design concepts either as negative, neutral or positive. The results for the *large hub* concept are reproduced in Table 1.2.

Table 1.2: Rankings of large hub concept

Cost and performance metrics					
Turbine capital costs	*Turbine spacing*	*Foundations, transport and erection*	*Annual energy production*	*Operational expenditure*	*Capacity factor*
negative	neutral	neutral	neutral	neutral	neutral

Science challenges				
Blade aerodynamics	*Wake*	*Aeroelasticity*	*Noise*	*Mesoscale*
positive	neutral	positive	positive	positive

Engineering challenges							
Materials	*Aerofoils*	*Structures*	*Controls*	*Integration / Manufacturing*	*Transport / Logistics / Installation*	*Reliability*	*Rest of turbine design*
positive	positive	positive	positive	positive	positive	positive	positive

(Source: NREL report -Investigation of Innovative Rotor Concepts for the Big Adaptive Rotor Project)

These results show that the workshop participants' perceived benefits to engineering and science challenges, were neutral on performance metrics, were neutral on operating costs and perceived a negative impact on turbine capital cost.

The report initially states that a large hub will increase overall energy production but then reports that workshop participants were neutral on the perceived impact of a large hub on overall energy production – possibly indicating some uncertainty.

Benini and Toffolo (2002), in a study on overall wind turbine design optimisation, assumed that optimum hub ratio falls somewhere between 0,05 and 0,20 (5% and 20%) and reported a "…*lack of knowledge in the open literature*…" in the area of hub ratio optimisation.

Noting the statement of Benini and Toffolo, a selection of relevant textbooks (listed below) were searched for the term "hub ratio". No occurrence of the term or coverage of hub ratio in any other form was found in:

Burton et al (2001) - *Wind Energy Handbook*
Hansen (2008) - *Aerodynamics of Wind Turbines*
Hemami (2012) - *Wind Turbine Technology*
Jain (2011) - *Wind Energy Engineering*
Johnson (2001) - *Wind Energy Systems*
Jamieson (2011) - *Innovation in wind turbine design*
Manwell (2009) - *Wind Energy Explained - Fundamentals, Resource Analysis and Economics*

Mathew (2006) - *Wind Energy Fundamentals, Resource Analysis and Economics*
Patel (2006) - *Wind and Solar Power Systems* - *Design, Analysis and Operation*
Spera (2009) - *Wind Turbine Technology* - *Fundamental concepts of wind turbine engineering*
Tavner (2012) - *Offshore Wind Turbines* - *Reliability, availability and maintenance*
Hau (2006) - *Wind Turbines* - *Fundamentals, Technologies, Applications, Economics*
Gasch and Twele (2012) - *Wind Power Plants* - *Fundamentals, Design, Construction and Operation*

Some insight is provided by Hau (2006) when commenting on the rotor blade root sections of the Enercon E-70 E4 (a HAWT with a relatively large hub ratio). Hau states that the nacelle shape and carefully designed blade root...

"...lead to an extraordinary acceleration ... around the nacelle ... which affects free stream velocity at blade roots ... [and] *... contributes to a noticeable increase in power coefficient"*.

1.4 Hypothesis - An optimum hub ratio for an ideal HAWT

Respectively, the Enercon and GE design choices described in section 1.1 show that:

- A relatively large hub size can produce an unusually high power coefficient if blade aerodynamic profile is uncompromised over the full span of the blade.
- There is an expectation, and wind tunnel test results, that support the idea that a large nose cone (aerodynamic hub) can reduce losses experienced by a rotor that has an aerodynamically compromised near-hub blade profile.

In the GE example, the improvement from the larger hub was expected to come from better use of the near-hub wind energy. In the near-hub region, without the larger nose cone, the almost cylindrical blade profile would have experienced significant drag and would have provided very little lift. This exercise by GE was therefore an exercise in design correction and the improvements expected from the larger hub were more a measure of how badly compromised the near-hub blade profiles were, than a measure of the value of a larger hub. For this reason, this thesis focuses exclusively on the effect of hub size on an uncompromised or 'ideal' rotor.

The efficiency challenges of the near-hub zone of rotors with minimal hub ratio have been discussed in Section 1.2, and can be reduced when larger hub ratios are used.

These efficiency benefits of larger hub ratios, suggest that an ideal rotor, with a relatively large hub ratio could produce more peak power than an ideal rotor with the same rotor diameter and with a minimal hub ratio. Figure 1.18 shows a large hub ratio above the central axis and a minimal hub ratio below.

Streamlines for the minimal hub are drawn in black and those for the large hub ratio are drawn in orange. The minimal hub ratio rotor has a constant axial velocity profile across the length of the blade and an inefficient zone near the central axis. The large hub diverts air that would have gone to the inefficient zone, towards larger radii - resulting in an axial velocity gradient over the length of the blade and a power gain. Because of the diversion of air, some flow that would have gone through the rotor plane spills over the edge of the rotor plane as a power loss or 'spillage' (and reduces the area A_1 of the stream tube).

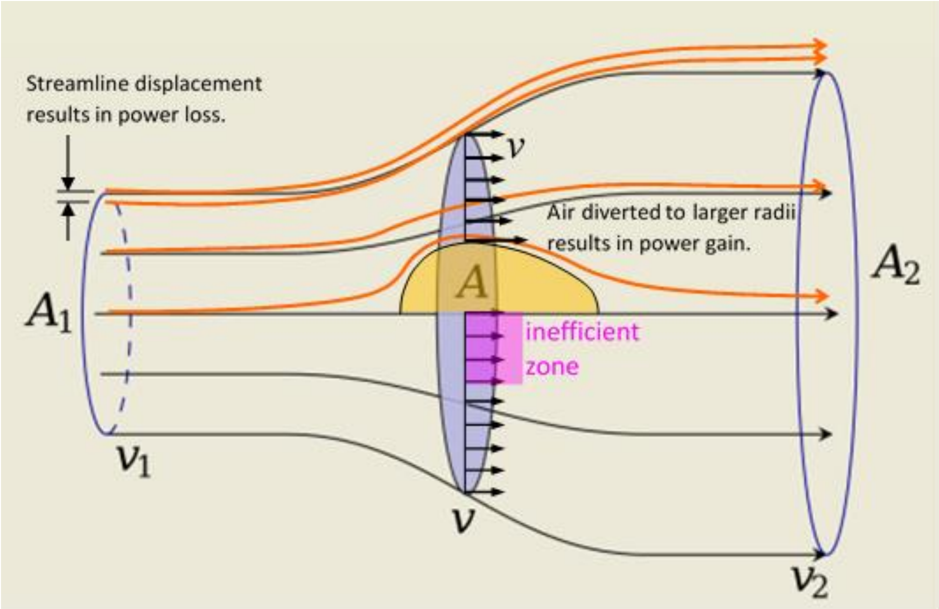

Figure 1.18: The effect of large hub ratio on flow through a HAWT rotor. Large hub ratio above the central axis and negligible hub ratio below

If the power gain provided by a large hub ratio is greater than the expected streamline displacement power loss, then an optimum, non-zero hub ratio exists.

Figure 1.19 shows the hypothetical curve of a hub-optimised ideal rotor with peak power occurring at an optimum hub ratio.

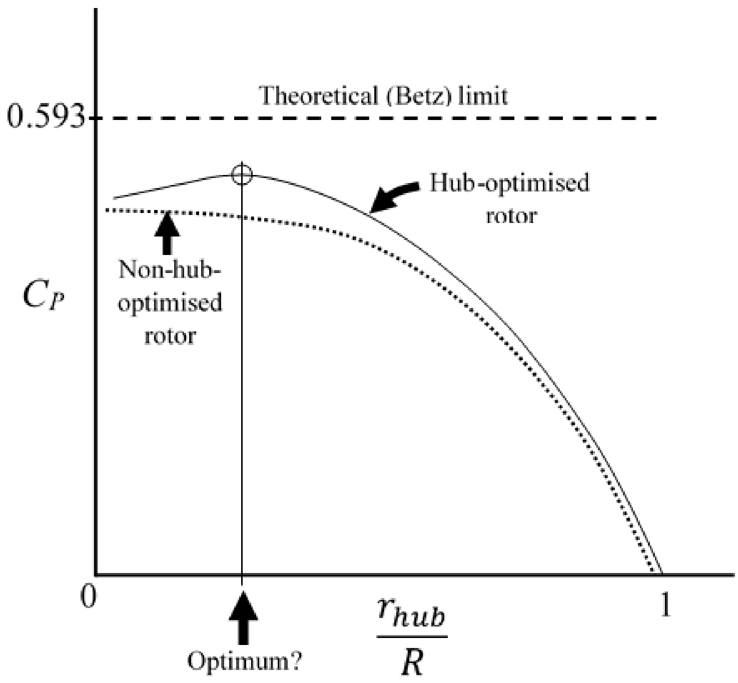

Figure 1.19: Power coefficient vs. hub ratio of a hypothetical hub-optimised rotor, a non-hub-optimised rotor and the theoretical Betz limit. Is there an optimum hub ratio for a hub-optimised rotor?

This thesis seeks to confirm the existence of an optimum (larger than negligible) hub ratio, to determine the optimum hub ratio for an ideal HAWT rotor, to quantify the increase in power from a larger hub ratio as opposed to a negligible hub ratio and to determine the limit to hub ratio, beyond which there is no performance benefit over a minimal hub.

CHAPTER TWO:
Overall methodology

The overall methodology included four investigations:

- Two sets of ϕ280 mm rotors, with varying hub ratios, were designed and peak rotor output power was predicted, using standard and adapted versions of the BEMM. The working fluid for the BEMM analyses was water so that results could be compared to CFD and physical test results. Part of this work included the development of an adaption to the BEMM that would take into account the acceleration of near-hub air due to larger hub ratios.

- CFD simulation of the same rotor sets, with Ansys Fluent, was used to determine peak rotor output power from virtual 3-D models of the rotors. The working fluid was water. The 3-D virtual models were designed in Solidworks using airfoil, chord and pitch data from the respective BEMM studies.

- Physical testing of the same rotors was performed on 3D-printed rotors, produced from the Solidworks solid models, and water was utilised as the working fluid. The constraints of physical testing largely determined the choice of working fluid, diameter of rotor and operating conditions, and for purposes of comparison, these same test parameters were applied in the BEMM design and performance predictions, and in the CFD simulations.

- A 'case study' investigation of an adapted set of 30 m rotors included design using an adapted BEMM and performance prediction using two variations of the adapted BEMM as well as the standard BEMM. The working fluid was air. This case study also compared the predictions against CFD simulations of the rotor set. The purpose of the case study was to test two different versions of the BEMM adaption and to investigate the effect of hub ratio in a large scale, fully turbulent flow regime. The case study methodology is discussed in Chapter 6.

Flow charts of the methodologies for the ϕ280 mm rotor study and the ϕ30 m case study are provided in Appendix P.

<u>The 280 mm rotor study</u>

The peak output power of two sets of four rotors per set, with hub ratios of 10%, 15%, 20% and 25% were compared with each other, and also compared with a 5% hub ratio rotor. In total, nine different rotors were designed, performance-simulated and physically tested. All rotors were three-bladed, had a diameter of 280 mm, a design tip speed ratio of 4.8 and the working fluid was water at 20 ^{o}C.

All rotors were designed using an initial Schmitz chord and blade twist as per Manwell (2009). Prandtl tip and hub losses were applied where appropriate. Final chords (incorporating tip chord optimization) were generated iteratively with the Maalawi chord function (El-Okda, 2015) and included adjustment to retain the overall rotor solidity of the original Schmitz chords. The power and induction prediction of the BEMM used the Buhl correction for axial induction greater than 0.4, and was applied according to Hansen (2008).

The hub ratio of 5% was small enough that the effect of using either the adapted or the standard BEMM in rotor design was negligible – allowing this rotor to be used as a baseline for comparison of both rotor sets.

Results from the BEMM, CFD simulation and physical testing compare rotor peak power for both rotor sets, relative to the peak power of the rotor with 5% hub ratio.

2.1 BEMM analyses - ϕ280 mm rotor

Analyses 1, 2 and 3 (below) were performed using the BEMM.

Analysis 1

- Rotor Set 1 (5%, 10%, 15%, 20% and 25% hub ratio rotors, designed using the standard BEMM).
- Induction and performance prediction also used the standard BEMM.
- Note that variation in hub ratio does not affect blade chord and twist in the standard BEMM so this was an analysis of large hubs being used on a rotor that was designed for a minimal hub.
- The rotor design data from this analysis was used for creating virtual models for CFD simulation and 3D models for physical testing.

Analysis 2

- Rotor Set 1
- Induction and performance prediction used the adapted BEMM.
- When compared to Analysis 1, this serves as an indicator of the effect of the BEMM adaption in the induction and performance prediction of the BEMM.

Analysis 3

- Rotor Set 2 (5% hub ratio rotor designed with standard BEMM, plus 10%, 15%, 20% and 25% hub ratio rotors designed using the adapted BEMM)
- Induction and performance prediction used the adapted BEMM.
- This, in theory, would be a better design than Rotor Set 1, and also the best estimate of induction and output power for rotors with different hub ratios since both the design of the rotor and the prediction of induction and power output take into account the near-hub acceleration generated

by larger hubs. Comparison of Analysis 2 and Analysis 3 provides an indication of the effect of the adapted BEMM design on the performance of the rotor.

- Again, rotor design data from this analysis was used for creating virtual models for CFD simulation and 3D models for physical testing.

The performances of Rotor Sets 1 and 3 were analysed using CFD simulation and physical testing.

2.2 Rotor and test parameters - ϕ280 mm rotor

Rotor output power for each rotor set was evaluated at hub ratios of 5%, 10%, 15%, 20% and 25%. This range was based on initial BEMM outputs, the work by Kanya and Visser (2010) and a pilot study (See Appendix A) of the rotor diameters used and investigated by industry.

Practical constraints of physical testing determined most of the rotor and test parameters that were applied across all investigations and scenarios. Water at 20 ºC was used as the working fluid - which allowed for measurable power output from the small (280 mm diameter), three-bladed rotors.

Ideally, these comparative tests needed to be performed in either a laminar or a turbulent flow regime since a regime transition across blade elements would affect blade profile lift and drag coefficients and introduce unnecessary complexity and uncertainty into the results. The possibility of performance benefit purely due to a flow regime change, as opposed to a flow change, was seen as something to be avoided. Large turbines operate at Reynolds numbers measured in millions, so do not experience a flow regime change under normal operating conditions. Practical rotor size limitation eliminated the possibility of testing within a fully turbulent flow regime, therefore a fully laminar flow regime was an objective in this testing. For an incompressible, undisturbed environment, a critical Reynolds number (before flow regime change) of approximately 5×10^4 was determined by Carmichael (1981) and corroborated by Derksen et al (2008), Huang and Lin (1995) and Tsuchiya et al (2013). Disturbed flow, such as early separation, lowers the critical Reynolds number, and Nava et al (2016) found that boundary layer transition for a similar (cambered plate) aerofoil was initiated from a Reynolds number of approximately 2×10^4, and progressed either slowly or suddenly to complete transition (depending on which numerical model was chosen) at a Reynolds number of approximately 2×10^5. Test parameters were therefore chosen to achieve Reynolds numbers well below 2×10^4 (with a maximum Reynolds number in the region of 13000) to achieve a fully laminar flow regime for the entire rotor.

A combination of water as working fluid, a water speed of 0.25 m/s and a tip speed ratio of 4.8 produced:

- physically measurable rotor output power.
- blade chord lengths that were large enough for successful 3D-printing and aerofoils that were thick enough to avoid excessive flexure or failure during physical testing.

- an acceptable range of Reynolds number (4000 > Re < 13000) for laminar flow to be expected across all blade elements, and
- an acceptably low rotor rotation speed to minimise radial flow across blades due to 'radial pumping' as described by Herraez (2014). The BEMM assumes no radial flow and there was some concern that excessive radial flow might exacerbate streamline displacement and 'spillage' of air past the outer diameter of the rotor, and offset the expected power gain from near-hub fluid acceleration. Large wind turbines typically have very slow rotation speeds (in the region of 20 rpm) compared to domestic (micro) turbines (at ≈ 400 rpm). Herraez identified centrifugal forces (not pressure gradients along the blade span) as being the major cause of 'radial pumping' and since centrifugal forces are proportional to rotation speed squared and only linearly proportional to the radius, this provided motivation for low rotation speeds (≈ 70 rpm) in testing.

The nature of testing in this research was comparative, not absolute. The objective of each methodology (BEMM, CFD and physical testing) was to determine rotor performance relative to the 5% baseline rotor, therefore results are reported as dimensionless ratios of power divided by the 5% baseline rotor power. In this study, the 5% baseline rotor was designed using the standard BEMM and performance prediction was also via the standard BEMM. Comparing absolute power output results of BEMM against those of CFD and physical testing was not the objective of this thesis.

CHAPTER THREE

Design and performance prediction using the BEMM

The BEMM is used for designing and predicting performance of HAWT rotors. The method has been used widely in academic research and industry owing to its ease of application within spreadsheet software, and low computing requirement when compared to CFD simulation software. The BEMM uses a combination of *blade element theory* and *momentum theory*.

William Froude introduced blade element theory – which entails cutting a rotor blade into sections (blade elements) which are then treated individually, using a two-dimensional model of lift and drag forces based on lift and drag coefficients for the blade aerofoil profile (Froude, 1878). William Rankine introduced momentum theory (otherwise known as axial momentum theory or disc actuator theory) (Rankine, 1865). This theory models the flow of fluid through the rotor while considering the rotor as an actuator disc (without defined blades). Hermann Glauert combined these two theories in 1926 and also developed the momentum theory to take into account wake rotation (Glauert, 1983).

Frederick Lanchester (in 2015), Albert Betz (in 2020), and Nikolay Joukowsky (in 2020), independently used momentum theory to determine the limit of power (59.3%) that can be absorbed by an ideal rotor in a fluid stream (now usually referred to as the *Betz limit*) (Van Kuik, 2007).

3.1 Classical blade element momentum theory

Hansen (2008) presents the underlying theory of the BEMM which is summarised below.

<u>Linear momentum theory</u>

Linear momentum is used to define axial induction and to derive important equations such as axial velocity and axial thrust. The HAWT rotor is modelled as a permeable, frictionless actuator disc that causes a pressure discontinuity and slows velocity in the fluid stream. The model assumes:

- incompressible, homogenous, steady state flow.
- uniform thrust on the actuator disc (which would require an infinite number of blades).
- pressures far upstream and downstream are equal.
- axial velocities immediately each side of the disc are equal.

In Figure 3.1, V_0 is the wind velocity upstream of the rotor, p_0 is static pressure, u is air velocity at rotor plane and u_1 is air velocity of the far wake.

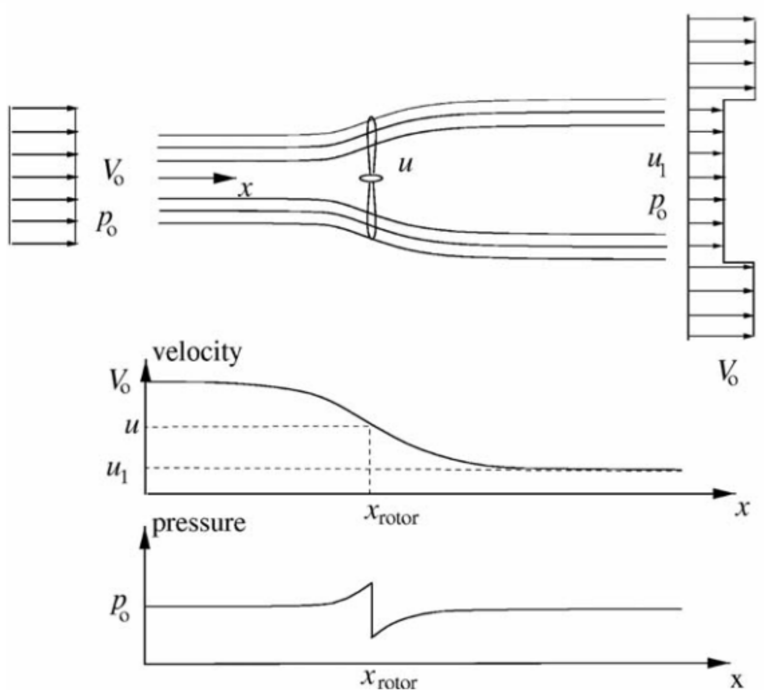

Figure 3.1: Control volume for linear momentum theory

(Source: Hansen, 2018)

Thrust on the rotor of radius R and area $A = \pi R^2$ can be written in terms of the pressure drop as

$$T = \Delta p A \tag{3.1}$$

The Bernoulli equation can be applied upstream and downstream of the rotor since no energy is added or removed before or after the rotor.

$$p_0 + \frac{\rho V_0^2}{2} = p + \frac{\rho u^2}{2} \qquad \text{(before)} \tag{3.2}$$

$$p - \Delta p + \frac{\rho u^2}{2} = p_0 + \frac{\rho u_1^2}{2} \qquad \text{(after)} \tag{3.3}$$

Combining (3.2) and (3.3) gives

$$\Delta p = \frac{1}{2}\rho(V_0^2 - u_1^2) \tag{3.4}$$

Thrust T on the rotor results from the momentum change

$$T = \dot{m}(V_0 - u_1) = \rho u A(V_0 - u_1) \tag{3.5}$$

Now if the thrust in (3.5) is substituted by (3.1), and (3.4) provides the pressure change, the result shows that the velocity in the rotor plane is the mean of the upstream wind and far wake velocities.

$$u = \frac{(V_0 + u_1)}{2} \tag{3.6}$$

Power P absorbed by the rotor is the product of thrust and velocity and if (3.5) and (3.6) are substituted, produces

$$P = Tu = \rho u A(V_0 - u_1)u = \rho u A(V_0 - u_1)\frac{(V_0 + u_1)}{2} = \frac{1}{2}\rho u A(V_0^2 - u_1^2) \tag{3.7}$$

The axial induction factor a is defined as the fractional reduction in wind velocity at the rotor,

$$u = (1 - a)V_0 \quad (3.8)$$

and combining (3.8) with (3.6) produces

$$u_1 = (1 - 2a)V_0 \quad (3.9)$$

If (3.8) is substituted into (3.5) and (3.8), and (3.9) into (3.7), this gives thrust and power as functions of wind speed and axial induction.

$$T = 2\rho V_0^2 a(1 - a)A \quad (3.10)$$

$$P = 2\rho V_0^3 a(1 - a)^2 A \quad (3.11)$$

Effect of wake rotation

A permeable disc does not model the angular velocity imparted to the wake (ϖ) as occurs in air flowing through the rotor of a HAWT. The wake of a HAWT rotates in opposite direction to the angular velocity of the rotor (ω) and an angular induction factor is defined as

$$a' = \varpi / 2\omega \quad (3.12)$$

This can also be expressed, using the tangential velocity of the wake (C_θ) as follows.

$$a' = C_\theta / 2\omega r \quad (3.13)$$

The induced velocity at the rotor includes both the axial velocity component Ua, and the tangential component in the rotor plane $a'\omega r$. These are components of the overall induced velocity w. Velocity triangles in Figure 3.2 show the relationship between these velocities at the rotor plane.

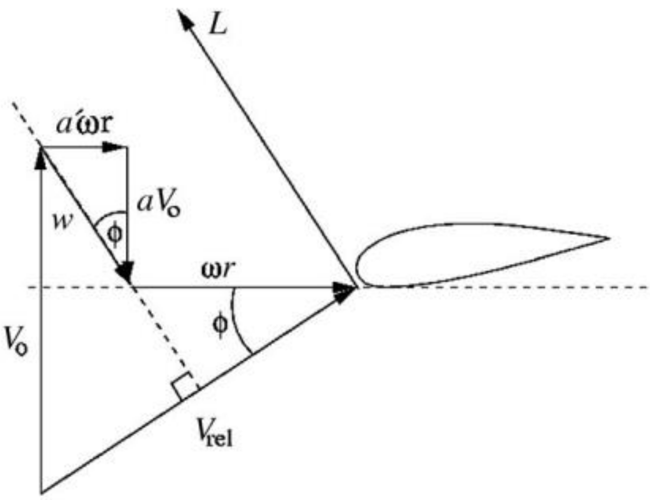

Figure 3.2: Velocity triangles showing the effect of induced velocity at the rotor plane (assuming a small angle of attack so that w is perpendicular to V_{re})

(Source: Hansen, 2008)

The relative wind angle ϕ, can therefore be defined from the velocity triangles in Figure 3.2.

$$\tan \phi = \frac{a'\omega r}{aV_0} \quad (3.14)$$

and

$$\tan\phi = \frac{(1-a)V_0}{(1+a')\omega r} \tag{3.15}$$

<u>The Blade Element Momentum Method</u>

The annular control volume shown in Figure 3.3 is used in the development of the BEMM. The stream tube from linear momentum theory is divided into N annular elements, each with height dr.

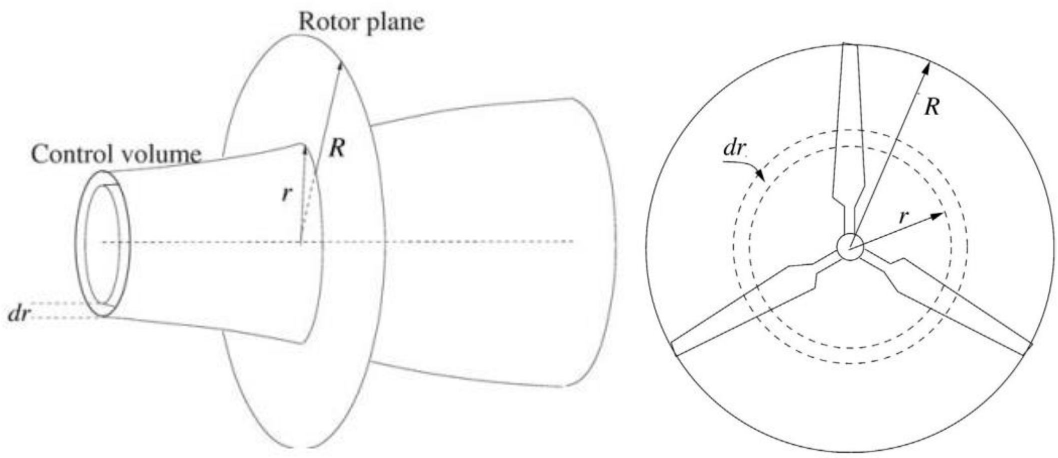

Figure 3.3: Annular element within the linear momentum control volume

(Source: Hansen, 2008)

Since the boundaries of the annular elements are streamlines, there is no flow across elements. Assumptions for this model are:

- Flow through each element is independent of flow through other elements.
- The entire annulus experiences the same force because the number of blades is assumed to be infinite. This assumption is corrected by the Prandtl tip loss correction later in the method.

Linear momentum conservation provides an expression for the thrust on the element at the rotor plane

$$dT = (V_0 - u_1)d\dot{m} = 2\pi r\rho u(V_0 - u_1)dr \tag{3.16}$$

Torque on the element (assuming zero rotation upstream and rotational velocity C_θ in the wake) is

$$dM = rC_\theta d\dot{m} = 2\pi r^2\rho u C_\theta dr \tag{3.17}$$

When (3.8) and (3.9) are substituted into (3.16) and (3.17) the element thrust and torque become

$$dT = 4\pi r\rho V_0^2 a(1-a)dr \tag{3.18}$$

and

$$dM = 4\pi r^3\rho V_0\omega(1-a)a'dr \tag{3.19}$$

Figure 3.2 can be re-drawn as shown in Figure 3.4.

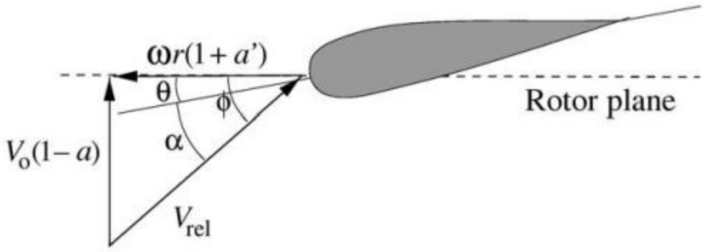

Figure 3.4: Velocities at the rotor plane

(Source: Hansen, 2008)

Angle of attack α is

$$\alpha = \phi - \theta \tag{3.20}$$

and

$$\tan \phi = \frac{(1 - a)V_0}{(1 + a')\omega r} \tag{3.21}$$

Lift and drag forces (per length) are defined as

$$L = \frac{1}{2}\rho V_{rel}^2 c C_L \tag{3.22}$$

$$D = \frac{1}{2}\rho V_{rel}^2 c C_D \tag{3.23}$$

and when these forces are projected to be normal and tangential to the rotor plane (see Figure 3.5), the projected forces become

$$p_N = L\cos\phi + D\sin\phi \tag{3.24}$$

and

$$p_T = L\sin\phi - D\cos\phi \tag{3.25}$$

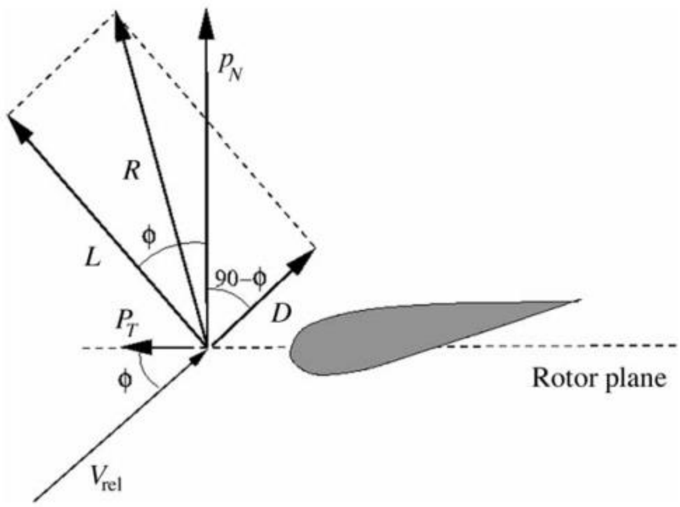

Figure 3.5: Normal and tangential components (p_N and p_T) of the resultant (*R*) of the lift force (L) and drag force (*D*)

(Source: Hansen, 2008)

Expressed as coefficients (dividing through by $\frac{1}{2}\rho V_{rel}^2 c$), p_N and p_T become

$$C_n = C_L \cos\phi + C_D \sin\phi \tag{3.26}$$

and

$$C_t = C_L \sin\phi - C_D \cos\phi \tag{3.27}$$

where

$$C_n = \frac{p_N}{0.5\rho V_{rel}^2 c} \tag{3.28}$$

and

$$C_t = \frac{p_T}{0.5\rho V_{rel}^2 c} \tag{3.29}$$

Figure 3.5 showed that

$$V_{rel} \sin\phi = V_0(1-a) \tag{3.30}$$

and

$$V_{rel} \cos\phi = \omega r(1+a') \tag{3.31}$$

Solidity σ of the annulus (local solidity) is defined as the fraction of the annular area that is occupied by the blades, where B is the number of blades.

$$\sigma = \frac{cB}{2\pi r} \tag{3.32}$$

Since p_N and p_T are forces per unit length, thrust and torque on the control volume of thickness dr are:

$$dT = Bp_N dr \tag{3.33}$$

$$dM = rBp_T dr \tag{3.34}$$

Using (3.28), (3.30) and (3.33), the annular thrust becomes

$$dT = \frac{1}{2}\rho B \frac{V_0^2(1-a)^2}{\sin^2\phi} cC_n dr \tag{3.35}$$

and from (3.29), (3.30), (3.31) and (3.34), annular torque is

$$dM = \frac{1}{2}\rho B \frac{V_0(1-a)\omega r(1+a')}{\sin\phi\cos\phi} cC_t r dr \tag{3.36}$$

Now if (3.35) and (3.18) are combined, an expression for a in terms of ϕ, σ and C_n is obtained.

$$a = \frac{1}{\frac{4sin^2\phi}{\sigma C_n} + 1} \tag{3.37}$$

Similarly a combination of (3.36) and (3.19) yields an expression for a' in terms of ϕ, σ and C_t.

$$a' = \frac{1}{\frac{4\sin\phi\cos\phi}{\sigma C_t} - 1} \tag{3.38}$$

The preceding theory in this chapter provides the basic equations that can be used in the BEMM, however, two corrections are seen as essential for a BEMM analysis – the Prandtl loss correction for finite number of blades and the Glauert correction for high values of axial induction.

Correction for finite number of blades – Prandtl tip loss factor

Prandtl (in Glauert, 1935) derived a correction factor for a finite number of blades (as opposed to the infinite blades simplification). The Prandtl tip loss factor is

$$F_{tip} = \frac{2}{\pi}\cos^{-1}\left(e^{-f}\right) \tag{3.39}$$

where

$$f = \frac{B}{2}\frac{(R-r)}{r\sin\phi} \tag{3.40}$$

This factor is applied to the equations for thrust and torque (3.18 and 3.19), which are adapted as shown below

$$dT = 4\pi r\rho V_0^2 a(1-a)F_{tip}dr \tag{3.41}$$

$$dM = 4\pi r^3\rho V_0\omega(1-a)a'F_{tip}dr \tag{3.42}$$

and (3.37) and (3.38) therefore become

$$a = \frac{1}{\frac{4F_{tip}sin^2\phi}{\sigma C_n}+1} \tag{3.43}$$

$$a' = \frac{1}{\frac{4F_{tip}\sin\phi\cos\phi}{\sigma C_t}-1} \tag{3.44}$$

Glauert correction for high values of axial induction

If axial induction is higher than approximately 0.4 (depending on which theory is chosen), the correction for turbulent wake state (at high values of axial induction) requires an alternative calculation of axial induction for this state. The Glauert correction as modified by Buhl (Moriarty and Hansen, 2005) was used to determine axial induction for axial induction greater than 0.4 and uses the equations below.

$$C_t = \frac{8}{9} + \left(4F - \frac{40}{9}\right)a + \left(\frac{50}{9} - 4F\right)a^2 \tag{3.45}$$

$$a = \frac{18F - 20 - 3\sqrt{C_t(50-36F) + 12F(3F-4)}}{36F - 50}$$

Prandtl hub loss correction

Since this study investigated the impact of improved flow in the near-hub region, a further correction that was used, in certain flow scenarios, was the Prandtl hub loss correction. The tip loss factor, hub loss factor and overall loss factor *F* are given by:

$$F_{tip} = \left({}^{2}/_{\pi}\right)\cos^{-1} e^{-\frac{B}{2}\left(\frac{R-r}{r\sin\phi}\right)}$$

$$F_{hub} = \left({}^{2}/_{\pi}\right)\cos^{-1} e^{-\frac{B}{2}\left(\frac{r-R_{hub}}{R_{hub}\sin\phi}\right)} \tag{3.46}$$

$$F = F_{tip} \times F_{hub} \tag{3.47}$$

The theory for this correction is identical to the tip loss correction but applies to the root of the blade, and the theory is only applicable if the blade is aerodynamically terminated prior to reaching the hub as shown in Figure 3.6.

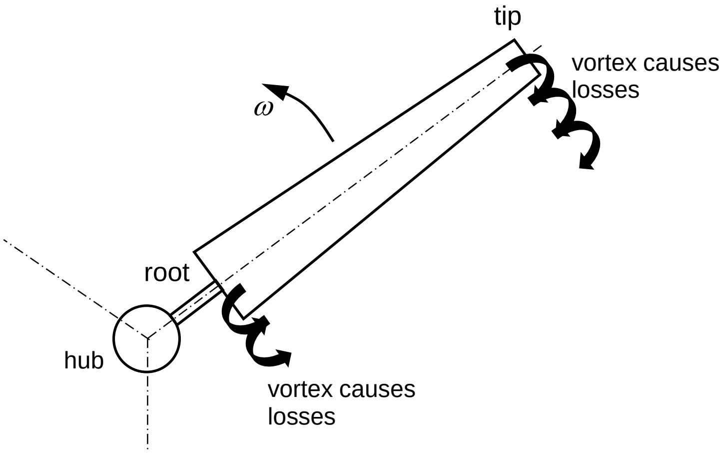

Figure 3.6: Prandtl hub loss theory applies to a blade aerodynamically terminated before reaching the hub

For larger hub ratios, and if uncompromised blade profiles are brought all the way to the hub and interfaced with the hub, no edge vortices at the root of the blade (as shown in Figure 3.6) will occur. However, an intense root vortex running axially downwind (with accompanying energy loss) is created due to a rapidly increasing angular induction as the rotor axis is approached and the tangential component of the resulting absolute air velocity leaving the rotor becoming greater and greater.
Figure 3.7 shows the location of the tip vortices and the root vortex.

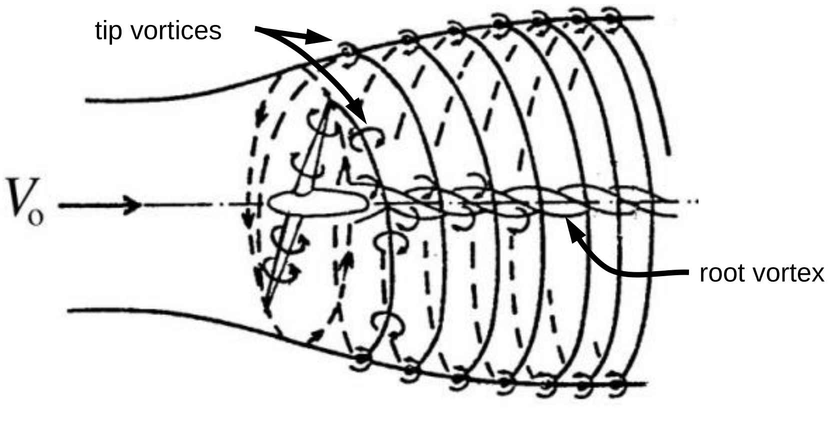

Figure 3.7: Location of tip and root vortices in a HAWT wake

(Source: Wilson and Lissaman, 1974 in Hansen, 2008)

Even though the Prandtl hub loss theory is specifically derived from blade termination effects (similar to tip losses), in practice, it is expected to approximately model the vortices from fully, partially or non-terminated blade roots, as well as the angular induction-induced root vortex. Branlard (2017) confirms that the nature of the hub losses are "... *somewhat different to the tip losses* ..." and that the Prandtl hub loss equation is used "... *for modelling convenience*". In this study, the Prandtl hub loss factor was applied to the 5% hub ratio rotor (to cater for an expected root vortex) and the same factor values were carried through to the corresponding elements of the rotors with larger hubs (to approximate the expected rapidly-diminishing root losses at larger hub ratios).

The BEMM to find the final flow condition (a, a' and ϕ)through a HAWT can now be performed in the following steps (for each blade element):

1) Initialize a and a' (0.3 and 0.1 respectively were used in this study).
2) Calculate local relative wind angle ϕ using (3.21).
3) Calculate local angle of attack α using (3.20).
4) Determine C_L and C_D from table/spreadsheet data.
5) Calculate C_n and C_t from (3.26) and (3.27) - or (3.43) for axial induction greater than 0.4.
6) Calculate a and a' from (3.41) and (3.42).
7) If a and a' have changed more than a particular tolerance, then go to step 2 or else finish.
8) Calculate local loads on the blade element.

The underlying classical theory, as presented in this section, provides a foundation upon which many choices can be made. For example, there are multiple ways that blade chord can be calculated – providing a variety of resulting blade geometries. A simpler (older) version of the BEMM excludes wake rotation. There is also lack of consensus on the use and relevance of the Prandtl hub factor (which is important in a study focussing on hub size). Because of the theory choices available, it is important to define the BEMM theory used in this study.

3.2 The 'standard' BEMM for this study

For this research the classical BEMM of Glauert as presented by Hansen (2008) was used. The method includes wake rotation theory, the Prandtl tip loss factor for correction for finite number of blades and the Glauert correction (with Buhl adaption) for high values of axial induction. During the blade design stage, the Schmitz equation as used by Manwell (2002) was used for initial chord calculation and the Maalawi chord (El-Okda, 2015) was used iteratively for chord optimization toward blade tips. The Prandtl hub loss factor was applied only to blade elements that were close to the centre of rotation where blade chords were semi-terminated (rapidly reducing chord towards centre of rotation) and where an intense axial root vortex was considered possible.

Owing to the possibility of variations in the BEMM the label 'standard' refers to the BEMM as presented by Hansen (2008) with the corrections as described above. The 'standard' design and BEMM study used in this research comprised three main stages:

Stage 1- Choice of main parameters and calculation of other constants

A sample portion of a typical BEMM spreadsheet is shown in Figure 3.8. Test and rotor parameters are chosen and other useful constants are calculated from these parameters.

Rotor diameter D (m)	0.28
Design tip speed ratio	4.8
Number of blades B	3
Element Δr_e (m)	0.0035
Number of blade elements N	40
Hub ratio	0.05
Hub radius r (m)	0.007
Fluid temp (°C)	20
Fluid density ρ (kg/m3)	998.4
Fluid dynamic viscosity μ (kg/m.s)	0.001027
Fluid speed U (m/s)	0.25

Figure 3.8: BEMM spreadsheet sample - Main rotor and test parameters

Apart from the above data, aerofoil performance data (α, C_L, C_D, C_L/C_D), at suitable intervals of Reynolds number and angle of attack are required for the following stages. In this study, XFLR5 (aerofoil flow modelling software) was used to determine the aerofoil performance data.

Stage 2 - Blade design - chord and pitch angle for each blade element

1) Blade length was divided into elements of equal width dr.

2) For each element, element centroid radius r, element radius ratio ${}^{r}/{}_{R}$, its inverse ${}^{R}/{}_{r}$ and local speed ratio $\lambda_r$were determined.

3) For each element, relative wind angle ϕ, chord c and Prandtl tip loss factor F_{tip} were determined using:

$$\phi = \left({}^{2}/{}_{3}\right)\tan^{-1}\left({}^{1}/{}_{\lambda_r}\right)$$

$$c = \left({}^{8\pi r}/{}_{BC_L}\right)(1-\cos\phi)$$

$$F_{tip} = \left({}^{2}/{}_{\pi}\right)cos^{-1}\, e^{-\frac{B}{2}\left(\frac{R-r}{r\sin\phi}\right)}$$

4) For each element, blade relative velocity $V_{rel}$and Reynolds number Re where estimated using the equations below and assuming an axial induction factor of a = 1/3 (for ideal flow)

$$V_{rel} = \sqrt{\left(V_0(1-a)\right)^2 + (\omega r_e)^2}$$

$$Re = {}^{\rho V_{rel} c}/{}_{\mu}$$

5) An iterative process was used to determine the final design chord and the resulting Reynolds number. Chord (with blade tip chord correction) was determined using the Maalawi equation (shown below) from El Okda (2015).

$$c = \frac{8\pi r F_{tip} sin\ \phi}{BC_L\left(\frac{\lambda_r + \tan\phi}{1-\lambda_r \tan\phi} - \frac{C_D}{C_L}\right)}$$

The lift coefficient and lift to drag ratio were determined from best-fit curve equations of C_L vs Re and C_L/C_D vs Re.

6) For each element, the section pitch angle θ was calculated from

$$\theta = \phi - \alpha$$

where α is the optimum angle of attack for each element, and was determined from a best-fit curve equation of α vs Re – from α data at maximum C_L/C_D for each step in Reynolds number.

7) For each element, local solidity σ was calculated from

$$\sigma = \frac{Bc}{2\pi r}$$

<u>Stage 3 - Applying the BEMM for prediction of induction, relative wind angle and power from the rotor</u>

The axial and angular induction factors were estimated ($a = 0.3$ and $a' = 0.1$) prior to the start of the first iteration. For each element, the following steps formed each iteration:

1) Relative wind angle ϕ was calculated using:

$$\tan\phi = \frac{(1-a)U}{(1+a')\Omega r}$$

2) Angle of attack α was calculated from

$$\alpha = \phi - \theta$$

3) Coefficients of lift and drag were interpolated from the airfoil data at angle of attack calculated above and Reynolds number calculated in Stage 2, Step 5.

4) Normal load coefficient C_n and tangential load coefficient C_t were calculated as follows.

$$C_n = C_L \cos\phi + C_D \sin\phi$$

$$C_t = C_L \sin\phi - C_D \cos\phi$$

5) Prandtl tip and hub loss factors (F_{tip} and F_{hub}) and overall tip and hub loss factor F were calculated. Note that hub loss factor was only calculated where blade root end effects or an intense root vortex were expected, otherwise it was assumed that $F_{hub} = 1$.

$$F_{tip} = \left({}^{2}/_{\pi}\right)\cos^{-1} e^{-\frac{B}{2}\left(\frac{R-r}{r\sin\phi}\right)}$$

$$F_{hub} = \left({}^{2}/_{\pi}\right)\cos^{-1} e^{-\frac{B}{2}\left(\frac{r-R_{hub}}{R_{hub}\sin\phi}\right)}$$

$$F = F_{tip} \times F_{hub}$$

6) The axial induction was calculated as follows.

$$a = \frac{1}{\frac{4F\sin^2\phi}{\sigma C_n} + 1}$$

The Glauert correction, as modified by Buhl (Moriarty and Hansen, 2005), was used to determine axial induction for axial induction greater than 0.4, and uses the equations below.

$$C_t = \frac{8}{9} + \left(4F - \frac{40}{9}\right)a + \left(\frac{50}{9} - 4F\right)a^2$$

$$a = \frac{18F - 20 - 3\sqrt{C_t(50 - 36F) + 12F(3F - 4)}}{36F - 50}$$

7) The angular induction factor was calculated.

$$a' = \frac{1}{\frac{4F\sin\phi\ cos\ \phi}{\sigma C_t} - 1}$$

Using the new induction factors (a and a') a new relative wind angle ϕ can now be calculated and the next iteration begins. After convergence, torque per annulus δM and power per annulus δP were determined from.

$$\mathrm{d}M = 4Fa'(1-a)\rho V_0 \pi r^3 \omega\ \mathrm{d}r$$

$$\mathrm{d}P = \omega\ \mathrm{d}Q$$

The sum of the power per annulus from all elements is the total power absorbed by the rotor at the chosen wind speed and rotor rotation speed.

3.3 The large-hub adaption to the BEMM

A spherical or axially symmetric streamlined or elliptical body within uniform flow of air causes acceleration of oncoming air near the body. A hub of an aerodynamically designed HAWT is similarly shaped and also experiences (in standard BEMM theory) a uniform flow of air in the axial direction. In this adaption to the BEMM, the assumption of uniform flow from the momentum theory is adapted by inclusion of a velocity profile applied to the upstream wind which best approximates the expected accelerations around the hub in the plane of the rotor.

Using three-dimensional potential flow theory, theoretical accelerations were predicted for flow around a Rankine half-body and flow around an airship shaped body. The velocity profile for both these forms was investigated for potential use in the BEMM adaption.

The Rankine half-body (a single point source within a uniform flow) is similar to flow over a long, cylindrical nacelle or flow adjacent to a long wide turbulent wake (such as from a significant root vortex). The airship form (a source followed by a line of sinks within a uniform flow) best describes flow that stays well attached to a streamlined nacelle (of any length). Arrangement of sources and sinks for each body are shown in Figure 3.9 and Figure 3.10.

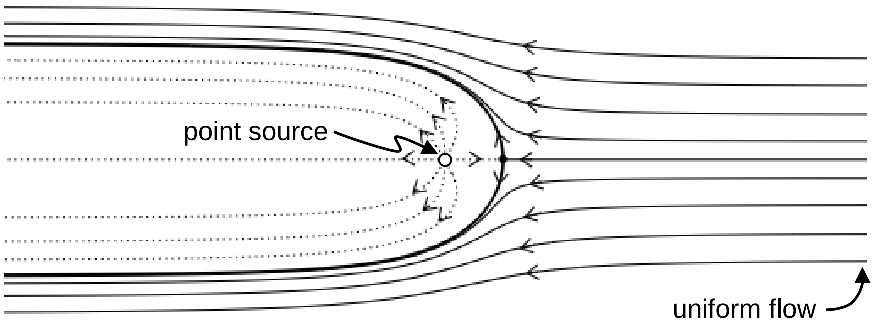

Figure 3.9: Flow over Rankine half-body – a point source within uniform flow

(Adapted from Kersalé, n.d.)

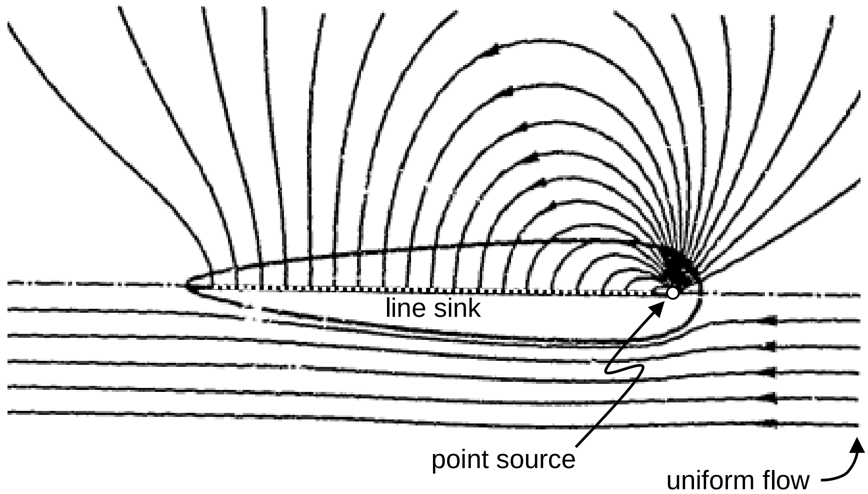

Figure 3.10: Flow over Airship form – a point source followed by a symmetrical line of distributed sinks within uniform flow

(Adapted from Kennard, 1967)

The following equations (from cylindrical coordinates) were used in describing the streamlines and body shape and for calculation of velocity vectors for the Rankine half-body (Kersalé, n.d.) and the Airship form (Kennard, 1967).

For the Rankine half-body, the stream function can be written as

$$\Psi(r,z) = \frac{Ur^2}{2} - \left(\frac{mz}{(r^2 + z^2)^{1/2}}\right) \tag{3.48}$$

For a long slender body of half-width a (at large z), where

$$a = 2\sqrt{m/U} \tag{3.49}$$

(3.48) and 3.49) can be combined to produce the stream function

$$\Psi(r, z) = \frac{U}{2} - \left(r^2 - \frac{a^2 z}{2(r^2 + z^2)^{1/2}}\right) \quad (3.50)$$

where U is the uniform flow (at the plane of the rotor), m is the source strength and r and z are the cylindrical coordinates as shown in Figure 3.11.

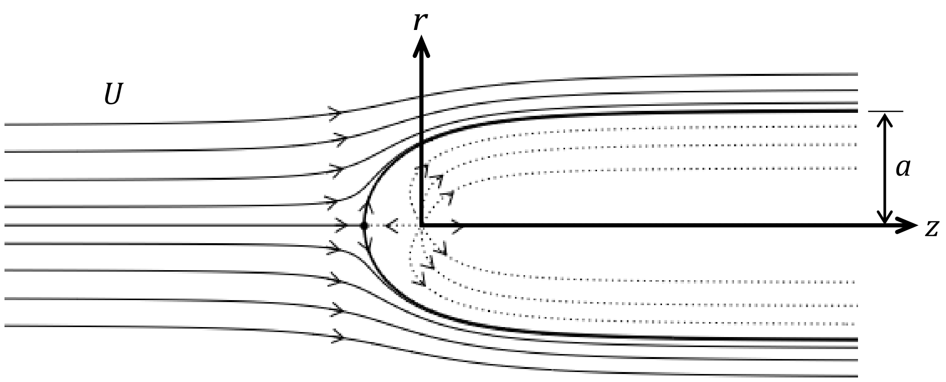

Figure 3.11: Variables and coordinate system for Rankine half-body

Body shape is obtained from

$$\frac{Ur^2}{2} = m\left(1 + \frac{z}{(r^2 + z^2)^{1/2}}\right) \quad (3.51)$$

and a stagnation point occurs at

$$z = -\sqrt{m/U} \quad (3.52)$$

Velocity component in the axial direction is given by

$$U_z = \frac{1}{r}\frac{\delta\Psi}{\delta r} \quad (3.53)$$

where

$$\frac{\delta\Psi}{\delta r} = Ur + \frac{mrz}{(r^2 + z^2)^{3/2}} \quad (3.54)$$

The velocity gradient for the BEMM adaption (if assuming a Rankine half-body flow profile over the hub) was generated from (3.53) and (3.54). The velocity gradients are presented in Figure 3.13 (later in this section).

The possibility that flow over the hub might not follow a profile similar to the Rankine half-body was also considered, and a velocity profile for flow that would closely follow the profile of a streamlined hub and nacelle was also modelled. A good approximation for this flow profile is the Airship form. Kennard (1967) provides equations for the Airship form using variables and coordinates as shown in Figure 3.12.

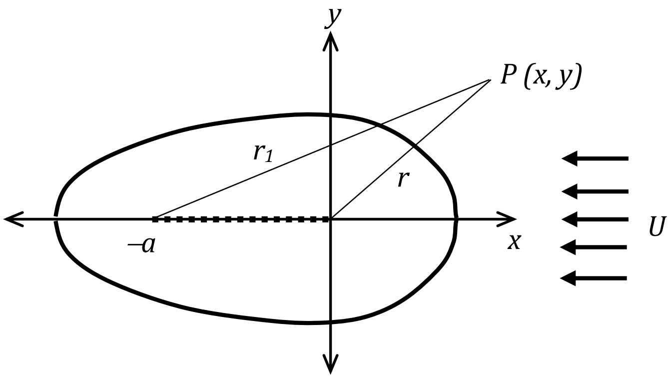

Figure 3.12: Variables and coordinate system for Airship form

(Adapted from Kennard, 1967)

The stream function for a point source of strength $4\pi A$ at the origin followed by a line of distributed point sinks of equal total strength is given by

$$\Psi = U\left(\frac{y^2}{2} + b^2 \frac{(r_1 - r)^2 - a^2}{2ar}\right) \tag{3.55}$$

where U is the uniform flow velocity

a is the length of the line sink

$b^2 = A/U$ (where b is a size factor) (3.56)

$A = (b/a)^2$ (airship thickness ratio) (3.57)

$r = (x^2 + y^2)^{1/2}$ (3.58)

and $r_1 = ((x + a)^2 + y^2)^{1/2}$ (3.59)

Body shape is given by

$$\frac{y^2}{a} = A\left(\frac{1 - (r_1/a - r/a)^2}{r/a}\right) \tag{3.60}$$

The velocity component in the axial direction at any point (P) is

$$v_x = U\big(-1 + b^2(x/r^3 - (1/r - 1/r_1)/a)\big) \tag{3.61}$$

The velocity profile for the Airship-adapted BEMM was generated using (3.56), (3.57), (3.58), (3.59) and (3.61).

The maximum integral of the axial velocity profile over the blade length was found to occur at a distance from the front of the airship of 1.21× maximum form radius. For the sake of comparison, this ratio was used to locate the rotor plane for both the Airship and Rankine half-body forms in the CFD models and the manufactured rotors for physical testing.

The results of the potential flow analyses produced the velocity profiles shown in Figure 3.13. Flow around a Rankine half-body produced a higher acceleration then around an Airship body. Larger hub ratio can be seen to produce a broader zone of accelerated air.

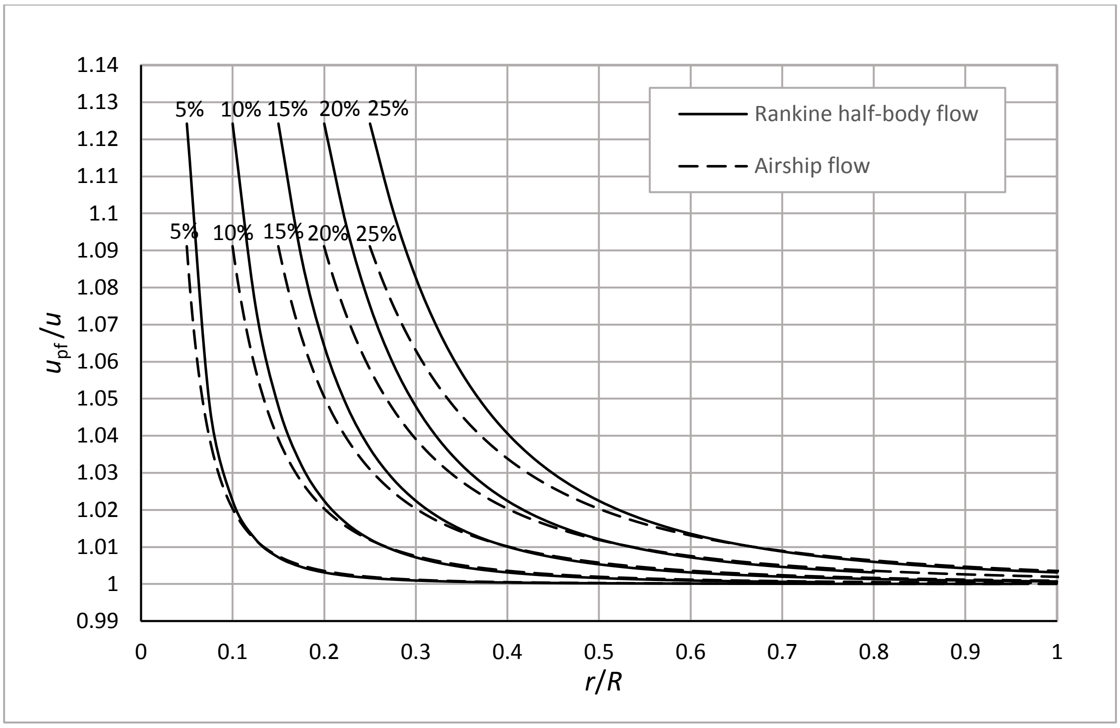

Figure 3.13: Potential flow velocity (U_{pf}) over theoretical uniform velocity at rotor plane (U) vs. blade radius ratio (r/R) – for 5%, 10%, 15%, 20% and 25% hub ratios - for ideal Airship and Rankine half-body flow around hub

Skin friction causes flow velocity at the hub surface to be close to zero, so in reality the theoretical increase in velocity (9% for Airship and 12.5% for Rankine half-body) at the hub surface would not be achieved. Instead, the velocity profile rises from zero at the hub surface and meets the curve at a point somewhere below the theoretical maximum values. Owing to the relatively thin boundary layer, compared to the width of the zone of accelerated air outside the boundary layer, this boundary layer effect was ignored in the BEMM adaption.

It is also noticeable in Figure 3.13 that for larger hub ratios a small amount of the theoretical gains in axial velocity extend beyond the tip of the rotor (r/R = 1). In practice this implies a loss of energy, due to deflection by the hub of air that would have passed through the rotor but now 'spills' over the edge of the rotor circle. This loss was quantified by numerically integrating dimensionless power per element-annulus over the length of the blade and subtracting this total dimensionless power with hub from the total dimensionless power with no hub (equal to 1) – to obtain a hub-induced deflection power loss fraction (or percentage). In equation form, this can be described as follows:

Power in a stream of air, of density ρ, velocity U and cross-sectional area A, is given by:

$$P = \frac{1}{2}\rho A U^3 \tag{3.62}$$

and since each annular stream tube has a different cross-sectional area and axial velocity, and because dimensionless power excludes constants, the relationship can be rewritten as:

$$P \propto AU^3 \tag{3.63}$$

For a blade element that has outer and inner dimensionless radii of $(r/R)_2$ and $(r/R)_1$, the dimensionless area can be written as:

$$A \propto \left[\left(\frac{r}{R}\right)_2^2 - \left(\frac{r}{R}\right)_1^2\right] \tag{3.64}$$

Now if U_{pf}/U is the average velocity ratio for that element from the potential flow-derived curve previously shown in Figure 3.13, then the dimensionless power per element can written as:

$$P \propto \left[\left(\frac{r}{R}\right)_2^2 - \left(\frac{r}{R}\right)_1^2\right]\left(\frac{U_{pf}}{U}\right)^3 \tag{3.65}$$

So when a large hub (and velocity gradient) is present, the total dimensionless power that would be expected from flow through the rotor is the integral of the dimensionless powers for each element from 1 to N, where element 1 is the first blade element starting at the hub.

$$P \propto \int_1^N \left[\left[\left(\frac{r}{R}\right)_2^2 - \left(\frac{r}{R}\right)_1^2\right]\left(\frac{U_{pf}}{U}\right)^3\right] \tag{3.66}$$

A stream of air without a hub (and without a velocity gradient) produces a dimensionless power of 1 and the existence of a hub, and using (3.66) reduces this to a fraction smaller than 1. The difference is the theoretical power loss that can be expressed as a percentage as shown in Figure 3.14.

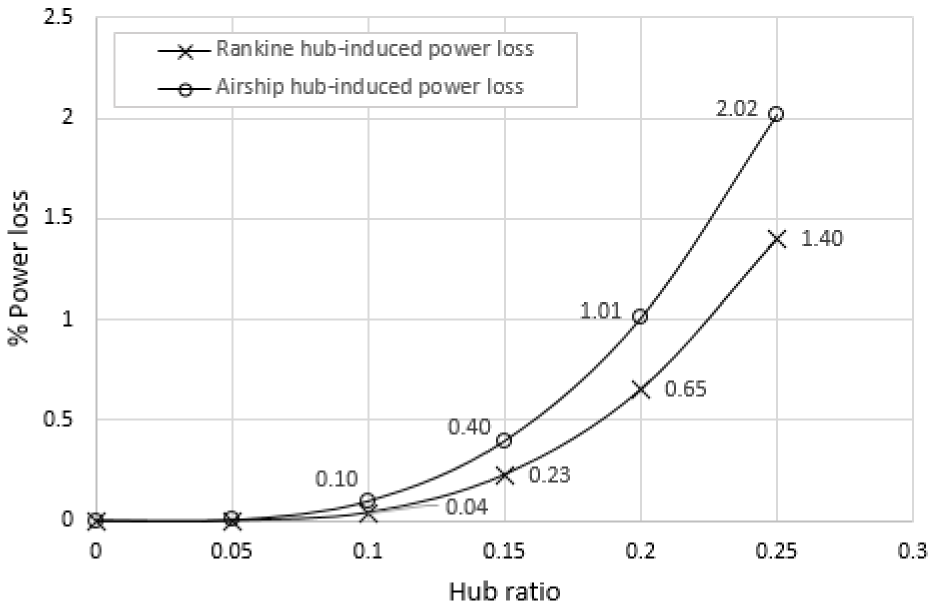

Figure 3.14: Hub-induced deflection power loss for Airship and Rankine half-body forms

This percentage power loss was subtracted from overall rotor power for all power predictions – because for large hubs, hub deflection ('spillage') losses would occur whether the standard or adapted BEMM was used, and should be seen as a necessary part of any BEMM study of rotors with large hub ratios.

The BEMM adaption for large hub ratios includes the following changes **(in bold type)** to the standard BEMM. A flow diagram of the adapted BEMM is provided in Appendix Q.

<u>Stage 1 - Choices of main parameters and calculation of other constants</u>

No change to this stage.

<u>Stage 2 - Blade design - chord and pitch angle for each blade element</u>

1) Blade length is divided into elements of equal width $\mathrm{d}r$. **(No change)**

2) For each element, element centroid radius r, element radius ratio r/R, its inverse R/r are determined. **(No change)**

2b) An imaginary non-uniform upstream wind velocity $V_0{}'$ is created by multiplying the free stream velocity V_0 by the air velocity ratio (u_{pf}/u) obtained from Figure 3.13. A corrected local speed ratio λ_r is calculated using $V_0{}'$ instead of V_0.

3) For each element, a **corrected** relative wind angle (ϕ), **corrected** chord (c) and **corrected** Prandtl loss factor (F) are determined by:

$$\phi = \left(2/3\right)\tan^{-1}\left(1/\lambda_r\right) \qquad \textbf{(using corrected } \boldsymbol{\lambda_r}\textbf{)}$$

$$c = \left(8\pi r/BC_L\right)(1-\cos\phi) \qquad \textbf{(using corrected } \boldsymbol{\phi}\textbf{)}$$

$$F = \left(2/\pi\right)cos^{-1}\, e^{-\frac{B}{2}\left(\frac{R-r}{r\sin\phi}\right)} \qquad \textbf{(using corrected } \boldsymbol{\phi}\textbf{)}$$

4) For each element, a **corrected** wind relative velocity (U_{rel}) and **corrected** Reynolds number (Re) are estimated using the equations below and assuming an axial induction factor of *a* = 1/3 (for ideal flow)

$$V_{rel} = \sqrt{\left(V_0{}'(1-a)\right)^2 + (\omega r)^2} \qquad \textbf{(using } \boldsymbol{V_0{}'}\textbf{ instead of } \boldsymbol{V_0}\textbf{)}$$

$$Re = \rho U_{rel}c/\mu \qquad \textbf{(using corrected } \boldsymbol{V_{rel}}\textbf{ and } \boldsymbol{c}\textbf{)}$$

5) A similar iterative process is used to determine the final design chord and the resulting Reynolds number. **Corrected** chord (with blade tip correction) is determined using the Maalawi equation (shown below) from El Okda (2015). **Corrected** C_L and C_D are determined at the **corrected** Reynolds number

$$c = \frac{8\pi rFsin\,\phi}{BC_L\left(\frac{\lambda_r + \tan\phi}{1-\lambda_r\tan\phi} - \frac{C_D}{C_L}\right)}$$

(using corrected $\boldsymbol{F, \phi, \lambda_r, C_L}$ *and* $\boldsymbol{C_D}$)

6) For each element, the **corrected** section pitch angle θ was calculated from

$$\theta = \phi - \alpha \qquad \textbf{(using corrected } \boldsymbol{\phi}\textbf{)}$$

Where α is the optimum angle of attack for each element and was determined, using **corrected** Reynolds number, from a best-fit curve equation of α vs Re – from α data at maximum (C_L/C_D) for each step in Reynolds number.

7) For each element, **corrected** local solidity σ is calculated using the **corrected chord** from

$$\sigma = \frac{Bc}{2\pi r_e}$$

Stage 3 - Applying the BEMM for prediction of induction, relative wind angle and power from the rotor

As with the standard BEMM, this is an iterative calculation and the axial and angular induction factors are estimated ($a = 0.3$ and $a' = 0.1$) prior to the start of the first iteration. For each element, the following steps form each iteration.

1) **Corrected** relative wind angle (ϕ) is calculated using the imaginary non-uniform upstream wind velocity $\boldsymbol{V_0}'$.

$$\tan\phi = \frac{(1-a)V_0'}{(1+a')\omega r}$$

All variables in the following steps 2 to 7 use corrected values if these values were corrected in Stage 2 – otherwise the overall method is identical.

2) Angle of attack (α) is calculated from:

$$\alpha = \phi - \theta$$

3) Coefficients of lift and drag are interpolated from the airfoil data at angle of attack calculated above and Reynolds number calculated in Stage 2, Step 5.

4) Normal load coefficient (C_n) and tangential load coefficient (C_t) are calculated as follows.

$$C_n = C_L \cos\phi + C_D \sin\phi$$

$$C_t = C_L \sin\phi - C_D \cos\phi$$

5) Prandtl tip and hub loss factors (F_{tip} and F_{hub}) and overall tip and hub loss factor (F) are calculated – noting that hub loss factor was only calculated where blade root end effects or an intense root vortex were expected, otherwise it was assumed that $F_{hub} = 1$.

$$F_{tip} = \left({}^{2}/_{\pi}\right)\cos^{-1} e^{-\frac{B}{2}\left(\frac{R-r}{r\sin\phi}\right)}$$

$$F_{hub} = \left({}^{2}/_{\pi}\right)\cos^{-1} e^{-\frac{B}{2}\left(\frac{r-R_{hub}}{R_{hub}\sin\phi}\right)}$$

$$F = F_{tip} \times F_{hub}$$

6) The axial induction is calculated as follows.

$$a = \frac{1}{\frac{4F\sin^2\phi}{\sigma C_n} + 1}$$

The Glauert correction as modified by Buhl (Moriarty and Hansen, 2005) is used to determine axial induction for axial induction greater than 0.4 and uses the equations below.

$$C_t = \frac{8}{9} + \left(4F - \frac{40}{9}\right)a + \left(\frac{50}{9} - 4F\right)a^2$$

$$a = \frac{18F - 20 - 3\sqrt{C_t(50 - 36F) + 12F(3F - 4)}}{36F - 50}$$

7) The angular induction factor is calculated.

$$a' = \frac{1}{\frac{4F\sin\phi\, cos\,\phi}{\sigma C_t} - 1}$$

Using the new induction factors (a and a'), a new relative wind angle ϕ is calculated and the next iteration begins. After convergence, torque per annulus $\mathrm{d}Q$ and power per annulus $\mathrm{d}P$ are determined.

$$\mathrm{d}Q = 4Fa'(1 - a)\rho V_0 \pi r^3 \omega\, \mathrm{d}r$$

$$\mathrm{d}P = \omega\, \mathrm{d}Q$$

The sum of the power per annulus from all elements is the total power absorbed by the blade at the chosen wind speed and rotor rotation speed.

8) This is an additional step, necessary to subtract the expected hub-induced deflection power loss. Values for % power loss are dependent on hub ratio and are obtained from Figure 3.14.

$$P_{final} = \sum dP \times \frac{(100 - \%\ \text{power loss})}{100}$$

3.4 Results of BEMM analyses

For a HAWT rotor of chosen diameter, number of blades, aerofoil and wind speed, the BEMM provides optimum blade chord and section pitch angle for blades. The BEMM was also used to predict relative wind angle, axial induction, angular induction and power absorption by the rotor at the necessary rotation speeds.

3.4.1 Blade designs

Blades were divided into 40 elements from rotor centre to blade tip. Design analysis predicted Reynolds numbers for the 5% hub rotor (based on chord) ranging from ≈ 8000 at hub to ≈ 12500 at blade centre and reducing back to ≈ 8000 at tip (2nd last element) with the last element at the tip dropping to ≈ 4500. A cambered plate aerofoil was identified as the most effective aerofoil type for this range of Reynolds number and a single profile was used in all elements of all rotors. The choice of airfoil is supported by the comparison of aerofoil types by Koning (2019) (see Figure 3.15) that shows which aerofoil types are expected to provide high performance within particular Reynolds number ranges.

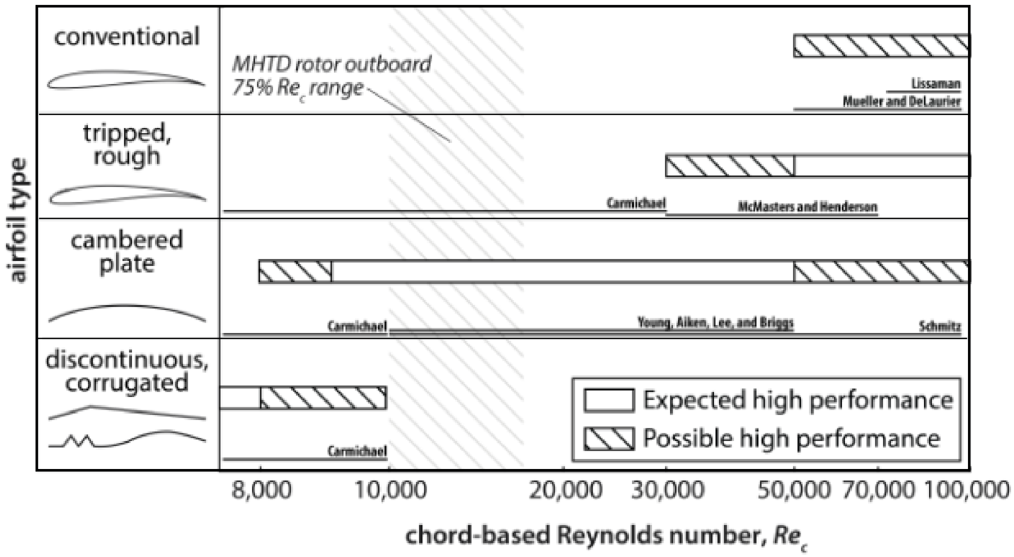

Figure 3.15: Performance of aerofoil types versus Reynolds number

(Source: Koning, 2019)

The cambered plate aerofoil used in this work was an adapted Eppler E61with trailing edge thickened to 5% to allow for successful 3D printing and for adequate strength and stiffness. Maximum thickness is 6.94% at position 42,21% and camber is 6.69% at position 50.09%.

The aerofoil profile is shown in Figure 3.16 and chord and twist data for all rotors is provided in Appendix B.

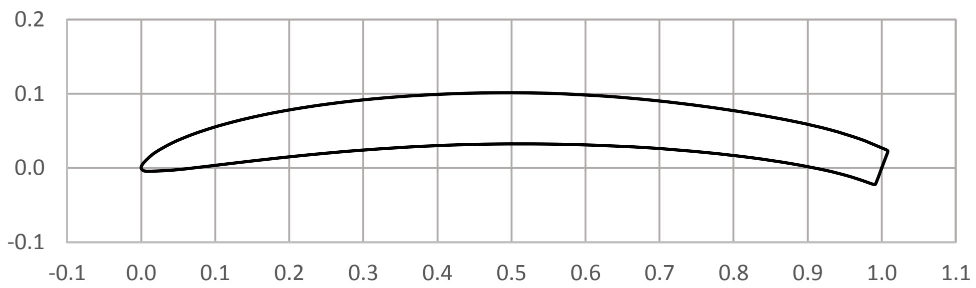

Figure 3.16: Cambered plate aerofoil – Adapted Eppler E61 airfoil with 5% trailing edge

Aerofoil performance data was obtained from aerofoil modelling software *XFLR5*. Outputs of C_L and C_D at Reynolds numbers ranging from 4000 to 13000 in intervals of 1000 and with angle of attack ranging from -2.5º to 16º in intervals of 0.25º were generated for use within the BEMM spreadsheet and performance curves are shown in Figure 3.17 and 3.18, and are tabulated in Appendix B.

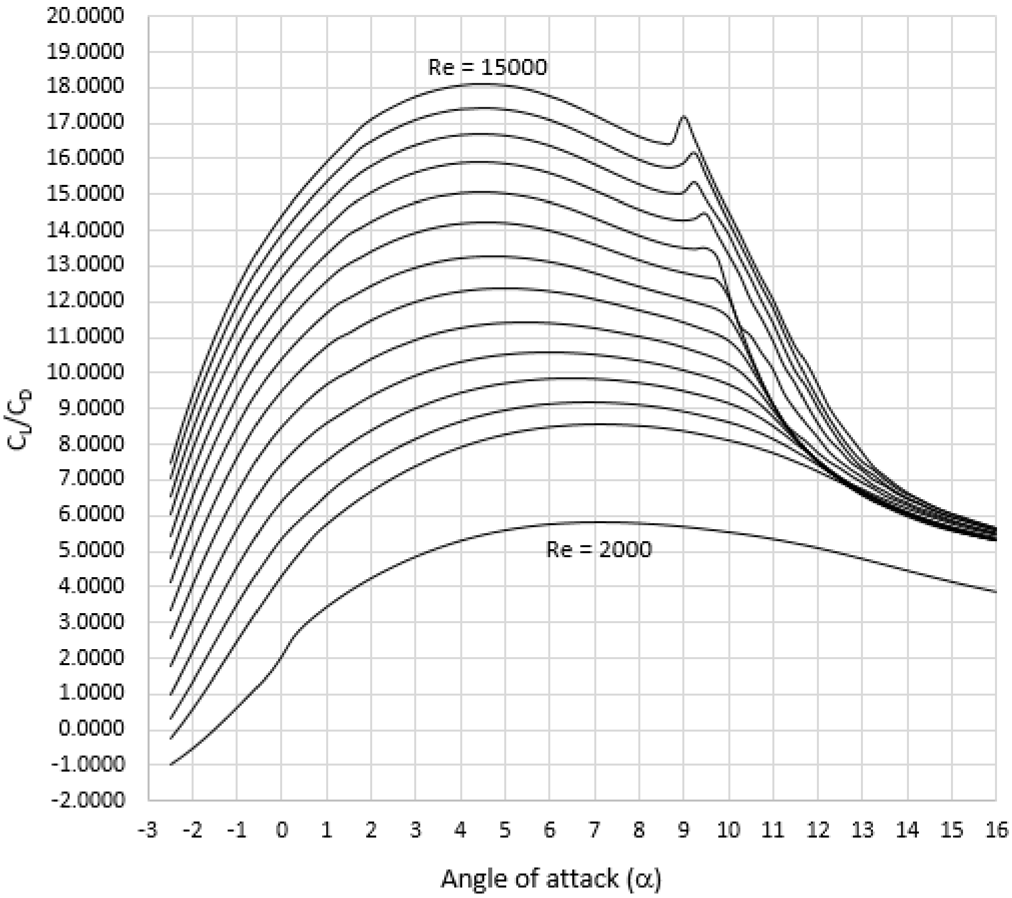

Figure 3.17: Lift –drag ratio vs. angle of attack for the cambered plate aerofoil. Reynolds number ranging from2000 to 15000 at intervals of 1000

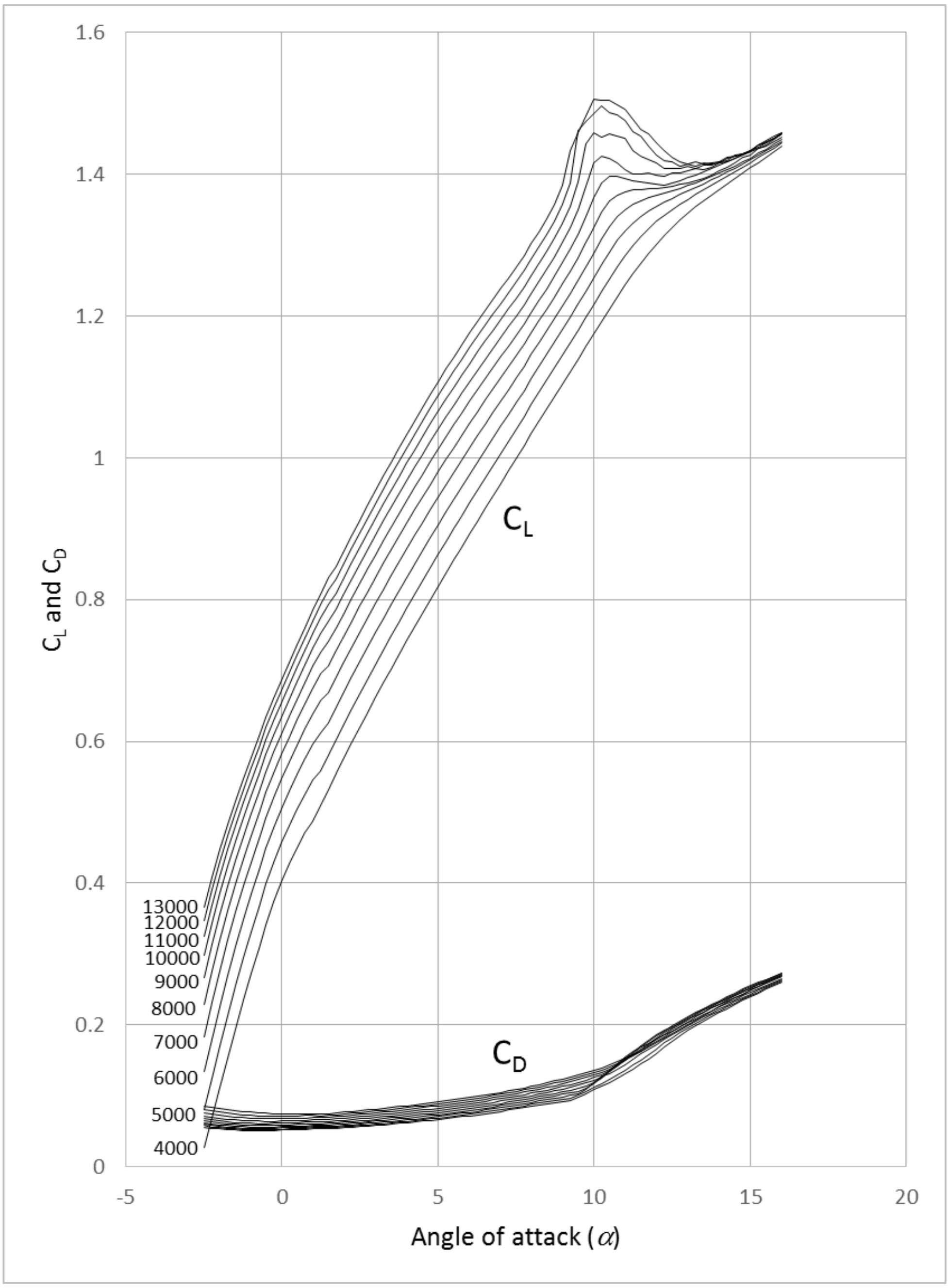

Figure 3.18: Lift and drag coefficients vs. angle of attack for 4000 ≤ Re ≤ 13000

3.4.2 Performance prediction

In all BEMM analyses, the 5% hub, designed and analysed with the 'standard' BEMM, was used as the reference 5% hub because initial analysis showed that for a rotor with a 5% hub there were negligible geometry differences, whether the rotor was designed with the 'standard' or the adapted BEMM.

Analysis 1 –All rotors (5%, 10%, 15%, 20% and 25% hub ratios) designed and analysed using the standard BEMM

The first analysis compared rotors, designed and analysed with the 'standard' BEMM, with hubs of increasing size. Using the standard BEMM design procedure, blade chord and twist at each blade element were identical across rotors because the standard BEMM design procedure doesn't take the effect of hub size into account. The BEMM results (see Figure 3.19) show that:

- peak power was achieved at a rotation speed of 63 rpm.
- power drops off sharply when rotation speeds are lower than rotation speed at peak power (when stall occurs).
- power was reduced by a greater margin with each increase in hub ratio.
- prediction, using the standard BEMM, of the effect of hub ratio, shows power was consistently reduced as hub ratio was increased (no benefit at all). This reduction in power with increasing hub ratio is expected since rotor swept area is reduced with each increase in hub size. This study seeks to determine if any benefit from a larger than minimal (5%) hub would increase power at a particular hub ratio, prior to the inevitable drop in power when the hub is made larger and larger.

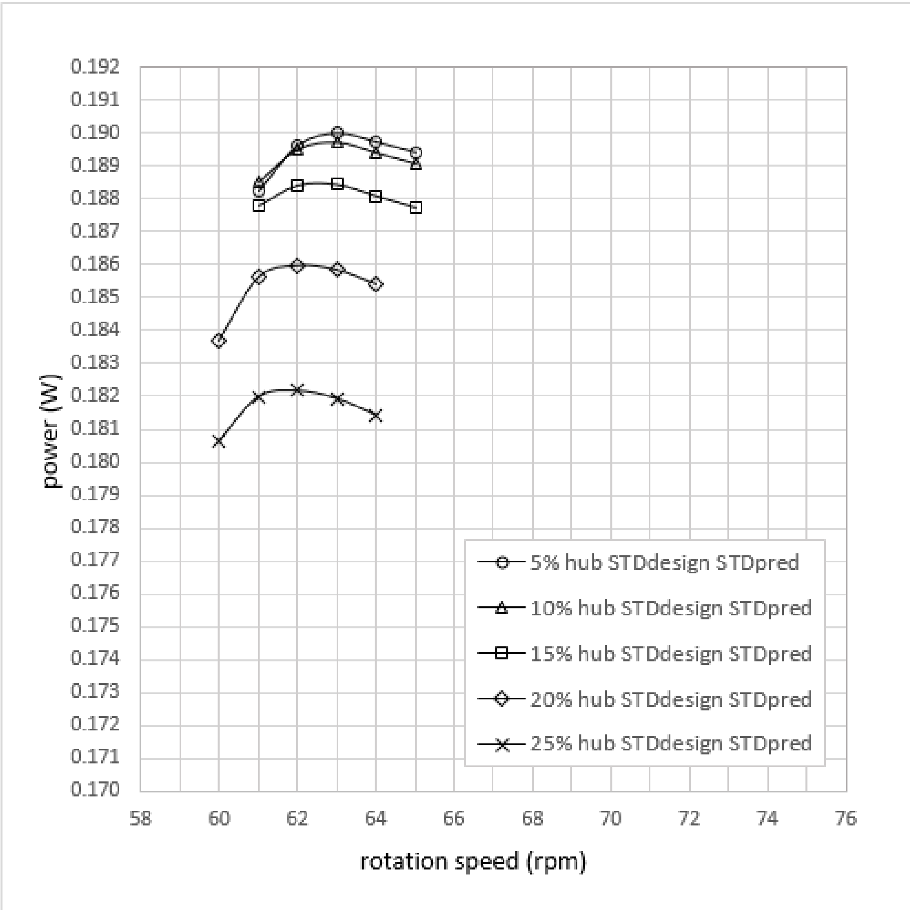

Figure 3.19: Analysis 1 - Power vs. rotation speed comparison. Rotors designed and analysed with the standard BEMM

Analysis 2 – Rotors (10%, 15%, 20% and 25% hub ratio) designed with the standard BEMM, but analysed with the adapted BEMM are compared with the baseline rotor of 5% hub ratio

In order to see the impact of the adapted BEMM analysis procedure (induction, relative wind angle, power absorbed), the 10%, 15%, 20% and 25% hub ratio rotors from Analysis 1 were re-tested using the adapted analysis procedure of the BEMM. These results should theoretically correspond with results from physical testing or CFD simulation of rotors designed with the standard BEMM. The results (see Figure 3.20) show that:

- peak power was achieved at a rotation speed ranging from 62 to 63 rpm.
- power was reduced by a smaller margin (than in Analysis 1) with each increase in hub ratio.
- prediction of effect of hub ratio, even using the adapted BEMM (which delivers accelerated fluid to the near-hub region), still shows only a reduction in power and no benefit for rotors with hub ratios larger than 5% that are designed with the standard BEMM.

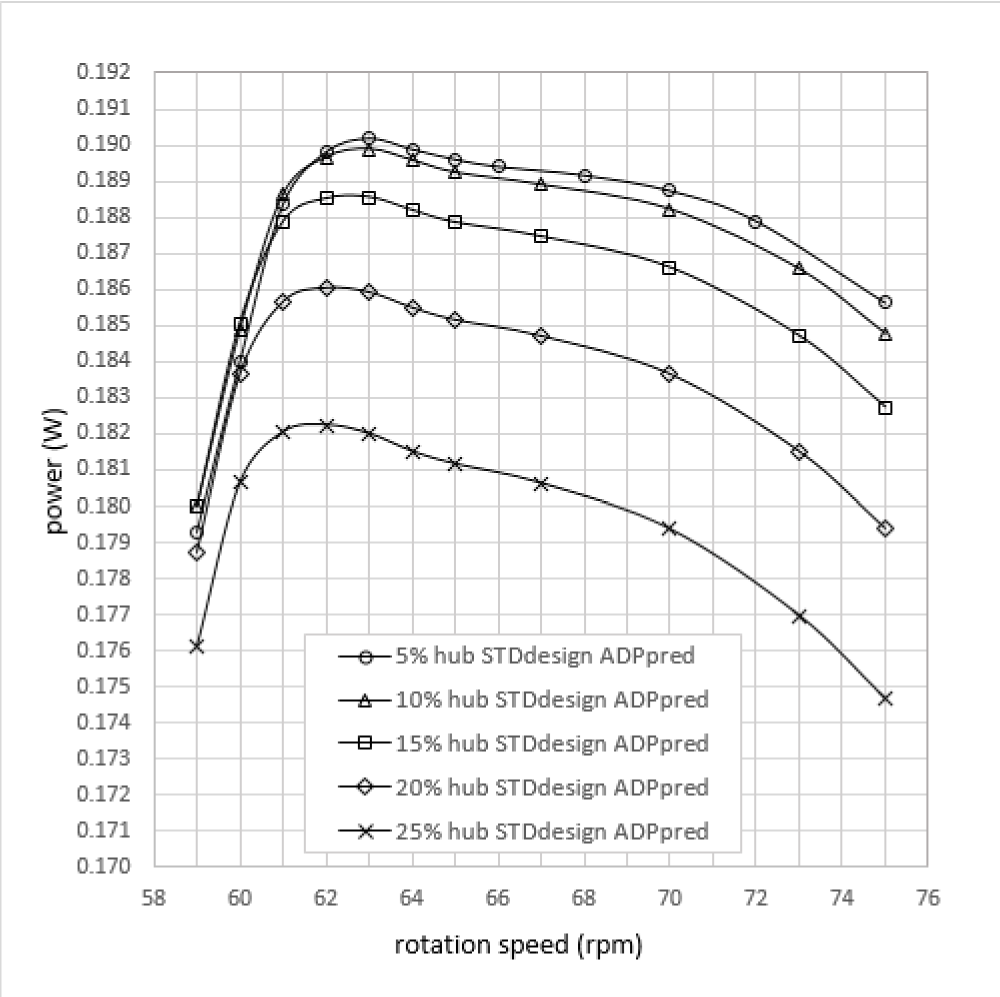

Figure 3.20: Analysis 2 - Power vs. rotation speed comparison. Rotors designed using standard BEMM and analysed with adapted BEMM

Analysis 3 –Custom rotors (10%, 15%, 20% and 25% hub ratio) designed and analysed with the adapted BEMM are compared with the baseline rotor of 5% hub ratio

This analysis compared the 5% hub ratio rotor to custom-designed rotors of increasing hub sizes, designed and analysed with the adapted BEMM. The results (see Figure 3.21) show that:

- peak power was achieved at rotation speed ranging from 63 to 64 rpm.
- the 10% and 15% rotors performed better than the 5% rotor.
- rotors with larger hub ratios (10% to 25%) and with blades that are custom-designed to the intended hub ratio are shown to perform significantly better than the larger hub ratio rotors in the previous analyses if both design and analysis make use of the adapted BEMM.

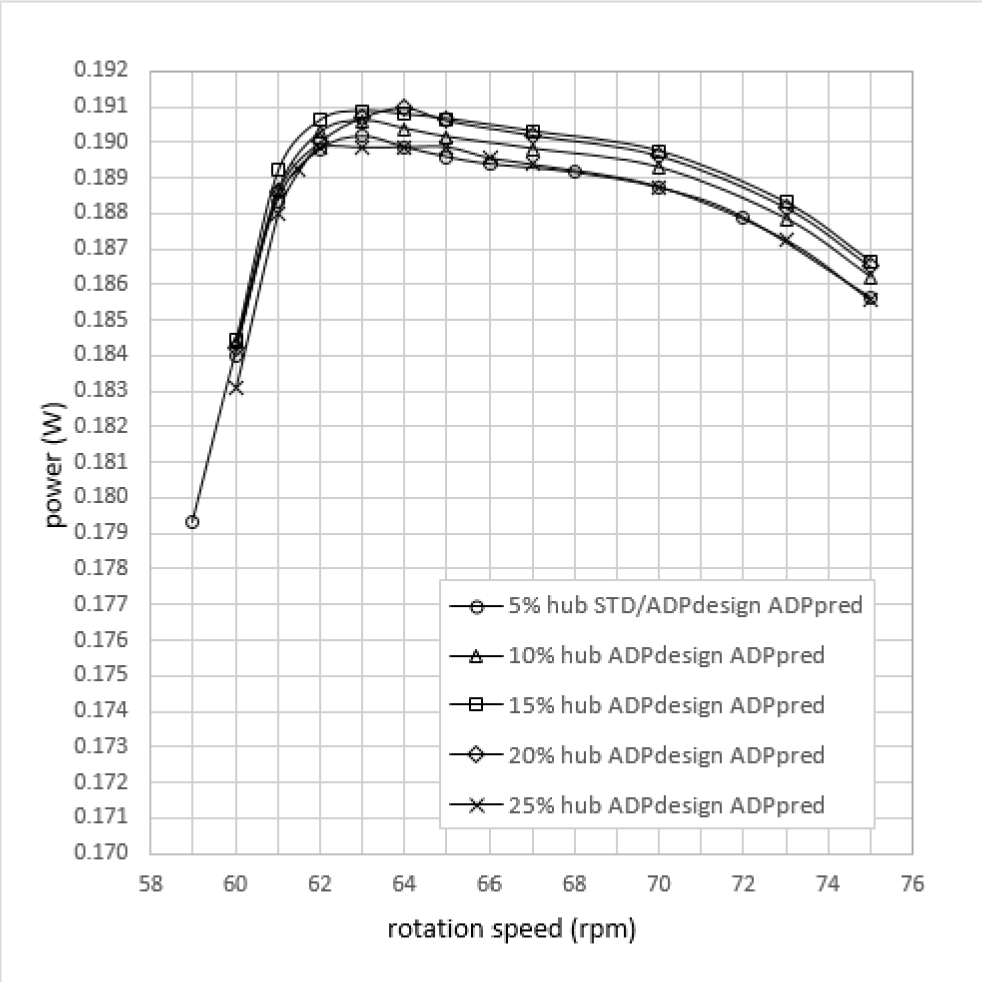

Figure 3.21: Analysis 3 - Power vs. rotation speed comparison. Rotors designed and analysed with the adapted BEMM

Note that 'spillage' losses expected from hub deflection are not included in Figs 3.19, 3.20 and 3.21, but are included in Fig 3.22.

When dimensionless relative peak power $(P/P_{5\%})$ for each curve in the three preceding analyses are plotted against hub ratio, the effect of hub ratio and the design and analysis method is more obvious.

These curves are plotted in Figure 3.22 and data is tabulated in Appendix I. Expected hub deflection losses have been applied to all three analyses and the dashed curves indicate BEMM results prior to power reduction to account for hub deflection “spillage’ losses.

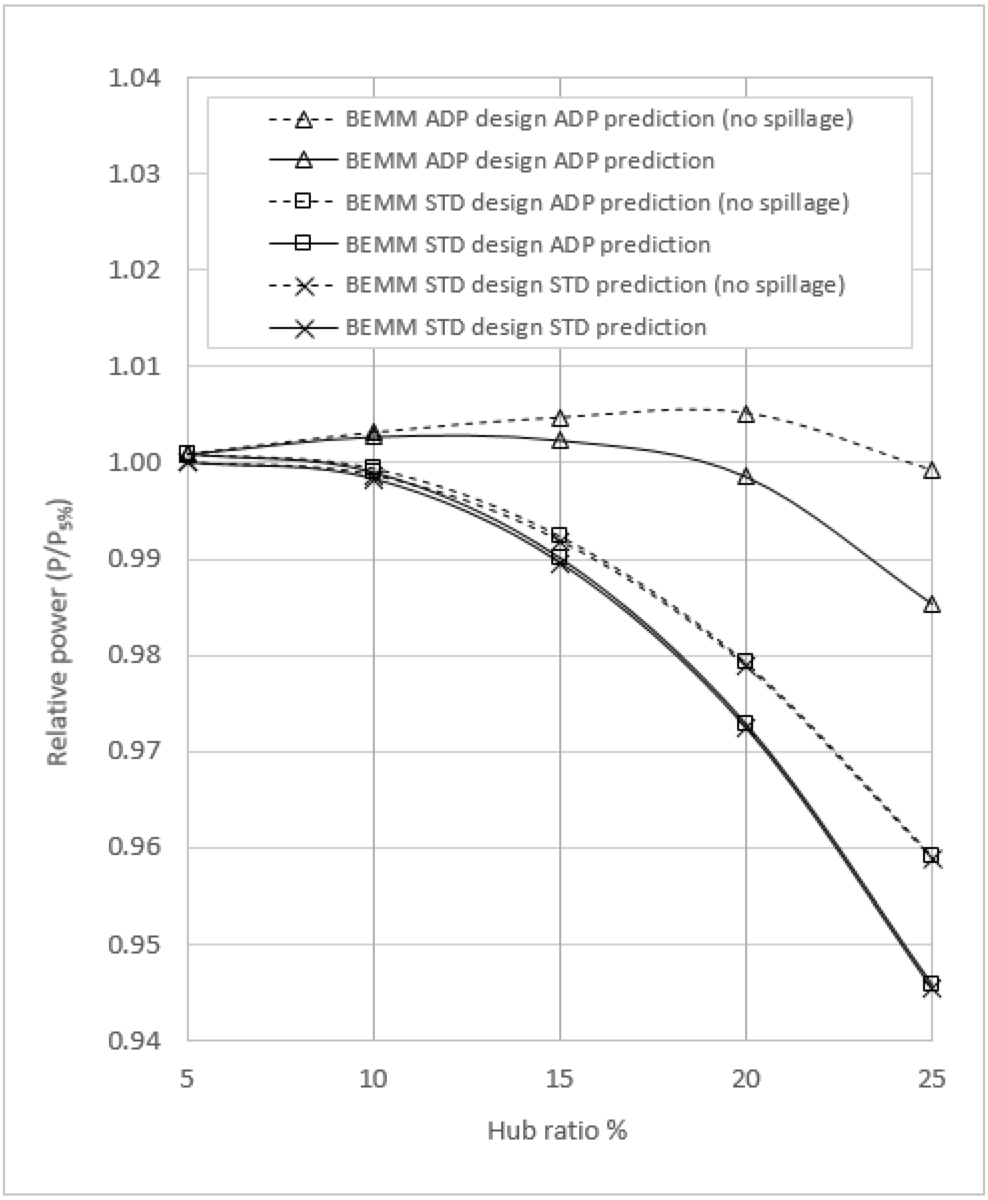

Figure 3.22: Relative power absorption of rotors – Comparison of standard (STD) vs. adapted (ADP) BEMM rotor design as well as STD vs. ADP BEMM prediction

The results show that:

- hub deflection (spillage) losses are significant for hub ratios beyond approximately 12% and need to be taken into account when predicting performance of HAWTs with hub ratios greater than 12% – irrespective of whether the standard or adapted BEMM is used.
- if hub deflection losses had been ignored, the 20% custom rotor using adapted BEMM would have been identified as the optimum hub ratio, whereas the optimum actually lies just beyond 10%.
- the sensitivity of relative power to hub ratio is low for the custom rotor using the adapted BEMM for design and analysis. While performance benefit from the 10% and 15% hub ratios, compared to the 5% hub ratio, is small, a relative reduction in power only occurs at hub ratios greater than about 18%, and this can be seen as a theoretical design limit if there are other compelling reasons to maximise hub ratio.

3.4.3 Error analysis

Precision

The BEMM analyses were performed in Microsoft Excel, which rounds cell values to 15 significant digits. Aerofoil data, copied to Excel from XFLR had four significant digits and for the targeted angle of attack ($\approx 5^{o}$), this produced precision error between 1/8000 (0.0125%) and 1/11000 (0.0091%). 'Stage 2' iterations, to obtain tip-adjusted chord and Reynolds number, were repeated (seven times) and achieved a maximum convergence of both Δc and ΔRe of 0.0013%. 'Stage 3' iterations for obtaining relative wind angle, power and axial and angular induction, typically converged within 20 iterations to a maximum $\Delta\phi$ of 0.00002%, Δa of 0.0000008% and $\Delta a'$ of 0.00006%.

Accuracy limitations of the BEMM

The method itself relies on simplifying assumptions (presented during the theoretical development in this chapter) and the design and BEMM analysis stages both included choice of underlying theory.

Accuracy of aerofoil data for the chosen profile is uncertain. However, since this study seeks comparison between rotors within the BEMM or within the CFD study or within the physical tests, the aerofoil profile and profile performance data was used by all rotors and is therefore seen as an input requiring consistency across rotors, but not necessarily a high level of accuracy.

CHAPTER FOUR

Computational fluid dynamics simulation

Virtual solid models, of the rotor designs that were analysed in the BEMM Analyses 1 and Analysis 3 (as presented in Chapters 2 and 3), were created and analysed using CFD software under the same conditions as the BEMM analyses.

4.1 Simulation methodology

In the methodology of the BEMM analyses in Chapters 2:

- **Analysis 1** entailed comparison of the 5% hub ratio (baseline) rotor, designed with the standard BEMM, against essentially the same rotor design – but with varying hub sizes (10%, 15%, 20% and 25%).
- **Analysis 3** was a comparison of the 5% hub ratio (baseline) rotor against rotors of increasing hub ratio that had been custom-designed for each hub size using the adapted BEMM.

For the sake of comparison with the BEMM analyses described in Chapter 2, the labels 'Analysis 1' and 'Analysis 3' and their meanings in terms of methodology will be retained in this and following chapters.

4.1.1 Rotor solid model and domain design

Nine solid models in total were created in the solid-modelling software, *Solidworks*. The CFD analysis made use of 'rotational periodicity' (analysis of a 120^o slice of the 3-bladed rotor) which meant that only the geometry of the 'slice' was required (one blade on a 120^o sliced hub) (see Figure 4.1).

In Figure 4.1, it can be seen that the blades designed with the adapted (ADP) BEMM have longer chords in the near-hub region when compared to the blades designed with the standard (STD) BEMM. This is because the velocity profile introduced into the rotor plane of the adapted BEMM raises the lift coefficient (C_L), raises the lift/drag ratio (C_L/C_D), reduces the local speed ratio (λ_r), which increases the relative wind angle (ϕ) – which together serve to increase the chord (c) as per the Maalawi equation:

$$c = \frac{8\pi rFsin\,\phi}{BC_L\left(\frac{\lambda_r + \tan\phi}{1-\lambda_r\tan\phi} - \frac{C_D}{C_L}\right)}$$

An increase in the relative wind angle also increases the required blade twist angle (θ_p)

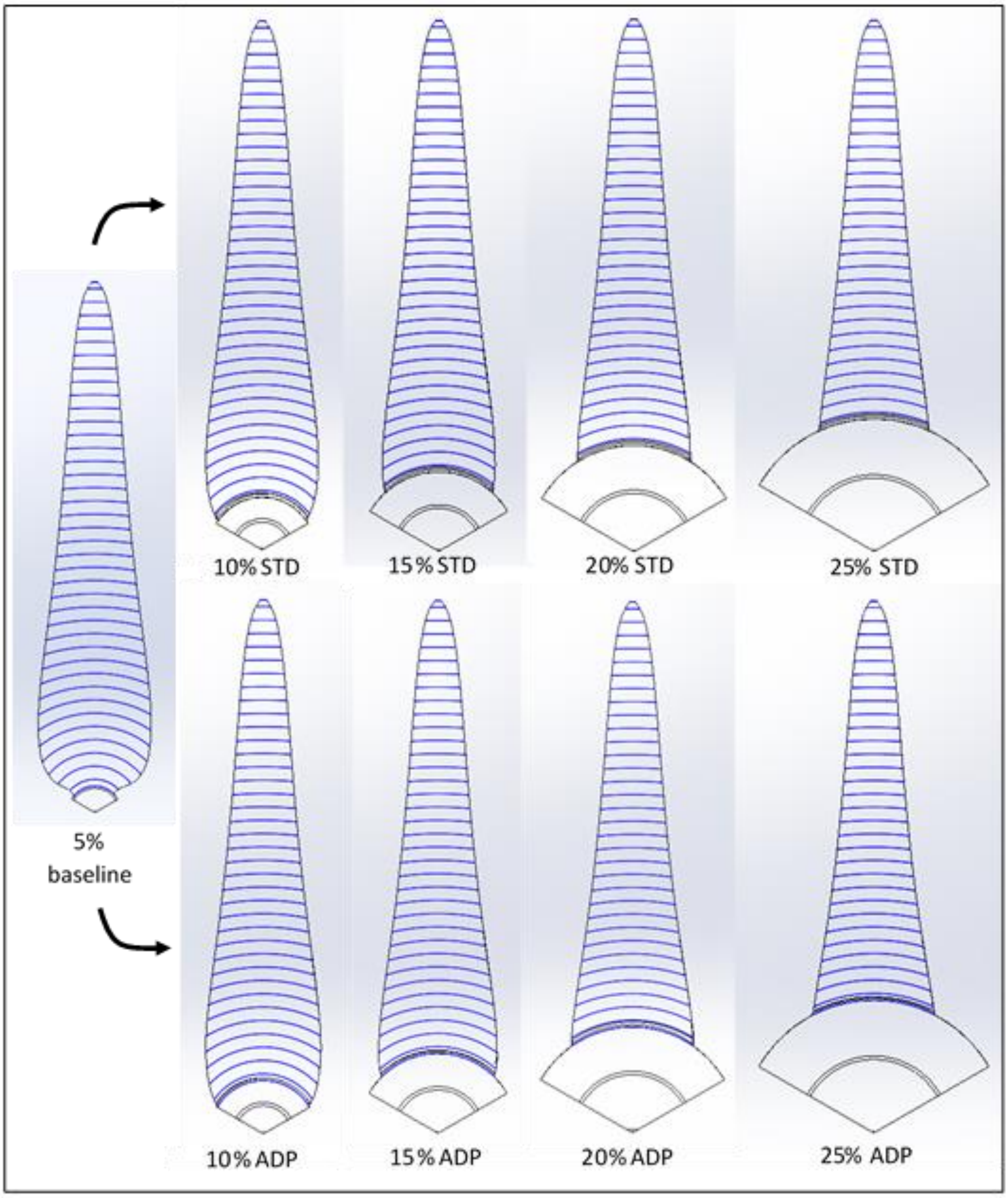

Figure 4.1: Rear view of the nine 120º 'sliced' solid models used in CFD testing

The design process for each solid model was identical. For each blade element, aerofoil profile, local chord and local pitch angle were combined to generate a planar local blade aerofoil profile. These planar profiles were then converted to profiles on concentric chord lines and were imported into *Solidworks*. Profiles were symmetrically arranged along the origin vertical axis. A solid model of the blade and hub-slice was then generated. The hub geometry included three sections – the rounded nose cone, a cylindrical mid-section (for blade attachment) and a truncated streamlined tail. Nose cones were elliptical, with an *l/d* ratio of 0.7143. Blade and hub were merged and a 1mm fillet was used at the intersection of blade and hub. The blade tip was a flat profile surface (of length ≈ 1.6 mm and area ≈ 0.15 mm^2), perpendicular to the rotor plane.

The hub was sliced symmetrically, in front view, using an 'extruded cut' 60° each side of the origin vertical axis. Side views of the 5% (baseline) rotor and the rotors designed using the adapted BEMM (Rotor Set 2) are shown in Figure 4.2. Rotor Set 1 and Rotor Set 2 had identical hubs.

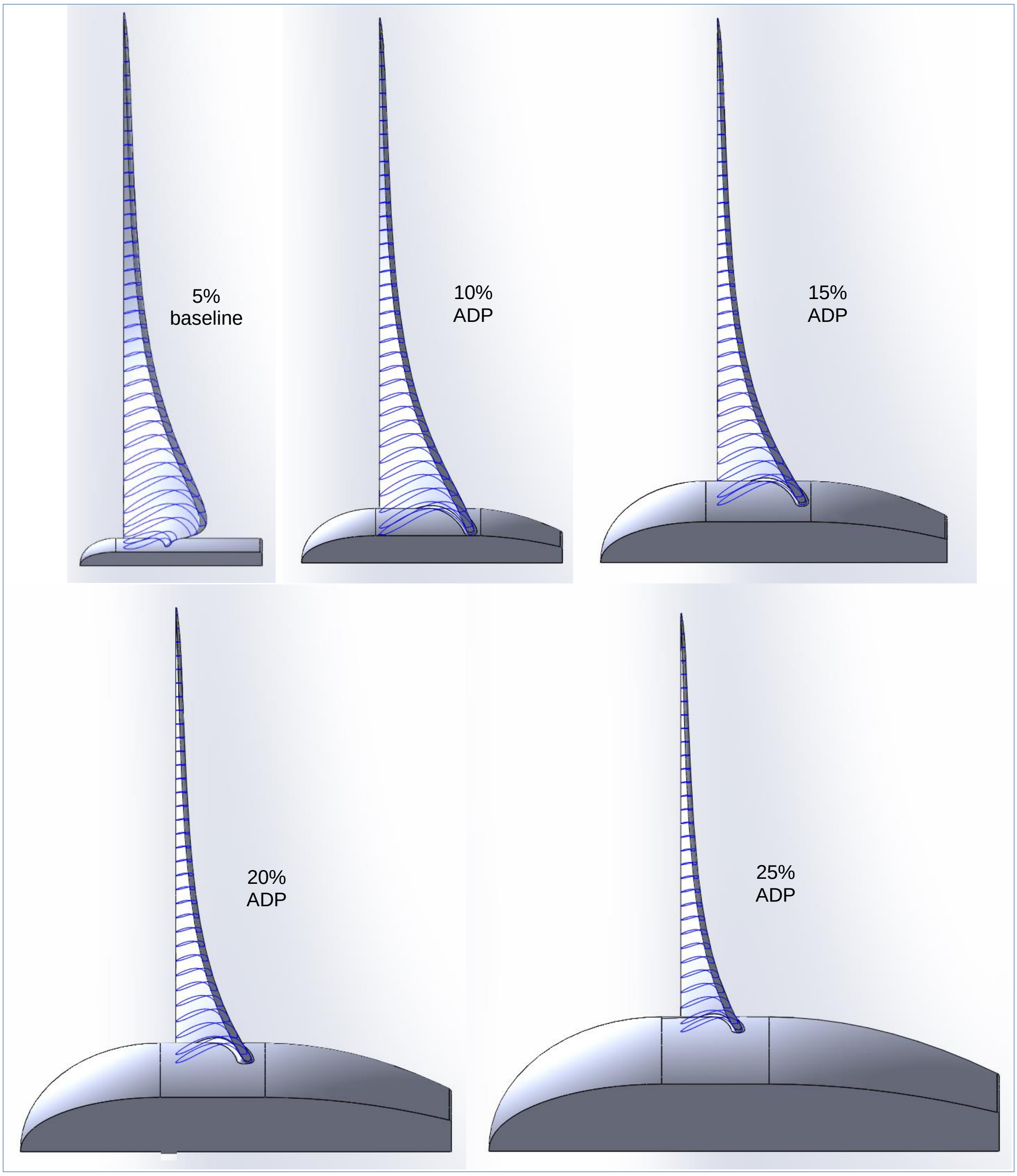

Figure 4.2: Side views of Rotor Set 2 – Baseline rotor and rotors designed with the adapted (ADP) BEMM

All solid model domains consisted of three parts (see Figure 4.3) that were 120° slices of:

- an outer fluid cylinder of diameter 2.000 m (7 rotor diameters), extending from 1.680 m (6 rotor diameters) upstream of the rotor plane to 2.520 m (9 rotor diameters) downstream of the rotor plane.
- an inner rotating fluid cylinder (identical for all rotors and containing the rotor), of diameter 360 mm, length upstream of rotor plane 90 mm and length downstream of rotor plane of 120 mm.
- a rotor (void) contained within the inner rotating fluid cylinder. Rotor dimensions were diameter 280 mm and total hub length ranged from 50 mm (5% hub ratio) to 133 mm (25% hub ratio).

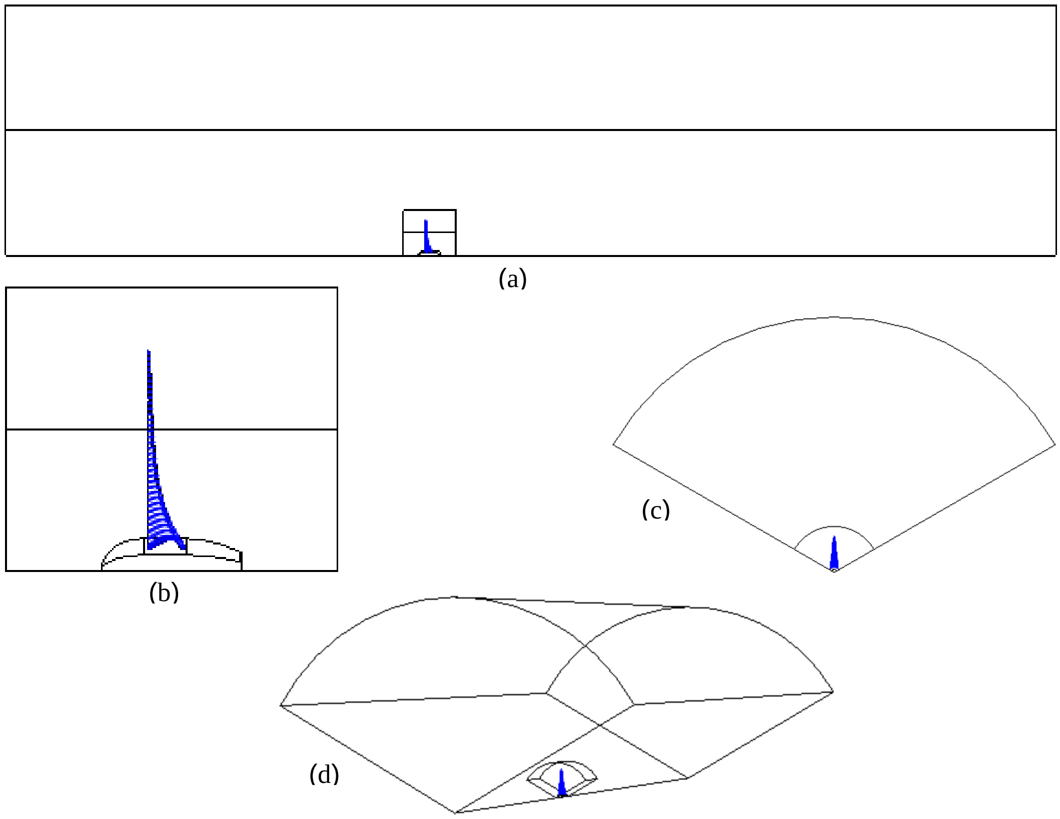

Figure 4.3: Domains of mesh for all rotors: (a) side view of entire domain, (b) side view of rotating domain, (c) axial view of entire domain and (d) isometric view of entire domain

4.1.2 Meshing for CFD

Solidworks solid models were imported to Ansys Workbench for preparation of models prior to meshing for CFD analysis. Meshing was performed with Ansys Fluent using a workflow that included the following main settings:

Blade local sizing:	Growth rate	1.2
	Size control type	face size
	Target mesh size	0.16
Hub local sizing:	Growth rate	1.2
	Size control type	face size
	Target mesh size	0.32
Surface mesh:	Minimum size	0.02
	Maximum size	105
	Growth rate	1.3
	Size functions	curvature and Proximity
	Curvature normal angle	18
	Cells per gap	1
	Scope proximity to	edges
Rotational periodic boundaries		Periodicity angle 120
Volume mesh - boundary layer settings		
	Offset method type	aspect ratio
	Number of layers	4
	First aspect ratio	20
	Growth rate	1.2
Volume settings		
	Fill with	poly-hexcore
	Buffer layers	1
	Peel layer	1

All volume meshes were improved to an Ansys cell quality of 0.18. Details of meshing within the boundary layer are provided in Appendix R and pictures of the mesh (10% hub, adapted BEMM used as sample) are provided in Appendix S.

4.1.3 CFD computational approach and solution parameters

Meshes and solutions were calculated on an Intel Core i3-6100 (3.7 GHz) with 32GB of RAM. For the simulations, the Reynolds averaged Navier-Stokes (RANS) equations were used within Ansys Fluent. Other approaches can be used, such as direct numerical simulation or large eddy simulation, but both these methods have high computational requirements, whereas the RANS equations, with an appropriate turbulence model, provide a practical solution with computational economy.

The turbulence models that are available in Ansys Fluent include:

- the one-equation model (Spalart-Allmaras)
- the two equation models (k-ε Standard, k-ε RNG, k-ε Realisable, k-ω Standard, k-ω BSL, k-ω GEKO and SST k-ω)
- Reynolds Stress models
- Transition Models (k-kl-, Intermittency Models and Transition SST)

The SST k-ω turbulence model was used in all simulations in this research as it is recommended for accurate resolution of the boundary layer and when modelling of flow separation is required (ANSYS, 2019). The SST k-ω model was expected to be suitable for the high Reynolds numbers of the 30 m case-study rotor as well as the low Reynolds numbers of the 280 mm test rotors. While the chord-based Reynolds number range of the 280 mm rotors indicated that the cambered plate aerofoil was operating within a laminar flow regime, the aerofoil performance (sensitivity reduction) relied on leading edge separation at higher angles of attack (Koning, 2019) and the SST k-ω model was expected to model this separation appropriately. For the 280 mm rotors, low Reynolds number correction was applied to the SST k-ω turbulence model.

All models were solved using identical case and solver settings. A complete sample report of all settings is provided in Appendix C. In summary, a double precision, 3-dimensional, steady, pressure-based solver with SST k-ω turbulence model with low Reynolds number correction and water (at 20 ^{o}C) as working fluid was used. The virtual model consisted of two fluid zones 'fluiddomain' (no frame motion) and 'rotating' (with rotational frame motion at rotor speed). Boundary conditions included rotor surfaces 'hub' and 'blade', fluid domain surfaces 'inlet', 'outlet' and 'outerwall' and the two cut surfaces (for rotational periodicity). The inlet to 'fluiddomain' provided a constant velocity of 0.25 m/s and the outlet was defined as a pressure-outlet.

Torques acting on the blade and hub were obtained via a torque report for each of those zones. Power was calculated ($P = T \cdot \omega$). The solution method was coupled pressure and velocity using a pseudo-transient solver with user-specified time steps. Time step was reduced whenever the scaled residual of both continuity and x, y and z fluid velocities reached a point of negligible change or oscillation. Convergence was assumed complete when the continuity residual reached $\approx 10^{-5}$ (where x, y and z-velocity residuals were $\approx 10^{-8}$). This convergence effectively brought the torque to a constant or oscillating 5th significant digit.

4.2 Results of CFD simulations

Rotor power at a range of rotor rotation speeds near the expected peak power were solved. Each data point of the results shown in Figure 4.4 represents an individual solved Ansys Fluent case. Power was calculated from the product of net torque and rotation speed (in rad/s). The net torque was the combined torque from all three blades less the opposing torque due to skin friction over the entire hub.

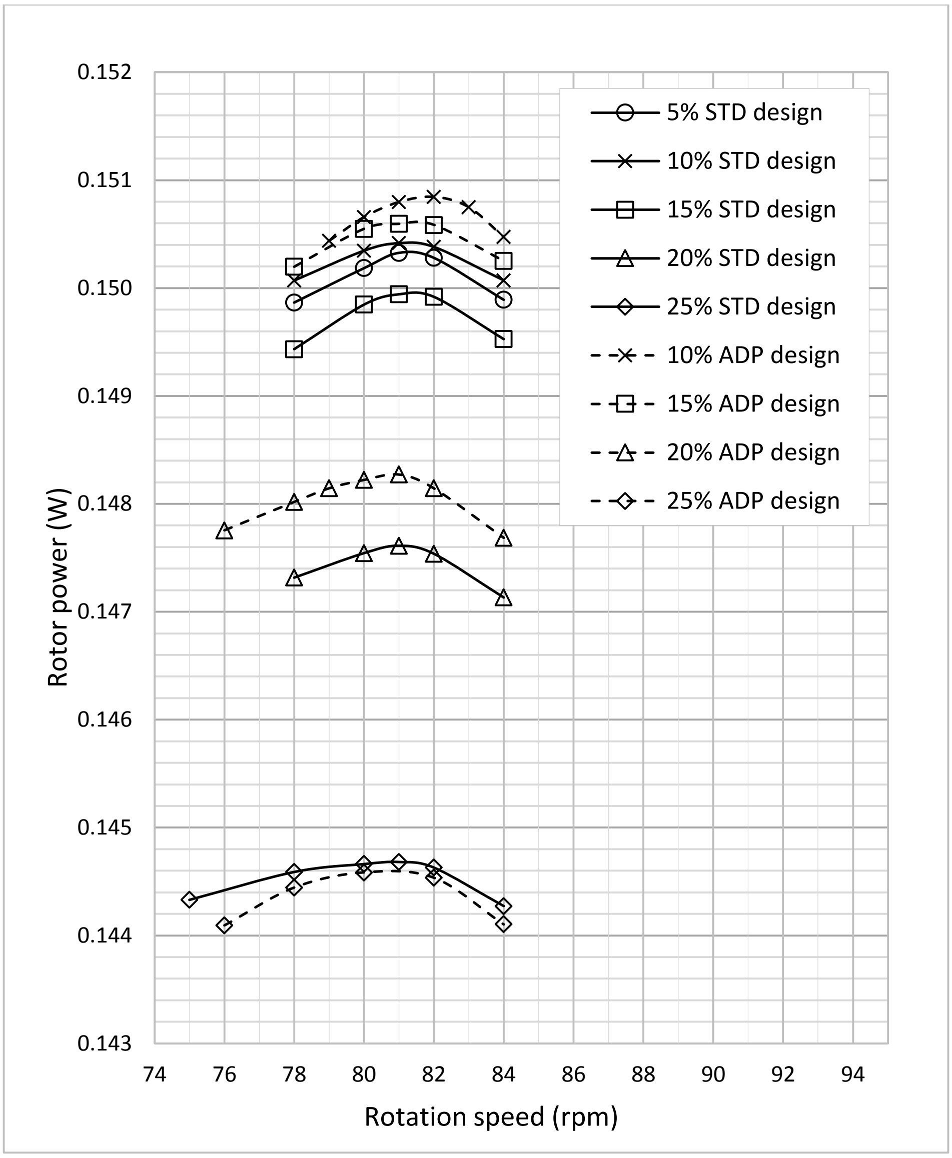

Figure 4.4: CFD simulation power curves of Analysis 1 and Analysis 3 rotors

CFD Flow analysis

The BEMM results showed that there is a significant difference between standard BEMM and adapted BEMM predictions and the CFD results tend to confirm the adapted BEMM predictions. The difference in relative power between CFD results (between adapted BEMM rotor design and standard BEMM rotor design) is however very little (in the order of 0.4% for the 15% and 20% hubs). A significant difference in axial, radial and tangential flow between adapted and standard rotor designs is therefore not expected. Flow analysis of the 20% hub rotors (adapted and standard designs) reveals a slightly lower radial flow in the near-hub region of the adapted rotor when compared to the standard rotor (see Figure 4.5). Grey areas at blade tips are out of range. The range was specifically chosen to provide as many distinct contour surfaces into the near-hub region. The contour plane is located 2.8 mm (1% of rotor diameter) upstream of the blade leading edge. Water speed is 0.25 m/s, both rotors are rotating at 81 rpm (peak power) and the rotors are turning clockwise. There is no noticeable difference when axial or tangential velocities are compared. The complete CFD flow analysis is shown in Appendix T.

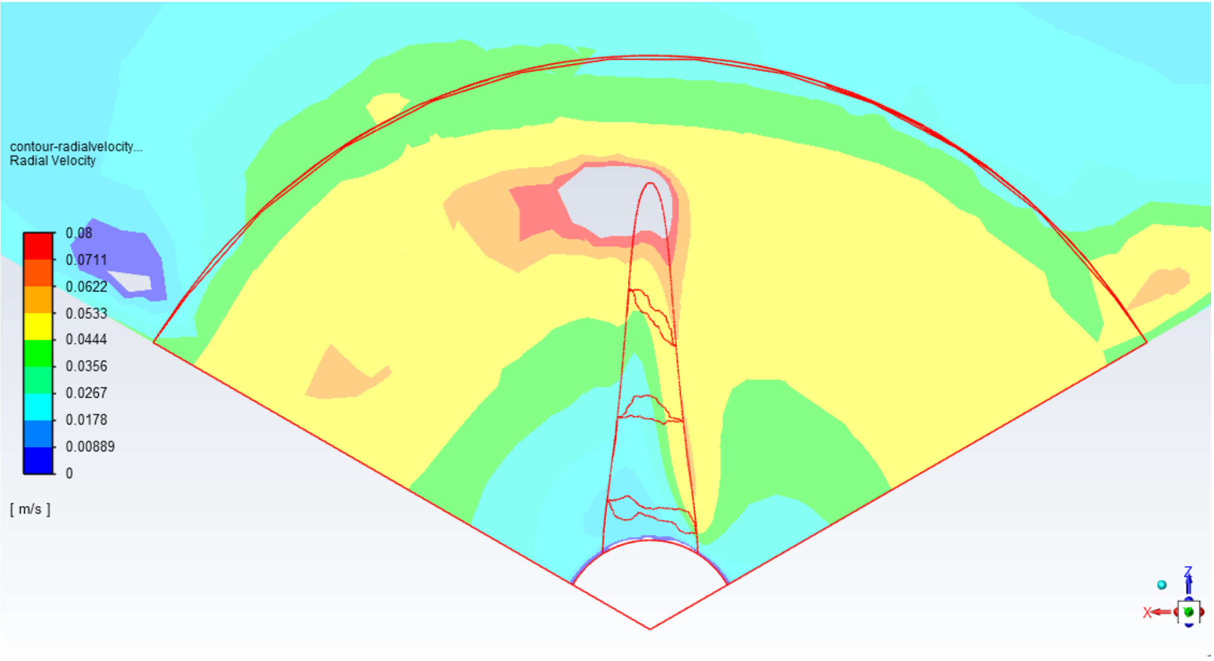

(a)

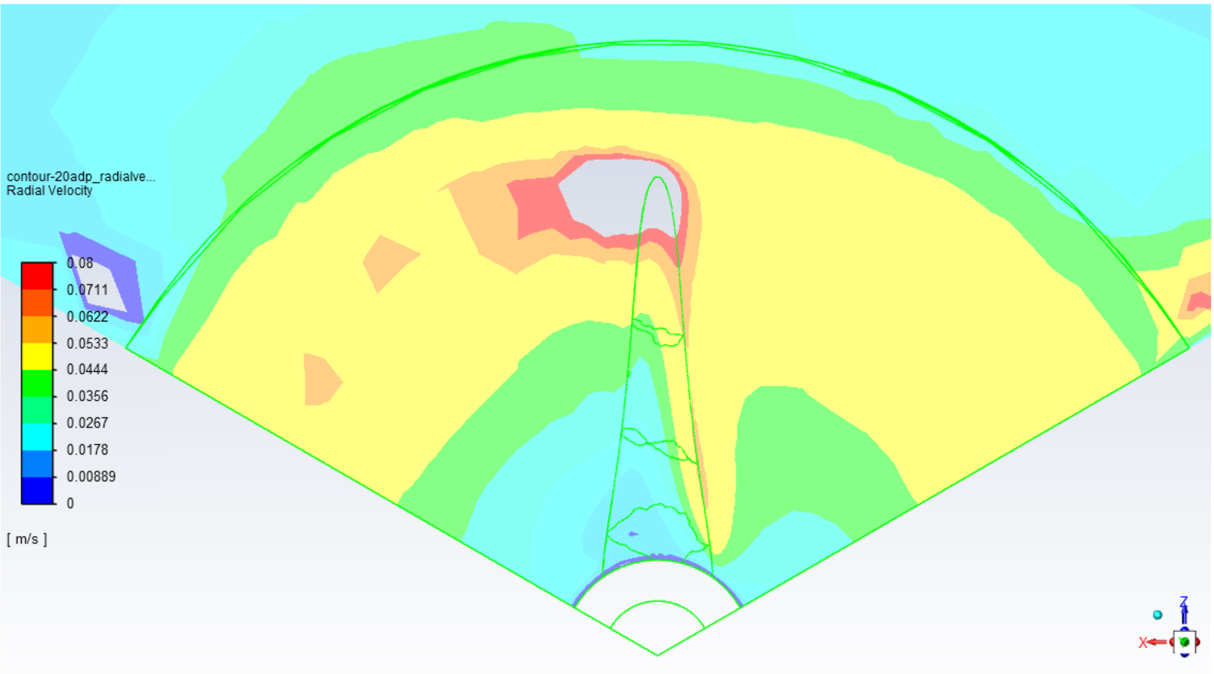

(b)

Figure 4.5: Radial flow through ϕ280 mm, 20% hub ratio rotors designed using (a) standard and (b) adapted BEMM

4.2.1 Mesh dependence, accuracy and uncertainty

A mesh dependence study was performed, solving for blade torque using meshes settings sized from 60% to 130% of the chosen mesh settings. Meshes with cell counts ranging from 3353083 to 7565848 cells were created by reducing/increasing local size targets as well as surface mesh minima and maxima. Expansion of surface mesh minimum greater than 0.026 mm (130%) resulted in repeated mesh failure which limited the upper range of meshes to 130%. Hardware limitations and the need for double precision resulted in solution failure for meshes finer than 70% (7565848 cells). The 60% mesh was achieved through retention of 100% local size targets but reduction of surface mesh minimum and maximum to 60%. An 87% mesh was considered for use but solution time was unacceptably slow.

The 5% hub ratio rotor was used for the mesh independence study and the results (Figure 4.6) show that the chosen (100%) mesh produces 1.5% more net torque than the 60% mesh. Considering that mesh micro-adjustments for the 5% hub ratio rotor produce a net torque range of approximately 0.6% (discussed later in this section), that the simulations are comparative, and that the cell count for the 60% and 87% meshes are both above 5500000 (resulting in impractical solution speeds), the 100% mesh settings (4470000 cells) were chosen for use in all of the 280 mm rotors.

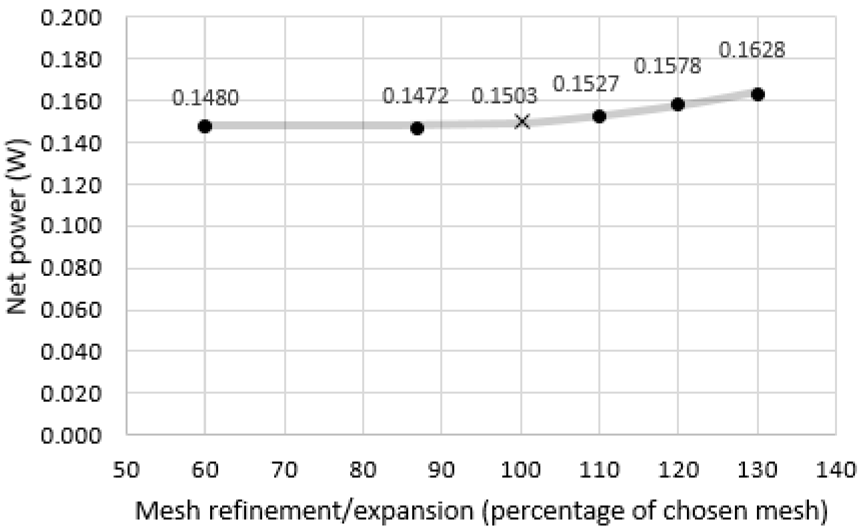

Figure 4.6: Mesh independence study results

<u>Initial power curves</u>

In order to identify approximate peak power and rotation speed at peak power, initial power curves were created using cell size settings as shown in Section 4.1.2. The major settings were:

Blade target mesh size		0.16 mm
Hub target mesh size		0.32 mm
Surface mesh:	Minimum size	0.02 mm
Maximum size	105 mm	

Mesh micro-adjustment for valid data comparison

Micro-adjustment (tenths of a percent) of the surface mesh maximum from the initial value of 105 mm produced new mesh arrangements which resulted in a range of rotor torques. Initial adjustments were 99.6%, 99.8%, 100.2% and 100.4%. Intermediate adjustments were added for important rotors (5%, 10% and 15%) or if the range of the micro-adjusted data for a rotor was significantly less than the highest range of any other rotor. The results (see Figure 4.6) showed that ranges of torque solutions of micro-adjusted meshes were between 0.381% and 0.594%.

Selection of appropriate micro-adjusted meshes provided an opportunity for better comparison if either the lower or upper limit meshes were used. In this analysis, the lower boundary of each data range was used for comparison across all rotors.

Relative uncertainties (the potential for the lower boundary to be lower) for each of the rotors, were calculated as shown in Table 4.1.

Table 4.1: Rotor data boundaries, ranges and relative uncertainty – ϕ280 mm rotors

Rotor	Upper boundary torque (T_U) (N·m) $\times 10^{-3}$	Lower boundary torque (T_L) (N·m) $\times 10^{-3}$	Range $R = T_U - T_L$ (N·m) $\times 10^{-3}$	Rel. uncertainty $\Delta(R^* - R)(100)/T_L$ (%)
5% STD BEMM	6.0079	5.9754	0.0324	-0.0437
10% STD BEMM	5.8685	5.8347	0.0338	-0.0202
15% STD BEMM	5.8344	5.8094	0.0250	-0.1725
20% STD BEMM	5.7341	5.7018	0.0322	-0.0488
25% STD BEMM	5.7236	5.7018	0.0218	-0.2319
10% ADP BEMM	5.8856	5.8538	0.0318	-0.0547
15% ADP BEMM	5.8618	5.8354	0.0264	-0.1476
20% ADP BEMM*	5.9078	5.8728	0.0350	0.0000
25% ADP BEMM	5.7329	5.7018	0.0311	-0.0690

Results of the micro-adjusted mesh solutions and boundary selection are shown in Figure 4.7.

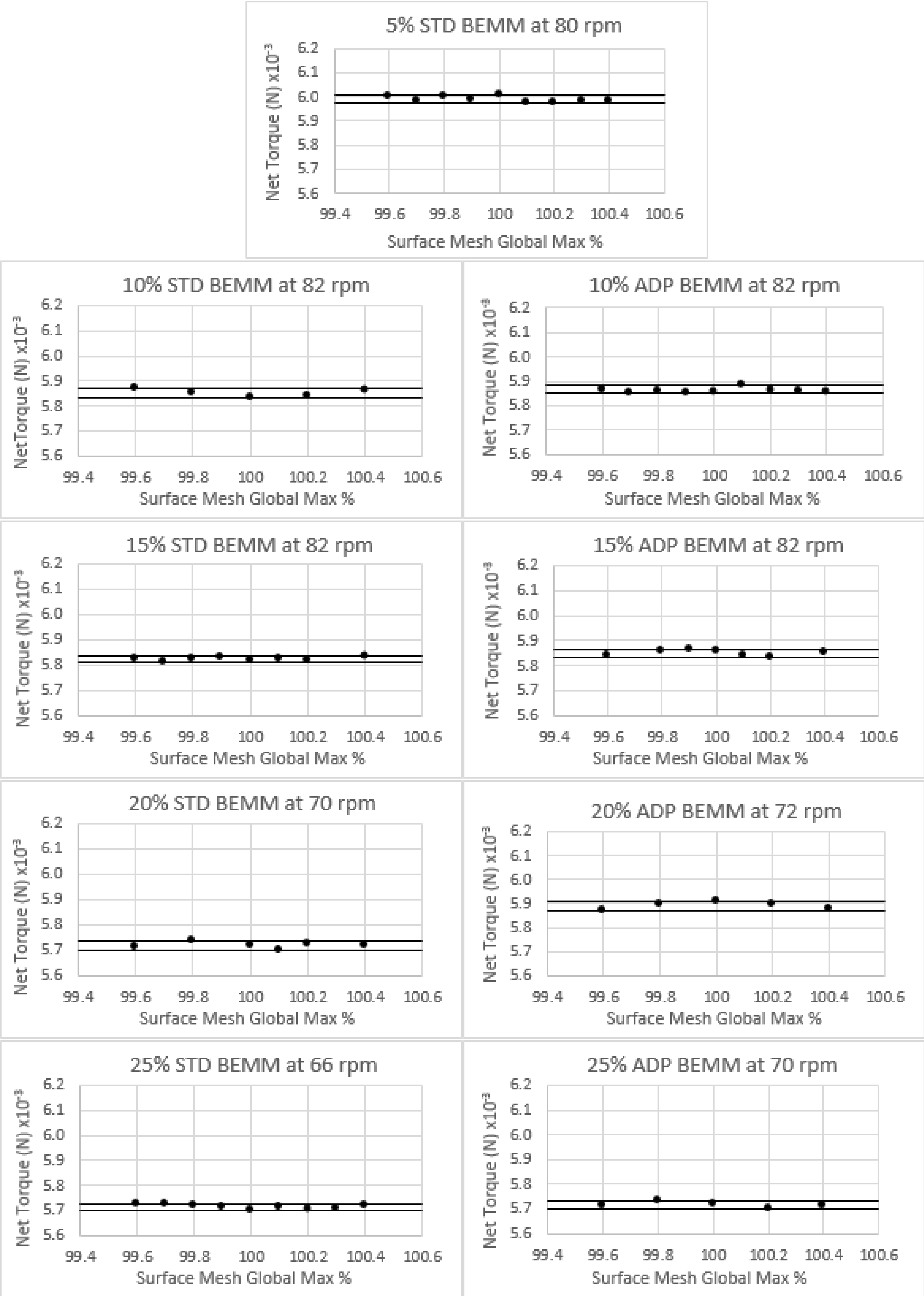

Figure 4.7: Results of mesh micro-adjustment for identification of best mesh for power curve data and comparison.

4.2.2 Rotor power

When peak relative power (relative to 5% rotor) from each curve is plotted against hub ratio, the relative performance of the custom designed rotors (using adapted BEMM) compared to the rotors designed using standard BEMM, can be seen more clearly (see Figure 4.8).

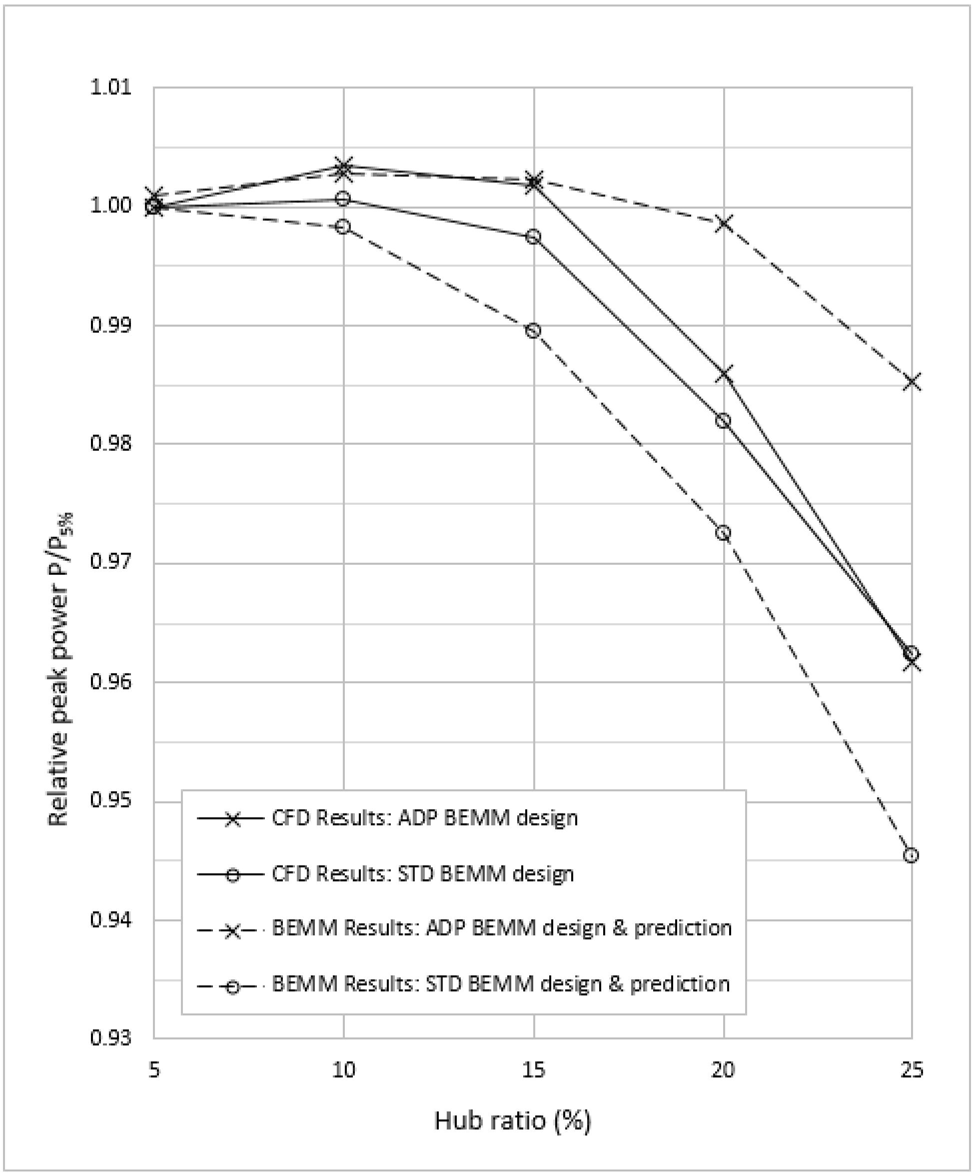

Figure 4.8: Dimensionless relative peak power vs. hub ratio. Rotors designed with standard BEMM compared to custom designed rotors using adapted BEMM. BEMM results from Section 3.3.2 are included for comparison

Some observations from the Ansys Fluent analysis of the ‘Analysis 1’ and ‘Analysis 3’ rotor sets were:

- The 10% hub ratio rotor, custom designed using the adapted BEMM, produced <u>0.35% more</u> peak power than the 5% baseline rotor and 0.29<u>% more</u> peak power than the 10% hub ratio rotor designed using the standard BEMM.

- The 15% hub ratio rotor, custom designed using the adapted BEMM, produced 0.18% more peak power than the 5% baseline rotor and 0.40% more peak power than the 15% hub ratio rotor designed using the standard BEMM.
- the 20% hub ratio rotor, custom designed using the adapted BEMM rotor produced 0.41% more peak power than the 20% hub ratio rotor designed using the standard BEMM.
- the 25% hub ratio rotor, custom designed using adapted BEMM, produced the same peak power as the 25% hub ratio rotor designed using the standard BEMM.

The CFD results in Figure 4.4, show how the rotors designed with the adapted BEMM consistently outperform the rotors designed with the standard BEMM (apart from the 25% hub ratio rotors). Comparison between CFD results and the BEMM predictions shows that the adapted BEMM predicts higher performance from the 20% and 25% rotors, relative to the 5% baseline rotor and the standard BEMM results consistently under-predict power output relative to the 5% baseline rotor.

Some possible reasons for the over-prediction of the adapted BEMM results at hub ratios greater than 15% are:

- The BEMM does not take into account radial flows (all flow is assumed 2-dimensional across the blade profile).
- The BEMM uses tabulated aerodynamic performance data for the blade profiles – which may not compare with the CFD simulation in consistency and accuracy, or if radial or other unexpected flow disturbances are affecting the aerofoil performance.
- Power loss through ‘spillage’ may be greater than was predicted by the potential flow analysis in this research.

CHAPTER FIVE
Physical Testing

As with the Ansys Fluent CFD analyses, standard and adapted BEMM rotor sets were physically tested to compare the performance of the adapted BEMM design against the standard BEMM design at different hub ratios. The nine rotors that required physical testing were 3D printed. Strength and cost limited the scale of the 3D-printed rotors to a size that excluded air as a possible working fluid in testing, due to its low power density. Water, as working fluid, provided adequate power density. Necessary diameter of the fluid domain (≈ 5× rotor diameter) and accuracy of 3D printing (0.1 - 0.2 mm) were determining factors for choosing a rotor diameter of 280 mm.

5.1 Test equipment

The testing equipment included the manufactured rotors and the 'water-drop' equipment - for propelling the rotors through the fluid at a constant relative velocity and for measuring and recording torque and rotation speed. Calibration equipment was used to find the torque produced by the generator at various electrical resistances and rotation speeds.

Manufactured rotors

Nine unique rotors were required for the 'Analysis 1' and 'Analysis 3" scenarios so that BEMM results, CFD results and physical test results could be compared. Because the standard BEMM generated identical blade twist and chord at different hub ratios, the 5% rotor blades were re-used, but with unique hub assembles that could be added to the 5% rotor for each of the required hub ratios. A typical hub assembly for the standard BEMM rotor consisted of five components - a nose cone, a 3-component centre-hub and a streamlined, truncated tail (see Figure 5.1).

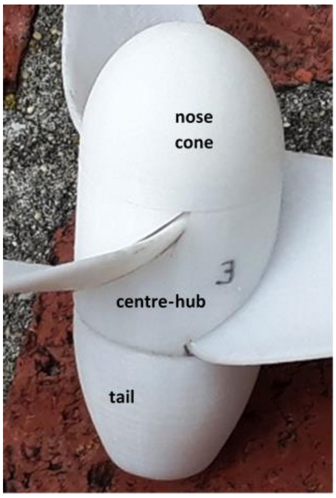

Figure 5.1: The 5-component hub assembly for the rotors designed with the standard BEMM (re-using the 5% rotor blades each time)

For rotors designed with the adapted BEMM, each rotor blade set was unique, and the complete rotors consisted of three parts, a nose cone, a set of blades (already printed on the appropriate cylindrical hub diameter) and the streamlined, truncated tail. All three parts were press fitted (by hand) and silicon was used to secure and fill the joints of rotor assemblies. All rotors were 3D printed, using polylactic acid (PLA).

The assembled standard BEMM rotors are shown in Figure 5.2.

Figure 5.2: Analysis 1 – Standard BEMM design - 5% rotor blade set fitted with hub assemblies of increasing diameter

For Analysis 3, three of the custom rotors used a 3-piece blade set and one (the 25% custom rotor) blade set was printed in one piece. See Figure 5.3.

Figure 5.3: Analysis 3 – Adapted BEMM design - rotor blade set with hub assemblies

After printing, a filler was applied if necessary, and all rotors were finished by sanding progressively to 600-grit water-paper. The design of all rotors for manufacture included an axial hole through the centre of rotation as well as a transverse pin hole for temporary attachment to the 6mm shaft of the water-drop equipment.

<u>Water-drop equipment</u>

The water drop equipment consisted of an insulated water-filled tank (diameter 1.40 × 1.49 m high) with a frame to support two vertical *guide rails* - square-section aluminium tubes (38 × 38 × 2 mm) above the tank. Insulation of the tank utilised 50 mm fibre blanket with construction grade bubble insulation as an outer skin. A 1500 W electric element was used for water heating when necessary. A *drop frame*, housed the *generator*, *rectifier*, top and bottom *bearings* for the *shaft*, *rotation speed encoder* (sensor, Arduino board and 8-slot encoder disc) and the 18-slot *linear encoder* scale for linear speed sensing. The shaft (13.4 mm × 1.2 mm wall, 316 stainless steel) with rotor attached is part of the drop-frame assembly.

Both angular and linear speed recording systems made use of *Arduino* boards with infra-red optical sensors. The Arduino board and sensor for linear speed measurement were mounted on one of the guide rails. Movement of the drop-frame was constrained by runners (nylon, ϕ20 mm) and controlled by a 2GT toothed-belt drive (6 mm width) and a stepper motor (0.98 N.m, 1.8^o per step) with variable voltage power supply. The drop-frame stepper motor was controlled by Arduino. Coding for the three Arduino systems (recording of angular velocity, recording of linear velocity and control of drop-frame velocity) is shown in Appendix H.

A stepper motor was also used as the generator (0.28 N.m, 1.8^o per step) where one field provided suitable torque resistance. The resistor bank used as electrical load for the generator consisted of 8 $\times$ 100 Ω, 2 $\times$ 20 Ω and 2 $\times$ 10 Ω power resistors. The resistor bank was semi-enclosed and temperature-controlled. Photographs of the water drop equipment are shown in Figures 5.4 and 5.5.

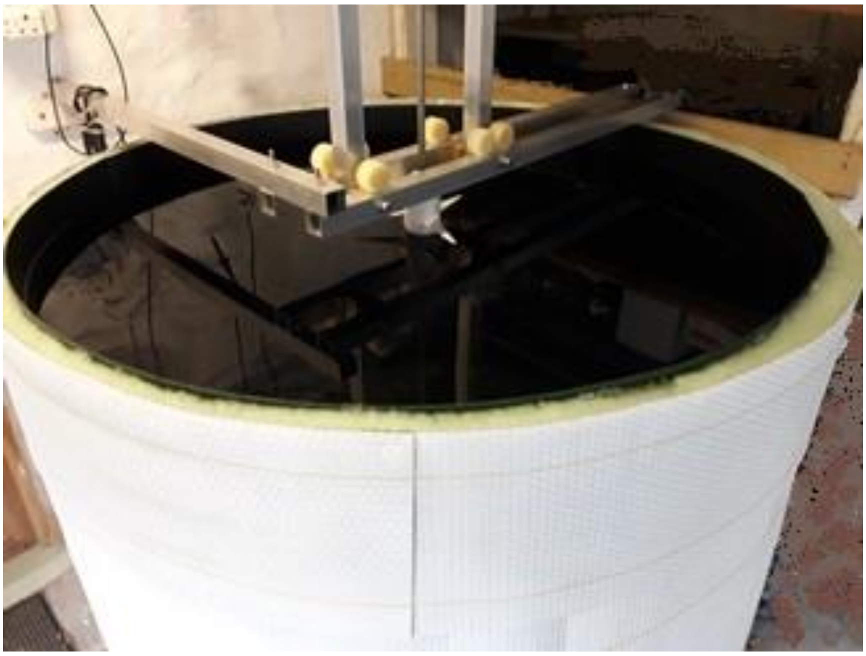

Figure 5.4: The insulated tank with frame supporting the guide rails

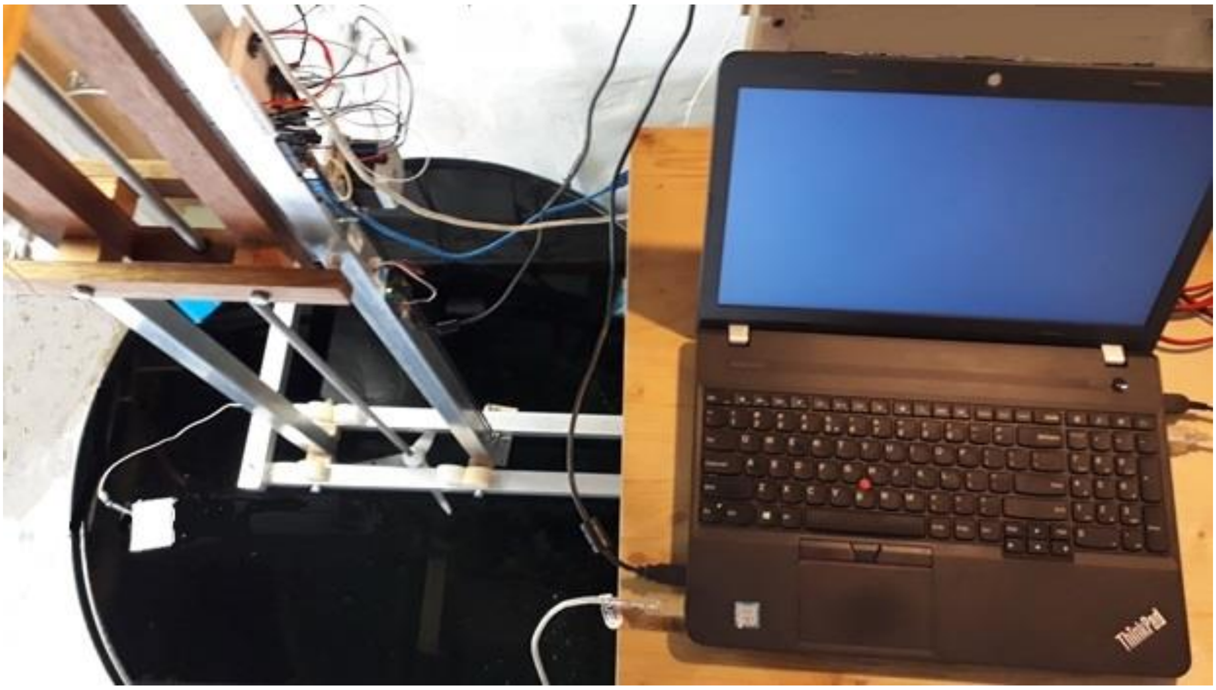

Figure 5.5: View of drop test assembly in raised position, tank and laptop

Principle of operation

1) A rotor is attached to the end of the shaft and the drop frame is raised to the upper position.

2) Arduino sensors (for angular and linear velocity) are initialised on the laptop.

3) The linear drive is engaged – driving the rotor at constant velocity down into the tank of water until the drop frame reaches the lowest position.

4) Data outputs from Arduino sensors are saved.

5) The drop frame is raised (manually) to the upper position, ready for the next run.

6) A period of 4mins between runs was found to be sufficient to allow turbulence to dissipate sufficiently.

An assembly diagram is shown in Figure 5.6.

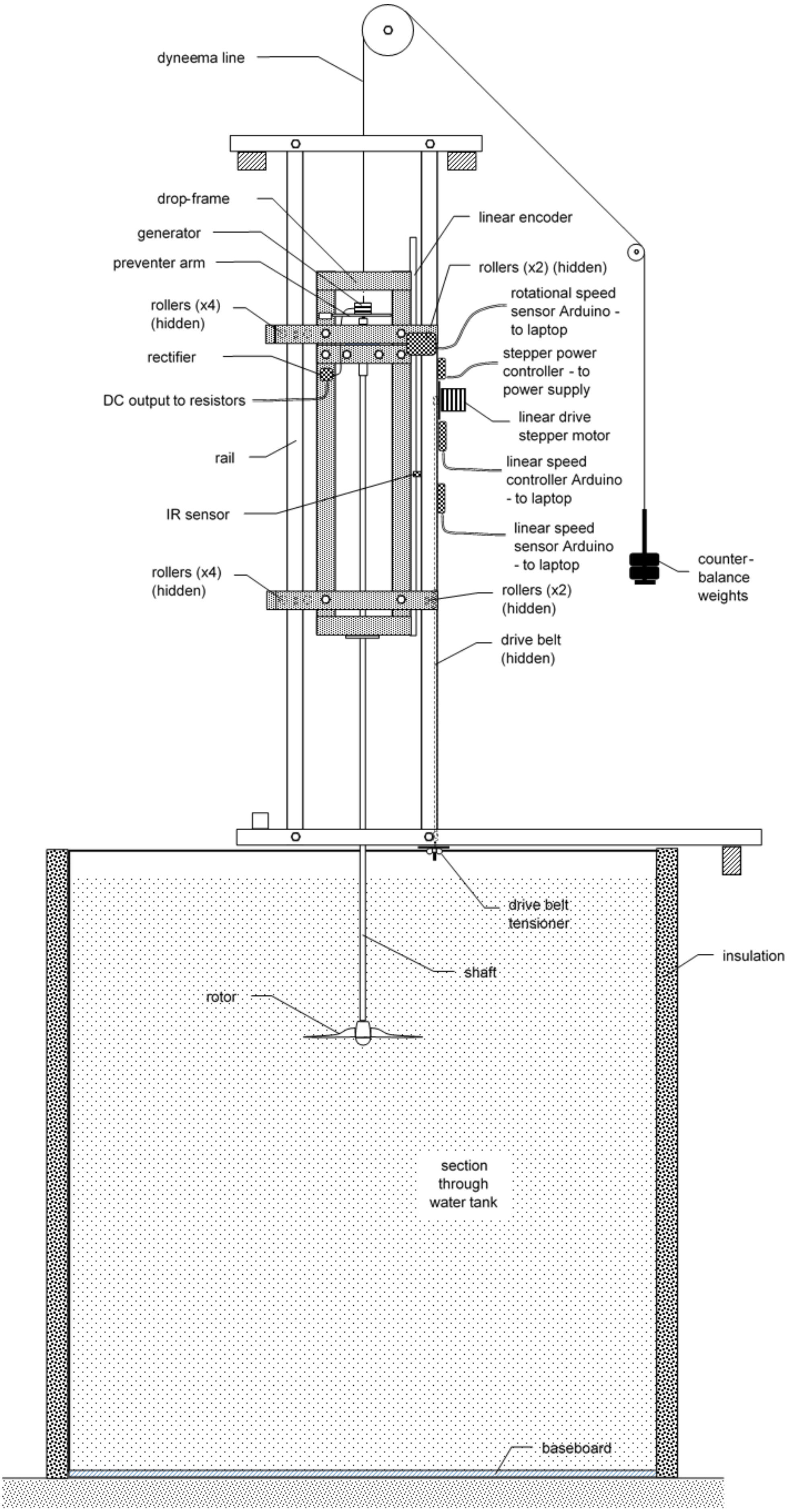

Figure 5.6: Front view of water-drop equipment

Blockage considerations

The effect of 'blockage' during testing was minimised through use of a water tank with adequate diameter. The 1.4 m diameter water tank and 280 mm diameter rotors resulted in a blockage ratio of 4%. Chen & Liou (2010) investigated the effect of wind tunnel blockage ratio and determined that a blockage ratio of 10% produces blockage error of less than 5% and that it was acceptable in research, to ignore blockage effects and not apply blockage correction when tests had blockage ratios of less than 10%. Ryi et al (2015) measured blockage effect on a wind turbine (1.408 m diameter) that was tested in three different sized wind tunnels and presented a relationship between thrust coefficient C_T, blockage ratio α and the corrected wind speed ratio U'/U for correction of blockage effect (see Figure 5.7).

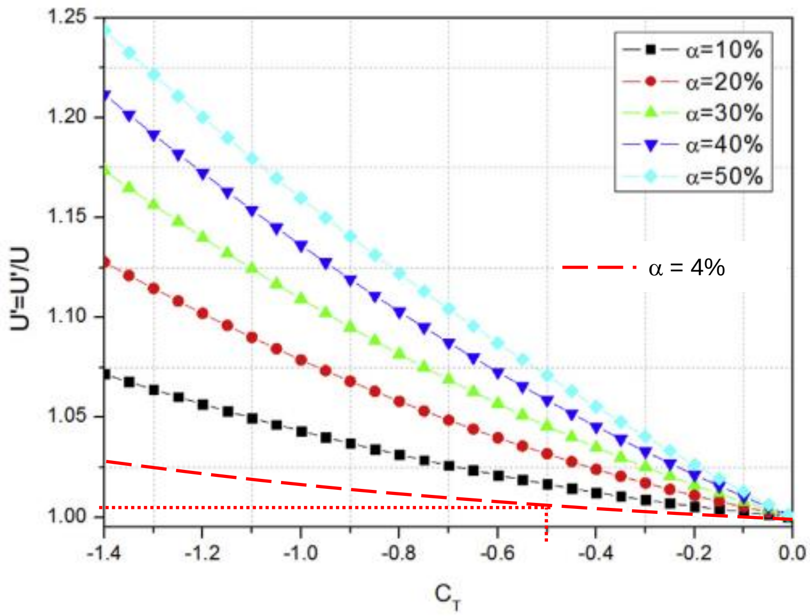

Figure 5.7: The relationship between blockage effect (*U'/U*), thrust coefficient (*C_T*) and blockage ratio (*α*)

(Adapted from Ryi et al, 2015)

Applying the above dimensionless relationship to this research, the thrust coefficient of the 280 mm rotor with the highest peak power output was approximately 0.5 and with the blockage ratio of 4% (shown by the added, dashed curve in Figure 5.7), the testing in this research experienced a blockage effect that would have required a wind speed correction of less than 1%.

Length of travel

Apart from subjecting the rotor to uniform and constant velocity of working fluid, the water-drop equipment also needed to provide adequate travel for the rotor to have sufficient time to generate a complete 'near-wake' – the part of the wake where flow is affected by the rotor blade geometry and which in-turn affects the rotation of the rotor, depending on the near-wake's level of completion. Beyond the near-wake, the wake is fully turbulent and in practice affects final rotor rotation speed very little.

There is lack of agreement as to the length of the near wake. Sanderse et al (2010) state that the near-wake length is 1 to 2 rotor diameters in length. Jha et al (2015) claim 2 to 3 rotor diameters, and Göçmen et al (2016), Okulov et al (2015) and Porté-Agel et al (2019) all report the near wake usually being 2 to 4 diameters in length. In this study, rotor travel of just over 3 diameters (≈ 900 mm) was provided and all rotation speed run data was subject to least squares curve fitting to an exponential decay function to generate a final expected rotation speed and to determine how close the measured final speed was to the theoretical asymptote of the final speed.

Overall requirements for the water-drop equipment were therefore:

- to lower the rotor into water at a constant speed of 0.25 m/s for a distance of at least 3 blade diameters (more information provided in Section 5.2).
- to sense and record rotor rotation speed at suitable time intervals.
- to retain the water at a constant temperature for consistent density and viscosity.
- to ensure a constant temperature for the power resistors that were used as electrical loads.

<u>Height of tank</u>

The height of the tank needed to accommodate the length of travel of the rotor, as well as an open space ahead of the rotor beyond the lowest point of travel. The readings towards the end of travel of the rotor provide the final rotation speed. If the rotor travelled all the way to the floor of the tank, the tank floor would affect induction through the rotor in the final stage of travel. An estimate (Figure 5.8), of how many rotor diameters of space are required to avoid affecting induction, was made by considering the change in velocity ratio ahead of an ideal rotor (actuator disc) at C_T = 0.89 and radius ratios 0.1, 0.5 and 0.9 at a range of stations - as presented by Madsen (1996). Against this data, an open zone height of two rotor diameters provided sufficient space for avoidance of induction interference by the tank floor.

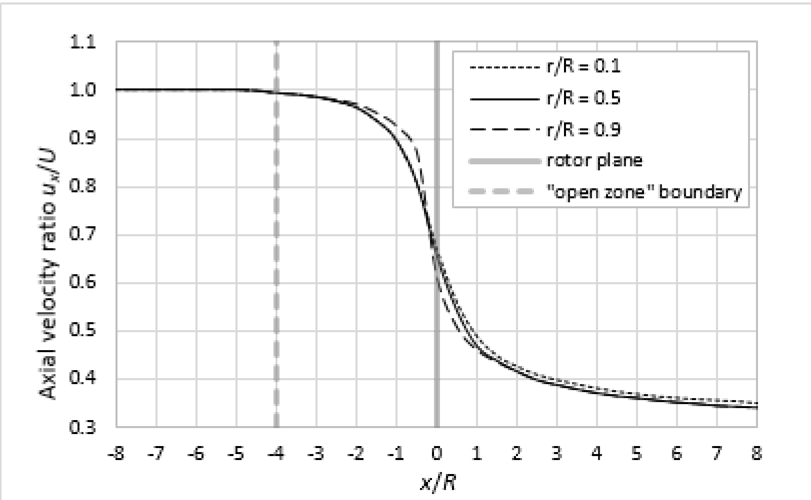

Figure 5.8: Boundary of 'open zone' to avoid upstream induction effects

(Adapted from Madsen, 1996)

Calibration equipment

To determine the torque produced by the rotor, the generator torque was measured for each resistance at a range of rotation speeds, using the calibration equipment. The result was a set of torque-speed curves, for one phase of the 0.28 N.m stepper generator, for each resistance that was used in testing.

The very small expected maximum generator torques (≈ 0.017 N.m), necessitated custom-built calibration equipment - consisting of the same vertical shaft and generator, mounted in the drop-frame (as in testing), driven from below by a stepper motor connected to the bottom of the shaft via a loose coupling and mounted on a horizontal, shaft-aligned, rotating platform. Generator torque was measured via polyester thread (0.025 g/m), lightweight nylon pulley and an electronic scale (200g/0.01g). See Fig 5.9.

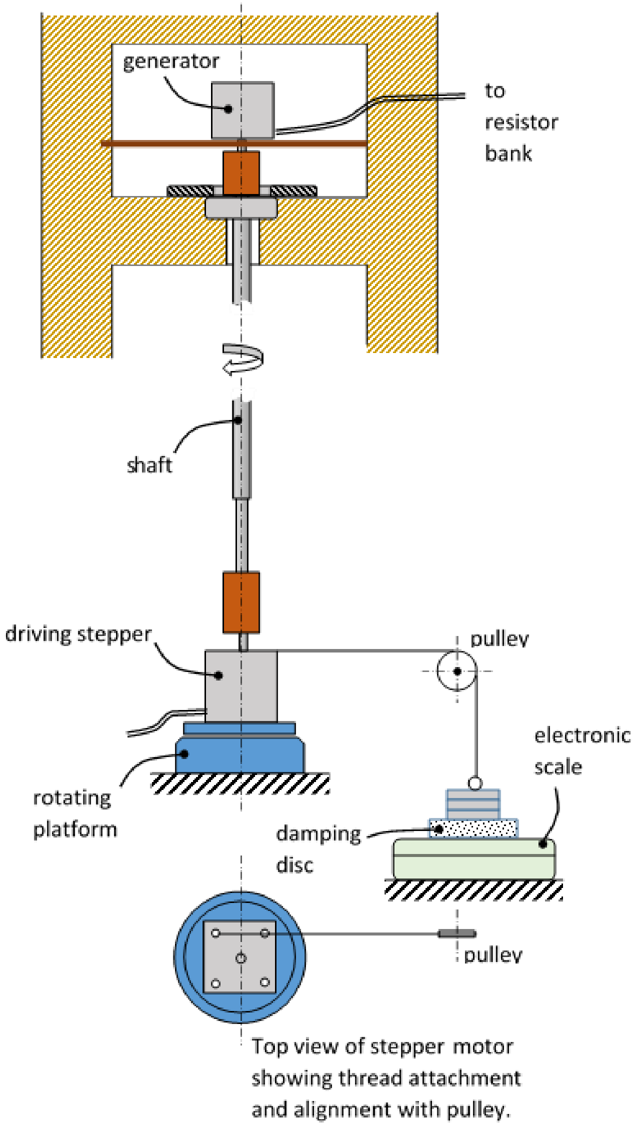

Figure 5.9 - Calibration equipment

5.2 Testing methodology

BEMM analyses and CFD simulations provided the range of rotor power, speed and torque expected during physical testing.

Rotor power data (per run) was produced in a three-stage process:

1) Rotor rotation speed was recorded while the rotor was provided a constant relative fluid velocity and the generator delivered power to a resistor.
2) An exponential decay curve was fitted to the raw rotation speed data and the asymptote was used as the final rotation speed for each run.
3) Rotor power was determined from the final rotor rotation speed using the generator rotation speed-resistance-torque calibration curves.

<u>Recording rotor rotation speed</u>

For each run, water temperature and resistor bank were maintained at 20 ^{o}C. The ten applied resistances for testing were, ∞, 860, 360, 160, 100, 60, 30, 10, 5 and 3 Ω. The drop frame (with rotor) was driven downwards into the tank of water by the stepper drive system and rotation speed was measured and recorded. Rotation speed sample period ranged from 0.19 to 0.22 seconds per sample through each run.

<u>Exponential decay curve fitting</u>

The exponential decay function,

$$Y = Y_0 + Ae^{-kt}$$

was used for curve fitting of rotation speed data. In this equation, Y is the curve value at any time t and Y_0 is the value of the asymptote. The constant A, describes amplitude of the curve and k is the decay rate constant. Excel *Solver* was utilised to minimise the sum of the δ^2 values by simultaneous optimization of Y_0, A and k for each data set. The mean asymptote value of five runs was recorded as final rotation speed.

At the start of a test run, prior to formation of a near-wake, rotation speed is high, and in the process of forming the near-wake, rotation speed drops until the near-wake formation is complete. The graphs of rotation data and exponential decay fitting show that in almost all test runs, the value of the exponential curve had approached the asymptote very closely by the end of the test run. This provides some evidence that the formation of the near-wake was achieved within the 3-diameter travel of the drop frame. A sample of the 15% adapted BEMM rotor (Run 5; Resistance ∞) is shown in Figure 5.10. A larger sample of rotation speed data is provided in Appendix D.

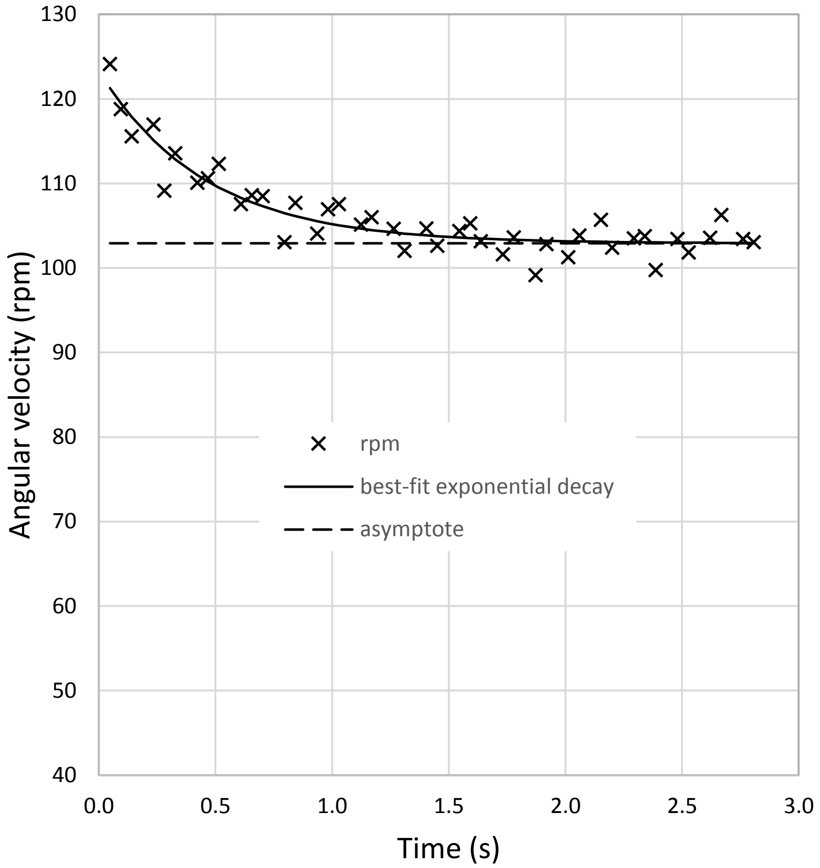

Figure 5.10: Exponential decay curve fitting and asymptote for angular velocity data (Sample: 15% custom rotor, Run 5, Resistance ∞)

<u>Creation of generator calibration curves</u>

Calibration of the generator torque-rotation speed-resistance relationship produced T-ω curves for the ten resistances used in testing. Second-order polynomial equations were fitted to the calibration data and were used to calculate torque from rotation speed – the product of torque and rotation speed then provided the rotor power.

This three-stage process avoided the need for considering generator efficiency and friction and torsion losses from the two shaft bearings. This process also avoided the need for recording of a transient generator torque on a moving frame.

The generator calibration curves for the ten resistances used in testing are shown in Figure 5.11. A table of calibration data is provided in Appendix K.

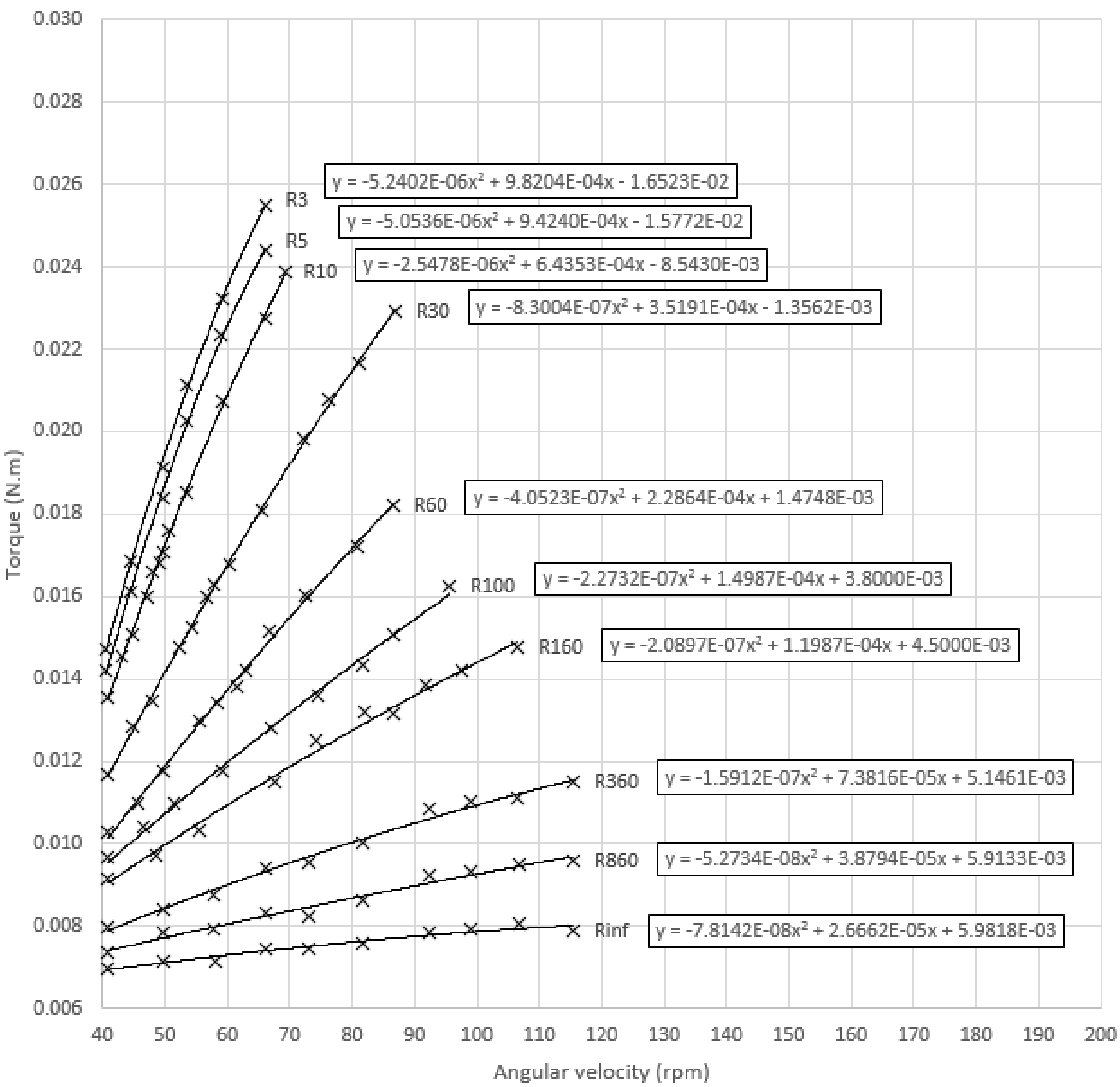

Figure 5.11: Calibration curves (T-ω) for generator at the ten test resistances

5.3 Test results

The physical testing of rotor sets 1 and 2 produced the power curves for each rotor as shown in Figure 5.12. Tables of physical test results are provided in Appendix K. The results show that:

- the adapted BEMM designed rotor for a 10% hub ratio was the highest peak power producer.
- the adapted BEMM 25% hub rotor performed better, at most rotation speeds, than the standard BEMM rotor with 25% hub ratio.
- all rotors except the adapted BEMM 25% hub rotor peaked within a narrow range of rotation speed (60 to 63 rpm).

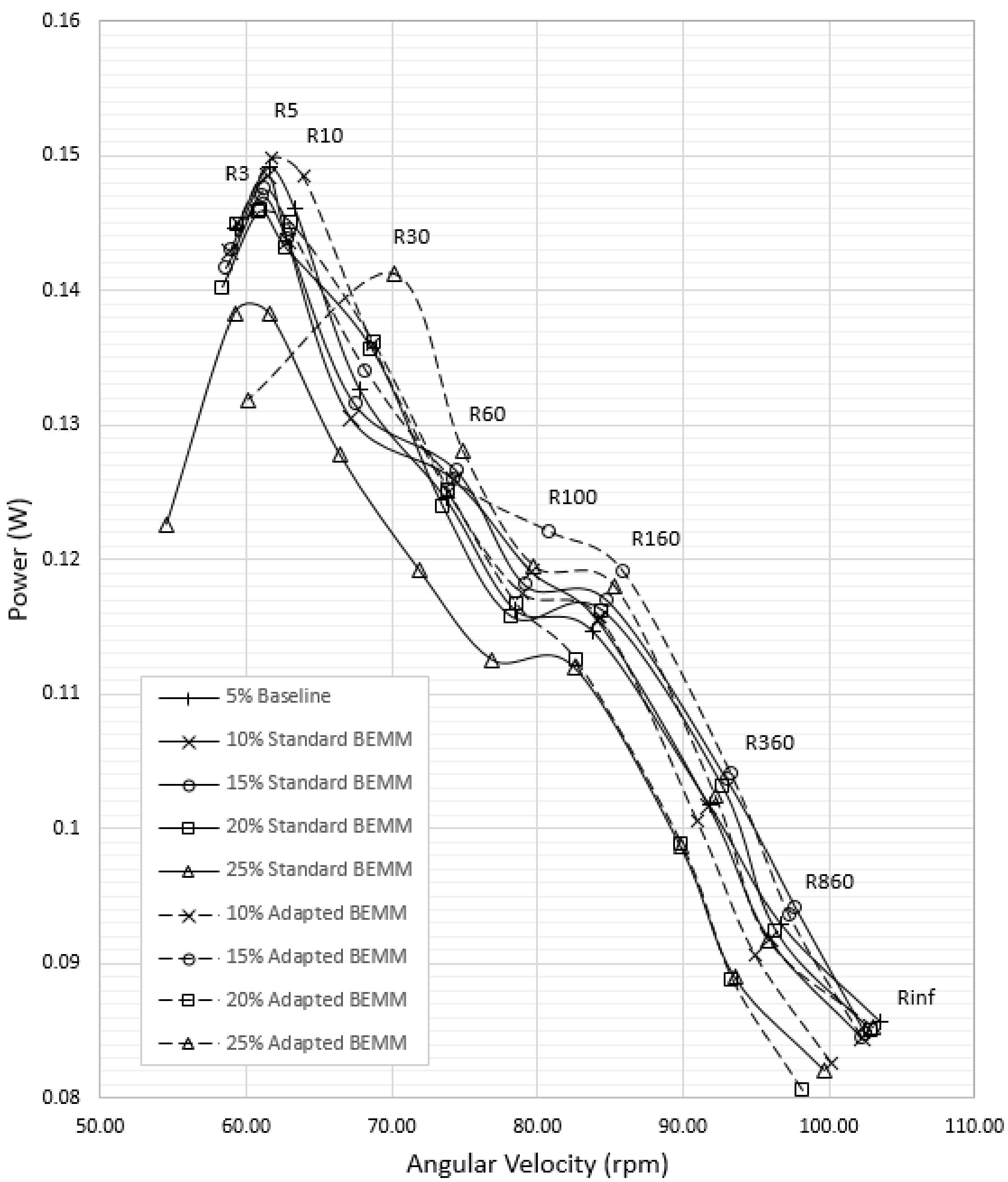

Figure 5.12: Physical Testing Results - Power vs. Rotation speed – all rotors

Congestion at peak values in Figure 5.12 makes comparison difficult so a comparison of peak power values for both rotor sets is shown in Figure 5.13. This comparison shows that:

- the adapted BEMM rotors performed better than the standard BEMM-rotors for 10%, 15% and 25% hub sizes and the 20% hub ratio rotors (standard and adapted) produced the same power.
- the adapted BEMM 10% rotor produced 0.4% more power than the 5% baseline rotor.

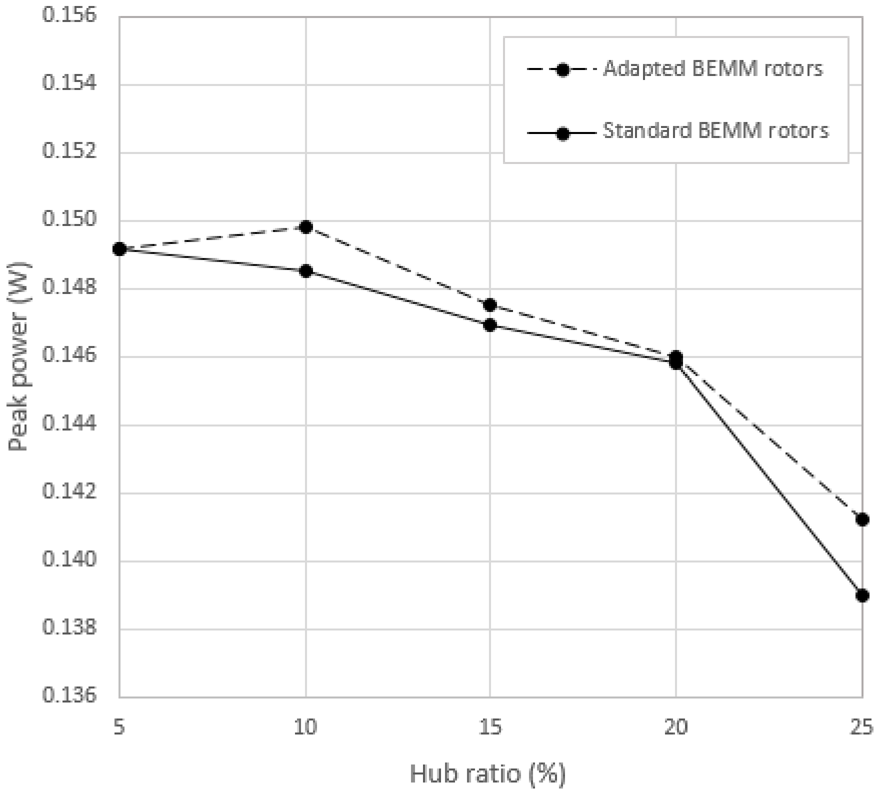

Figure 5.13: Peak power vs. Hub ratio from physical testing of rotors design using the standard and adapted BEMM

5.4 Testing accuracy

Accuracy for the three-stage physical testing methodology is discussed below.

Accuracy in recording rotor rotation speed

Tank water and ambient temperature of resistor bank were maintained between 19.5 and 20.5 ^{o}C. This translates to a viscosity (and Reynolds number) range of 2.4% and an electrical resistance range of 0.01% (based on the resistor specification of 100 ppm/^{o}C). Resistances for testing were checked by multi-meter (Brymen TBM867) for each set of five runs. Specifications for the Brymen TBM867 are provided in Appendix E. The drop frame speed was controlled by stepper motor and a maximum speed range from 0.249 to 0.251 m/s was achieved across all tests. A cyclical error was generated by the 8-slot optical encoder for rotation speed and this 8-point repeated pattern can be noticed on the rotation speed vs. time graphs (Figure 5.10 in Section 5.2). The extent of influence of this cyclical error on final rotation speed values is difficult to quantify but is ameliorated by use of the exponential decay curve fitting protocol.

Accuracy in generator calibration

Accurate calibration of the generator depended on:

1) consistent load resistance.
2) bearing friction and shaft bending that was consistent with the conditions when rotor rotation speed was recorded.
3) accurate transmission of force to the electronic scale for torque measurement.

Electrical load resistance was checked as in the recording of rotor rotation speed. Shaft bearings were de-sealed to reduce friction and oiled with a light oil at the start of each test session. Inconsistent shaft bending could have occurred due to the need to constrain (in two dimensions) the bottom end of the shaft where the driving stepper motor was fixed to the horizontal rotating surface. Increased shaft bending would have produced a consistently higher torque reading during calibration which would have resulted in elevated values of rotor power across all rotors.

Generator torque was measured via lightweight polyester thread (0.025 g/m), lightweight nylon pulley and an electronic scale (200g/0.01g). Torque reading required alignment (by eye) of the thread in relation to the driving stepper motor.

Accuracy of the physical tests is insufficient to confirm relative performance of rotors to within 10ths of a percentage. The results of the physical tests should therefore be seen as providing some evidence of general trends in the relative performance of the rotors. Sufficient accuracy is claimed for the CFD simulations (which benefitted from perfect repeatability and input variable control).

Accuracy of 3D-printed rotor geometry

All rotors were printed with ABS (Acrylonitrile-Butadiene Styrene) on a Creality CR10S PRO. With a nozzle size of 0.4 mm and a layer height ranging from 0.1-0.4 mm, the accuracy of print for this printer is specified as +/- 0.1 mm. In order to maximise strength and minimise flexure, all rotors were printed oriented with the rotor plane parallel to the print bed so that lines of filament would run parallel to the length of each blade. Support material removal necessitated surface improvement and surfaces were smoothed to 600-grit water-paper. Some flexure was noticed during testing but was not measured. It was expected that flexure would affect results but it was not possible to quantify this during testing. No blades broke during testing.

CHAPTER SIX

Case Study: Analysis of a 30 m diameter HAWT rotor

Case Study methodology

The adaption to the BEMM was tested on a 30 m diameter, 339 kW HAWT rotor to see outcomes for a much larger geometry with a fully turbulent flow regime. This allowed for more conventional high-performance aerofoil profiles. Four analyses were performed:

1) An adapted BEMM design and performance analysis using the potential flow 'Rankine half-body' velocity gradient within the BEMM (as was used in the 280mm rotors and discussed in Section 3.2).
2) An adapted BEMM design and performance analysis using the potential flow 'Airship' velocity gradient within the BEMM (as discussed in Section 3.2).
3) A standard BEMM design and performance analysis.

4) CFD (Ansys Fluent) simulation of the rotor that was designed with the Rankine-half-body-adapted BEMM. The Rankine half-body-adapted BEMM rotor design was chosen for CFD simulation because the BEMM predictions showed that this design would produce the best performance.

Case Study blade and hub design

The rotor was three-bladed, designed for a wind speed of 12 m/s and had a tip-speed ratio of 4. A single blade profile (NREL S830) (see Figure 6.1) was used throughout the span of the blade and ideal chords and twist angles were retained all the way to the hub interface. S830 data is provided in Appendix G.

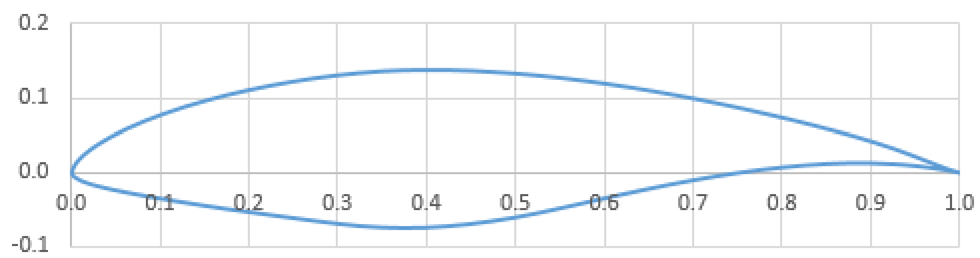

Figure 6.1: NREL S830 profile for the 30 m diameter rotor

(Data sourced from airfoiltools.com)

Leading edges of blade profiles were aligned to a rotor plane, perpendicular to the axis of rotation. Planar blade profiles were transformed to concentric chord lines and a 3 mm radius was applied to trailing edges. Chord lengths for the blades with smallest (5%) hub ratio ranged from 2.264 m at the hub interface to 3.495 m at widest point, and with a chord of 0.388 m at the tip.

Lift and drag coefficients for the NREL S830 aerofoil were generated using XFLR5 software and are shown in Figure 6.2. The chord-based Reynolds number ranged from 1.2×10^6 to 5.5×10^6 and angle of attack shown from zero to 16 degrees.

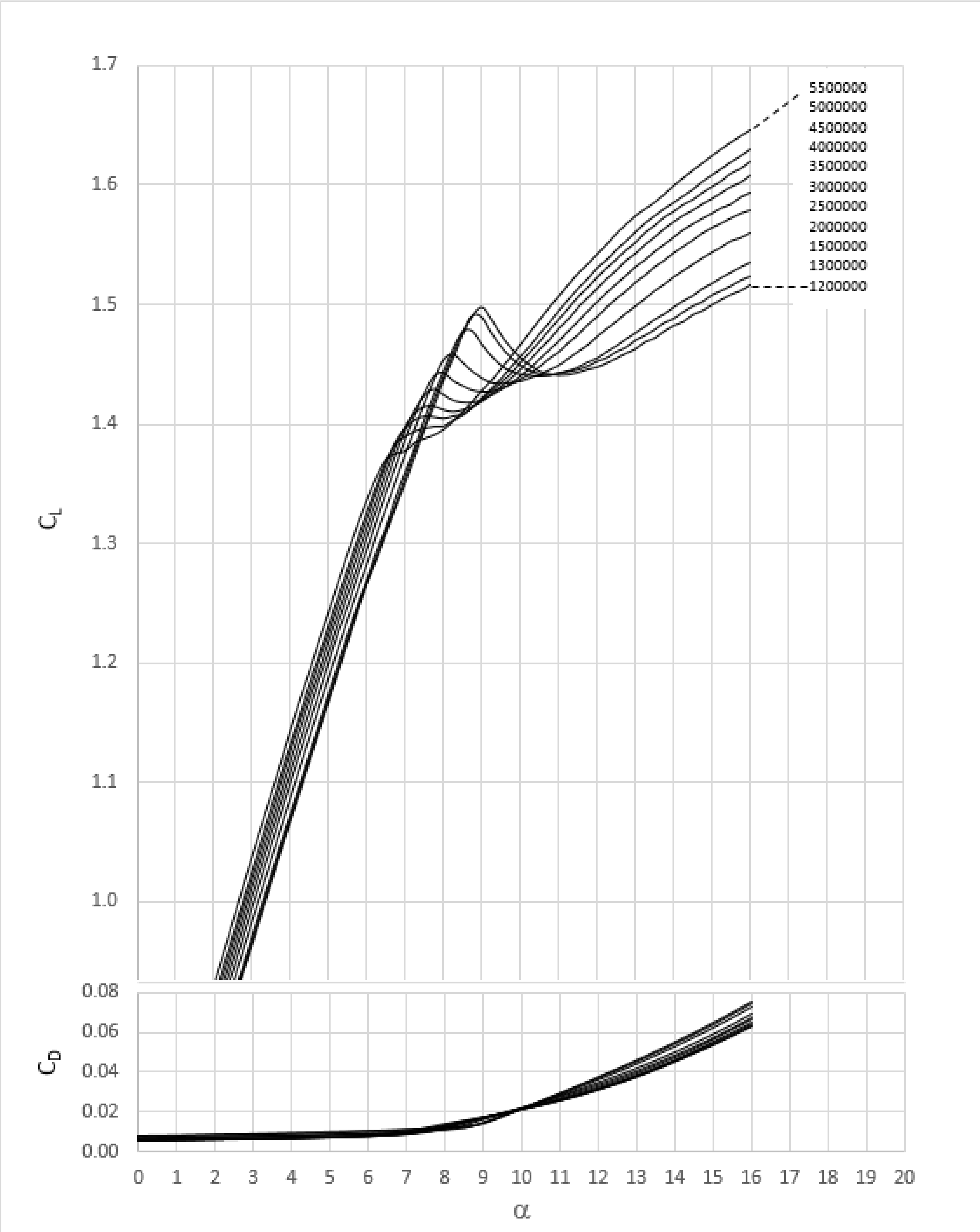

Figure 6.2: Lift and drag coefficients for the NREL S830 aerofoil

Chord and twist data for all rotors is provided in Appendix G.

The hub was an airship design with a length/diameter ratio of 2.0. A front and side view of the 5% hub ratio rotor and 'airship' shaped hub are shown in Figure 6.3.

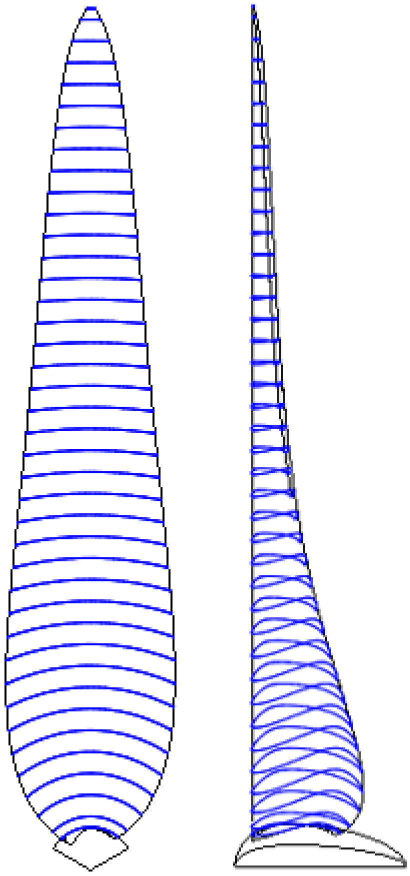

Figure 6.3: Front and side views of the 5% hub ratio, 30 m rotor, blade and hub (hub cut to a 120° 'slice')

Case Study CFD simulation and domains

Ansys Fluent was used for the CFD simulation. A pressure-based, SST k-omega solver was used for all rotors, with air at density and viscosity of 1.2041 kg/m^3 and 1.8134×10^{-5} kg/m.s. A complete Ansys Fluent input summary is provided in Appendix F and details of meshing within the boundary layer is provided in Appendix R. The cylindrical outer domain had a diameter of 224 m. Length upstream was also 224 m and length downstream was 256 m. The rotor geometry was Boolean-extracted from an inner cylindrical rotating domain with a diameter of 38 m, length upstream of 10 m and length downstream of 16 m. As in the 280 mm diameter rotor CFD study, a 120° slice of the domains and rotor was analysed using rotational periodicity. The domains are shown in Figure 6.4.

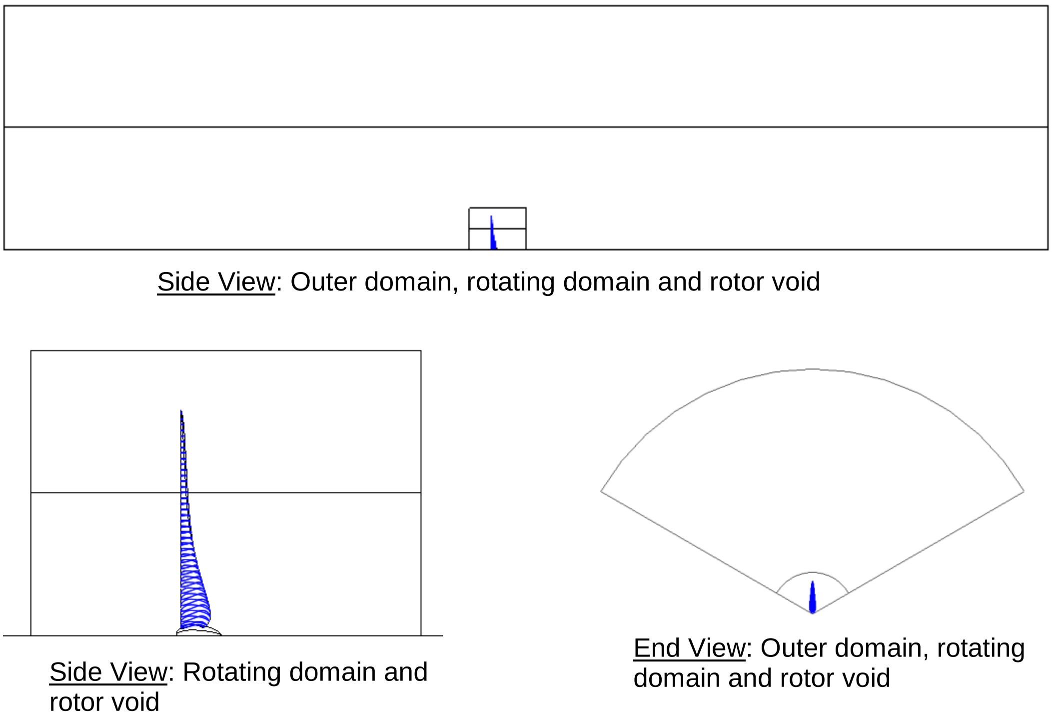

Figure 6.4: CFD domains for the 30 m diameter rotors

Details of meshing within the boundary layer are provided in Appendix R and pictures of the mesh (10% hub, adapted BEMM as sample) are provided in Appendix S.

Mesh dependence and data uncertainty

A mesh dependence study (Fig 6.5), of the 5% hub ratio rotor, shows the relationship between the chosen (100%) mesh and meshes of increased and reduced local size target setting for blade and hub. The '100%' mesh settings were then applied to all five rotors in this study.

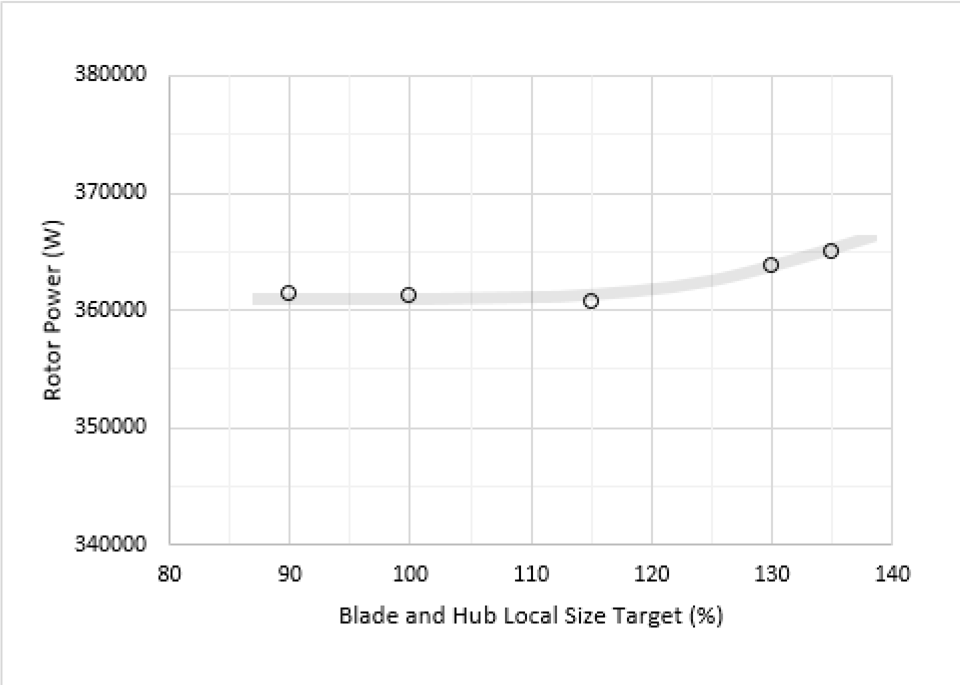

Figure 6.5: Mesh dependence study – 30 m 5% hub ratio rotor

Micro adjustment of the chosen (100%) mesh for all five rotors generated the data ranges shown in Fig 6.6. A minimum of four micro-adjustments were used per rotor and more meshes were solved for the critical rotors (5%, 10% and 15%) or if the range was particularly narrow.

Mesh dependence and micro-adjustment data is tabulated in Appendix N.

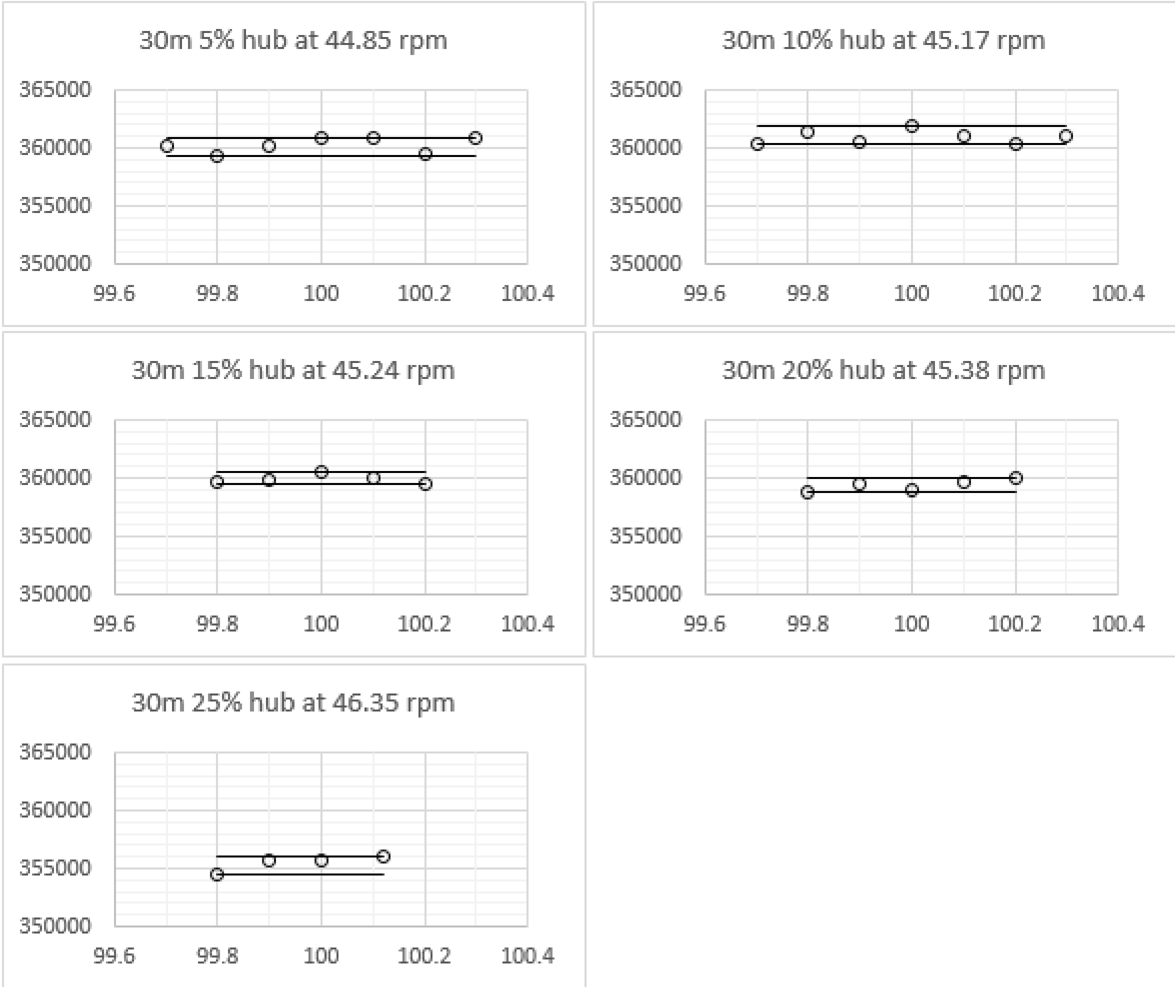

Figure 6.6: Micro-adjusted mesh data ranges – 30 m rotors

The difference between data ranges across rotors provides an indicator of relative uncertainty. Since lower boundary meshes were used for power curves, relative uncertainty is downwards (negative) only. Relative uncertainty assumes that all rotors would ultimately produce a data range equal in size to the rotor with the largest data range – i.e. the rotor with the narrowest data range has the largest relative uncertainty because its range might extend by the largest amount when compared to the other rotors. This analysis is shown in Table 6.1.

Table 6.1: Rotor data boundaries, ranges and relative uncertainty – ϕ30 m rotors

Rotor	Upper boundary power (P_U) (N·m) $\times 10^{-3}$	Lower boundary power (P_L) (N·m) $\times 10^{-3}$	Range $R = P_U - P_L$ (N·m) $\times 10^{-3}$	Rel. uncertainty $\Delta(R^* - R)(100)/P_L$ (%)
5% STD BEMM*	360954	359333	1621	0.000
10% ADP BEMM	361890	360301	1589	-0.009
15% ADP BEMM	360446	359452	994	-0.174
20% ADP BEMM	359653	358884	769	-0.237
25% ADP BEMM	355984	354504	1480	-0.040

Case Study Results

The results of the three BEMM analyses and the CFD simulation are presented in Fig 6.7. The Case Study BEMM results are tabulated in Appendix M and CFD results are provided in Appendix N. Overall results are tabulated in Appendix O.

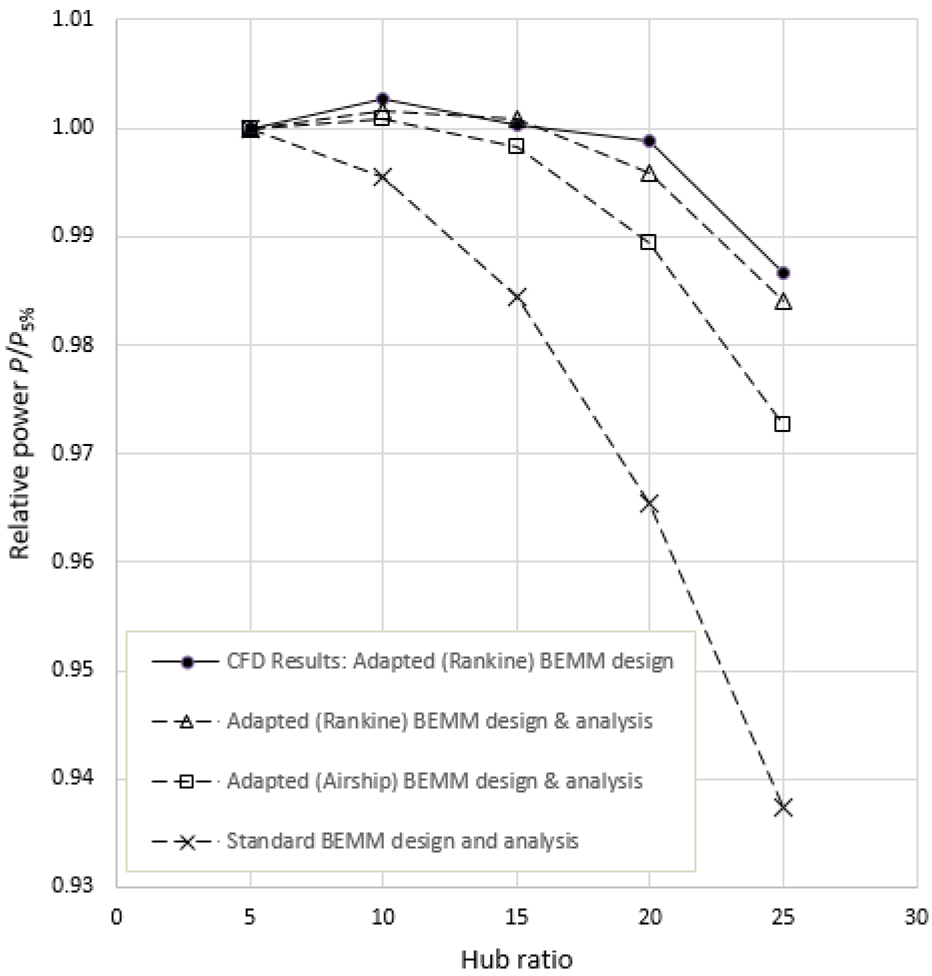

Figure 6.7: Results of BEMM analyses and CFD simulation of the 30 m diameter rotors

All power data was converted to dimensionless ratios of the 5% baseline (standard BEMM designed) rotor. While the standard BEMM predicted no positive benefit to increased hub ratio, both the Rankine and Airship BEMM adaptions predicted a maximum power benefit at a hub ratio of approximately 10%. The Rankine BEMM adaption showed that positive performance benefit extended to a hub ratio of up to 15%, while the Airship BEMM adaption predicted a benefit for hub ratios up to 11%. The CFD results correlated closely with the Rankine-adapted BEMM prediction, with CFD results slightly higher than prediction results at hub ratios of 20% and 25%.

A spillage power loss estimate based on the mean of the Rankine and Airship spillage power loss estimates was applied to the standard BEMM prediction.

This case study provides some insight into the effect of the potential flow model (Rankine half-body or Airship) used in creating the hub-induced velocity gradient in the rotor plane and for estimating spillage losses. The CFD results correlate closely with the adapted BEMM predictions and show that both of the BEMM adaption models were better predictors of relative rotor power than the standard BEMM design and analysis.

CHAPTER SEVEN

Discussion of results

The standard BEMM predicts no benefit from increasing hub ratio of an ideal HAWT rotor beyond the minimum (5% in this study). The standard BEMM relies on assumptions that limit its capacity to account for the potential benefit from larger hubs, and an adaption to the BEMM was developed in order to address this limitation.

The adapted BEMM predicts that ideal HAWT rotors that are custom-designed using this adapted BEMM, will produce higher peak power than ideal HAWT rotors that are designed with the standard BEMM, for all hub ratios. The adapted BEMM accounts for expected acceleration of air around larger hubs, and also provides a means to include this acceleration in rotor design. The adaption is based on rotor plane dimensionless velocity profiles, obtained through potential flow theory, which are applied to the upstream fluid.

The success of the Rankine-adapted BEMM in designing and predicting power from ideal, ϕ280 mm HAWT rotors was compared with CFD simulation and physical test results.

The CFD simulations benefit from perfect control of input variables and zero rotor flexure but are dependent on the accuracy of the mesh and solver and the choice of turbulence model. The accuracy challenges in physical testing include control of the input variables, rotor flexure and calibration of instruments.

The results for the BEMM predictions, CFD simulations and physical testing of the 280 mm rotors are combined and shown in Figure 7.1.

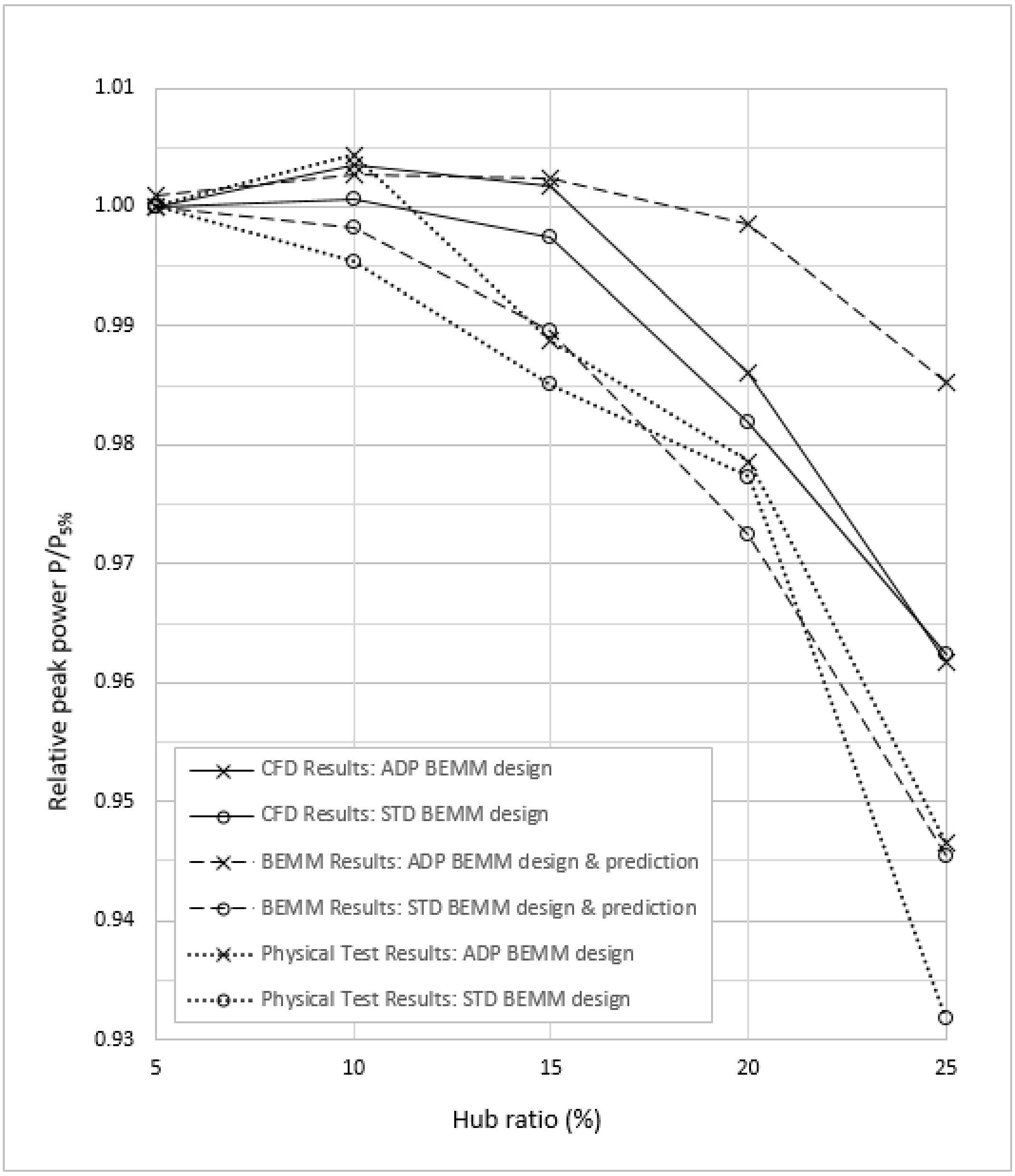

Figure 7.1: Results of BEMM predictions, CFD analyses and physical testing of 280 mm diameter rotors designed with the standard BEMM and an adapted BEMM

For the 280 mm rotors, both the CFD simulation and physical testing show that the adapted BEMM design procedure generally produces rotors that perform better than those designed with the standard BEMM. The 10% hub ratio rotor recorded improvement of 0.29% (CFD) and 0.90% (physical testing) and the 15% hub ratio rotor recorded a 0.44% (CFD) and 0.37% (physical testing) improvement.

The adapted BEMM is a better predictor of relative peak power for the CFD analyses of the 280 mm, 10% and 15% hub ratio rotors. Beyond a 15% hub ratio, the CFD analyses fall roughly between the standard and adapted BEMM predictions.

The adapted BEMM predictions, CFD analyses and physical tests all showed that the 280 mm, 10% hub ratio rotor, designed with the adapted BEMM, produced more power than the 5% baseline rotor. The adapted BEMM predicted a 0.28% performance increase for the 10% rotor, and the CFD analyses and physical testing produced performance increases of 0.35% and 0.44% respectively.

At hub ratios beyond 15%, for the 280 mm rotors, the adapted BEMM over-predicts relative peak power (compared to the physical tests and CFD simulations). A possible explanation is that the power loss, from radial flow and ‘spillage’, was underestimated by the adapted BEMM. The power loss model for the adaption to the BEMM, was based on ideal potential flow theory and the assumption of zero radial flow at the rotor plane (which is also an assumption of BEMM theory). Another possible explanation is that, at hub ratios beyond 15%, the performance of the cambered plate aerofoil in the physical tests and CFD simulations was lower than from the XFLR5 software-predicted performance curves that were used in both the standard and adapted BEMMs.

Physical test results of the 280 mm rotors showed that rotors that were designed using the adapted BEMM all performed better in the physical tests than rotors designed using the standard BEMM. The physical test results correlated approximately with the standard BEMM prediction. Physical test results were significantly lower than CFD simulation results for rotors that had hub ratios larger than 10%. This was possibly due to the flexure of the 3D-printed blades (compared to the fixed dimensions of the CFD solid model), which would have resulted in greater radial flow and ‘spillage’.

For the 280 mm rotors, design and prediction with the Rankine half-body-adapted BEMM shows peak rotor power to be greater than the 5% baseline rotor for hub ratios of up to 17.5%. Physical testing of the 280 mm rotor indicates a limit of benefit closer to 11%.

The 30 m diameter rotor case study investigated the choice of near-hub flow assumption in the BEMM adaption (Rankine-half-body or Airship) and compared these with standard BEMM design and prediction. The results are reproduced in Figure 7.2.

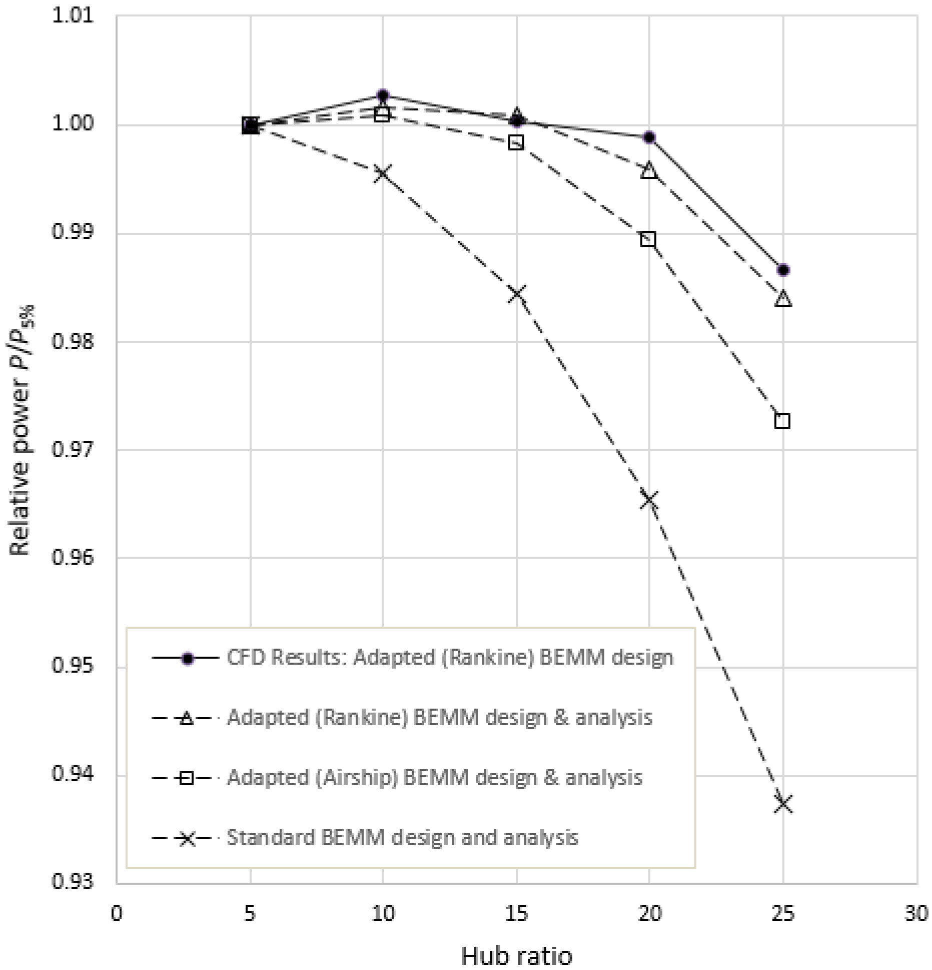

Figure 7.2: Results of BEMM analyses and CFD simulation of the 30 m diameter rotor

The 30 m diameter rotors benefitted from a high-performance conventional aerofoil and fully turbulent boundary layer. CFD results correlate closely with the Rankine half-body-adapted BEMM (noting that the rotors for the CFD simulation were designed using the Rankine half-body-adapted BEMM). The 30 m rotors were also designed using the standard BEMM and using an Airship-adapted BEMM. BEMM predictions for these rotors are included in Fig 7.2. CFD simulations were performed for the Rankine half-body-adapted BEMM-designed rotors because this adaption was predicted to result in the best performance.

The 30 m diameter rotor study confirmed the increase in power from the 10% hub ratio rotor, with the Rankine-adapted BEMM prediction of 0.15% and the CFD result of 0.27%.

The CFD results correlated quite well with the Rankine half-body-adapted BEMM predictions at all hub ratios.

For the 30 m rotors, design and prediction with the Rankine half-body-adapted BEMM shows peak rotor power to be greater than the 5% baseline rotor for hub ratios of up to 15%. The CFD analyses of both the 280 mm and the 30 m rotors showed that a hub ratio of 15% was the limit of benefit from a large hub.

CONCLUSION

This study set out to answer four questions concerning ideal HAWT rotors and hub ratio:

1) *Is there an improved peak performance for a larger-than-negligible hub ratio*? The results of CFD simulation and physical testing of a 280 mm diameter HAWT rotor and simulation of a 30 m diameter rotor show that, when comparing ideal rotors, improved performance can be expected from a larger-than-negligible hub ratio.

2) *What is the optimum hub ratio to maximise performance*? CFD simulation results for both the 280 mm and the 30 m diameter rotors, as well as physical test results of the 280 mm rotors predict an optimum hub ratio close to 10%.

3) *What gain in output power can be achieved if an optimum hub ratio is chosen instead of a minimum hub size for an ideal HAWT rotor*? For the 280 mm rotors, the Rankine-adapted BEMM predicted a relative power gain of 0.28%. CFD simulation and physical testing measured relative power gains of 0.35% and 0.44% respectively. The 30 m case study rotor achieved a relative power gain of 0.27%. These relative power gains are small, but if a large hub ratio is required for an annular generator or for increasing the diameter of a turbine, then the small power gain from the larger hub is an additional potential benefit on top of the primary reason for the large hub ratio.

Also, this study compared larger hub ratio rotors against a 5% hub ratio rotor that was designed as ‘ideal’ (ideal chord, thickness and twist extending all the way to the hub interface). In reality, large hub ratio turbines are competing against small-hub turbines that have aerofoil profiles transitioning from a cylindrical blade root for a significant length of the blade and which are quite far from an ideal aerodynamic design. A larger hub ratio also has blade-hub geometry that provides more space for a more ideal blade-hub interface. As has been discussed, in the literature review, large hub ratio turbines in industry have achieved power coefficients close to 50%, whereas conventional minimal hub ratio turbines are closer to 45%. Expected power gain from large-hub turbines are partly from the benefit of air accelerations close to the hub, but also from the potential to improve the hub-blade interface and blade aerodynamic profile in the near and not-so-near-hub region.

4) *What is the limit to hub ratio, beyond which there is no performance benefit over a minimal hub*? The Rankine-adapted BEMM predictions for the 280 mm and the 30 m diameter rotors show benefit from large hub ratios up to 17.5% and 15% respectively. This is supported by the CFD simulations that predict benefit to 15% for both the 280 mm and the 30 m rotors. Physical testing of the 280 mm rotor suggests that the maximum hub ratio before loss of benefit is in the region of 11%. The standard BEMM predicts no benefit beyond a minimum hub ratio (5% in this research), and this is to be expected because the

standard BEMM does not make use of the potential benefit from the acceleration of fluid around large hubs – either in rotor design or in performance prediction.

In the process of finding the answers to these questions, the creation of an adaption to the standard BEMM was required as well as a suitable physical testing method for the nine test rotors.

The BEMM adaption presented in this research was necessary in order to include the flow benefits that arise from larger hub ratios into the rotor design method and performance prediction of the BEMM. Results of this research show that use of the BEMM adaption in the design of HAWT rotors, up to a hub ratio of 20%, produces a higher peak performance than rotors designed using the standard BEMM. The 280 mm rotor physical tests and simulations show that the Rankine half-body-adapted BEMM was a better predictor of power for the 280 mm rotors with hub ratios up to 15%, and for all the 30 m rotors (up to 25%). It is recommended that the 'large hub adaption' from this study be included when using the BEMM to design rotors with hub ratios greater than 5%.

The physical 'water-drop' testing method, with rotor velocity (controlled by stepper motor) into a static body of water, was an accurate, repeatable and economical method of achieving flow of water through the ϕ280 mm rotors. Testing in water produced a measurable rotor power at low rotation speeds from the ϕ280 mm rotors. The 1.4 m diameter of the water tank was sufficient for blockage effects to be ignored. In almost all test runs, rotor rotation speed reached the expected asymptote of the exponential decay function that best described the recorded rotation speed data – indicating complete development of the rotor near-wake. The measurement of generator torque accurately to fractions of a percent is challenging and a potential source of error. The in-situ calibration of the generator torque-resistance-rotation speed relationship was to avoid unknown torque losses from shaft bending, bearing friction and generator efficiency. Model testing of wind turbines requires same tip-speed ratio for similarity of rotor geometry. Testing model rotors in water allows models to be tested at lower rotation speeds (closer to the prototype rotation speed) than if tested in air. This is beneficial for similarity of inertial forces. Overall, the testing method has good potential for future use in testing of small wind turbine rotors and rotor modelling.

FUTURE WORK

Improvement to the BEMM adaption for large hubs

The BEMM adaption developed in this work uses a number of simplifying assumptions. The following areas could benefit from further investigation:

- Both the rotor plane velocity gradient and the spillage losses were generated from a potential flow model. The potential flow model assumes infinite number of blades (permeable disc) - as does the 'standard' BEMM, prior to the application of the Prandtl tip loss correction. The accuracies of the rotor plane velocity gradient and the spillage loss are uncertain since the overall result is based on the input from both models. Further investigation could improve the velocity gradient and spillage loss modelling in the BEMM adaption.
- It is not clear whether the improved performance through design with the adapted BEMM is optimized performance. A CFD investigation of whether relative wind angle along the blade is as the adapted BEMM predicts, would be necessary to determine whether the angle of attack is optimised – or only improved.

Testing of BEMM large hub adaption in large HAWT CFD models

The testing and simulation of 280mm diameter rotors with water as working fluid was for the feasibility of physical testing in a laboratory. Use of the BEMM large hub adaption to create CFD models of large HAWTs, as in the 30 m diameter rotor case study, would provide data for large Reynolds number HAWT designs where working fluid would be air and a turbulent boundary layer would predominate.

Testing of BEMM large hub adaption with optimised aerofoil profiles

To reduce confounding variables, this research used a single aerofoil profile across the entire span of the blade. Further investigation into optimization, but using more appropriate aerofoil profiles at blade root and tip would also be important for showing the application of the BEMM large hub adaption to more efficient blade designs.

Improvement to the 'water-drop' testing system for physical testing of small HAWT models

The water-drop system developed and used in this research provided a high level of accuracy in delivery of a constant velocity of working fluid to the rotor and provided accurate rotor rotation speed data. The system is very economical and uses components and materials that are readily available. The system is also very compact (compared to a wind or water tunnel of equivalent test section area) and occupies very little floor area. Scaling up to larger systems (50% to 100% larger) would allow for investigations where a turbulent boundary layer predominates. The advantages of the water-drop system justify its further development.

Reduction of spillage and radial flow in large hub or high rotation speed rotors using an annular aerofoil

Radial displacement of fluid in the rotor plane, due to the presence of a large hub, causes streamlines of fluid which would have passed through the rotor plane, to be deflected outside of the rotor plane. This is what has been termed 'spillage' in this document, and it is particularly significant in rotors with hub ratios greater than 15%. Another cause of radial movement of fluid in the rotor plane is 'radial pumping' – attributed to centrifugal forces, which are proportional to the square of the rotation speed. This spillage, as well as the radial flow over the blades, results in a loss of fluid power. Shrouds have been used in HAWTs to enclose the entire rotor, and improve induction, by preventing unwanted streamline deflection. However, these are bulky and add significant expense and strength considerations to the overall design – especially for large turbines. The possibility of using a stationary, annular aerofoil at an intermediate radius, either before or after the rotor plane, to improve induction through rotors with large hub ratios and/or to reduce radial flow, deserves investigation. Compared to a shrouded HAWT, use of an annular aerofoil, as suggested, would be less costly, more compact and pose a lesser structural challenge to the overall design of the turbine.

Appendix A: Pilot study of HAWT hub ratios in industry

A pilot study to determine hub ratio of wind turbines in industry was conducted from June 2017 to June 2018. The graph below is a plot of rated power (log scale) against hub ratio and shows:

- for turbines up to 1 MW there is a broad range (0.01 to 0.12) of hub ratio.
- for turbines greater than 1 MW, most had a hub ratio between 0.015 and 0.035 and a few were in the range of 0.035 to 0.095.

The two turbines with hub ratios of 0.18 are the GE ecoROTR (a single 1.7 MW prototype investigation) and the SWAY turbine (a concept 10 MW turbine that was designed, but never built).

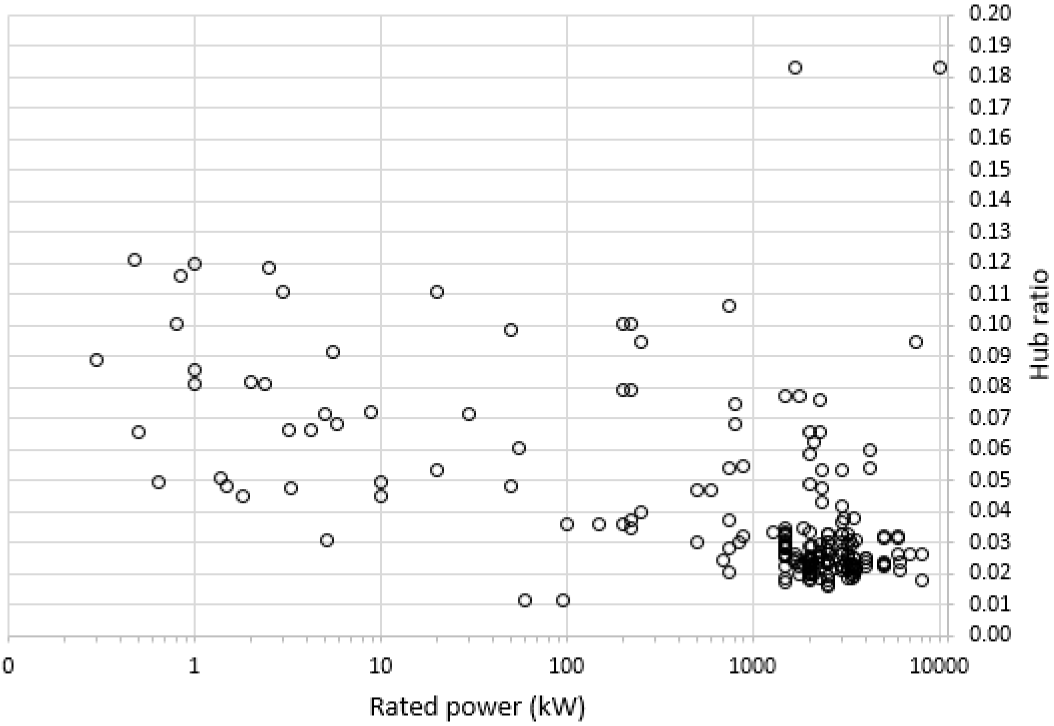

Hub ratio vs. Rated power (log scale)

The following data is a list of wind turbines from information in the public domain that was accessed between June 2017 and June 2018. Manufacturers seldom provide information about hub size and in many cases, hub ratio was calculated from estimated dimensions. The list is arranged from smallest to largest hub ratio.

Manufacturer	Model	Rated Power [kW]	Rotor Diameter [m]	Hub Diameter [m]	Estimated Hub Ratio	Rated Wind Speed [m/s]
Northern Power Systems	NPS100C-24	95	24.4	0.28	0.011	12.0
Northern Power Systems	NPS60-24	60	24.4	0.14	0.012	11.0
Gamesa	G126-2.5	2500	126	2	0.016	10.0
Siemens	SWT-2.5-120	2500	120	2	0.017	11.5
Acciona	AW 82/1500	1500	82	1.4	0.017	10.5
Gamesa	G114-2.0	2000	114	2	0.018	12.5
Gamesa	G114-2.5	2500	114	2	0.018	11.0
Adwen	AD 8-180	8000	180	3.2	0.018	12.0
Vestas	V110-2.0	2000	110	2	0.018	12.0
Sinovel	SL1500/82	1500	82	1.5	0.018	11.0
Siemens	SWT-2.3-108	2300	108	2	0.019	11.5
Siemens	SWT-3.2-108	3200	108	2	0.019	13.5
Siemens	SWT-3.4-108	3400	108	2	0.019	14.5
Gamesa	G106-2.5	2500	106	2	0.019	12.0
Vestas	V136-3.45	3450	136	2.6	0.019	11.0
Senvion	3.4M122 NES	3400	122	2.4	0.020	12.0
Suzlon	S111	2100	111.8	2.2	0.020	10.0
Sinovel	SL2000/121	2000	121	2.4	0.020	8.7
Vestas	V100-1.8	1800	100	2	0.020	12.0
Vestas	V100-2.0	2000	100	2	0.020	12.0
Vestas	V100-2.0	2000	100	2	0.020	12.0
Pioneer Wincon	P750/49	750	49	1	0.020	15.0
Gamesa	G97-2.0	2000	97	2	0.021	14.0
Suzlon	S97	2100	97	2	0.021	11.0
Vestas	V126-3.45	3450	126	2.6	0.021	11.5
Acciona	AW125/3000	3000	125	2.6	0.021	10.5
Senvion	6.2M152	6150	152	3.2	0.021	12.0
Senvion	3.2M114 NES	3200	114	2.4	0.021	12.0
Senvion	3.6M114 NES	3600	114	2.4	0.021	12.0
Senvion	3.4M140 EBC	3400	140	3	0.021	11.0
Senvion	3.6M140 EBC	3600	140	3	0.021	11.0
GE	2.75-120	2750	120	2.6	0.022	12.5
Kenersys	K120	2300	120	2.6	0.022	11.0
Senvion	MM100	2000	100	2.2	0.022	11.5
Vestas	V117-3.45	3450	117	2.6	0.022	11.5
ENO Energy	eno 126/3500	3500	126	2.8	0.022	12.5
ENO Energy	eno 126/4000	4000	126	2.8	0.022	13.0
Adwen	AD 5-135	5000	135	3	0.022	11.4
Gamesa	G90-2.0	2000	90	2	0.022	12.0
Sinovel	SL1500/90	1500	90	2	0.022	10.0
Sinovel	SL3000/90	3000	90	2	0.022	13.0
Vestas	V90-1.8	1800	90	2	0.022	13.0

Vestas	V90-2.0	2000	90	2	0.022	13.5
Doosan	WinDS3000/134	3000	134	3	0.022	10.0
Acciona	AW116/3000	3000	116	2.6	0.022	10.6
Senvion	MM92	2050	92.5	2.1	0.023	13.0
Adwen	AD 5-132	5000	132	3	0.023	13.5
Gamesa	G132-3.3	3300	132	3	0.023	11.0
Gamesa	G132-5.0	5000	132	3	0.023	13.5
Gamesa	G87-2.0	2000	87	2	0.023	14.0
GE	1.85-82.5	1850	82.5	1.9	0.023	13.0
Senvion	3.4M104	3400	104	2.4	0.023	13.0
Vestas	V112-3.45	3450	112	2.6	0.023	12.5
Goldwind	GW 103/2500	2500	103	2.4	0.023	10.8
Gamesa	G128-5.0	5000	128	3	0.023	14.5
ENO Energy	eno 92/2200	2200	92.8	2.2	0.024	13.0
Garuda	1700.84	1700	84	2	0.024	11.0
Senvion	6.2M126	6150	126	3	0.024	14.0
Siemens	SWT-4.0-130	4000	130	3.1	0.024	12.0
Goldwind	GW 109/2500	2500	109	2.6	0.024	10.3
Kenersys	K110	2400	109	2.6	0.024	12.0
Siemens	SWT-3.15-142	3150	142	3.4	0.024	11.0
Kenersys	K100	2500	100	2.4	0.024	14.0
Sinovel	SL2000/100	2000	100	2.4	0.024	10.5
Garuda	700.54	700	54	1.3	0.024	12.5
Kenersys	K82	2000	82	2	0.024	13.5
Senvion	MM82	2050	82	2	0.024	14.5
Vestas	V82-1.65	1650	82	2	0.024	13.0
Vestas	V105-3.45	3450	105	2.6	0.025	13.5
ENO Energy	eno 100/2200	2200	100.5	2.5	0.025	13.0
Gamesa	G80-2.0	2000	80	2	0.025	15.0
Siemens	SWT-4.0-120	4000	120	3	0.025	13.5
ENO Energy	eno 114/3500	3500	114.9	2.9	0.025	13.0
ENO Energy	eno 114/4000	4000	114.9	2.9	0.025	13.5
GE	1.7-103	1700	103	2.6	0.025	9.6
GE	3.2-103	3200	103	2.6	0.025	15.0
Guangdong Mingyang	MY1.5Sh	1500	82.6	2.1	0.025	14.0
Sinovel	SL1500/93	1500	93	2.4	0.026	9.5
Avantis	AV 1010/2300	2300	100.6	2.6	0.026	12.0
Sinovel	SL2000/116	2000	116	3	0.026	9.0
Acciona	AW 77/1500	1500	77	2	0.026	11.1
Siemens	SWT-6.0-154	6000	154	4	0.026	13.0
Siemens	SWT-7.0-154	7000	154	4	0.026	13.0
Siemens	SWT-8.0-154	8000	154	4	0.026	14.0
Sinovel	SL1500/77	1500	77	2	0.026	12.0
Acciona	AW100/3000	3000	100	2.6	0.026	11.7
GE	1.7-100	1700	100	2.6	0.026	11.0
Nordex	N100/2500	2500	100	2.6	0.026	12.5

Siemens	SWT-3.2-113	3200	113	3	0.027	13.5
Sinovel	SL3000/113	3000	113	3	0.027	11.5
Nordex	N90/2300	2300	90	2.4	0.027	13.0
Guangdong Mingyang	SCD2500/108	2500	108	3	0.028	12.5
Guangdong Mingyang	SCD3000/108	3000	108	3	0.028	12.0
Avantis	AV 928/2500	2450	93.2	2.6	0.028	11.6
Goldwind	GW 82/1500	1500	82.3	2.3	0.028	10.3
IMPSA	IV 82	1500	82.3	2.3	0.028	12.5
Hyosung	HS50	750	50	1.4	0.028	13.0
Acciona	AW 70/1500	1500	70	2	0.029	11.6
IMPSA	IV 70	1500	70	2	0.029	15.0
Sinovel	SL1500/70	1500	70	2	0.029	12.0
Sinovel	SL2000/110	2000	110	3.2	0.029	9.5
ENO Energy	eno 82/2050	2050	82.4	2.4	0.029	13.0
ENO Energy	eno 82/1500	1500	82.4	2.4	0.029	12.0
Siemens	SWT-2.3-101	2300	101	3	0.030	12.0
Siemens	SWT-3.2-101	3200	101	3	0.030	14.5
Siemens	SWT-3.4-101	3400	101	3	0.030	14.5
Goldwind	GW 77/1500	1500	76.9	2.3	0.030	11.1
PowerWind	60-850 kW	850	60	1.8	0.030	12.0
PowerWind	500	500	60	1.8	0.030	9.2
Guangdong Mingyang	SCD2500/100	2500	100	3	0.030	12.5
Guangdong Mingyang	SCD3000/100	3000	100	3	0.030	12.5
Nordex	N80/2500	2500	80	2.4	0.030	15.0
Goldwind	GW 93/1500	1500	92.6	2.8	0.030	9.5
Siemens	SWT-3.3-130 Low Noise	3300	130	4	0.031	11.4
Siemens	SWT-3.6-130	3600	130	4	0.031	12.2
Unitron Energy	UE-42 Plus	5.100	5.24	0.16	0.031	11.0
Sinovel	SL5000/128	5000	128	4	0.031	12.5
Sinovel	SL6000/128	6000	128	4	0.031	13.0
PowerWind	56	900	56	1.8	0.032	12.5
Goldwind	GW 87/1500	1500	87	2.8	0.032	9.9
Sinovel	SL5000/155	5000	155	5	0.032	10.0
Sinovel	SL6000/155	6000	155	5	0.032	11.0
IMPSA	IV 77	1500	77	2.5	0.032	13.0
Guangdong Mingyang	SCD2500/92	2500	92	3	0.033	12.5
Guangdong Mingyang	SCD3000/92	3000	92	3	0.033	14.0
Enercon (2017)	E115	3000	115.7	3.8	0.033	12.0
Enercon (2017)	E115	3200	115.7	3.8	0.033	13.0
Mapna Group	Mapna 2.5 MW	2500	104	3.4	0.033	12.0
Goldwind	GW 70/1500	1500	70.3	2.3	0.033	11.6
Hyosung	HS90	2000	90.6	3	0.033	12.0
Nordex	N60/1300	1300	60	2	0.033	17.0
Sinovel	SL1500/90	1500	90	3	0.033	10.0
GE	1.85-87	1850	87	3	0.034	13.0
IMPSA	IV 87	1500	87	3	0.034	12.0

RRB Energy	V27-225 kW	225	29	1	0.034	14.5
Electria Wind	Garbi 100/28	100	28	1.0	0.036	9.0
Electria Wind	Garbi 150/28	150	28	1.0	0.036	10.4
Electria Wind	Garbi 200/28	200	28	1.0	0.036	11.0
Sinovel	SL3000/121	3000	121	4.4	0.036	10.5
Norwin	54-ASR-750 kW	750	54	2	0.037	13.0
RRB Energy	V27-225 kW	225	27	1	0.037	14.5
Enercon (2017)	E-101	3050	101	3.8	0.038	13.0
Enercon (2017)	E-101	3500	101	3.8	0.038	15.0
NEPC India Ltd	SRC 31 - 250/50	250	31	4.2	0.040	13.0
Sinovel	SL3000/105	3000	105	4.4	0.042	12.0
Enercon (2017)	E-103	2350	103	4.4	0.043	12.0
Aeolos	H-10kW	10.000	8	0.18	0.045	10.0
Unitron Energy	UE-15 Plus	1.800	3.4	0.08	0.045	10.5
Nordex	N43/600	600	43	4.8	0.047	14.0
Norwin	47-ASR-500 kW	500	47	5	0.047	13.0
Unitron Energy	UE-33	3.300	4.65	0.11	0.047	10.5
Enercon (2017)	E-92	2350	92	4.4	0.048	14.0
Unitron Energy	UE-15	1.500	3.2	0.08	0.048	10.5
Aeolos	H-50kW	50.000	18	0.44	0.048	10.0
IMPSA	IWP 100	2000	103	5	0.049	11.0
Fortis	Alize	10.000	7	0.17	0.049	13.0
Unitron Energy	UE-6	0.650	2.2	0.05	0.049	10.5
Fortis	Passaat 1.4kW	1.400	3.12	0.08	0.051	16.0
Aeolos	H-20kW	20.000	10	0.27	0.053	10.0
Enercon (2017)	E-82	2350	82	4.4	0.054	14.0
Enercon (2017)	E-82	3000	82	4.4	0.054	16.0
Norwin	47-ASR-750 kW	750	47	5	0.054	15.0
Enercon (2017)	E141 EP4	4200	141	7.6	0.054	14.0
Enercon (2017)	E-44	900	44	2.4	0.055	15.5
IMPSA	IWP 85	2000	85	5	0.059	12.0
Enercon (2017)	E126 EP4	4200	127	7.6	0.060	14.0
NEPC India Ltd	SRC 16 -55/11	55	16.6	1	0.060	11.0
IMPSA	IWP 83	2100	83	5.2	0.063	13.5
Aeolos	H-500W	0.500	1.7	0.06	0.066	12.0
Enercon (2017)	E-82	2300	82	5.4	0.066	13.5
Enercon (2017)	E-82	2000	82	5.4	0.066	12.3
Unitron Energy	UE-42	4.200	4.9	0.16	0.066	11.0
Ennera	Windera S	3.200	4.36	0.14	0.066	11.0
Enercon (2017)	E-53	800	52.9	3.6	0.068	12.5
Fortis	Montana 5kW	5.800	5	0.17	0.068	17.0
Aeolos	H-30kW	30.000	15.6	0.55	0.071	9.0
Aeolos	H-5000W	5.000	6.4	0.23	0.072	10.0
Bergey	10kW	8.900	7	0.25	0.072	11.0
Enercon (2017)	E-48	800	48	3.6	0.075	13.5
Enercon (2017)	E-70	2300	71	5.4	0.076	15.0

IMPSA	IWP 70	1500	70	5.4	0.077	13.0
IMPSA	IWP 70	1800	70	5.4	0.077	13.0
Norwin	29-Stall-200 kW	200	29.1	2.3	0.079	16.0
Norwin	29-Stall-225 kW	225	29.1	2.3	0.079	16.0
Aeolos	H-1000W	1.000	3.2	0.13	0.081	12.0
Exzeres Wind	Skystream 3.7	2.400	3.72	0.15	0.081	13.0
Aeolos	H-2000W	2.000	4	0.16	0.082	12.0
Bergey	1kW	1.000	2.5	0.11	0.086	11.0
Qingdao Windwings	FZY300	0.300	2.2	0.10	0.089	8.0
Bergey	6kW	5.500	6.2	0.28	0.091	11.0
Enercon	E126	7500	127	12	0.094	17.0
Pioneer Wincon	P250/29	250	29.6	2.8	0.095	15.0
Polaris	50kW	50.000	15.2	1.5	0.099	12.0
Kestrel	e230i 800W	0.800	2.3	0.12	0.100	12.5
NEPC India Ltd	SRC 29.8 -200/40	200	29.8	3	0.101	15.0
NEPC India Ltd	SCR 29.8 - 225/40	225	29.8	3	0.101	14.0
Wind Engineering SPA	WESPA 750/47	750	47	5	0.106	14.5
Polaris	20kW	20.000	10	0.55	0.111	10.0
Aeolos	H-3000W	3.000	4.8	0.27	0.111	12.0
Marlec	Rutland 1803	0.840	1.8	0.10	0.116	15.0
Kestrel	e400nb 3.5kW	2.500	4	0.24	0.119	11.0
Kestrel	e300i 1kW	1.000	3	0.18	0.120	10.5
Marlec	Rutland 1200	0.483	1.22	0.07	0.121	15.0
SWAY Turbine AS	SWAY ST10	10000	164	30	0.183	13.0
GE Test Eco Rotr	Eco Rotr Test	1700	100	18.3	0.183	10.0

Appendix B: Aerofoil data: ϕ280 mm rotors

Blade chord and twist

25% hub - 'adapted BEMM'			
Blade element	Chord c (m)	Twist θ_p (°)	Hub
40	0.0039	1.331	
39	0.0066	2.854	
38	0.0082	3.613	
37	0.0094	4.057	
36	0.0103	4.377	
35	0.0111	4.652	
34	0.0118	4.919	
33	0.0125	5.195	
32	0.0131	5.485	
31	0.0136	5.795	
30	0.0142	6.127	
29	0.0148	6.483	
28	0.0154	6.865	
27	0.0160	7.275	
26	0.0166	7.718	
25	0.0173	8.195	
24	0.0180	8.712	
23	0.0187	9.273	
22	0.0195	9.883	
21	0.0204	10.550	
20	0.0214	11.280	
19	0.0224	12.084	
18	0.0235	12.973	
17	0.0248	13.961	
16	0.0261	15.063	
15	0.0276	16.300	
14	0.0293	17.697	
13	0.0311	19.281	
12	0.0331	21.086	
11	0.0353	23.148	25%

20% hub - 'adapted BEMM'			
Blade element	Chord c (m)	Twist θ_p (°)	Hub
40	0.0039	1.315	
39	0.0066	2.833	
38	0.0082	3.592	
37	0.0093	4.036	
36	0.0103	4.356	
35	0.0111	4.631	
34	0.0118	4.897	
33	0.0124	5.171	
32	0.0130	5.459	
31	0.0136	5.766	
30	0.0141	6.094	
29	0.0147	6.446	
28	0.0153	6.823	
27	0.0159	7.228	
26	0.0165	7.663	
25	0.0171	8.132	
24	0.0178	8.638	
23	0.0185	9.187	
22	0.0193	9.782	
21	0.0202	10.431	
20	0.0211	11.140	
19	0.0220	11.917	
18	0.0231	12.774	
17	0.0243	13.721	
16	0.0255	14.774	
15	0.0269	15.950	
14	0.0284	17.271	
13	0.0300	18.762	
12	0.0318	20.457	
11	0.0338	22.392	25%
10	0.0358	24.610	
9	0.0379	27.157	20%

15% hub - 'adapted BEMM'			
Blade element	Chord c (m)	Twist θ_p (°)	Hub
40	0.0039	1.309	
39	0.0066	2.823	
38	0.0082	3.581	
37	0.0093	4.025	
36	0.0103	4.344	
35	0.0111	4.619	
34	0.0118	4.884	
33	0.0124	5.156	
32	0.0130	5.442	
31	0.0135	5.747	
30	0.0141	6.073	
29	0.0146	6.421	
28	0.0152	6.795	
27	0.0158	7.195	
26	0.0164	7.625	
25	0.0170	8.088	
24	0.0177	8.588	
23	0.0184	9.128	
22	0.0192	9.714	
21	0.0200	10.350	
20	0.0209	11.044	
19	0.0218	11.803	
18	0.0228	12.637	
17	0.0239	13.556	
16	0.0251	14.572	
15	0.0264	15.702	
14	0.0278	16.963	
13	0.0293	18.378	
12	0.0309	19.973	
11	0.0326	21.779	25%
10	0.0344	23.835	
9	0.0362	26.184	20%
8	0.0379	28.879	
7	0.0394	31.977	15%

10% hub - 'adapted BEMM'			
Blade element	Chord c (m)	Twist θ_p (°)	Hub
40	0.0039	1.301	
39	0.0066	2.814	
38	0.0082	3.573	
37	0.0093	4.017	
36	0.0103	4.337	
35	0.0110	4.612	
34	0.0117	4.877	
33	0.0124	5.149	
32	0.0130	5.435	
31	0.0135	5.739	
30	0.0141	6.064	
29	0.0146	6.411	
28	0.0152	6.783	
27	0.0158	7.182	
26	0.0164	7.610	
25	0.0170	8.070	
24	0.0176	8.566	
23	0.0183	9.102	
22	0.0191	9.681	
21	0.0199	10.311	
20	0.0207	10.996	
19	0.0217	11.743	
18	0.0226	12.562	
17	0.0237	13.462	
16	0.0248	14.455	
15	0.0260	15.553	
14	0.0274	16.773	
13	0.0287	18.134	
12	0.0302	19.657	
11	0.0318	21.367	25%
10	0.0333	23.295	
9	0.0349	25.473	20%
8	0.0363	27.941	
7	0.0375	30.741	15%
6	0.0382	33.921	
5	0.0379	37.521	10%

5% hub - 'standard BEMM'			
Blade element	Chord c (m)	Twist θ_p (°)	Hub
40	0.0039	1.298	
39	0.0066	2.810	
38	0.0082	3.569	
37	0.0093	4.013	
36	0.0103	4.333	
35	0.0111	4.608	
34	0.0118	4.873	
33	0.0124	5.145	
32	0.0130	5.430	
31	0.0135	5.734	
30	0.0141	6.058	
29	0.0146	6.405	
28	0.0152	6.776	
27	0.0158	7.174	
26	0.0164	7.601	
25	0.0170	8.060	
24	0.0176	8.554	
23	0.0183	9.088	
22	0.0191	9.665	
21	0.0199	10.291	
20	0.0207	10.972	
19	0.0216	11.715	
18	0.0226	12.527	
17	0.0236	13.419	
16	0.0247	14.400	
15	0.0259	15.484	
14	0.0272	16.684	
13	0.0286	18.018	
12	0.0300	19.503	
11	0.0314	21.161	25%
10	0.0329	23.011	
9	0.0343	25.076	20%
8	0.0355	27.375	
7	0.0364	29.922	15%
6	0.0367	32.720	
5	0.0360	35.752	10%
4	0.0334	38.981	
3	0.0282	42.405	5%

Airfoil performance data

Re =	2000		
alpha	CL	CD	CL/CD
-2.50	-0.1041	0.1055	-0.9868
-2.25	-0.0794	0.1031	-0.7704
-2.00	-0.0534	0.1007	-0.5301
-1.75	-0.0262	0.0985	-0.2660
-1.50	0.0016	0.0964	0.0166
-1.25	0.0298	0.0944	0.3158
-1.00	0.0579	0.0924	0.6267
-0.75	0.0855	0.0904	0.9457
-0.50	0.1126	0.0883	1.2753
-0.25	0.1395	0.0858	1.6253
0.00	0.1724	0.0830	2.0769
0.25	0.2140	0.0826	2.5895
0.50	0.2440	0.0833	2.9295
0.75	0.2684	0.0839	3.1998
1.00	0.2910	0.0845	3.4446
1.25	0.3122	0.0851	3.6678
1.50	0.3326	0.0858	3.8765
1.75	0.3522	0.0865	4.0712
2.00	0.3710	0.0873	4.2512
2.25	0.3892	0.0881	4.4192
2.50	0.4069	0.0889	4.5760
2.75	0.4241	0.0898	4.7217
3.00	0.4408	0.0908	4.8562
3.25	0.4573	0.0918	4.9826
3.50	0.4733	0.0929	5.0975
3.75	0.4890	0.0940	5.2032
4.00	0.5044	0.0952	5.2994
4.25	0.5195	0.0965	5.3862
4.50	0.5344	0.0978	5.4653
4.75	0.5489	0.0992	5.5338
5.00	0.5633	0.1007	5.5961
5.25	0.5774	0.1022	5.6486
5.50	0.5914	0.1039	5.6948
5.75	0.6051	0.1056	5.7323
6.00	0.6188	0.1074	5.7638
6.25	0.6322	0.1093	5.7867
6.50	0.6455	0.1112	5.8038
6.75	0.6587	0.1133	5.8148
7.00	0.6719	0.1154	5.8208
7.25	0.6849	0.1177	5.8205
7.50	0.6978	0.1200	5.8150
7.75	0.7106	0.1224	5.8051
8.00	0.7234	0.1249	5.7914
8.25	0.7360	0.1275	5.7725
8.50	0.7485	0.1302	5.7506
8.75	0.7609	0.1329	5.7254
9.00	0.7731	0.1358	5.6950
9.25	0.7853	0.1387	5.6615
9.50	0.7973	0.1418	5.6239
9.75	0.8092	0.1449	5.5842
10.00	0.8209	0.1481	5.5421
10.25	0.8325	0.1514	5.4987
10.50	0.8440	0.1548	5.4536
10.75	0.8550	0.1582	5.4039
11.00	0.8657	0.1618	5.3501
11.25	0.8761	0.1655	5.2927
11.50	0.8861	0.1694	5.2308
11.75	0.8957	0.1734	5.1652
12.00	0.9049	0.1776	5.0954
12.25	0.9136	0.1819	5.0228
12.50	0.9218	0.1863	4.9471
12.75	0.9296	0.1909	4.8693
13.00	0.9368	0.1956	4.7889
13.25	0.9436	0.2004	4.7076
13.50	0.9499	0.2054	4.6255
13.75	0.9558	0.2104	4.5434
14.00	0.9614	0.2155	4.4617
14.25	0.9665	0.2206	4.3806
14.50	0.9713	0.2258	4.3012
14.75	0.9756	0.2310	4.2228
15.00	0.9795	0.2362	4.1466
15.25	0.9829	0.2414	4.0722
15.50	0.9859	0.2465	4.0002
15.75	0.9885	0.2515	3.9304
16.00	0.9909	0.2565	3.8630

Re =	3000		
alpha	CL	CD	CL/CD
-2.50	-0.0216	0.0927	-0.2330
-2.25	0.0151	0.0903	0.1671
-2.00	0.0528	0.0882	0.5987
-1.75	0.0911	0.0863	1.0561
-1.50	0.1297	0.0846	1.5336
-1.25	0.1678	0.0831	2.0195
-1.00	0.2051	0.0818	2.5073
-0.75	0.2409	0.0807	2.9862
-0.50	0.2751	0.0796	3.4552
-0.25	0.3076	0.0786	3.9115
0.00	0.3383	0.0777	4.3539
0.25	0.3668	0.0771	4.7562
0.50	0.3893	0.0758	5.1332
0.75	0.4119	0.0749	5.4986
1.00	0.4371	0.0757	5.7764
1.25	0.4612	0.0765	6.0311
1.50	0.4846	0.0773	6.2699
1.75	0.5075	0.0782	6.4939
2.00	0.5297	0.0790	6.7017
2.25	0.5515	0.0800	6.8963
2.50	0.5730	0.0809	7.0802
2.75	0.5940	0.0819	7.2501
3.00	0.6147	0.0830	7.4087
3.25	0.6351	0.0841	7.5562
3.50	0.6553	0.0852	7.6931
3.75	0.6751	0.0864	7.8173
4.00	0.6948	0.0876	7.9324
4.25	0.7142	0.0889	8.0374
4.50	0.7334	0.0902	8.1317
4.75	0.7524	0.0916	8.2167
5.00	0.7713	0.0930	8.2927
5.25	0.7899	0.0945	8.3578
5.50	0.8084	0.0961	8.4147
5.75	0.8268	0.0977	8.4626
6.00	0.8450	0.0994	8.5019
6.25	0.8631	0.1012	8.5320
6.50	0.8811	0.1030	8.5552
6.75	0.8991	0.1049	8.5702
7.00	0.9169	0.1069	8.5772
7.25	0.9346	0.1090	8.5767
7.50	0.9522	0.1111	8.5683
7.75	0.9699	0.1134	8.5552
8.00	0.9874	0.1157	8.5349
8.25	1.0048	0.1181	8.5088
8.50	1.0221	0.1206	8.4758
8.75	1.0395	0.1232	8.4361
9.00	1.0569	0.1260	8.3888
9.25	1.0743	0.1289	8.3318
9.50	1.0917	0.1321	8.2673
9.75	1.1093	0.1353	8.2000
10.00	1.1269	0.1386	8.1288
10.25	1.1444	0.1421	8.0541
10.50	1.1617	0.1458	7.9705
10.75	1.1788	0.1496	7.8776
11.00	1.1957	0.1538	7.7749
11.25	1.2122	0.1583	7.6600
11.50	1.2283	0.1631	7.5333
11.75	1.2438	0.1681	7.3978
12.00	1.2586	0.1735	7.2533
12.25	1.2728	0.1792	7.1047
12.50	1.2862	0.1850	6.9524
12.75	1.2991	0.1910	6.8016
13.00	1.3114	0.1971	6.6531
13.25	1.3232	0.2033	6.5086
13.50	1.3344	0.2095	6.3691
13.75	1.3453	0.2157	6.2369
14.00	1.3556	0.2218	6.1110
14.25	1.3655	0.2279	5.9925
14.50	1.3751	0.2338	5.8810
14.75	1.3844	0.2397	5.7768
15.00	1.3935	0.2454	5.6792
15.25	1.4023	0.2510	5.5877
15.50	1.4111	0.2564	5.5029
15.75	1.4197	0.2618	5.4235
16.00	1.4282	0.2670	5.3493

Re =	4000		
alpha	CL	CD	CL/CD
-2.50	0.0277	0.0856	0.3234
-2.25	0.0696	0.0839	0.8294
-2.00	0.1115	0.0822	1.3564
-1.75	0.1534	0.0805	1.9061
-1.50	0.1947	0.0790	2.4636
-1.25	0.2345	0.0778	3.0126
-1.00	0.2723	0.0769	3.5423
-0.75	0.3079	0.0761	4.0460
-0.50	0.3415	0.0755	4.5250
-0.25	0.3731	0.0750	4.9780
0.00	0.4020	0.0746	5.3873
0.25	0.4268	0.0746	5.7227
0.50	0.4496	0.0747	6.0179
0.75	0.4709	0.0748	6.2997
1.00	0.4871	0.0737	6.6056
1.25	0.5090	0.0741	6.8719
1.50	0.5322	0.0750	7.0998
1.75	0.5548	0.0759	7.3115
2.00	0.5770	0.0768	7.5101
2.25	0.5987	0.0778	7.6944
2.50	0.6201	0.0788	7.8663
2.75	0.6411	0.0799	8.0248
3.00	0.6619	0.0810	8.1726
3.25	0.6823	0.0821	8.3086
3.50	0.7025	0.0833	8.4344
3.75	0.7224	0.0845	8.5481
4.00	0.7421	0.0858	8.6522
4.25	0.7616	0.0871	8.7470
4.50	0.7808	0.0884	8.8306
4.75	0.7999	0.0898	8.9066
5.00	0.8187	0.0913	8.9711
5.25	0.8374	0.0928	9.0286
5.50	0.8560	0.0943	9.0765
5.75	0.8744	0.0959	9.1169
6.00	0.8926	0.0976	9.1474
6.25	0.9107	0.0993	9.1703
6.50	0.9287	0.1011	9.1850
6.75	0.9466	0.1030	9.1921
7.00	0.9643	0.1049	9.1908
7.25	0.9820	0.1069	9.1836
7.50	0.9995	0.1090	9.1689
7.75	1.0169	0.1112	9.1481
8.00	1.0342	0.1134	9.1207
8.25	1.0515	0.1157	9.0858
8.50	1.0689	0.1182	9.0431
8.75	1.0863	0.1208	8.9933
9.00	1.1038	0.1236	8.9333
9.25	1.1215	0.1265	8.8663
9.50	1.1393	0.1296	8.7929
9.75	1.1572	0.1327	8.7178
10.00	1.1750	0.1361	8.6365
10.25	1.1927	0.1396	8.5437
10.50	1.2102	0.1435	8.4364
10.75	1.2274	0.1477	8.3118
11.00	1.2441	0.1523	8.1677
11.25	1.2600	0.1574	8.0046
11.50	1.2749	0.1629	7.8248
11.75	1.2888	0.1688	7.6346
12.00	1.3017	0.1750	7.4391
12.25	1.3136	0.1813	7.2439
12.50	1.3248	0.1878	7.0539
12.75	1.3352	0.1943	6.8708
13.00	1.3449	0.2008	6.6974
13.25	1.3540	0.2072	6.5338
13.50	1.3627	0.2136	6.3809
13.75	1.3710	0.2197	6.2392
14.00	1.3790	0.2258	6.1072
14.25	1.3868	0.2317	5.9846
14.50	1.3945	0.2376	5.8691
14.75	1.4020	0.2433	5.7615
15.00	1.4095	0.2489	5.6625
15.25	1.4169	0.2544	5.5705
15.50	1.4244	0.2597	5.4856
15.75	1.4319	0.2648	5.4071
16.00	1.4393	0.2698	5.3347

Re =	5000		
alpha	CL	CD	CL/CD
-2.50	0.0805	0.0811	0.9927
-2.25	0.1253	0.0789	1.5881
-2.00	0.1699	0.0770	2.2059
-1.75	0.2134	0.0755	2.8284
-1.50	0.2554	0.0742	3.4439
-1.25	0.2950	0.0732	4.0328
-1.00	0.3319	0.0724	4.5868
-0.75	0.3664	0.0718	5.1045
-0.50	0.3989	0.0713	5.5915
-0.25	0.4294	0.0711	6.0419
0.00	0.4569	0.0710	6.4316
0.25	0.4815	0.0713	6.7579
0.50	0.5044	0.0715	7.0516
0.75	0.5259	0.0719	7.3113
1.00	0.5455	0.0723	7.5481
1.25	0.5580	0.0716	7.7922
1.50	0.5806	0.0725	8.0105
1.75	0.6029	0.0734	8.2128
2.00	0.6248	0.0744	8.4001
2.25	0.6463	0.0754	8.5739
2.50	0.6674	0.0764	8.7345
2.75	0.6882	0.0775	8.8834
3.00	0.7087	0.0786	9.0188
3.25	0.7289	0.0797	9.1421
3.50	0.7489	0.0809	9.2560
3.75	0.7686	0.0821	9.3583
4.00	0.7880	0.0834	9.4496
4.25	0.8072	0.0847	9.5301
4.50	0.8262	0.0861	9.6014
4.75	0.8450	0.0874	9.6638
5.00	0.8637	0.0889	9.7176
5.25	0.8821	0.0904	9.7610
5.50	0.9003	0.0919	9.7965
5.75	0.9184	0.0935	9.8235
6.00	0.9364	0.0951	9.8423
6.25	0.9541	0.0968	9.8523
6.50	0.9718	0.0986	9.8560
6.75	0.9893	0.1004	9.8516
7.00	1.0067	0.1023	9.8407
7.25	1.0239	0.1042	9.8225
7.50	1.0410	0.1063	9.7967
7.75	1.0580	0.1084	9.7647
8.00	1.0751	0.1105	9.7268
8.25	1.0922	0.1128	9.6826
8.50	1.1095	0.1152	9.6311
8.75	1.1268	0.1177	9.5702
9.00	1.1444	0.1205	9.4995
9.25	1.1622	0.1233	9.4227
9.50	1.1803	0.1263	9.3445
9.75	1.1984	0.1294	9.2591
10.00	1.2165	0.1328	9.1611
10.25	1.2345	0.1365	9.0440
10.50	1.2522	0.1407	8.9004
10.75	1.2693	0.1454	8.7273
11.00	1.2852	0.1508	8.5220
11.25	1.2995	0.1568	8.2903
11.50	1.3123	0.1631	8.0445
11.75	1.3235	0.1698	7.7935
12.00	1.3336	0.1767	7.5455
12.25	1.3425	0.1838	7.3057
12.50	1.3505	0.1907	7.0814
12.75	1.3579	0.1976	6.8734
13.00	1.3648	0.2043	6.6817
13.25	1.3714	0.2108	6.5054
13.50	1.3779	0.2172	6.3433
13.75	1.3843	0.2235	6.1951
14.00	1.3908	0.2295	6.0601
14.25	1.3972	0.2354	5.9359
14.50	1.4037	0.2411	5.8221
14.75	1.4102	0.2467	5.7174
15.00	1.4169	0.2521	5.6215
15.25	1.4236	0.2573	5.5328
15.50	1.4304	0.2624	5.4512
15.75	1.4373	0.2673	5.3769
16.00	1.4441	0.2720	5.3098

Re =	6000		
alpha	CL	CD	CL/CD
-2.50	0.1334	0.0762	1.7500
-2.25	0.1802	0.0741	2.4309
-2.00	0.2260	0.0724	3.1237
-1.75	0.2697	0.0709	3.8045
-1.50	0.3107	0.0697	4.4558
-1.25	0.3490	0.0688	5.0705
-1.00	0.3845	0.0682	5.6403
-0.75	0.4177	0.0677	6.1699
-0.50	0.4491	0.0674	6.6642
-0.25	0.4785	0.0673	7.1110
0.00	0.5049	0.0675	7.4833
0.25	0.5297	0.0678	7.8161
0.50	0.5531	0.0682	8.1159
0.75	0.5750	0.0686	8.3868
1.00	0.5955	0.0691	8.6167
1.25	0.6118	0.0694	8.8143
1.50	0.6269	0.0696	9.0098
1.75	0.6489	0.0705	9.2029
2.00	0.6705	0.0715	9.3802
2.25	0.6917	0.0725	9.5433
2.50	0.7126	0.0735	9.6939
2.75	0.7331	0.0746	9.8297
3.00	0.7533	0.0757	9.9538
3.25	0.7733	0.0768	10.0664
3.50	0.7929	0.0780	10.1654
3.75	0.8123	0.0792	10.2537
4.00	0.8315	0.0805	10.3330
4.25	0.8504	0.0818	10.3999
4.50	0.8691	0.0831	10.4572
4.75	0.8875	0.0845	10.5042
5.00	0.9058	0.0859	10.5424
5.25	0.9238	0.0874	10.5710
5.50	0.9417	0.0889	10.5904
5.75	0.9594	0.0905	10.6023
6.00	0.9769	0.0921	10.6058
6.25	0.9942	0.0938	10.6003
6.50	1.0114	0.0955	10.5884
6.75	1.0284	0.0973	10.5683
7.00	1.0453	0.0992	10.5415
7.25	1.0619	0.1011	10.5066
7.50	1.0785	0.1031	10.4658
7.75	1.0952	0.1051	10.4206
8.00	1.1119	0.1072	10.3703
8.25	1.1288	0.1094	10.3143
8.50	1.1459	0.1118	10.2532
8.75	1.1631	0.1143	10.1803
9.00	1.1806	0.1169	10.0966
9.25	1.1985	0.1197	10.0109
9.50	1.2167	0.1226	9.9225
9.75	1.2352	0.1257	9.8258
10.00	1.2539	0.1292	9.7081
10.25	1.2726	0.1332	9.5576
10.50	1.2906	0.1379	9.3610
10.75	1.3067	0.1435	9.1040
11.00	1.3205	0.1500	8.8022
11.25	1.3316	0.1571	8.4777
11.50	1.3408	0.1644	8.1552
11.75	1.3486	0.1719	7.8457
12.00	1.3553	0.1793	7.5580
12.25	1.3611	0.1866	7.2930
12.50	1.3664	0.1938	7.0524
12.75	1.3715	0.2007	6.8346
13.00	1.3765	0.2074	6.6376
13.25	1.3815	0.2139	6.4592
13.50	1.3866	0.2202	6.2976
13.75	1.3919	0.2263	6.1510
14.00	1.3973	0.2322	6.0174
14.25	1.4030	0.2380	5.8962
14.50	1.4088	0.2435	5.7852
14.75	1.4148	0.2489	5.6838
15.00	1.4209	0.2542	5.5904
15.25	1.4273	0.2593	5.5055
15.50	1.4337	0.2642	5.4276
15.75	1.4401	0.2688	5.3577
16.00	1.4468	0.2733	5.2934

Re =	7000		
alpha	CL	CD	CL/CD
-2.50	0.1834	0.0719	2.5518
-2.25	0.2312	0.0699	3.3099
-2.00	0.2768	0.0682	4.0604
-1.75	0.3195	0.0668	4.7822
-1.50	0.3589	0.0658	5.4586
-1.25	0.3954	0.0650	6.0878
-1.00	0.4295	0.0644	6.6713
-0.75	0.4616	0.0640	7.2114
-0.50	0.4922	0.0638	7.7135
-0.25	0.5204	0.0639	8.1491
0.00	0.5465	0.0641	8.5231
0.25	0.5714	0.0645	8.8617
0.50	0.5952	0.0649	9.1724
0.75	0.6177	0.0653	9.4536
1.00	0.6385	0.0658	9.7022
1.25	0.6570	0.0664	9.8976
1.50	0.6692	0.0665	10.0601
1.75	0.6910	0.0674	10.2477
2.00	0.7124	0.0684	10.4198
2.25	0.7334	0.0694	10.5738
2.50	0.7541	0.0704	10.7162
2.75	0.7743	0.0714	10.8359
3.00	0.7945	0.0725	10.9556
3.25	0.8143	0.0736	11.0578
3.50	0.8337	0.0748	11.1442
3.75	0.8529	0.0760	11.2209
4.00	0.8717	0.0773	11.2827
4.25	0.8904	0.0785	11.3369
4.50	0.9087	0.0799	11.3772
4.75	0.9269	0.0812	11.4094
5.00	0.9447	0.0827	11.4287
5.25	0.9624	0.0841	11.4408
5.50	0.9799	0.0856	11.4434
5.75	0.9971	0.0872	11.4346
6.00	1.0142	0.0888	11.4199
6.25	1.0311	0.0905	11.3971
6.50	1.0478	0.0922	11.3657
6.75	1.0643	0.0940	11.3272
7.00	1.0806	0.0958	11.2797
7.25	1.0967	0.0977	11.2263
7.50	1.1129	0.0996	11.1692
7.75	1.1292	0.1017	11.1087
8.00	1.1457	0.1037	11.0461
8.25	1.1624	0.1059	10.9795
8.50	1.1793	0.1081	10.9093
8.75	1.1965	0.1105	10.8310
9.00	1.2139	0.1131	10.7339
9.25	1.2317	0.1159	10.6309
9.50	1.2501	0.1187	10.5289
9.75	1.2693	0.1219	10.4152
10.00	1.2890	0.1255	10.2717
10.25	1.3087	0.1300	10.0708
10.50	1.3263	0.1356	9.7810
10.75	1.3401	0.1425	9.4049
11.00	1.3502	0.1502	8.9882
11.25	1.3574	0.1582	8.5781
11.50	1.3627	0.1663	8.1967
11.75	1.3668	0.1741	7.8502
12.00	1.3703	0.1818	7.5395
12.25	1.3735	0.1891	7.2622
12.50	1.3768	0.1963	7.0152
12.75	1.3802	0.2031	6.7947
13.00	1.3838	0.2098	6.5971
13.25	1.3877	0.2162	6.4198
13.50	1.3920	0.2224	6.2604
13.75	1.3965	0.2283	6.1161
14.00	1.4014	0.2341	5.9856
14.25	1.4065	0.2398	5.8665
14.50	1.4119	0.2452	5.7584
14.75	1.4176	0.2505	5.6595
15.00	1.4220	0.2549	5.5787
15.25	1.4308	0.2599	5.5046
15.50	1.4345	0.2637	5.4407
15.75	1.4432	0.2686	5.3732
16.00	1.4495	0.2728	5.3130

Re =	8000		
alpha	CL	CD	CL/CD
-2.50	0.2280	0.0681	3.3495
-2.25	0.2757	0.0661	4.1691
-2.00	0.3204	0.0645	4.9644
-1.75	0.3616	0.0633	5.7143
-1.50	0.3992	0.0623	6.4067
-1.25	0.4341	0.0616	7.0482
-1.00	0.4669	0.0611	7.6416
-0.75	0.4983	0.0608	8.1944
-0.50	0.5280	0.0607	8.6971
-0.25	0.5554	0.0609	9.1259
0.00	0.5814	0.0612	9.5078
0.25	0.6064	0.0615	9.8554
0.50	0.6305	0.0620	10.1759
0.75	0.6536	0.0624	10.4710
1.00	0.6753	0.0629	10.7378
1.25	0.6948	0.0634	10.9555
1.50	0.7063	0.0636	11.1053
1.75	0.7280	0.0645	11.2903
2.00	0.7494	0.0654	11.4605
2.25	0.7704	0.0663	11.6129
2.50	0.7910	0.0673	11.7481
2.75	0.8113	0.0684	11.8698
3.00	0.8313	0.0694	11.9767
3.25	0.8510	0.0705	12.0692
3.50	0.8703	0.0717	12.1465
3.75	0.8894	0.0728	12.2120
4.00	0.9081	0.0741	12.2633
4.25	0.9266	0.0753	12.3038
4.50	0.9448	0.0766	12.3310
4.75	0.9627	0.0780	12.3471
5.00	0.9803	0.0794	12.3510
5.25	0.9977	0.0808	12.3447
5.50	1.0148	0.0823	12.3290
5.75	1.0317	0.0839	12.3026
6.00	1.0484	0.0855	12.2677
6.25	1.0649	0.0871	12.2248
6.50	1.0812	0.0888	12.1743
6.75	1.0972	0.0906	12.1144
7.00	1.1130	0.0924	12.0455
7.25	1.1288	0.0943	11.9728
7.50	1.1446	0.0962	11.8981
7.75	1.1606	0.0982	11.8187
8.00	1.1767	0.1003	11.7377
8.25	1.1932	0.1024	11.6569
8.50	1.2101	0.1045	11.5766
8.75	1.2275	0.1068	11.4956
9.00	1.2453	0.1093	11.3976
9.25	1.2635	0.1119	11.2883
9.50	1.2828	0.1147	11.1820
9.75	1.3034	0.1178	11.0645
10.00	1.3254	0.1216	10.8988
10.25	1.3467	0.1269	10.6131
10.50	1.3624	0.1341	10.1634
10.75	1.3711	0.1424	9.6278
11.00	1.3755	0.1511	9.1008
11.25	1.3775	0.1598	8.6207
11.50	1.3786	0.1682	8.1986
11.75	1.3793	0.1762	7.8289
12.00	1.3802	0.1839	7.5068
12.25	1.3815	0.1912	7.2243
12.50	1.3833	0.1983	6.9758
12.75	1.3855	0.2051	6.7552
13.00	1.3883	0.2117	6.5594
13.25	1.3905	0.2175	6.3928
13.50	1.3943	0.2224	6.2691
13.75	1.3991	0.2272	6.1577
14.00	1.4043	0.2321	6.0499
14.25	1.4099	0.2370	5.9489
14.50	1.4163	0.2419	5.8554
14.75	1.4245	0.2470	5.7667
15.00	1.4272	0.2514	5.6770
15.25	1.4360	0.2565	5.5980
15.50	1.4398	0.2607	5.5220
15.75	1.4456	0.2652	5.4506
16.00	1.4523	0.2698	5.3833

Re =	9000		
alpha	CL	CD	CL/CD
-2.50	0.2661	0.0648	4.1052
-2.25	0.3133	0.0630	4.9762
-2.00	0.3566	0.0615	5.8021
-1.75	0.3961	0.0603	6.5699
-1.50	0.4323	0.0594	7.2790
-1.25	0.4660	0.0588	7.9319
-1.00	0.4978	0.0583	8.5342
-0.75	0.5284	0.0581	9.0947
-0.50	0.5574	0.0581	9.5955
-0.25	0.5845	0.0583	10.0274
0.00	0.6104	0.0586	10.4182
0.25	0.6355	0.0590	10.7767
0.50	0.6598	0.0594	11.1059
0.75	0.6833	0.0599	11.4112
1.00	0.7058	0.0604	11.6951
1.25	0.7261	0.0608	11.9464
1.50	0.7407	0.0612	12.1128
1.75	0.7597	0.0618	12.2869
2.00	0.7812	0.0627	12.4593
2.25	0.8023	0.0636	12.6128
2.50	0.8230	0.0646	12.7498
2.75	0.8434	0.0655	12.8685
3.00	0.8634	0.0666	12.9718
3.25	0.8831	0.0676	13.0597
3.50	0.9025	0.0687	13.1330
3.75	0.9216	0.0699	13.1921
4.00	0.9403	0.0710	13.2362
4.25	0.9587	0.0723	13.2655
4.50	0.9769	0.0736	13.2821
4.75	0.9947	0.0749	13.2857
5.00	1.0122	0.0762	13.2765
5.25	1.0295	0.0777	13.2565
5.50	1.0464	0.0791	13.2238
5.75	1.0632	0.0807	13.1829
6.00	1.0796	0.0822	13.1290
6.25	1.0958	0.0839	13.0670
6.50	1.1117	0.0856	12.9932
6.75	1.1273	0.0873	12.9085
7.00	1.1427	0.0892	12.8148
7.25	1.1581	0.0911	12.7194
7.50	1.1737	0.0930	12.6231
7.75	1.1894	0.0949	12.5279
8.00	1.2054	0.0970	12.4332
8.25	1.2218	0.0990	12.3414
8.50	1.2387	0.1011	12.2534
8.75	1.2564	0.1032	12.1709
9.00	1.2751	0.1055	12.0874
9.25	1.2947	0.1079	11.9957
9.50	1.3158	0.1105	11.9034
9.75	1.3400	0.1136	11.7947
10.00	1.3674	0.1181	11.5773
10.25	1.3885	0.1253	11.0841
10.50	1.3965	0.1341	10.4131
10.75	1.3969	0.1433	9.7454
11.00	1.3944	0.1526	9.1394
11.25	1.3915	0.1615	8.6150
11.50	1.3891	0.1700	8.1712
11.75	1.3874	0.1781	7.7922
12.00	1.3865	0.1857	7.4659
12.25	1.3844	0.1922	7.2048
12.50	1.3884	0.1972	7.0391
12.75	1.3908	0.2026	6.8661
13.00	1.3963	0.2076	6.7259
13.25	1.3992	0.2129	6.5721
13.50	1.4030	0.2181	6.4319
13.75	1.4076	0.2233	6.3048
14.00	1.4126	0.2283	6.1866
14.25	1.4176	0.2334	6.0735
14.50	1.4226	0.2385	5.9652
14.75	1.4276	0.2436	5.8615
15.00	1.4326	0.2486	5.7620
15.25	1.4367	0.2535	5.6686
15.50	1.4419	0.2581	5.5857
15.75	1.4497	0.2631	5.5103
16.00	1.4569	0.2679	5.4386

Re =	10000		
alpha	CL	CD	CL/CD
-2.50	0.2979	0.0621	4.8002
-2.25	0.3443	0.0603	5.7126
-2.00	0.3862	0.0589	6.5613
-1.75	0.4243	0.0578	7.3459
-1.50	0.4593	0.0569	8.0664
-1.25	0.4921	0.0564	8.7314
-1.00	0.5234	0.0560	9.3464
-0.75	0.5534	0.0558	9.9122
-0.50	0.5817	0.0559	10.4098
-0.25	0.6086	0.0561	10.8485
0.00	0.6345	0.0564	11.2480
0.25	0.6597	0.0568	11.6165
0.50	0.6841	0.0572	11.9556
0.75	0.7080	0.0577	12.2746
1.00	0.7310	0.0582	12.5688
1.25	0.7526	0.0586	12.8452
1.50	0.7702	0.0590	13.0542
1.75	0.7867	0.0595	13.2196
2.00	0.8083	0.0603	13.3958
2.25	0.8295	0.0612	13.5517
2.50	0.8504	0.0621	13.6918
2.75	0.8709	0.0631	13.8128
3.00	0.8911	0.0640	13.9169
3.25	0.9109	0.0650	14.0052
3.50	0.9304	0.0661	14.0756
3.75	0.9496	0.0672	14.1310
4.00	0.9684	0.0683	14.1703
4.25	0.9870	0.0695	14.1953
4.50	1.0052	0.0708	14.2058
4.75	1.0230	0.0720	14.2004
5.00	1.0406	0.0734	14.1829
5.25	1.0578	0.0748	14.1512
5.50	1.0747	0.0762	14.1037
5.75	1.0913	0.0777	14.0450
6.00	1.1076	0.0793	13.9743
6.25	1.1236	0.0809	13.8905
6.50	1.1393	0.0826	13.7980
6.75	1.1548	0.0843	13.6954
7.00	1.1701	0.0861	13.5869
7.25	1.1854	0.0880	13.4750
7.50	1.2008	0.0899	13.3645
7.75	1.2164	0.0918	13.2549
8.00	1.2324	0.0937	13.1498
8.25	1.2488	0.0957	13.0477
8.50	1.2658	0.0977	12.9547
8.75	1.2838	0.0998	12.8702
9.00	1.3034	0.1019	12.7947
9.25	1.3246	0.1041	12.7243
9.50	1.3495	0.1066	12.6654
9.75	1.3827	0.1099	12.5837
10.00	1.4161	0.1167	12.1335
10.25	1.4258	0.1260	11.3159
10.50	1.4228	0.1355	10.5019
10.75	1.4154	0.1449	9.7681
11.00	1.4073	0.1542	9.1259
11.25	1.4009	0.1629	8.5987
11.50	1.4005	0.1686	8.3091
11.75	1.4018	0.1740	8.0563
12.00	1.3984	0.1804	7.7521
12.25	1.3975	0.1862	7.5042
12.50	1.4019	0.1916	7.3176
12.75	1.4027	0.1974	7.1052
13.00	1.4044	0.2031	6.9155
13.25	1.4080	0.2087	6.7481
13.50	1.4062	0.2145	6.5563
13.75	1.4104	0.2198	6.4176
14.00	1.4168	0.2251	6.2952
14.25	1.4177	0.2305	6.1516
14.50	1.4223	0.2358	6.0331
14.75	1.4282	0.2409	5.9291
15.00	1.4318	0.2458	5.8248
15.25	1.4408	0.2510	5.7407
15.50	1.4450	0.2558	5.6483
15.75	1.4505	0.2607	5.5639
16.00	1.4569	0.2656	5.4847

Re =	11000		
alpha	CL	CD	CL/CD
-2.50	0.3245	0.0597	5.4346
-2.25	0.3697	0.0580	6.3741
-2.00	0.4105	0.0567	7.2462
-1.75	0.4475	0.0556	8.0442
-1.50	0.4816	0.0549	8.7771
-1.25	0.5138	0.0544	9.4535
-1.00	0.5446	0.0540	10.0796
-0.75	0.5743	0.0539	10.6529
-0.50	0.6021	0.0540	11.1500
-0.25	0.6288	0.0542	11.5972
0.00	0.6547	0.0545	12.0062
0.25	0.6799	0.0549	12.3821
0.50	0.7044	0.0553	12.7309
0.75	0.7285	0.0558	13.0579
1.00	0.7519	0.0563	13.3624
1.25	0.7744	0.0567	13.6530
1.50	0.7938	0.0571	13.9117
1.75	0.8097	0.0575	14.0817
2.00	0.8314	0.0583	14.2632
2.25	0.8528	0.0591	14.4249
2.50	0.8739	0.0600	14.5699
2.75	0.8946	0.0609	14.6945
3.00	0.9149	0.0618	14.8018
3.25	0.9349	0.0628	14.8893
3.50	0.9546	0.0638	14.9624
3.75	0.9738	0.0649	15.0104
4.00	0.9930	0.0660	15.0569
4.25	1.0116	0.0671	15.0783
4.50	1.0300	0.0683	15.0849
4.75	1.0480	0.0695	15.0748
5.00	1.0656	0.0708	15.0466
5.25	1.0829	0.0722	15.0048
5.50	1.0999	0.0736	14.9504
5.75	1.1166	0.0750	14.8820
6.00	1.1329	0.0766	14.7995
6.25	1.1490	0.0781	14.7063
6.50	1.1647	0.0798	14.6007
6.75	1.1801	0.0815	14.4833
7.00	1.1954	0.0832	14.3609
7.25	1.2106	0.0851	14.2340
7.50	1.2259	0.0869	14.1086
7.75	1.2415	0.0888	13.9872
8.00	1.2574	0.0907	13.8694
8.25	1.2738	0.0926	13.7589
8.50	1.2911	0.0945	13.6610
8.75	1.3098	0.0964	13.5815
9.00	1.3307	0.0984	13.5247
9.25	1.3549	0.1004	13.4937
9.50	1.3887	0.1027	13.5219
9.75	1.4433	0.1087	13.2766
10.00	1.4586	0.1186	12.3016
10.25	1.4526	0.1277	11.3733
10.50	1.4573	0.1317	11.0678
10.75	1.4537	0.1374	10.5801
11.00	1.4501	0.1431	10.1313
11.25	1.4332	0.1516	9.4538
11.50	1.4261	0.1587	8.9856
11.75	1.4207	0.1657	8.5719
12.00	1.4169	0.1726	8.2077
12.25	1.4087	0.1805	7.8053
12.50	1.4076	0.1869	7.5309
12.75	1.4084	0.1930	7.2978
13.00	1.4106	0.1988	7.0959
13.25	1.4078	0.2053	6.8573
13.50	1.4122	0.2109	6.6957
13.75	1.4122	0.2169	6.5099
14.00	1.4182	0.2223	6.3808
14.25	1.4191	0.2278	6.2293
14.50	1.4268	0.2330	6.1247
14.75	1.4291	0.2383	5.9963
15.00	1.4330	0.2436	5.8833
15.25	1.4381	0.2488	5.7811
15.50	1.4438	0.2538	5.6894
15.75	1.4512	0.2588	5.6083
16.00	1.4590	0.2638	5.5311

Re =	12000		
alpha	CL	CD	CL/CD
-2.50	0.3468	0.0577	6.0114
-2.25	0.3910	0.0561	6.9759
-2.00	0.4306	0.0548	7.8620
-1.75	0.4667	0.0538	8.6747
-1.50	0.5002	0.0531	9.4200
-1.25	0.5320	0.0526	10.1083
-1.00	0.5625	0.0524	10.7429
-0.75	0.5918	0.0523	11.3198
-0.50	0.6194	0.0524	11.8229
-0.25	0.6460	0.0526	12.2790
0.00	0.6718	0.0529	12.6946
0.25	0.6970	0.0533	13.0794
0.50	0.7217	0.0537	13.4395
0.75	0.7459	0.0542	13.7747
1.00	0.7696	0.0546	14.0875
1.25	0.7926	0.0551	14.3874
1.50	0.8139	0.0555	14.6781
1.75	0.8294	0.0558	14.8771
2.00	0.8513	0.0565	15.0646
2.25	0.8729	0.0573	15.2339
2.50	0.8941	0.0581	15.3810
2.75	0.9150	0.0590	15.5137
3.00	0.9356	0.0599	15.6246
3.25	0.9558	0.0608	15.7178
3.50	0.9757	0.0618	15.7931
3.75	0.9952	0.0628	15.8497
4.00	1.0144	0.0639	15.8872
4.25	1.0333	0.0650	15.9092
4.50	1.0518	0.0661	15.9123
4.75	1.0700	0.0673	15.8990
5.00	1.0878	0.0685	15.8710
5.25	1.1053	0.0698	15.8262
5.50	1.1225	0.0712	15.7654
5.75	1.1393	0.0726	15.6907
6.00	1.1557	0.0741	15.6007
6.25	1.1718	0.0756	15.4959
6.50	1.1875	0.0772	15.3781
6.75	1.2029	0.0789	15.2497
7.00	1.2182	0.0806	15.1160
7.25	1.2335	0.0824	14.9787
7.50	1.2489	0.0841	14.8431
7.75	1.2644	0.0860	14.7092
8.00	1.2804	0.0878	14.5831
8.25	1.2971	0.0897	14.4669
8.50	1.3149	0.0915	14.3705
8.75	1.3346	0.0933	14.3029
9.00	1.3575	0.0951	14.2790
9.25	1.3872	0.0968	14.3247
9.50	1.4620	0.1011	14.4667
9.75	1.4737	0.1064	13.9023
10.00	1.4855	0.1118	13.3380
10.25	1.4972	0.1172	12.7737
10.50	1.4876	0.1233	12.0610
10.75	1.4844	0.1289	11.5141
11.00	1.4761	0.1354	10.9050
11.25	1.4601	0.1431	10.2005
11.50	1.4532	0.1498	9.6996
11.75	1.4392	0.1581	9.1031
12.00	1.4273	0.1665	8.5739
12.25	1.4189	0.1746	8.1275
12.50	1.4172	0.1814	7.8108
12.75	1.4119	0.1892	7.4637
13.00	1.4147	0.1952	7.2486
13.25	1.4115	0.2022	6.9824
13.50	1.4160	0.2076	6.8198
13.75	1.4147	0.2140	6.6111
14.00	1.4168	0.2198	6.4459
14.25	1.4231	0.2252	6.3187
14.50	1.4253	0.2310	6.1704
14.75	1.4285	0.2365	6.0409
15.00	1.4332	0.2417	5.9297
15.25	1.4418	0.2468	5.8429
15.50	1.4461	0.2519	5.7417
15.75	1.4513	0.2569	5.6502
16.00	1.4574	0.2618	5.5662

Re =	13000		
alpha	CL	CD	CL/CD
-2.50	0.3658	0.0559	6.5391
-2.25	0.4089	0.0544	7.5221
-2.00	0.4476	0.0531	8.4230
-1.75	0.4829	0.0522	9.2474
-1.50	0.5160	0.0516	10.0058
-1.25	0.5475	0.0511	10.7059
-1.00	0.5778	0.0509	11.3494
-0.75	0.6068	0.0509	11.9308
-0.50	0.6343	0.0510	12.4397
-0.25	0.6608	0.0512	12.9037
0.00	0.6866	0.0515	13.3295
0.25	0.7118	0.0519	13.7228
0.50	0.7365	0.0523	14.0876
0.75	0.7608	0.0527	14.4310
1.00	0.7847	0.0532	14.7528
1.25	0.8081	0.0537	15.0596
1.50	0.8306	0.0541	15.3644
1.75	0.8465	0.0542	15.6123
2.00	0.8686	0.0550	15.8071
2.25	0.8904	0.0557	15.9828
2.50	0.9118	0.0565	16.1381
2.75	0.9329	0.0573	16.2753
3.00	0.9536	0.0582	16.3905
3.25	0.9741	0.0591	16.4878
3.50	0.9942	0.0600	16.5672
3.75	1.0139	0.0610	16.6268
4.00	1.0334	0.0620	16.6677
4.25	1.0524	0.0631	16.6889
4.50	1.0712	0.0642	16.6958
4.75	1.0895	0.0653	16.6820
5.00	1.1076	0.0665	16.6531
5.25	1.1252	0.0678	16.6057
5.50	1.1425	0.0691	16.5412
5.75	1.1594	0.0704	16.4594
6.00	1.1760	0.0719	16.3652
6.25	1.1922	0.0734	16.2536
6.50	1.2080	0.0749	16.1282
6.75	1.2236	0.0765	15.9927
7.00	1.2390	0.0782	15.8501
7.25	1.2544	0.0799	15.7055
7.50	1.2699	0.0816	15.5606
7.75	1.2857	0.0834	15.4198
8.00	1.3019	0.0852	15.2877
8.25	1.3189	0.0869	15.1702
8.50	1.3373	0.0887	15.0784
8.75	1.3581	0.0904	15.0299
9.00	1.3840	0.0919	15.0549
9.25	1.4339	0.0934	15.3457
9.50	1.4579	0.0984	14.8706
9.75	1.4819	0.1033	14.3954
10.00	1.5059	0.1082	13.9203
10.25	1.5044	0.1134	13.2675
10.50	1.5038	0.1186	12.6753
10.75	1.4976	0.1245	12.0251
11.00	1.4919	0.1305	11.4296
11.25	1.4769	0.1377	10.7224
11.50	1.4630	0.1452	10.0744
11.75	1.4572	0.1517	9.6045
12.00	1.4443	0.1599	9.0348
12.25	1.4332	0.1682	8.5218
12.50	1.4242	0.1766	8.0655
12.75	1.4177	0.1849	7.6686
13.00	1.4141	0.1924	7.3498
13.25	1.4173	0.1983	7.1480
13.50	1.4153	0.2053	6.8935
13.75	1.4155	0.2118	6.6826
14.00	1.4180	0.2178	6.5115
14.25	1.4234	0.2232	6.3787
14.50	1.4252	0.2290	6.2239
14.75	1.4285	0.2345	6.0914
15.00	1.4337	0.2398	5.9787
15.25	1.4407	0.2450	5.8815
15.50	1.4477	0.2503	5.7843
15.75	1.4533	0.2555	5.6890
16.00	1.4591	0.2605	5.6009

Re =	14000		
alpha	CL	CD	CL/CD
-2.50	0.3822	0.0544	7.0244
-2.25	0.4244	0.0529	8.0272
-2.00	0.4622	0.0517	8.9383
-1.75	0.4969	0.0508	9.7738
-1.50	0.5296	0.0502	10.5456
-1.25	0.5609	0.0498	11.2563
-1.00	0.5910	0.0496	11.9081
-0.75	0.6198	0.0496	12.4934
-0.50	0.6472	0.0498	13.0090
-0.25	0.6737	0.0500	13.4821
0.00	0.6995	0.0503	13.9149
0.25	0.7247	0.0506	14.3165
0.50	0.7495	0.0510	14.6903
0.75	0.7738	0.0515	15.0398
1.00	0.7978	0.0519	15.3689
1.25	0.8215	0.0524	15.6835
1.50	0.8446	0.0528	15.9902
1.75	0.8641	0.0530	16.3038
2.00	0.8837	0.0536	16.4993
2.25	0.9057	0.0543	16.6826
2.50	0.9272	0.0551	16.8398
2.75	0.9485	0.0559	16.9830
3.00	0.9695	0.0567	17.1048
3.25	0.9901	0.0575	17.2072
3.50	1.0104	0.0584	17.2895
3.75	1.0304	0.0594	17.3556
4.00	1.0500	0.0604	17.3985
4.25	1.0692	0.0614	17.4157
4.50	1.0883	0.0624	17.4323
4.75	1.1068	0.0635	17.4217
5.00	1.1250	0.0647	17.3906
5.25	1.1429	0.0659	17.3429
5.50	1.1604	0.0672	17.2781
5.75	1.1775	0.0685	17.1948
6.00	1.1942	0.0699	17.0942
6.25	1.2105	0.0713	16.9776
6.50	1.2265	0.0728	16.8475
6.75	1.2424	0.0744	16.7079
7.00	1.2581	0.0760	16.5605
7.25	1.2737	0.0776	16.4115
7.50	1.2894	0.0793	16.2598
7.75	1.3053	0.0810	16.1128
8.00	1.3218	0.0827	15.9773
8.25	1.3391	0.0844	15.8605
8.50	1.3581	0.0861	15.7772
8.75	1.3806	0.0876	15.7585
9.00	1.4122	0.0889	15.8799
9.25	1.4992	0.0927	16.1691
9.50	1.5015	0.0965	15.5531
9.75	1.5038	0.1009	14.9039
10.00	1.5067	0.1056	14.2666
10.25	1.5083	0.1107	13.6546
10.50	1.5098	0.1158	13.0425
10.75	1.5056	0.1213	12.4112
11.00	1.5016	0.1269	11.8329
11.25	1.4878	0.1337	11.1262
11.50	1.4744	0.1409	10.4679
11.75	1.4611	0.1484	9.8470
12.00	1.4482	0.1564	9.2608
12.25	1.4365	0.1647	8.7214
12.50	1.4274	0.1731	8.2456
12.75	1.4207	0.1815	7.8284
13.00	1.4172	0.1893	7.4853
13.25	1.4198	0.1954	7.2661
13.50	1.4175	0.2028	6.9914
13.75	1.4168	0.2095	6.7621
14.00	1.4183	0.2157	6.5756
14.25	1.4250	0.2208	6.4529
14.50	1.4268	0.2269	6.2877
14.75	1.4300	0.2327	6.1442
15.00	1.4340	0.2383	6.0169
15.25	1.4386	0.2437	5.9029
15.50	1.4438	0.2489	5.8003
15.75	1.4495	0.2540	5.7074
16.00	1.4555	0.2589	5.6210

Re =	15000		
alpha	CL	CD	CL/CD
-2.50	0.3966	0.0531	7.4760
-2.25	0.4379	0.0516	8.4930
-2.00	0.4749	0.0504	9.4151
-1.75	0.5091	0.0496	10.2620
-1.50	0.5415	0.0490	11.0420
-1.25	0.5726	0.0487	11.7625
-1.00	0.6026	0.0485	12.4247
-0.75	0.6313	0.0485	13.0165
-0.50	0.6586	0.0486	13.5403
-0.25	0.6851	0.0489	14.0188
0.00	0.7108	0.0492	14.4589
0.25	0.7361	0.0495	14.8707
0.50	0.7608	0.0499	15.2495
0.75	0.7852	0.0503	15.6072
1.00	0.8094	0.0508	15.9456
1.25	0.8332	0.0512	16.2639
1.50	0.8566	0.0517	16.5719
1.75	0.8787	0.0520	16.8981
2.00	0.8970	0.0523	17.1412
2.25	0.9191	0.0530	17.3317
2.50	0.9409	0.0538	17.4986
2.75	0.9624	0.0545	17.6490
3.00	0.9836	0.0553	17.7770
3.25	1.0044	0.0562	17.8846
3.50	1.0249	0.0570	17.9712
3.75	1.0450	0.0579	18.0390
4.00	1.0649	0.0589	18.0890
4.25	1.0844	0.0599	18.1186
4.50	1.1035	0.0609	18.1288
4.75	1.1222	0.0619	18.1175
5.00	1.1406	0.0631	18.0875
5.25	1.1587	0.0642	18.0427
5.50	1.1764	0.0654	17.9768
5.75	1.1937	0.0667	17.8912
6.00	1.2105	0.0681	17.7827
6.25	1.2273	0.0694	17.6743
6.50	1.2436	0.0709	17.5427
6.75	1.2596	0.0724	17.4002
7.00	1.2755	0.0739	17.2505
7.25	1.2913	0.0755	17.0943
7.50	1.3072	0.0772	16.9392
7.75	1.3233	0.0788	16.7889
8.00	1.3400	0.0805	16.6501
8.25	1.3578	0.0821	16.5364
8.50	1.3776	0.0837	16.4647
8.75	1.4024	0.0850	16.4911
9.00	1.4962	0.0869	17.2155
9.25	1.4976	0.0904	16.5682
9.50	1.4987	0.0945	15.8576
9.75	1.5016	0.0989	15.1784
10.00	1.5071	0.1035	14.5642
10.25	1.5112	0.1083	13.9525
10.50	1.5097	0.1136	13.2908
10.75	1.5082	0.1190	12.6697
11.00	1.5060	0.1245	12.1012
11.25	1.4936	0.1310	11.4041
11.50	1.4821	0.1376	10.7687
11.75	1.4774	0.1435	10.2926
12.00	1.4643	0.1510	9.6948
12.25	1.4476	0.1599	9.0526
12.50	1.4396	0.1676	8.5905
12.75	1.4336	0.1753	8.1798
13.00	1.4272	0.1836	7.7743
13.25	1.4209	0.1926	7.3771
13.50	1.4206	0.1996	7.1172
13.75	1.4196	0.2068	6.8649
14.00	1.4201	0.2135	6.6515
14.25	1.4219	0.2198	6.4679
14.50	1.4247	0.2258	6.3084
14.75	1.4286	0.2315	6.1708
15.00	1.4339	0.2369	6.0540
15.25	1.4418	0.2418	5.9618
15.50	1.4465	0.2473	5.8501
15.75	1.4519	0.2525	5.7496
16.00	1.4583	0.2577	5.6492

Appendix C: Ansys Fluent simulation settings – ϕ280 mm rotors

Fluent
Version: 3d, dp, pbns, sstkw (3d, double precision, pressure-based, SST k-omega)

Models

Model Settings

Space 3D
Time Steady
Viscous SST k-omega turbulence model
Heat Transfer Disabled
Solidification and Melting Disabled
Species Disabled
Coupled Dispersed Phase Disabled
NOx Pollutants Disabled
SOx Pollutants Disabled
Soot Disabled
Mercury Pollutants Disabled
Structure Disabled

Material Properties

Material: water (fluid)

Property Units Method Value(s)

Density kg/m3 constant 998.21
Cp (Specific Heat) j/kg-k constant 1006.43
Thermal Conductivity w/m-k constant 0.0242
Viscosity kg/m-s constant 0.001002
Molecular Weight kg/kmol constant 28.966
Thermal Expansion Coefficient 1/k constant 0
Speed of Sound m/s none #f

Cell Zone Conditions

Zones

name id type

fluiddomain 157 fluid
rotating 154 fluid

Setup Conditions

fluiddomain

Condition Value

Frame Motion? no
Reference Frame Y-Origin of Rotation-Axis (m) -2
Reference Frame Y-Component of Rotation-Axis 1
Reference Frame Z-Component of Rotation-Axis 0

rotating

Condition Value

Frame Motion? yes
Reference Frame Rotation Speed (rpm) -81
Reference Frame Y-Origin of Rotation-Axis (m) -2
Reference Frame Y-Component of Rotation-Axis 1
Reference Frame Z-Component of Rotation-Axis 0

Boundary Conditions

Zones

name id type

inlet 73 velocity-inlet
outlet 74 pressure-outlet
blade 79 wall
hub 80 wall
outerwall 81 wall
pie1 75 periodic
pie1.1 76 periodic

Setup Conditions

inlet

Condition Value

Velocity Magnitude (m/s) 0.25

outlet

Condition Value

blade

Condition Value

Wall Motion 1
Shear Boundary Condition 0
Wall Surface Roughness 0

Define wall motion relative to adjacent cell zone? no
Apply a rotational velocity to this wall? yes
Rotation Speed (rpm) -81
Y-Position of Rotation-Axis Origin (m) -2
Y-Component of Rotation-Axis Direction 1
Z-Component of Rotation-Axis Direction 0

hub

Condition Value

Wall Motion 1
Shear Boundary Condition 0
Wall Surface Roughness 0
Define wall motion relative to adjacent cell zone? no
Apply a rotational velocity to this wall? yes
Rotation Speed (rpm) -81
Y-Position of Rotation-Axis Origin (m) -2
Y-Component of Rotation-Axis Direction 1
Z-Component of Rotation-Axis Direction 0

outerwall

Condition Value

Wall Motion 0
Shear Boundary Condition 0
Wall Surface Roughness 0

pie1

Condition Value

Rotationally Periodic? yes

pie1.1

Condition Value

Rotationally Periodic? yes

Solver Settings

Equations

Equation Solved

Flow yes
Turbulence yes

Numerics

Numeric Enabled

Absolute Velocity Formulation yes

Relaxation

Variable Relaxation Factor

Density 1
Body Forces 1
Turbulent Kinetic Energy 0.75
Specific Dissipation Rate 0.75
Turbulent Viscosity 1

Linear Solver

Solver Termination Residual Reduction
Variable Type Criterion Tolerance

Flow F-Cycle 0.1
Turbulent Kinetic Energy F-Cycle 0.1
Specific Dissipation Rate F-Cycle 0.1

Pressure-Velocity Coupling

Parameter Value

Type Coupled
Pseudo Transient yes
Explicit momentum under-relaxation 0.5
Explicit pressure under-relaxation 0.5

Discretization Scheme

Variable Scheme

Pressure Second Order
Momentum Second Order Upwind
Turbulent Kinetic Energy First Order Upwind
Specific Dissipation Rate First Order Upwind

Solution Limits

Quantity Limit

Minimum Absolute Pressure 1
Maximum Absolute Pressure 5e+10
Minimum Temperature 1
Maximum Temperature 5000
Minimum Turb. Kinetic Energy 1e-14
Minimum Spec. Dissipation Rate 1e-20
Maximum Turb. Viscosity Ratio 100000

Appendix D: Samples of rotation speed data from physical testing

For physical testing, nine rotors were each tested five times (runs) at ten different resistances. This produced 450 angular velocity vs. time graphs, which were then curve fitted using an exponential decay function and *Excel Solver* to minimise the square of the deviations. A sample of these 450 graphs is provided in the following pages of this appendix and includes:

- 5% baseline rotor, resistance 10 Ω , Runs 1-5 (to show consistency between runs at the same resistance)
- 5% baseline rotor, Run 5 only, resistances 3 Ω, 5 Ω, 10 Ω, 30 Ω and 60 Ω (to show variation of data at different resistances)
- 25% adapted BEMM design rotor, Run 5 only, resistances 10 Ω, 30 Ω 60 Ω, 100 Ω and 160 Ω (to show data for the largest hub at different resistances). This rotor was stalled at the 3 Ω and 5 Ω resistances.

Peak power was occurring mostly in the resistor range of 5 Ω to 10 Ω, but shifted towards 30 Ω for the 25% hub ratio rotor.

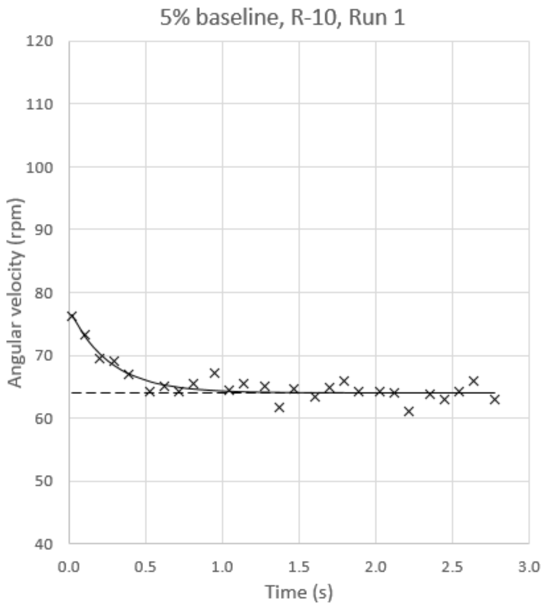

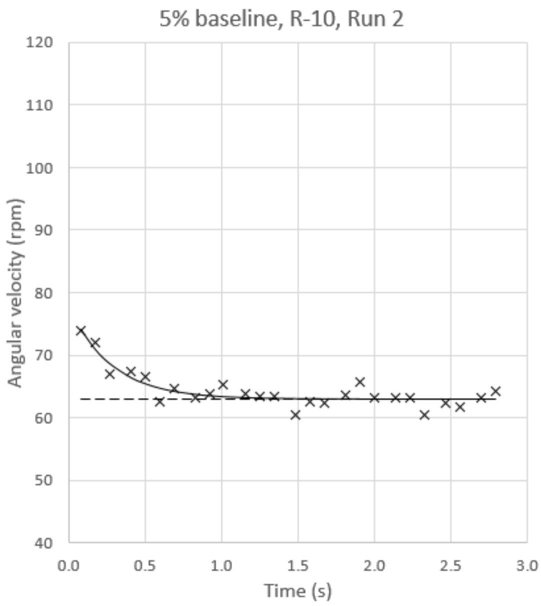

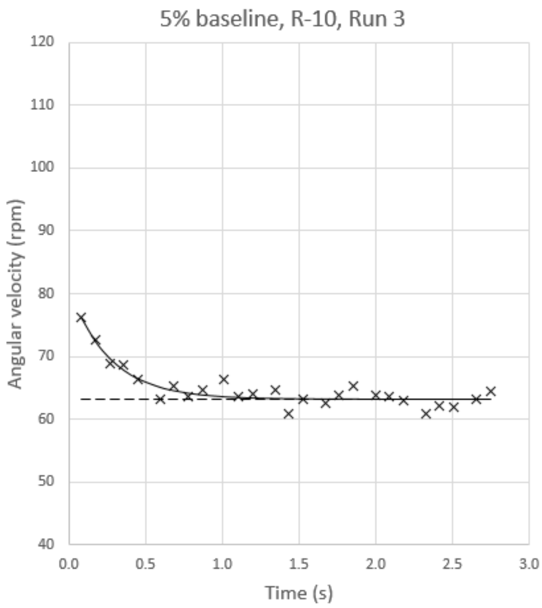

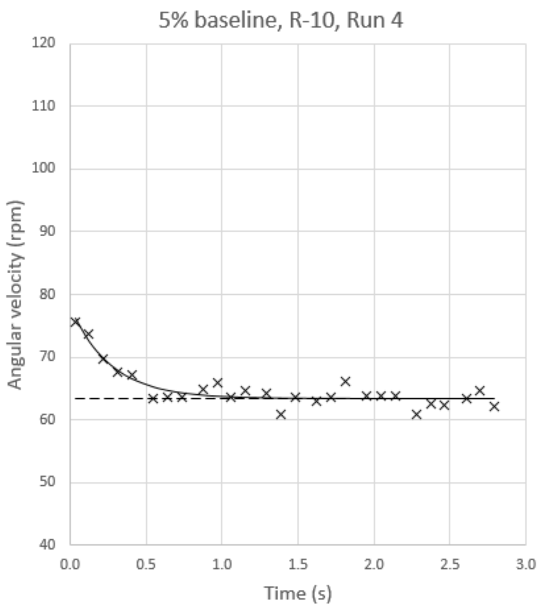

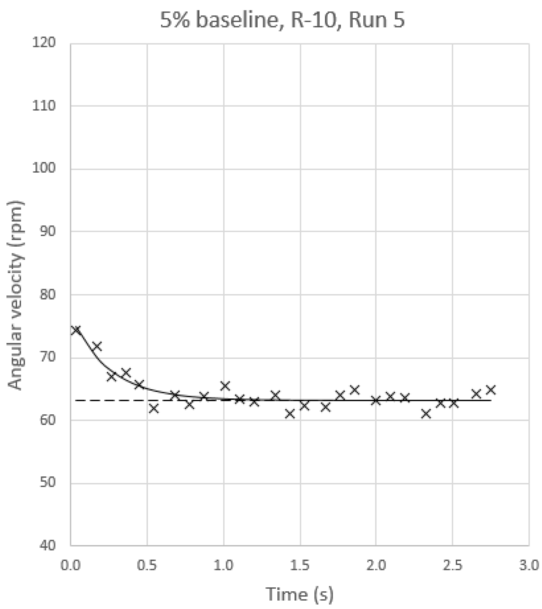

Five runs of the 5% baseline rotor at resistance 10 Ω.

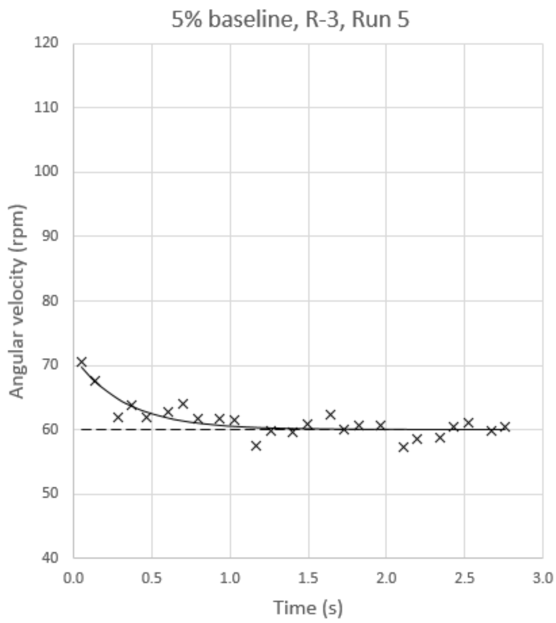

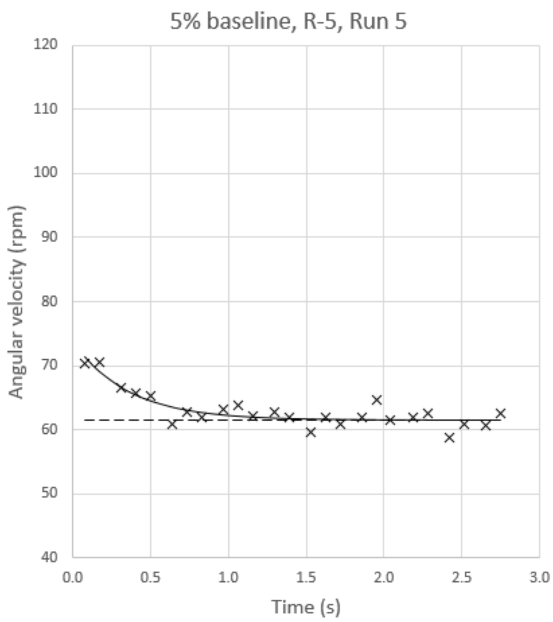

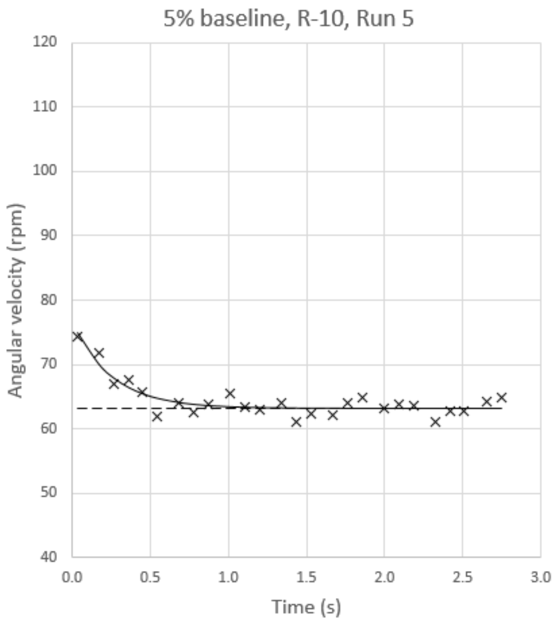

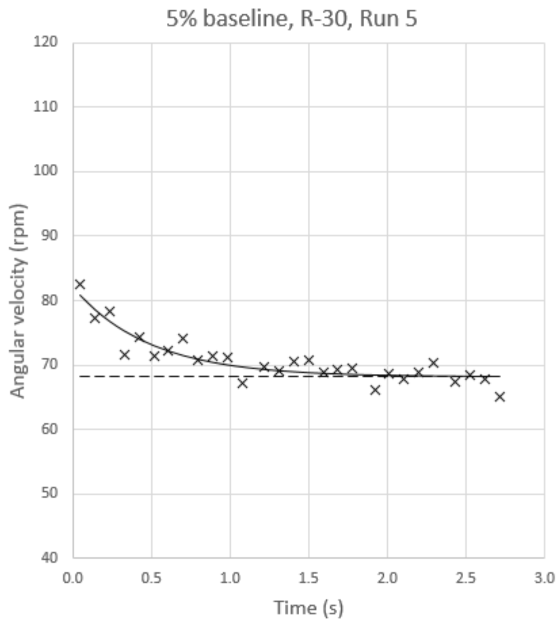

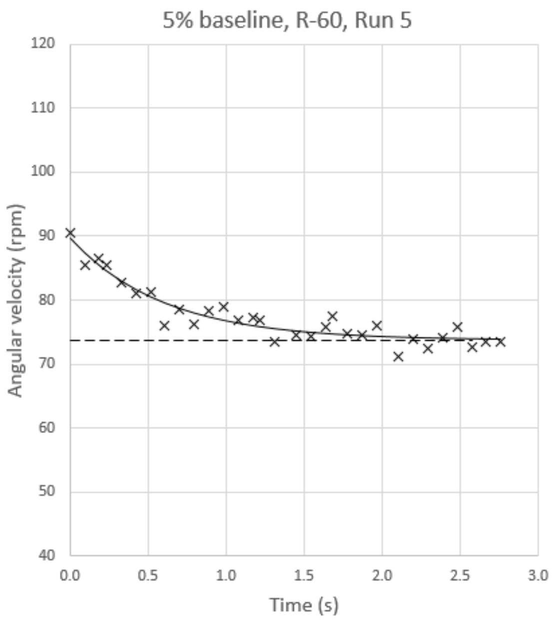

Run 5 of the 5% baseline rotor at resistances 3 Ω, 5 Ω, 10 Ω, 30 Ω and 60 Ω.

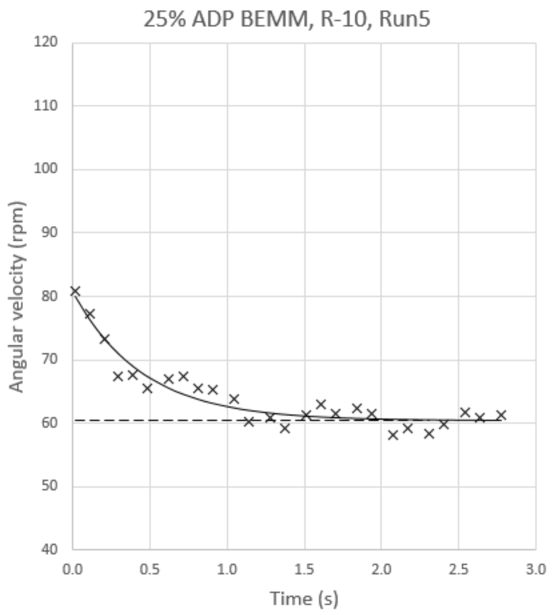

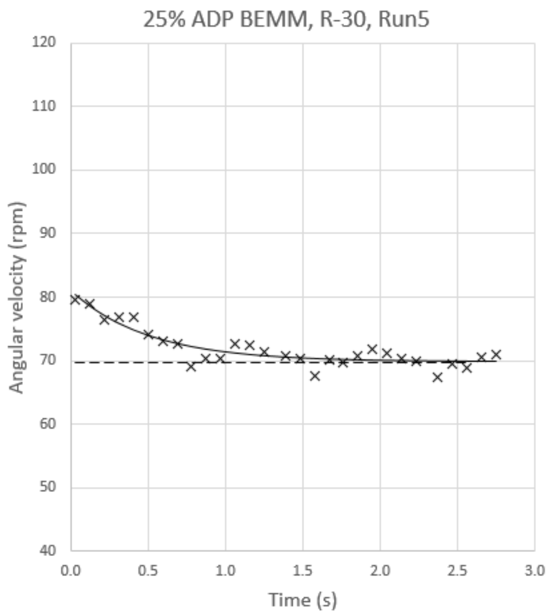

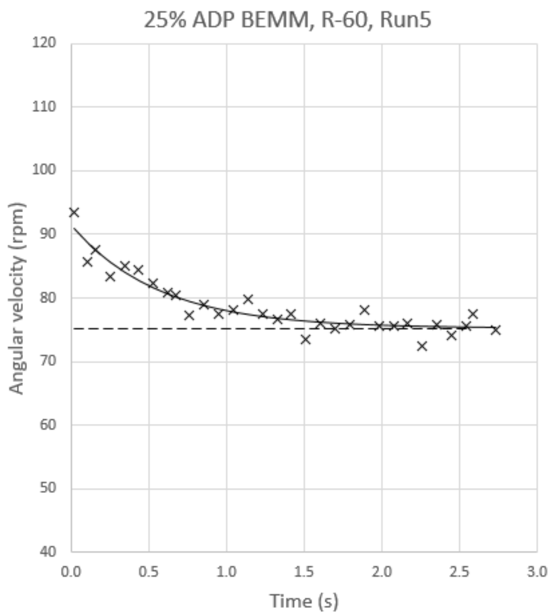

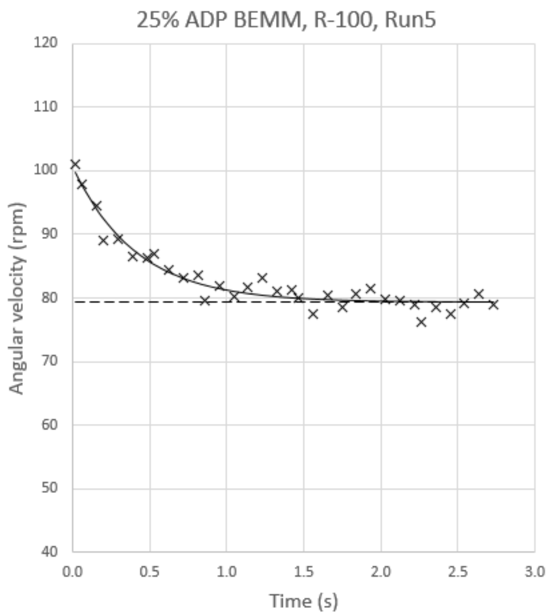

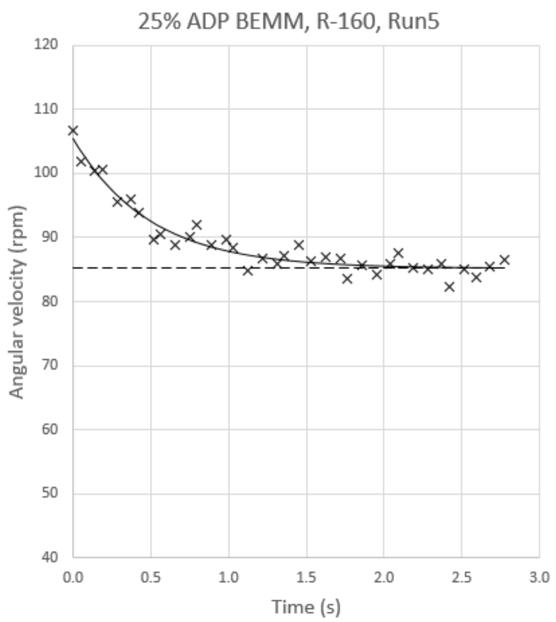

Run 5 of the 25% ADP BEMM rotor at resistances 10 Ω, 30 Ω, 60 Ω, 100 Ω and 160 Ω. Rotor was stalled at 3 Ω and 5 Ω.

Appendix E: Accuracy specifications: Brymen TBM867 multimeter

Electrical Specifications

Accuracy is ±(% reading digits + number of digits) or otherwise specified, at 23°C ± 5°C & less than 75% relative humidity.

True RMS voltage & current accuracies are specified from 5 % to 100 % of range or otherwise specified. Maximum Crest Factor < 2.1:1 at full scale & < 4.2:1 at half scale, and with frequency components within the specified frequency bandwidth for non-sinusoidal waveforms.

DC Voltage

RANGE	869s	867s
Accuracy		
500.00mV, 5.0000V,	0.02% + 2d	0.03% + 2d
50.000V	0.03% + 2d	0.04% + 2d
500.00V	0.04% + 2d	0.05% + 2d
1000.0V	0.15% + 2d	0.15% + 2d

Input Impedance: 10MΩ, 60pF nominal (80pF nominal for 500mV range)

Ohms

RANGE	869s	867s
Accuracy		
500.00Ω	0.07%+10d	0.1%+10d
5.0000kΩ	0.07%+2d	0.1%+6d
50.000kΩ	0.1%+2d	0.1%+6d
500.00kΩ	0.1%+2d	0.1%+6d
5.0000MΩ	0.3%+6d	0.4%+6d
50.000MΩ	2.0%+6d	2.0%+6d
99.99nS*	2.0%+10d	2.0%+10d

Open Circuit Voltage: < 1.3VDC (< 3VDC for 500Ω range)
*From 0% to 10% of range: Specified accuracy + 30d

Audible Continuity Tester

Audible threshold: between 20Ω and 200Ω
Response time < 100µs

Crest mode (Instantaneous Peak Hold)

Resolution: 5000 counts
Accuracy: Specified accuracy ± 100 digits for changes > 0.8ms in duration

AC Voltage

RANGE	869s	867s
Accuracy *		
20Hz ~ 45Hz		
500.00mV, 5.0000V, 50.000V	1.2% + 40d	Unspec'd
500.00V, 1000.0V	Unspec'd	
45Hz ~ 300Hz		
500.00mV	0.3% + 20d	0.8%+60d
5.0000V, 50.000V	0.4% + 30d	
500.00V, 1000.0V	0.5% + 40d	
	300Hz ~ 5kHz	300Hz ~ 1kHz
500.00mV	0.3% + 20d	0.8%+40d
5.0000V, 50.000V, 500.00V	0.4% + 40d	2.0%+60d
1000.0V	0.8% + 40d**	1.0%+40d
	5kHz ~ 20kHz	1kHz ~ 20kHz
500.00mV	0.5%+30d	1dB***
5.0000V, 50.000V	0.7%+40d	2dB***
500.00V	0.5%+40d	3dB***
1000.0V	Unspec'd	Unspec'd
20kHz ~ 100kHz		
500.00mV	2.5%+40d	Unspec'd
5.0000V, 50.000V	4.0%+40d***	
500.00V	Unspec'd	
1000.0V		

*From 5% to 10% of range: Specified accuracy + 80d
**Specified bandwidth 300Hz ~ 1kHz
***From 5% to 10% of range: Specified accuracy + 180d
From 10% to 15% of range: Specified

Appendix F: Ansys Fluent settings – Case Study - ϕ30 m rotors

Fluent
Version: 3d, sp, pbns, sstkw (3d, single precision, pressure-based, SST k-omega)

Models

Model Settings

Space 3D
Time Steady
Viscous SST k-omega turbulence model
Heat Transfer Disabled
Solidification and Melting Disabled
Species Disabled
Coupled Dispersed Phase Disabled
NOx Pollutants Disabled
SOx Pollutants Disabled
Soot Disabled
Mercury Pollutants Disabled
Structure Disabled

Material Properties

Material: air (fluid)

Property Units Method Value(s)

Density kg/m3 constant 1.2041
Cp (Specific Heat) j/kg-k constant 1006.43
Thermal Conductivity w/m-k constant 0.0242
Viscosity kg/m-s constant 1.8134e-05
Molecular Weight kg/kmol constant 28.966
Thermal Expansion Coefficient 1/k constant 0
Speed of Sound m/s none #f

Cell Zone Conditions

Zones

name id type

outerdomain 106 fluid
innerdomain 102 fluid

Setup Conditions

outerdomain

Condition Value

Frame Motion? no
Reference Frame Y-Origin of Rotation-Axis (m) -230
Reference Frame Y-Component of Rotation-Axis 1
Reference Frame Z-Component of Rotation-Axis 0

innerdomain

Condition Value

Frame Motion? yes
Reference Frame Rotation Speed (rpm) -47.059
Reference Frame Y-Origin of Rotation-Axis (m) -230
Reference Frame Y-Component of Rotation-Axis 1
Reference Frame Z-Component of Rotation-Axis 0

Boundary Conditions

Zones

name id type

inlet 65 velocity-inlet
outlet 66 pressure-outlet
outerwall 67 wall
blade 73 wall
hub 72 wall
pie1 68 periodic
pie1.1 69 periodic

Setup Conditions

inlet

Condition Value

Velocity Magnitude (m/s) 12

outlet

Condition Value

outerwall

Condition Value

Wall Motion 0
Shear Boundary Condition 0
Wall Surface Roughness 0

blade

<u>Condition Value</u>

Wall Motion 1
Shear Boundary Condition 0
Wall Surface Roughness 0
Define wall motion relative to adjacent cell zone? no
Apply a rotational velocity to this wall? yes
Rotation Speed (rpm) -47.059
Y-Position of Rotation-Axis Origin (m) -230
Y-Component of Rotation-Axis Direction 1
Z-Component of Rotation-Axis Direction 0

hub

<u>Condition Value</u>

Wall Motion 1
Shear Boundary Condition 0
Wall Surface Roughness 0
Define wall motion relative to adjacent cell zone? no
Apply a rotational velocity to this wall? yes
Rotation Speed (rpm) -47.059
Y-Position of Rotation-Axis Origin (m) -230
Y-Component of Rotation-Axis Direction 1
Z-Component of Rotation-Axis Direction 0

pie1

<u>Condition Value</u>

Rotationally Periodic? yes

pie1.1

<u>Condition Value</u>

Rotationally Periodic? yes

<u>Solver Settings</u>

Equations

<u>Equation Solved</u>

Flow yes
Turbulence yes

Numerics

<u>Numeric Enabled</u>

Absolute Velocity Formulation yes

Relaxation

<u>Variable Relaxation Factor</u>

Density 1
Body Forces 1
Turbulent Kinetic Energy 0.75
Specific Dissipation Rate 0.75
Turbulent Viscosity 1

Linear Solver

Solver Termination Residual Reduction
<u>Variable Type Criterion Tolerance</u>

Flow F-Cycle 0.1
Turbulent Kinetic Energy F-Cycle 0.1
Specific Dissipation Rate F-Cycle 0.1

Pressure-Velocity Coupling

<u>Parameter Value</u>

Type Coupled
Pseudo Transient yes
Explicit momentum under-relaxation 0.5
Explicit pressure under-relaxation 0.5

Discretization Scheme

<u>Variable Scheme</u>

Pressure Second Order
Momentum Second Order Upwind
Turbulent Kinetic Energy First Order Upwind
Specific Dissipation Rate First Order Upwind

Solution Limits

<u>Quantity Limit</u>

Minimum Absolute Pressure 1
Maximum Absolute Pressure 5e+10
Minimum Temperature 1
Maximum Temperature 5000
Minimum Turb. Kinetic Energy 1e-14
Minimum Spec. Dissipation Rate 1e-20
Maximum Turb. Viscosity Ratio 100000

Appendix G: NREL S830 aerofoil data: ϕ30 m rotors

<u>Chord and twist data – NREL S830, ϕ30 m rotor blades</u>

	25% hub - 'adapted BEMM'		
	Blade element	Chord c (m)	Twist θ_p (°)
	40	0.389	3.26
	39	0.685	4.11
	38	0.881	4.60
	37	1.035	5.01
	36	1.162	5.37
	35	1.271	5.72
	34	1.368	6.06
	33	1.457	6.42
	32	1.539	6.78
	31	1.617	7.16
	30	1.693	7.56
	29	1.768	7.98
	28	1.842	8.43
	27	1.917	8.91
	26	1.994	9.42
	25	2.074	9.97
	24	2.157	10.56
	23	2.243	11.20
	22	2.335	11.89
	21	2.432	12.63
	20	2.535	13.45
	19	2.645	14.35
	18	2.763	15.33
	17	2.889	16.41
	16	3.024	17.61
	15	3.168	18.94
	14	3.322	20.42
	13	3.484	22.08
	12	3.653	23.94
25%	11	3.822	26.02

	20% hub - 'adapted BEMM'		
	Blade element	Chord c (m)	Twist θ_p (°)
	40	0.388	3.24
	39	0.683	4.09
	38	0.879	4.58
	37	1.031	4.99
	36	1.158	5.34
	35	1.266	5.69
	34	1.362	6.03
	33	1.450	6.38
	32	1.531	6.74
	31	1.608	7.11
	30	1.683	7.51
	29	1.756	7.93
	28	1.828	8.37
	27	1.901	8.84
	26	1.976	9.34
	25	2.052	9.88
	24	2.132	10.46
	23	2.214	11.08
	22	2.301	11.75
	21	2.392	12.48
	20	2.489	13.27
	19	2.591	14.13
	18	2.699	15.08
	17	2.814	16.11
	16	2.935	17.25
	15	3.064	18.51
	14	3.199	19.91
	13	3.340	21.47
	12	3.485	23.22
25%	11	3.630	25.18
	10	3.770	27.38
20%	9	3.892	29.86

	15% hub - 'adapted BEMM'		
	Blade element	Chord c (m)	Twist θ_p (°)
	40	0.388	3.23
	39	0.682	4.08
	38	0.878	4.56
	37	1.030	4.97
	36	1.155	5.33
	35	1.263	5.68
	34	1.359	6.02
	33	1.446	6.36
	32	1.526	6.72
	31	1.602	7.09
	30	1.676	7.48
	29	1.748	7.89
	28	1.819	8.33
	27	1.890	8.79
	26	1.963	9.29
	25	2.038	9.82
	24	2.115	10.39
	23	2.195	11.00
	22	2.278	11.66
	21	2.366	12.37
	20	2.458	13.14
	19	2.554	13.99
	18	2.656	14.90
	17	2.763	15.91
	16	2.875	17.00
	15	2.992	18.21
	14	3.113	19.55
	13	3.237	21.03
	12	3.361	22.68
25%	11	3.481	24.51
	10	3.593	26.57
20%	9	3.686	28.85
	8	3.750	31.48
15%	7	3.764	34.37

	10% hub - 'adapted BEMM'		
	Blade element	Chord c (m)	Twist θ_p (°)
	40	0.388	3.23
	39	0.681	4.07
	38	0.877	4.56
	37	1.028	4.96
	36	1.154	5.32
	35	1.262	5.67
	34	1.357	6.01
	33	1.444	6.35
	32	1.524	6.71
	31	1.600	7.07
	30	1.673	7.47
	29	1.744	7.87
	28	1.815	8.31
	27	1.886	8.78
	26	1.957	9.27
	25	2.031	9.79
	24	2.107	10.36
	23	2.185	10.96
	22	2.267	11.61
	21	2.353	12.32
	20	2.442	13.08
	19	2.535	13.91
	18	2.633	14.81
	17	2.735	15.78
	16	2.840	16.86
	15	2.950	18.03
	14	3.061	19.32
	13	3.172	20.75
	12	3.282	22.32
25%	11	3.385	24.07
	10	3.475	26.01
20%	9	3.544	28.14
	8	3.580	30.58
15%	7	3.566	33.25
	6	3.479	36.36
10%	5	3.290	40.10

	5% hub - 'standard BEMM'		
	Blade element	Chord c (m)	Twist θ_p (°)
	40	0.387	3.22
	39	0.681	4.06
	38	0.876	4.55
	37	1.028	4.96
	36	1.153	5.32
	35	1.261	5.66
	34	1.356	6.00
	33	1.443	6.35
	32	1.523	6.70
	31	1.598	7.07
	30	1.671	7.46
	29	1.742	7.87
	28	1.813	8.30
	27	1.883	8.77
	26	1.955	9.26
	25	2.028	9.78
	24	2.103	10.34
	23	2.181	10.95
	22	2.262	11.60
	21	2.346	12.29
	20	2.435	13.05
	19	2.526	13.87
	18	2.622	14.76
	17	2.722	15.74
	16	2.825	16.79
	15	2.930	17.95
	14	3.037	19.22
	13	3.143	20.62
	12	3.245	22.16
25%	11	3.338	23.86
	10	3.415	25.73
20%	9	3.467	27.77
	8	3.481	30.01
15%	7	3.440	32.52
	6	3.320	35.34
10%	5	3.095	38.62
	4	2.733	42.92
5%	3	2.202	49.75

<u>Lift and drag coefficients – NREL S830 aerofoil</u>

Re = 1200000			
alpha	CL	CD	CL/CD
-2.50	0.3865	0.007180	53.83
-2.25	0.4121	0.007310	56.37
-2.00	0.4394	0.007320	60.03
-1.75	0.4643	0.007400	62.74
-1.50	0.4892	0.007480	65.40
-1.25	0.5159	0.007540	68.42
-1.00	0.5431	0.007570	71.74
-0.75	0.5692	0.007620	74.70
-0.50	0.5940	0.007710	77.04
-0.25	0.6239	0.007738	80.62
0.00	0.6538	0.007767	84.18
0.25	0.6800	0.007833	86.80
0.50	0.7062	0.007897	89.43
0.75	0.7313	0.007960	91.88
1.00	0.7579	0.008040	94.26
1.25	0.7847	0.008123	96.60
1.50	0.8111	0.008197	98.95
1.75	0.8363	0.008310	100.64
2.00	0.8617	0.008390	102.71
2.25	0.8888	0.008487	104.73
2.50	0.9152	0.008567	106.83
2.75	0.9408	0.008663	108.60
3.00	0.9657	0.008770	110.11
3.25	0.9916	0.008877	111.71
3.50	1.0177	0.008977	113.37
3.75	1.0435	0.009090	114.79
4.00	1.0685	0.009200	116.14
4.25	1.0934	0.009320	117.32
4.50	1.1190	0.009447	118.46
4.75	1.1442	0.009567	119.60
5.00	1.1689	0.009690	120.63
5.25	1.1939	0.009820	121.58
5.50	1.2187	0.009960	122.36
5.75	1.2438	0.010100	123.15
6.00	1.2675	0.010260	123.54
6.25	1.2875	0.010410	123.68
6.50	1.3096	0.010580	123.78
6.75	1.3310	0.010790	123.35
7.00	1.3515	0.011010	122.75
7.25	1.3740	0.011223	122.42
7.50	1.3961	0.011460	121.82
7.75	1.4156	0.011720	120.78
8.00	1.4374	0.011980	119.98
8.25	1.4557	0.012297	118.38
8.50	1.4754	0.012620	116.91
8.75	1.4904	0.013063	114.09
9.00	1.4977	0.013867	108.00
9.25	1.4870	0.015520	95.81
9.50	1.4739	0.017427	84.58
9.75	1.4635	0.019360	75.59
10.00	1.4553	0.021313	68.28
10.25	1.4490	0.023303	62.18
10.50	1.4441	0.025350	56.97
10.75	1.4418	0.027358	52.70
11.00	1.4408	0.029357	49.08
11.25	1.4413	0.031367	45.95
11.50	1.4431	0.033363	43.25
11.75	1.4457	0.035367	40.88
12.00	1.4476	0.037500	38.60
12.25	1.4510	0.039583	36.66
12.50	1.4549	0.041683	34.90
12.75	1.4591	0.043827	33.29
13.00	1.4628	0.046067	31.75
13.25	1.4686	0.048133	30.51
13.50	1.4718	0.050533	29.12
13.75	1.4776	0.052707	28.03
14.00	1.4824	0.055023	26.94
14.25	1.4856	0.057553	25.81
14.50	1.4914	0.059837	24.93
14.75	1.4947	0.062433	23.94
15.00	1.4994	0.064923	23.10
15.25	1.5038	0.067487	22.28
15.50	1.5080	0.070083	21.52
15.75	1.5112	0.072863	20.74
16.00	1.5159	0.075460	20.09

Re = 1300000			
alpha	CL	CD	CL/CD
-2.50	0.3869	0.006970	55.51
-2.25	0.4140	0.007110	58.23
-2.00	0.4404	0.007140	61.68
-1.75	0.4658	0.007190	64.78
-1.50	0.4911	0.007240	67.83
-1.25	0.5183	0.007300	71.00
-1.00	0.5448	0.007340	74.22
-0.75	0.5699	0.007420	76.81
-0.50	0.5963	0.007480	79.72
-0.25	0.6260	0.007527	83.17
0.00	0.6557	0.007573	86.58
0.25	0.6822	0.007623	89.48
0.50	0.7076	0.007707	91.81
0.75	0.7340	0.007777	94.38
1.00	0.7608	0.007840	97.04
1.25	0.7872	0.007923	99.35
1.50	0.8126	0.008020	101.33
1.75	0.8379	0.008080	103.70
2.00	0.8653	0.008180	105.78
2.25	0.8918	0.008257	108.01
2.50	0.9174	0.008363	109.69
2.75	0.9422	0.008460	111.38
3.00	0.9684	0.008577	112.91
3.25	0.9947	0.008680	114.59
3.50	1.0207	0.008770	116.39
3.75	1.0459	0.008860	118.04
4.00	1.0708	0.008993	119.07
4.25	1.0966	0.009090	120.64
4.50	1.1218	0.009220	121.67
4.75	1.1465	0.009350	122.62
5.00	1.1714	0.009477	123.61
5.25	1.1961	0.009600	124.60
5.50	1.2214	0.009740	125.40
5.75	1.2465	0.009890	126.04
6.00	1.2685	0.010020	126.59
6.25	1.2901	0.010183	126.69
6.50	1.3123	0.010350	126.79
6.75	1.3336	0.010530	126.64
7.00	1.3560	0.010750	126.14
7.25	1.3783	0.010967	125.68
7.50	1.3986	0.011200	124.87
7.75	1.4206	0.011447	124.11
8.00	1.4406	0.011733	122.78
8.25	1.4601	0.012043	121.24
8.50	1.4781	0.012407	119.14
8.75	1.4915	0.012960	115.08
9.00	1.4897	0.014163	105.18
9.25	1.4763	0.015980	92.39
9.50	1.4649	0.017843	82.10
9.75	1.4560	0.019727	73.81
10.00	1.4494	0.021613	67.06
10.25	1.4450	0.023513	61.46
10.50	1.4422	0.025430	56.71
10.75	1.4416	0.027323	52.76
11.00	1.4428	0.029190	49.43
11.25	1.4443	0.031113	46.42
11.50	1.4461	0.033107	43.68
11.75	1.4489	0.035087	41.29
12.00	1.4529	0.037033	39.23
12.25	1.4558	0.039147	37.19
12.50	1.4610	0.041123	35.53
12.75	1.4645	0.043307	33.82
13.00	1.4706	0.045297	32.47
13.25	1.4746	0.047543	31.02
13.50	1.4794	0.049747	29.74
13.75	1.4852	0.051900	28.62
14.00	1.4886	0.054350	27.39
14.25	1.4943	0.056607	26.40
14.50	1.4990	0.059010	25.40
14.75	1.5025	0.061570	24.40
15.00	1.5080	0.063943	23.58
15.25	1.5118	0.066550	22.72
15.50	1.5158	0.069180	21.91
15.75	1.5204	0.071757	21.19
16.00	1.5237	0.074537	20.44

Re = 1500000			
alpha	CL	CD	CL/CD
-2.50	0.3907	0.006640	58.84
-2.25	0.4168	0.006710	62.12
-2.00	0.4407	0.006850	64.34
-1.75	0.4680	0.006880	68.02
-1.50	0.4953	0.006910	71.68
-1.25	0.5215	0.006950	75.04
-1.00	0.5469	0.007010	78.02
-0.75	0.5744	0.007050	81.48
-0.50	0.6019	0.007090	84.89
-0.25	0.6299	0.007162	87.95
0.00	0.6579	0.007233	90.95
0.25	0.6844	0.007300	93.75
0.50	0.7114	0.007350	96.79
0.75	0.7375	0.007437	99.17
1.00	0.7631	0.007530	101.35
1.25	0.7896	0.007597	103.94
1.50	0.8160	0.007670	106.39
1.75	0.8423	0.007757	108.59
2.00	0.8684	0.007843	110.72
2.25	0.8945	0.007933	112.75
2.50	0.9204	0.008020	114.77
2.75	0.9459	0.008123	116.44
3.00	0.9724	0.008197	118.63
3.25	0.9983	0.008283	120.52
3.50	1.0239	0.008387	122.09
3.75	1.0496	0.008490	123.62
4.00	1.0742	0.008600	124.91
4.25	1.0992	0.008720	126.06
4.50	1.1248	0.008837	127.29
4.75	1.1499	0.008950	128.48
5.00	1.1750	0.009070	129.55
5.25	1.2000	0.009190	130.57
5.50	1.2250	0.009310	131.58
5.75	1.2485	0.009460	131.98
6.00	1.2704	0.009610	132.20
6.25	1.2939	0.009783	132.26
6.50	1.3140	0.009950	132.06
6.75	1.3389	0.010153	131.86
7.00	1.3602	0.010373	131.12
7.25	1.3809	0.010580	130.52
7.50	1.4043	0.010820	129.79
7.75	1.4248	0.011063	128.79
8.00	1.4443	0.011360	127.14
8.25	1.4631	0.011697	125.09
8.50	1.4769	0.012220	120.86
8.75	1.4773	0.013310	110.99
9.00	1.4662	0.014977	97.90
9.25	1.4563	0.016697	87.22
9.50	1.4484	0.018437	78.56
9.75	1.4438	0.020120	71.76
10.00	1.4415	0.021797	66.13
10.25	1.4404	0.023493	61.31
10.50	1.4397	0.025280	56.95
10.75	1.4404	0.027073	53.20
11.00	1.4422	0.028873	49.95
11.25	1.4443	0.030737	46.99
11.50	1.4471	0.032633	44.34
11.75	1.4513	0.034480	42.09
12.00	1.4547	0.036477	39.88
12.25	1.4601	0.038350	38.07
12.50	1.4649	0.040323	36.33
12.75	1.4707	0.042283	34.78
13.00	1.4758	0.044343	33.28
13.25	1.4813	0.046420	31.91
13.50	1.4869	0.048523	30.64
13.75	1.4916	0.050760	29.38
14.00	1.4972	0.052937	28.28
14.25	1.5023	0.055223	27.20
14.50	1.5066	0.057627	26.14
14.75	1.5124	0.059913	25.24
15.00	1.5168	0.062403	24.31
15.25	1.5217	0.064857	23.46
15.50	1.5262	0.067403	22.64
15.75	1.5304	0.070000	21.86
16.00	1.5344	0.072680	21.11

Re = 2000000			
alpha	CL	CD	CL/CD
-2.50	0.3970	0.006160	64.45
-2.25	0.4243	0.006200	68.44
-2.00	0.4509	0.006230	72.38
-1.75	0.4771	0.006295	75.78
-1.50	0.5032	0.006360	79.12
-1.25	0.5306	0.006400	82.91
-1.00	0.5572	0.006470	86.12
-0.75	0.5829	0.006550	88.99
-0.50	0.6097	0.006653	91.64
-0.25	0.6392	0.006653	96.07
0.00	0.6687	0.006653	100.50
0.25	0.6951	0.006727	103.33
0.50	0.7219	0.006787	106.37
0.75	0.7485	0.006857	109.17
1.00	0.7749	0.006930	111.81
1.25	0.8014	0.007000	114.48
1.50	0.8278	0.007073	117.03
1.75	0.8539	0.007163	119.20
2.00	0.8799	0.007253	121.31
2.25	0.9067	0.007323	123.81
2.50	0.9329	0.007413	125.84
2.75	0.9593	0.007487	128.13
3.00	0.9851	0.007580	129.96
3.25	1.0107	0.007683	131.55
3.50	1.0368	0.007767	133.49
3.75	1.0627	0.007853	135.32
4.00	1.0882	0.007950	136.88
4.25	1.1139	0.008040	138.54
4.50	1.1393	0.008143	139.91
4.75	1.1646	0.008247	141.22
5.00	1.1892	0.008370	142.08
5.25	1.2134	0.008500	142.75
5.50	1.2382	0.008640	143.31
5.75	1.2615	0.008793	143.46
6.00	1.2843	0.008950	143.50
6.25	1.3086	0.009130	143.33
6.50	1.3305	0.009300	143.06
6.75	1.3535	0.009490	142.62
7.00	1.3760	0.009687	142.05
7.25	1.3974	0.009910	141.01
7.50	1.4185	0.010157	139.66
7.75	1.4380	0.010470	137.34
8.00	1.4546	0.010887	133.61
8.25	1.4588	0.011818	123.43
8.50	1.4519	0.013197	110.02
8.75	1.4444	0.014690	98.33
9.00	1.4388	0.016183	88.91
9.25	1.4351	0.017677	81.19
9.50	1.4343	0.019110	75.05
9.75	1.4353	0.020533	69.90
10.00	1.4364	0.022043	65.16
10.25	1.4391	0.023537	61.14
10.50	1.4420	0.025103	57.44
10.75	1.4459	0.026683	54.19
11.00	1.4497	0.028333	51.17
11.25	1.4555	0.029917	48.65
11.50	1.4611	0.031557	46.30
11.75	1.4667	0.033277	44.07
12.00	1.4738	0.034927	42.20
12.25	1.4803	0.036667	40.37
12.50	1.4863	0.038497	38.61
12.75	1.4932	0.040293	37.06
13.00	1.4990	0.042253	35.48
13.25	1.5051	0.044217	34.04
13.50	1.5116	0.046197	32.72
13.75	1.5170	0.048327	31.39
14.00	1.5233	0.050393	30.23
14.25	1.5286	0.052613	29.05
14.50	1.5339	0.054863	27.96
14.75	1.5391	0.057177	26.92
15.00	1.5440	0.059543	25.93
15.25	1.5484	0.062027	24.96
15.50	1.5535	0.064430	24.11
15.75	1.5561	0.067180	23.16
16.00	1.5603	0.069760	22.37

Re = 2500000			
alpha	CL	CD	CL/CD
-2.50	0.4046	0.005880	68.81
-2.25	0.4310	0.005900	73.05
-2.00	0.4587	0.005920	77.48
-1.75	0.4857	0.005950	81.62
-1.50	0.5126	0.005980	85.72
-1.25	0.5383	0.006050	88.98
-1.00	0.5655	0.006100	92.70
-0.75	0.5931	0.006130	96.75
-0.50	0.6200	0.006180	100.32
-0.25	0.6487	0.006245	103.87
0.00	0.6773	0.006310	107.34
0.25	0.7045	0.006353	110.89
0.50	0.7314	0.006417	113.98
0.75	0.7581	0.006480	117.00
1.00	0.7850	0.006540	120.03
1.25	0.8110	0.006620	122.51
1.50	0.8378	0.006687	125.29
1.75	0.8644	0.006770	127.68
2.00	0.8907	0.006837	130.29
2.25	0.9172	0.006910	132.74
2.50	0.9432	0.007000	134.75
2.75	0.9695	0.007083	136.88
3.00	0.9960	0.007160	139.11
3.25	1.0219	0.007250	140.96
3.50	1.0483	0.007327	143.08
3.75	1.0743	0.007410	144.98
4.00	1.1003	0.007497	146.77
4.25	1.1255	0.007603	148.02
4.50	1.1505	0.007710	149.22
4.75	1.1755	0.007820	150.32
5.00	1.2013	0.007930	151.48
5.25	1.2260	0.008060	152.11
5.50	1.2480	0.008190	152.38
5.75	1.2730	0.008360	152.27
6.00	1.2954	0.008510	152.22
6.25	1.3196	0.008687	151.91
6.50	1.3428	0.008860	151.56
6.75	1.3650	0.009060	150.66
7.00	1.3875	0.009257	149.90
7.25	1.4077	0.009527	147.77
7.50	1.4260	0.009870	144.47
7.75	1.4398	0.010400	138.44
8.00	1.4422	0.011377	126.77
8.25	1.4356	0.012727	112.80
8.50	1.4314	0.014057	101.83
8.75	1.4278	0.015403	92.70
9.00	1.4266	0.016727	85.29
9.25	1.4269	0.018057	79.02
9.50	1.4297	0.019317	74.02
9.75	1.4327	0.020650	69.38
10.00	1.4371	0.021977	65.39
10.25	1.4417	0.023360	61.72
10.50	1.4477	0.024727	58.55
10.75	1.4544	0.026107	55.71
11.00	1.4599	0.027620	52.86
11.25	1.4676	0.029037	50.54
11.50	1.4743	0.030573	48.22
11.75	1.4825	0.032057	46.25
12.00	1.4893	0.033697	44.20
12.25	1.4970	0.035307	42.40
12.50	1.5041	0.037017	40.63
12.75	1.5103	0.038830	38.90
13.00	1.5177	0.040593	37.39
13.25	1.5236	0.042550	35.81
13.50	1.5306	0.044447	34.44
13.75	1.5359	0.046537	33.00
14.00	1.5424	0.048560	31.76
14.25	1.5477	0.050733	30.51
14.50	1.5530	0.052940	29.34
14.75	1.5589	0.055140	28.27
15.00	1.5634	0.057543	27.17
15.25	1.5673	0.060030	26.11
15.50	1.5716	0.062533	25.13
15.75	1.5754	0.065107	24.20
16.00	1.5781	0.067857	23.26

Re = 3000000			
alpha	CL	CD	CL/CD
-2.50	0.4117	0.005670	72.61
-2.25	0.4397	0.005660	77.69
-2.00	0.4668	0.005670	82.33
-1.75	0.4933	0.005720	86.24
-1.50	0.5198	0.005770	90.09
-1.25	0.5474	0.005770	94.87
-1.00	0.5743	0.005810	98.85
-0.75	0.6005	0.005880	102.13
-0.50	0.6266	0.005950	105.31
-0.25	0.6561	0.005998	109.38
0.00	0.6856	0.006047	113.38
0.25	0.7125	0.006103	116.74
0.50	0.7395	0.006153	120.18
0.75	0.7661	0.006230	122.97
1.00	0.7933	0.006283	126.25
1.25	0.8202	0.006343	129.30
1.50	0.8468	0.006407	132.18
1.75	0.8733	0.006480	134.76
2.00	0.8995	0.006560	137.12
2.25	0.9261	0.006630	139.68
2.50	0.9527	0.006700	142.19
2.75	0.9791	0.006777	144.48
3.00	1.0057	0.006853	146.74
3.25	1.0321	0.006927	149.00
3.50	1.0583	0.007007	151.04
3.75	1.0840	0.007103	152.60
4.00	1.1097	0.007190	154.34
4.25	1.1355	0.007270	156.19
4.50	1.1616	0.007370	157.61
4.75	1.1875	0.007480	158.75
5.00	1.2106	0.007610	159.08
5.25	1.2351	0.007747	159.43
5.50	1.2586	0.007880	159.72
5.75	1.2817	0.008040	159.41
6.00	1.3067	0.008200	159.35
6.25	1.3298	0.008370	158.88
6.50	1.3525	0.008540	158.37
6.75	1.3758	0.008737	157.47
7.00	1.3961	0.009010	154.95
7.25	1.4128	0.009410	150.13
7.50	1.4248	0.009987	142.67
7.75	1.4298	0.010850	131.78
8.00	1.4249	0.012117	117.60
8.25	1.4203	0.013417	105.86
8.50	1.4185	0.014653	96.81
8.75	1.4188	0.015867	89.42
9.00	1.4207	0.017057	83.29
9.25	1.4248	0.018217	78.21
9.50	1.4296	0.019397	73.70
9.75	1.4345	0.020627	69.55
10.00	1.4410	0.021843	65.97
10.25	1.4472	0.023123	62.59
10.50	1.4551	0.024360	59.73
10.75	1.4626	0.025673	56.97
11.00	1.4700	0.027050	54.35
11.25	1.4785	0.028393	52.07
11.50	1.4864	0.029837	49.82
11.75	1.4949	0.031267	47.81
12.00	1.5023	0.032837	45.75
12.25	1.5102	0.034420	43.88
12.50	1.5174	0.036107	42.02
12.75	1.5245	0.037830	40.30
13.00	1.5318	0.039580	38.70
13.25	1.5376	0.041513	37.04
13.50	1.5446	0.043387	35.60
13.75	1.5504	0.045413	34.14
14.00	1.5566	0.047447	32.81
14.25	1.5628	0.049513	31.56
14.50	1.5677	0.051750	30.29
14.75	1.5723	0.054057	29.09
15.00	1.5766	0.056457	27.93
15.25	1.5812	0.058850	26.87
15.50	1.5844	0.061467	25.78
15.75	1.5901	0.063807	24.92
16.00	1.5938	0.066433	23.99

Re = 3500000			
alpha	CL	CD	CL/CD
-2.50	0.4180	0.005500	76.00
-2.25	0.4453	0.005530	80.52
-2.00	0.4727	0.005540	85.32
-1.75	0.5002	0.005555	90.04
-1.50	0.5276	0.005570	94.72
-1.25	0.5542	0.005620	98.61
-1.00	0.5804	0.005660	102.54
-0.75	0.6075	0.005690	106.77
-0.50	0.6349	0.005710	111.19
-0.25	0.6639	0.005775	114.96
0.00	0.6928	0.005840	118.64
0.25	0.7195	0.005900	121.95
0.50	0.7463	0.005960	125.22
0.75	0.7735	0.006013	128.64
1.00	0.8005	0.006070	131.88
1.25	0.8274	0.006133	134.91
1.50	0.8540	0.006207	137.59
1.75	0.8806	0.006273	140.37
2.00	0.9074	0.006337	143.19
2.25	0.9338	0.006403	145.83
2.50	0.9605	0.006467	148.54
2.75	0.9871	0.006550	150.70
3.00	1.0136	0.006630	152.89
3.25	1.0397	0.006693	155.34
3.50	1.0658	0.006770	157.43
3.75	1.0920	0.006867	159.02
4.00	1.1184	0.006937	161.23
4.25	1.1450	0.007020	163.11
4.50	1.1706	0.007130	164.17
4.75	1.1939	0.007240	164.90
5.00	1.2195	0.007367	165.54
5.25	1.2422	0.007500	165.63
5.50	1.2661	0.007650	165.50
5.75	1.2907	0.007820	165.05
6.00	1.3141	0.007980	164.68
6.25	1.3370	0.008140	164.25
6.50	1.3604	0.008327	163.38
6.75	1.3819	0.008570	161.24
7.00	1.3985	0.008980	155.73
7.25	1.4097	0.009577	147.21
7.50	1.4146	0.010432	135.61
7.75	1.4149	0.011460	123.46
8.00	1.4118	0.012663	111.49
8.25	1.4103	0.013860	101.76
8.50	1.4120	0.014957	94.41
8.75	1.4149	0.016070	88.05
9.00	1.4189	0.017167	82.66
9.25	1.4252	0.018227	78.19
9.50	1.4316	0.019323	74.09
9.75	1.4383	0.020453	70.32
10.00	1.4458	0.021607	66.92
10.25	1.4539	0.022773	63.84
10.50	1.4627	0.023943	61.09
10.75	1.4705	0.025223	58.30
11.00	1.4801	0.026437	55.99
11.25	1.4879	0.027817	53.49
11.50	1.4974	0.029120	51.42
11.75	1.5053	0.030580	49.22
12.00	1.5130	0.032103	47.13
12.25	1.5212	0.033640	45.22
12.50	1.5282	0.035317	43.27
12.75	1.5364	0.036943	41.59
13.00	1.5423	0.038787	39.76
13.25	1.5497	0.040560	38.21
13.50	1.5560	0.042483	36.63
13.75	1.5629	0.044383	35.21
14.00	1.5689	0.046427	33.79
14.25	1.5743	0.048557	32.42
14.50	1.5786	0.050827	31.06
14.75	1.5838	0.053078	29.84
15.00	1.5882	0.055430	28.65
15.25	1.5932	0.057773	27.58
15.50	1.5982	0.060150	26.57
15.75	1.6019	0.062720	25.54
16.00	1.6078	0.065057	24.71

Re = 4000000			
alpha	CL	CD	CL/CD
-2.50	0.4213	0.005440	77.44
-2.25	0.4505	0.005390	83.58
-2.00	0.4790	0.005400	88.70
-1.75	0.5063	0.005420	93.41
-1.50	0.5336	0.005440	98.09
-1.25	0.5596	0.005510	101.56
-1.00	0.5872	0.005520	106.38
-0.75	0.6146	0.005530	111.14
-0.50	0.6412	0.005570	115.12
-0.25	0.6701	0.005633	118.96
0.00	0.6991	0.005697	122.72
0.25	0.7262	0.005740	126.51
0.50	0.7531	0.005790	130.07
0.75	0.7801	0.005847	133.43
1.00	0.8068	0.005917	136.37
1.25	0.8338	0.005977	139.51
1.50	0.8610	0.006037	142.63
1.75	0.8879	0.006110	145.31
2.00	0.9146	0.006163	148.39
2.25	0.9411	0.006233	150.98
2.50	0.9678	0.006297	153.71
2.75	0.9943	0.006380	155.85
3.00	1.0205	0.006450	158.22
3.25	1.0470	0.006523	160.50
3.50	1.0737	0.006597	162.76
3.75	1.1006	0.006680	164.76
4.00	1.1270	0.006750	166.97
4.25	1.1527	0.006840	168.52
4.50	1.1767	0.006940	169.56
4.75	1.2029	0.007070	170.14
5.00	1.2259	0.007190	170.51
5.25	1.2502	0.007330	170.56
5.50	1.2743	0.007490	170.13
5.75	1.2982	0.007657	169.55
6.00	1.3215	0.007827	168.84
6.25	1.3446	0.008003	168.00
6.50	1.3665	0.008223	166.17
6.75	1.3856	0.008547	162.12
7.00	1.3964	0.009160	152.45
7.25	1.4035	0.009903	141.72
7.50	1.4063	0.010833	129.81
7.75	1.4057	0.011920	117.93
8.00	1.4046	0.013060	107.55
8.25	1.4064	0.014130	99.54
8.50	1.4084	0.015223	92.51
8.75	1.4139	0.016227	87.14
9.00	1.4202	0.017240	82.38
9.25	1.4277	0.018233	78.30
9.50	1.4350	0.019287	74.41
9.75	1.4422	0.020400	70.70
10.00	1.4516	0.021450	67.67
10.25	1.4603	0.022577	64.68
10.50	1.4690	0.023753	61.84
10.75	1.4787	0.024913	59.35
11.00	1.4876	0.026177	56.83
11.25	1.4967	0.027460	54.50
11.50	1.5059	0.028777	52.33
11.75	1.5137	0.030243	50.05
12.00	1.5223	0.031700	48.02
12.25	1.5300	0.033267	45.99
12.50	1.5372	0.034930	44.01
12.75	1.5449	0.036580	42.23
13.00	1.5513	0.038400	40.40
13.25	1.5595	0.040083	38.91
13.50	1.5655	0.042037	37.24
13.75	1.5724	0.043933	35.79
14.00	1.5773	0.046083	34.23
14.25	1.5831	0.048177	32.86
14.50	1.5872	0.050483	31.44
14.75	1.5930	0.052650	30.26
15.00	1.5980	0.054940	29.09
15.25	1.6029	0.057297	27.98
15.50	1.6093	0.059513	27.04
15.75	1.6132	0.062070	25.99
16.00	1.6192	0.064383	25.15

Re = 4500000			
alpha	CL	CD	CL/CD
-2.50	0.4255	0.005320	79.98
-2.25	0.4550	0.005260	86.50
-2.00	0.4832	0.005290	91.34
-1.75	0.5110	0.005310	96.23
-1.50	0.5388	0.005330	101.09
-1.25	0.5665	0.005350	105.89
-1.00	0.5935	0.005390	110.11
-0.75	0.6200	0.005430	114.18
-0.50	0.6461	0.005480	117.90
-0.25	0.6756	0.005525	122.27
0.00	0.7050	0.005570	126.58
0.25	0.7318	0.005613	130.37
0.50	0.7587	0.005663	133.97
0.75	0.7854	0.005723	137.23
1.00	0.8125	0.005777	140.65
1.25	0.8397	0.005833	143.94
1.50	0.8667	0.005897	146.98
1.75	0.8938	0.005960	149.97
2.00	0.9208	0.006017	153.05
2.25	0.9474	0.006083	155.74
2.50	0.9737	0.006153	158.24
2.75	1.0001	0.006233	160.44
3.00	1.0266	0.006300	162.96
3.25	1.0536	0.006360	165.66
3.50	1.0806	0.006440	167.80
3.75	1.1072	0.006510	170.08
4.00	1.1330	0.006610	171.41
4.25	1.1576	0.006700	172.78
4.50	1.1842	0.006810	173.89
4.75	1.2078	0.006930	174.28
5.00	1.2324	0.007060	174.57
5.25	1.2567	0.007210	174.29
5.50	1.2802	0.007360	173.94
5.75	1.3042	0.007517	173.51
6.00	1.3277	0.007690	172.65
6.25	1.3492	0.007910	170.57
6.50	1.3700	0.008170	167.69
6.75	1.3840	0.008677	159.51
7.00	1.3901	0.009447	147.16
7.25	1.3943	0.010297	135.42
7.50	1.3965	0.011277	123.84
7.75	1.3981	0.012273	113.91
8.00	1.3984	0.013360	104.67
8.25	1.4037	0.014300	98.16
8.50	1.4076	0.015325	91.85
8.75	1.4142	0.016273	86.90
9.00	1.4221	0.017207	82.65
9.25	1.4302	0.018180	78.67
9.50	1.4386	0.019183	74.99
9.75	1.4479	0.020180	71.75
10.00	1.4571	0.021230	68.63
10.25	1.4658	0.022347	65.59
10.50	1.4760	0.023427	63.01
10.75	1.4852	0.024613	60.34
11.00	1.4951	0.025797	57.96
11.25	1.5042	0.027073	55.56
11.50	1.5133	0.028397	53.29
11.75	1.5214	0.029830	51.00
12.00	1.5305	0.031240	48.99
12.25	1.5373	0.032870	46.77
12.50	1.5457	0.034427	44.90
12.75	1.5528	0.036137	42.97
13.00	1.5607	0.037800	41.29
13.25	1.5680	0.039567	39.63
13.50	1.5740	0.041503	37.92
13.75	1.5801	0.043467	36.35
14.00	1.5852	0.045583	34.78
14.25	1.5908	0.047693	33.35
14.50	1.5961	0.049877	32.00
14.75	1.6028	0.051940	30.86
15.00	1.6083	0.054173	29.69
15.25	1.6137	0.056463	28.58
15.50	1.6192	0.058773	27.55
15.75	1.6242	0.061193	26.54
16.00	1.6299	0.063540	25.65

Re = 5500000			
alpha	CL	CD	CL/CD
-2.50	0.4311	0.005180	83.22
-2.25	0.4602	0.005150	89.36
-2.00	0.4893	0.005120	95.57
-1.75	0.5181	0.005130	100.99
-1.50	0.5469	0.005140	106.40
-1.25	0.5752	0.005160	111.47
-1.00	0.6024	0.005220	115.40
-0.75	0.6295	0.005260	119.68
-0.50	0.6568	0.005280	124.39
-0.25	0.6857	0.005347	128.25
0.00	0.7146	0.005413	132.00
0.25	0.7414	0.005450	136.04
0.50	0.7685	0.005487	140.07
0.75	0.7956	0.005530	143.87
1.00	0.8228	0.005580	147.46
1.25	0.8501	0.005630	150.99
1.50	0.8774	0.005673	154.66
1.75	0.9046	0.005750	157.32
2.00	0.9314	0.005810	160.32
2.25	0.9584	0.005877	163.09
2.50	0.9853	0.005937	165.97
2.75	1.0124	0.006000	168.73
3.00	1.0391	0.006057	171.56
3.25	1.0655	0.006130	173.82
3.50	1.0917	0.006200	176.08
3.75	1.1176	0.006290	177.68
4.00	1.1448	0.006370	179.72
4.25	1.1703	0.006480	180.60
4.50	1.1942	0.006600	180.94
4.75	1.2198	0.006730	181.25
5.00	1.2439	0.006860	181.32
5.25	1.2683	0.007010	180.93
5.50	1.2931	0.007153	180.76
5.75	1.3161	0.007327	179.64
6.00	1.3374	0.007560	176.91
6.25	1.3565	0.007867	172.44
6.50	1.3709	0.008360	163.99
6.75	1.3753	0.009193	149.59
7.00	1.3775	0.010100	136.39
7.25	1.3845	0.010877	127.29
7.50	1.3879	0.011797	117.65
7.75	1.3909	0.012767	108.95
8.00	1.3955	0.013703	101.83
8.25	1.4025	0.014570	96.26
8.50	1.4105	0.015447	91.31
8.75	1.4188	0.016327	86.90
9.00	1.4283	0.017210	82.99
9.25	1.4368	0.018160	79.12
9.50	1.4468	0.019090	75.79
9.75	1.4566	0.020070	72.57
10.00	1.4667	0.021077	69.59
10.25	1.4773	0.022097	66.85
10.50	1.4876	0.023173	64.19
10.75	1.4976	0.024317	61.59
11.00	1.5068	0.025550	58.98
11.25	1.5165	0.026793	56.60
11.50	1.5258	0.028110	54.28
11.75	1.5335	0.029577	51.85
12.00	1.5419	0.031043	49.67
12.25	1.5502	0.032580	47.58
12.50	1.5590	0.034107	45.71
12.75	1.5668	0.035760	43.81
13.00	1.5739	0.037500	41.97
13.25	1.5797	0.039413	40.08
13.50	1.5852	0.041413	38.28
13.75	1.5918	0.043347	36.72
14.00	1.5992	0.045260	35.33
14.25	1.6057	0.047287	33.96
14.50	1.6122	0.049353	32.67
14.75	1.6180	0.051517	31.41
15.00	1.6242	0.053683	30.26
15.25	1.6301	0.055940	29.14
15.50	1.6356	0.058270	28.07
15.75	1.6407	0.060670	27.04
16.00	1.6457	0.063117	26.07

Appendix H: Arduino coding

Linear velocity sensor

```
//Linear motion sensor - photo-interrupt module - by Howard Fawkes

volatile unsigned long StartTime;
float Period;
unsigned long PreviousStart;

void setup()
{
  Serial.begin(9600);  // Begin serial communication.
  attachInterrupt(digitalPinToInterrupt(2), PulseEvent, RISING);
}
void loop()
{
}
void PulseEvent()
{
  StartTime = micros();
  Period = (StartTime - PreviousStart) / 1000000.0000;
    if ((Period < 4000) && (Period > 0.16)) //Adjust according to expected period
  {
        //Serial.print(" Period (s): ");
        Serial.println(Period, 4);
        //delay(10);
        PreviousStart = StartTime;
  }
}
```

Angular velocity sensor

```
//Tachometer for photo-interrupt module - by Howard Fawkes

volatile unsigned long StartTime;
float Period;
unsigned long PreviousStart;
float Rpm;                  //Define as float to enable decimal places

void setup()
{
  Serial.begin(9600);  // Begin serial communication.
  attachInterrupt(digitalPinToInterrupt(2), PulseEvent, RISING);
```

```
}

void loop()
{
}

void PulseEvent()
{
  StartTime = micros();
  Period = (StartTime - PreviousStart) / 1000000.0000;
  Rpm = 60/8/((float)Period);    //Eight cutouts. Temporarily use float of Period so that the division
includes decimals of Period.
  if ((Rpm < 150) && (Rpm > 0.2))
  {
        //Serial.print("Start: ");
        //Serial.print(StartTime);
        //Serial.print(" Prev_start: ");
        //Serial.print(PreviousStart);
        //Serial.print(" Period: ");
        //Serial.print(Period, 5);
        //Serial.print(" RPM: ");
        Serial.println(Rpm, 3);
        //delay(10);
        PreviousStart = StartTime;
  }
}
```

<u>Drop-frame speed control</u>

```
//Stepper control - by Howard Fawkes

// define pins numbers
const int stepPin = 3;
const int dirPin = 4;
const int enPin = 5;
const int buttonPin = 2;     // the number of the pushbutton pin

    //Variable for calculations
    volatile unsigned long StartTime;
    volatile unsigned long FinishTime;
    float APeriod;
    float VPeriod;
    float DPeriod;
```

```
  float RPM;
  double AccDecFactor;
  double DelayA;
  double DelayD;
  float DelayADelta;
  double InversePulsesA;
  float PowerReducer;
  int buttonState = LOW;         // variable for reading the pushbutton status

  //Variables for adjustment
  const int PulsesV = 1874; //Number of pulses at constant velocity
  const int PulsesA = 290; //Number of pulses for acceleration
  const int DelayV = 791; //Delay for adjustment of constant velocity
  float DelayRatio = 3.5; //Ratio of initial delay/DelayV and final delay/DelayV
                         //(for initial startup and final rotation speed of acceleration).

void setup() {
    Serial.begin(9600);
 // Sets the two pins as Outputs
 pinMode(stepPin,OUTPUT);
 pinMode(dirPin,OUTPUT);
 pinMode(buttonPin, INPUT);  // initialize the pushbutton pin as an input:
 DelayADelta = DelayV * DelayRatio;
  }
void loop() {
digitalWrite(enPin,HIGH); // Enables driver turn-off)
buttonOn1:
 buttonState = digitalRead(buttonPin); // read the state of the pushbutton value:
 if (buttonState == LOW) {
goto buttonOn1;
 }
 digitalWrite(enPin,LOW); // Enables driver turn-on)
 digitalWrite(dirPin,HIGH); // Enables the motor to move anticlockwise (DOWNWARDS)

 // Makes pulses for acceleration (A) rotation
 for(int x = 0; x < PulsesA; x++) {
  DelayA = DelayV + DelayADelta * (PulsesA - x) / PulsesA;
  digitalWrite(stepPin,HIGH);
  delayMicroseconds(DelayA);
  digitalWrite(stepPin,LOW);
  delayMicroseconds(DelayA);
 }
```

```
// Makes pulses for constant velocity (V) rotation
//StartTime = micros();
for(int x = 0; x < PulsesV; x++) {
  digitalWrite(stepPin,HIGH);
  delayMicroseconds(DelayV);
  digitalWrite(stepPin,LOW);
  delayMicroseconds(DelayV);
}
```

Appendix I: Results - 280 mm rotor - BEMM predictions

BEMM Results - 280 mm rotors
(excluding and including expected power losses from hub streamtube deflection or 'spillage')

BEMM Results - STD design STD prediction

Hub ratio	Power (W)	Rel. power ($P/P_{5\%STDSTD}$)	Less spillage power loss (W)	Rel. power ($P/P_{5\%STDSTD}$)
5	0.19000	1.0000	0.19000	1.0000
10	0.18975	0.9987	0.18968	0.9983
15	0.18845	0.9918	0.18802	0.9896
20	0.18598	0.9788	0.18476	0.9724
25	0.18218	0.9588	0.17963	0.9454

BEMM Results - STD design ADP prediction

Hub ratio	Power (W)	Rel. power ($P/P_{5\%STDSTD}$)	Less spillage power loss (W)	Rel. power ($P/P_{5\%STDSTD}$)
5	0.19018	1.0009	0.19018	1.0009
10	0.18989	0.9994	0.18982	0.9990
15	0.18855	0.9924	0.18812	0.9901
20	0.18605	0.9792	0.18483	0.9728
25	0.18224	0.9592	0.17969	0.9457

BEMM Results - ADP design ADP prediction

Hub ratio	Power (W)	Rel. power ($P/P_{5\%STDSTD}$)	Less spillage power loss (W)	Rel. power ($P/P_{5\%STDSTD}$)
5	0.19018	1.0009	0.19018	1.0009
10	0.19060	1.0032	0.19052	1.0028
15	0.19089	1.0047	0.19045	1.0024
20	0.19098	1.0052	0.18973	0.9986
25	0.18987	0.9993	0.18721	0.9853

Power loss from streamline deflection around hub

Hub ratio (%)	Power loss (%)
5	0.000
10	0.039
15	0.229
20	0.653
25	1.400

Appendix J: Results - 280 mm rotor - CFD simulations

5 STD kw-sst for rough peak

Fluent angular velocity (rpm)	Fluent angular velocity (rad/s)	Torque on blade only (Fluent, one blade, 120° slice) (Nm)	Power (blade only, one blade, 120° slice) (W)	Power (blades only, whole rotor) (W)	Total Torque on Hub only (Fluent, 120° slice) (Nm)	Adjusted Torque on Hub based on fraction of surface area that would be rotating (fraction below) 0.79	Net Torque (Ansys, one blade, 120° slice) (Nm)	Ratio: hub torque / blade torque	Net Power (one blade with hub, 120° slice) (W)	Net Power (whole rotor) (W)
76	7.959	6.3005E-03	0.05014	0.15043	9.2713E-07	7.285E-07	6.300E-03	0.00012	0.05014	0.15041
78	8.168	6.1542E-03	0.05027	0.15081	9.4048E-07	7.389E-07	6.153E-03	0.00012	0.05026	0.15079
80	8.378	6.0204E-03	0.05044	0.15131	9.5645E-07	7.515E-07	6.020E-03	0.00012	0.05043	0.15129
82	8.587	5.8675E-03	0.05038	0.15115	1.1530E-06	9.059E-07	5.867E-03	0.00015	0.05038	0.15113
84	8.796	5.7173E-03	0.05029	0.15088	1.1879E-06	9.334E-07	5.716E-03	0.00016	0.05028	0.15085

5 STD kw-sst 100.1p final graph

78	8.168	6.1166E-03	0.04996	0.14988	9.3590E-07	7.354E-07	6.116E-03	0.00012	0.04996	0.14987
80	8.378	5.9764E-03	0.05007	0.15020	9.5130E-07	7.475E-07	5.976E-03	0.00013	0.05006	0.15018
81	8.482	5.9082E-03	0.05012	0.15035	9.6333E-07	7.569E-07	5.907E-03	0.00013	0.05011	0.15033
82	8.587	5.8345E-03	0.05010	0.15030	1.1372E-06	8.935E-07	5.834E-03	0.00015	0.05009	0.15028
84	8.796	5.6809E-03	0.04997	0.14992	1.1695E-06	9.189E-07	5.680E-03	0.00016	0.04996	0.14989

Mesh dependence study 5 STD kwsst rotor

60p	81	8.482	5.8153E-03	0.04933	0.14798	1.1589E-06	9.106E-07	5.814E-03	0.00016	0.04932	0.14796
87p	81	8.482	5.7857E-03	0.04908	0.14723	1.1833E-06	9.297E-07	5.785E-03	0.00016	0.04907	0.14720
100p	81	8.482	5.9082E-03	0.05012	0.15035	9.6333E-07	7.569E-07	5.907E-03	0.00013	0.05011	0.15033
110p	81	8.482	6.0033E-03	0.05092	0.15277	9.6686E-07	7.597E-07	6.003E-03	0.00013	0.05092	0.15275
120p	81	8.482	6.2032E-03	0.05262	0.15785	9.4683E-07	7.439E-07	6.202E-03	0.00012	0.05261	0.15783
130p	81	8.482	6.3980E-03	0.05427	0.16281	9.3705E-07	7.363E-07	6.397E-03	0.00012	0.05426	0.16279

10STD kwsst for rough peak

Fluent angular velocity (rpm)	Fluent angular velocity (rad/s)	Torque on blade only (Fluent, one blade, 120° slice) (Nm)	Power (blade only, one blade, 120° slice) (W)	Power (blades only, whole rotor) (W)	Total Torque on Hub only (Fluent, 120° slice) (Nm)	Adjusted Torque on Hub based on fraction of surface area that would be rotating (fraction below) 0.64	Net Torque (Ansys, one blade, 120° slice) (Nm)	Ratio: hub torque / blade torque	Net Power (one blade with hub, 120° slice) (W)	Net Power (whole rotor) (W)
80	8.378	5.9872E-03	0.05016	0.15047	7.9527E-06	5.104E-06	5.982E-03	0.00085	0.05012	0.15035
82	8.587	5.8427E-03	0.05017	0.15051	8.0207E-06	5.148E-06	5.838E-03	0.00088	0.05013	0.15038
84	8.796	5.6920E-03	0.05007	0.15021	8.0822E-06	5.187E-06	5.687E-03	0.00091	0.05002	0.15007

10STD kwsst 100p final graph

78	8.168	6.1292E-03	0.05006	0.15019	7.7968E-06	5.004E-06	6.124E-03	0.00082	0.05002	0.15007
80	8.378	5.9872E-03	0.05016	0.15047	7.9527E-06	5.104E-06	5.982E-03	0.00085	0.05012	0.15035
81	8.482	5.9161E-03	0.05018	0.15055	7.9885E-06	5.127E-06	5.911E-03	0.00087	0.05014	0.15042
82	8.587	5.8427E-03	0.05017	0.15051	8.0207E-06	5.148E-06	5.838E-03	0.00088	0.05013	0.15038
84	8.796	5.6920E-03	0.05007	0.15021	8.0822E-06	5.187E-06	5.687E-03	0.00091	0.05002	0.15007
86	9.006	5.5288E-03	0.04979	0.14938	8.1557E-06	5.234E-06	5.524E-03	0.00095	0.04974	0.14923

15STD kwsst for rough peak

Fluent angular velocity (rpm)	Fluent angular velocity (rad/s)	Torque on blade only (Fluent, one blade, 120° slice) (Nm)	Power (blade only, one blade, 120° slice) (W)	Power (blades only, whole rotor) (W)	Total Torque on Hub only (Fluent, 120° slice) (Nm)	Adjusted Torque on Hub based on fraction of surface area that would be rotating (fraction below) 0.60	Net Torque (Ansys, one blade, 120° slice) (Nm)	Ratio: hub torque / blade torque	Net Power (one blade with hub, 120° slice) (W)	Net Power (whole rotor) (W)
80	8.378	5.9850E-03	0.05014	0.15042	2.5081E-05	1.494E-05	5.970E-03	0.00250	0.05001	0.15004
82	8.587	5.8429E-03	0.05017	0.15052	2.5290E-05	1.506E-05	5.828E-03	0.00258	0.05004	0.15013
84	8.796	5.6901E-03	0.05005	0.15016	2.5481E-05	1.517E-05	5.675E-03	0.00267	0.04992	0.14976
15STD kwsst 99_7p final graph										
78	8.168	6.1130E-03	0.04993	0.14980	2.4781E-05	1.476E-05	6.098E-03	0.00241	0.04981	0.14943
80	8.378	5.9771E-03	0.05007	0.15022	2.5002E-05	1.489E-05	5.962E-03	0.00249	0.04995	0.14985
81	8.482	5.9073E-03	0.05011	0.15032	2.5105E-05	1.495E-05	5.892E-03	0.00253	0.04998	0.14994
82	8.587	5.8346E-03	0.05010	0.15031	2.5203E-05	1.501E-05	5.820E-03	0.00257	0.04997	0.14992
84	8.796	5.6813E-03	0.04998	0.14993	2.5390E-05	1.512E-05	5.666E-03	0.00266	0.04984	0.14953

20STD kwsst for rough peak

Fluent angular velocity (rpm)	Fluent angular velocity (rad/s)	Torque on blade only (Fluent, one blade, 120° slice) (Nm)	Power (blade only, one blade, 120o slice) (W)	Power (blades only, whole rotor) (W)	Total Torque on Hub only (Fluent, 120° slice) (Nm)	Adjusted Torque on Hub based on fraction of surface area that would be rotating (fraction below) 0.57	Net Torque (Ansys, one blade, 120° slice) (Nm)	Ratio: hub torque / blade torque	Net Power (one blade with hub, 120° slice) (W)	Net Power (whole rotor) (W)
80	8.378	5.9181E-03	0.04958	0.14874	5.7649E-05	3.272E-05	5.885E-03	0.00553	0.04931	0.14792
82	8.587	5.7773E-03	0.04961	0.14883	5.8637E-05	3.328E-05	5.744E-03	0.00576	0.04932	0.14797
84	8.796	5.6210E-03	0.04944	0.14833	5.9400E-05	3.371E-05	5.587E-03	0.00600	0.04915	0.14745
20STD kwsst 100_1p final graph										
78	8.168	6.0442E-03	0.04937	0.14811	5.7030E-05	3.237E-05	6.012E-03	0.00536	0.04911	0.14732
80	8.378	5.9034E-03	0.04946	0.14837	5.7829E-05	3.282E-05	5.871E-03	0.00556	0.04918	0.14754
81	8.482	5.8338E-03	0.04948	0.14845	5.8157E-05	3.301E-05	5.801E-03	0.00566	0.04920	0.14761
82	8.587	5.7604E-03	0.04946	0.14839	5.8562E-05	3.324E-05	5.727E-03	0.00577	0.04918	0.14754
84	8.796	5.6091E-03	0.04934	0.14802	5.9296E-05	3.365E-05	5.575E-03	0.00600	0.04904	0.14713

25STD kwsst for rough peak

Fluent angular velocity (rpm)	Fluent angular velocity (rad/s)	Torque on blade only (Fluent, one blade, 120° slice) (Nm)	Power (blade only, one blade, 120o slice) (W)	Power (blades only, whole rotor) (W)	Total Torque on Hub only (Fluent, 120° slice) (Nm)	Adjusted Torque on Hub based on fraction of surface area that would be rotating (fraction below) 0.55	Net Torque (Ansys, one blade, 120° slice) (Nm)	Ratio: hub torque / blade torque	Net Power (one blade with hub, 120° slice) (W)	Net Power (whole rotor) (W)
78	8.168	5.9650E-03	0.04872	0.14617	1.1650E-04	6.394E-05	5.901E-03	0.01072	0.04820	0.14460
80	8.378	5.8218E-03	0.04877	0.14632	1.2002E-04	6.588E-05	5.756E-03	0.01132	0.04822	0.14466
82	8.587	5.6820E-03	0.04879	0.14637	1.2200E-04	6.696E-05	5.615E-03	0.01179	0.04822	0.14465

25STD kwsst 100p final graph

75	7.854	6.1879E-03	0.04860	0.14580	1.1358E-04	6.234E-05	6.126E-03	0.01007	0.04811	0.14433
78	8.168	5.9644E-03	0.04872	0.14615	1.1640E-04	6.389E-05	5.901E-03	0.01071	0.04820	0.14459
80	8.378	5.8218E-03	0.04877	0.14632	1.2002E-04	6.588E-05	5.756E-03	0.01132	0.04822	0.14466
81	8.482	5.7522E-03	0.04879	0.14638	1.2132E-04	6.659E-05	5.686E-03	0.01158	0.04823	0.14468
82	8.587	5.6815E-03	0.04879	0.14636	1.2249E-04	6.723E-05	5.614E-03	0.01183	0.04821	0.14463
84	8.796	5.5357E-03	0.04869	0.14608	1.2500E-04	6.861E-05	5.467E-03	0.01239	0.04809	0.14427

10 ADP - kw-sst for rough peak

Fluent angular velocity (rpm)	Fluent angular velocity (rad/s)	Torque on blade only (Fluent, one blade, 120° slice) (Nm)	Power (blade only, one blade, 120° slice) (W)	Power (blades only, whole rotor) (W)	Total Torque on Hub only (Fluent, 120° slice) (Nm)	Adjusted Torque on Hub based on fraction of surface area that would be rotating (fraction below) 0.64	Net Torque (Ansys, one blade, 120° slice) (Nm)	Ratio: hub torque / blade torque	Net Power (one blade with hub, 120° slice) (W)	Net Power (whole rotor) (W)
80	8.378	6.0108E-03	0.05036	0.15107	8.1448E-06	5.227E-06	6.006E-03	0.00087	0.05031	0.15094
82	8.587	5.8674E-03	0.05038	0.15115	8.1922E-06	5.258E-06	5.862E-03	0.00090	0.05034	0.15101
84	8.796	5.7152E-03	0.05027	0.15082	8.2349E-06	5.285E-06	5.710E-03	0.00092	0.05023	0.15068

10 ADP - kw-sst 99_9p final graph

79	8.273	6.0667E-03	0.05019	0.15057	8.1023E-06	5.200E-06	6.062E-03	0.00086	0.05015	0.15044
80	8.378	5.9997E-03	0.05026	0.15079	8.1239E-06	5.214E-06	5.994E-03	0.00087	0.05022	0.15066
81	8.482	5.9312E-03	0.05031	0.15093	8.1505E-06	5.231E-06	5.926E-03	0.00088	0.05027	0.15080
82	8.587	5.8608E-03	0.05033	0.15098	8.1780E-06	5.249E-06	5.856E-03	0.00090	0.05028	0.15085
83	8.692	5.7866E-03	0.05030	0.15089	8.2060E-06	5.267E-06	5.781E-03	0.00091	0.05025	0.15075
84	8.796	5.7073E-03	0.05020	0.15061	8.2312E-06	5.283E-06	5.702E-03	0.00093	0.05016	0.15047

15ADP kw-SST for rough peak

Fluent angular velocity (rpm)	Fluent angular velocity (rad/s)	Torque on blade only (Fluent, one blade, 120^o slice) (Nm)	Power (blade only, one blade, 120^o slice) (W)	Power (blades only, whole rotor) (W)	Total Torque on Hub only (Fluent, 120^o slice) (Nm)	Adjusted Torque on Hub based on fraction of surface area that would be rotating (fraction below) 0.60	Net Torque (Ansys, one blade, 120^o slice) (Nm)	Ratio: hub torque / blade torque	Net Power (one blade with hub, 120^o slice) (W)	Net Power (whole rotor) (W)
78	8.168	6.1440E-03	0.05019	0.15056	2.4500E-05	1.459E-05	6.129E-03	0.00237	0.05007	0.15020
80	8.378	6.0048E-03	0.05031	0.15092	2.4647E-05	1.468E-05	5.990E-03	0.00244	0.05018	0.15055
82	8.587	5.8602E-03	0.05032	0.15096	2.4785E-05	1.476E-05	5.845E-03	0.00252	0.05019	0.15058
84	8.796	5.7085E-03	0.05021	0.15064	2.4929E-05	1.485E-05	5.694E-03	0.00260	0.05008	0.15025
86	9.006	5.5536E-03	0.05002	0.15005	2.5084E-05	1.494E-05	5.539E-03	0.00269	0.04988	0.14964

15ADP kw-SST 100_2p final graph

78	8.168	6.1440E-03	0.05019	0.15056	2.4500E-05	1.459E-05	6.129E-03	0.00237	0.05007	0.15020
80	8.378	6.0048E-03	0.05031	0.15092	2.4647E-05	1.468E-05	5.990E-03	0.00244	0.05018	0.15055
81	8.482	5.9327E-03	0.05032	0.15097	2.4718E-05	1.472E-05	5.918E-03	0.00248	0.05020	0.15059
82	8.587	5.8602E-03	0.05032	0.15096	2.4785E-05	1.476E-05	5.845E-03	0.00252	0.05019	0.15058
84	8.796	5.7085E-03	0.05021	0.15064	2.4929E-05	1.485E-05	5.694E-03	0.00260	0.05008	0.15025
86	9.006	5.5536E-03	0.05002	0.15005	2.5084E-05	1.494E-05	5.539E-03	0.00269	0.04988	0.14964

20 ADP kwsst for rough peak

Fluent angular velocity (rpm)	Fluent angular velocity (rad/s)	Torque on blade only (Fluent, one blade, 120° slice) (Nm)	Power (blade only, one blade, 120° slice) (W)	Power (blades only, whole rotor) (W)	Total Torque on Hub only (Fluent, 120° slice) (Nm)	Adjusted Torque on Hub based on fraction of surface area that would be rotating (fraction below) 0.57	Net Torque (Ansys, one blade, 120° slice) (Nm)	Ratio: hub torque / blade torque	Net Power (one blade with hub, 120° slice) (W)	Net Power (whole rotor) (W)
78	8.168	6.0940E-03	0.04978	0.14933	5.6300E-05	3.195E-05	6.062E-03	0.00524	0.04952	0.14855
80	8.378	5.9648E-03	0.04997	0.14991	5.6984E-05	3.234E-05	5.932E-03	0.00542	0.04970	0.14910
82	8.587	5.8195E-03	0.04997	0.14992	5.8187E-05	3.303E-05	5.786E-03	0.00567	0.04969	0.14907

20 ADP kwsst 99_6p final graph

76	7.959	6.2200E-03	0.04950	0.14851	5.5680E-05	3.160E-05	6.188E-03	0.00508	0.04925	0.14775
78	8.168	6.0724E-03	0.04960	0.14880	5.6254E-05	3.193E-05	6.040E-03	0.00526	0.04934	0.14802
79	8.273	6.0012E-03	0.04965	0.14894	5.6541E-05	3.209E-05	5.969E-03	0.00535	0.04938	0.14814
80	8.378	5.9301E-03	0.04968	0.14904	5.7296E-05	3.252E-05	5.898E-03	0.00548	0.04941	0.14822
81	8.482	5.8592E-03	0.04970	0.14910	5.7212E-05	3.247E-05	5.827E-03	0.00554	0.04942	0.14827
82	8.587	5.7834E-03	0.04966	0.14899	5.7596E-05	3.269E-05	5.751E-03	0.00565	0.04938	0.14814
84	8.796	5.6295E-03	0.04952	0.14856	5.8340E-05	3.311E-05	5.596E-03	0.00588	0.04923	0.14769

25ADP kwsst for rough peak

Fluent angular velocity (rpm)	Fluent angular velocity (rad/s)	Torque on blade only (Fluent, one blade, 120° slice) (Nm)	Power (blade only, one blade, 120° slice) (W)	Power (blades only, whole rotor) (W)	Total Torque on Hub only (Fluent, 120° slice) (Nm)	Adjusted Torque on Hub based on fraction of surface area that would be rotating (fraction below) 0.55	Net Torque (Ansys, one blade, 120° slice) (Nm)	Ratio: hub torque / blade torque	Net Power (one blade with hub, 120° slice) (W)	Net Power (whole rotor) (W)
78	8.168	5.9792E-03	0.04884	0.14652	1.1532E-04	6.330E-05	5.916E-03	0.01059	0.04832	0.14497
80	8.378	5.8387E-03	0.04891	0.14674	1.1797E-04	6.475E-05	5.774E-03	0.01109	0.04837	0.14512
82	8.587	5.6973E-03	0.04892	0.14677	1.2096E-04	6.639E-05	5.631E-03	0.01165	0.04835	0.14506

25ADP kwsst 100_2p final graph

76	7.959	6.0974E-03	0.04853	0.14558	1.1347E-04	6.228E-05	6.035E-03	0.01021	0.04803	0.14410
78	8.168	5.9581E-03	0.04867	0.14600	1.1563E-04	6.347E-05	5.895E-03	0.01065	0.04815	0.14444
80	8.378	5.8177E-03	0.04874	0.14621	1.1819E-04	6.487E-05	5.753E-03	0.01115	0.04819	0.14458
82	8.587	5.6768E-03	0.04875	0.14624	1.2063E-04	6.621E-05	5.611E-03	0.01166	0.04818	0.14453
84	8.796	5.5286E-03	0.04863	0.14590	1.2372E-04	6.791E-05	5.461E-03	0.01228	0.04803	0.14410

Results: Micro-adjustment and uncertainty

5 Baseline (STD)						
LS	blade	0.16		Rough peak rpm		80
	hub	0.32				
SM	min	0.02				
	max	105				
Mesh check						
SM max%	Cells	Torque (blade) (N)	Torque (hub) (N)	Torque (b - h) (N x10^{-3})	Final PTS	Rotatn speed (rpm)
99.6	4637392	6.0029E-03	9.5063E-07	6.0019	0.1	80
100	**4634894**	**6.0088E-03**	**9.4955E-07**	**6.0079**	**0.1**	**80**
100.2	4642183	5.9777E-03	9.3356E-07	5.9768	0.1	80
100.1	**4633252**	**5.9764E-03**	**9.5130E-07**	**5.9754**	**0.1**	**80**
99.9	4639228	5.9862E-03	9.5234E-07	5.9852	0.1	80
100.4	4636796	5.9845E-03	9.5512E-07	5.9835	0.1	80
100.3	4639112	5.9834E-03	9.4531E-07	5.9825	0.1	80
99.8	4641977	6.0044E-03	9.5778E-07	6.0034	0.1	80
99.7	4629860	5.9827E-03	9.5397E-07	5.9817	0.1	80
Torque range and uncertainty						
99.4	6.0079	T range	0.0324	T%rangemax - T%range		0.054
100.6	6.0079	T midrange	5.992			
99.4	5.9754	T % range	0.541			
100.6	5.9754					

10 STD						
LS	blade	0.16		Rough peak rpm		82
LS	hub	0.32				
SM	min	0.02				
SM	max	105				
SM max%	Cells	Torque (blade) (N)	Torque (hub) (N)	Torque (b - h) (N x10-3)	Final PTS	Rotatn speed (rpm)
99.6	**4498729**	**5.8766E-03**	**8.0876E-06**	**5.8685**	**0.1**	**82**
99.8	4501609	5.8588E-03	7.9771E-06	5.8508	0.1	82
100	**4497971**	**5.8427E-03**	**8.0207E-06**	**5.8347**	**0.1**	**82**
100.2	4501949	5.8470E-03	8.1078E-06	5.8389	0.1	82
100.4	4496992	5.8709E-03	7.9983E-06	5.8629	0.1	82
Torque range and uncertainty						
99.4	5.8685	T range	0.0338	T%rangemax - T%range		0.016
100.6	5.8685	T midrange	5.852			
99.4	5.8347	T % range	0.578			
100.6	5.8347					

15 STD						
LS	blade	0.16			Rough peak rpm	82
	hub	0.32				
SM	min	0.02				
	max	105				
SM max%	Cells	Torque (blade) (N)	Torque (hub) (N)	Torque (b - h) (N x10-3)	Final PTS	Rotatn speed (rpm)
99.6	4339731	5.8475E-03	2.5352E-05	5.8221	0.1000	82
99.8	4339199	5.8523E-03	2.5476E-05	5.8268	0.1000	82
100	4338767	5.8429E-03	2.5290E-05	5.8176	0.1000	82
100.2	4337708	5.8418E-03	2.5362E-05	5.8164	0.1000	82
100.4	**4343286**	**5.8597E-03**	**2.5311E-05**	**5.8344**	**0.1000**	**82**
100.1	4338884	5.8486E-03	2.5223E-05	5.8234	0.1000	82
99.9	4334449	5.8562E-03	2.5100E-05	5.8311	0.1000	82
99.7	**4338606**	**5.8346E-03**	**2.5203E-05**	**5.8094**	**0.1000**	**82**
Torque range and uncertainty						
99.4	5.8344	T range	0.0250	T%rangemax - T%range		0.165
100.6	5.8344	T midrange	5.822			
99.4	5.8094	T % range	0.429			
100.6	5.8094					

20 STD						
LS	blade	0.16			Rough peak rpm	82
	hub	0.32				
SM	min	0.02				
	max	105				
SM max%	Cells	Torque (blade) (N)	Torque (hub) (N)	Torque (b - h) (N x10-3)	Final PTS	Rotatn speed (rpm)
99.6	4158297	5.7695E-03	5.8380E-05	5.7111	0.0035	82
99.8	**4156533**	**5.7931E-03**	**5.9033E-05**	**5.7341**	**0.0042**	**82**
100	4162080	5.7773E-03	5.8637E-05	5.7187	0.0049	82
100.2	4156665	5.7818E-03	5.8985E-05	5.7228	0.1000	82
100.4	4156829	5.7735E-03	5.7904E-05	5.7156	0.0040	82
100.1	**4159727**	**5.7604E-03**	**5.8562E-05**	**5.7018**	**0.0200**	**82**
Torque range and uncertainty						
99.4	5.7341	T range	0.0322	T%rangemax - T%range		0.031
100.6	5.7341	T midrange	5.718			
99.4	5.7018	T % range	0.564			
100.6	5.7018					

25 STD						
LS blade	0.16			Rough peak rpm		80
hub	0.32					
SM min	0.02					
max	105					
Mesh check						
SM max%	Cells	Torque (blade) (N)	Torque (hub) (N)	Torque (b - h) (N x10-3)	Final PTS	Rotatn speed (rpm)
99.6	4204130	5.8440E-03	1.2137E-04	5.7226	0.0500	80
99.8	4203619	5.8389E-03	1.2133E-04	5.7176	0.1000	80
100	**4202371**	**5.8218E-03**	**1.2002E-04**	**5.7018**	**0.1000**	**80**
100.2	4207153	5.8303E-03	1.2097E-04	5.7093	0.1000	80
100.4	4209309	5.8371E-03	1.1947E-04	5.7176	0.0100	80
100.1	4203072	5.8322E-03	1.2078E-04	5.7114	0.1000	80
99.9	4204985	5.8339E-03	1.2044E-04	5.7135	0.1000	80
100.3	4206625	5.8278E-03	1.2181E-04	5.7060	0.1000	80
99.7	**4199495**	**5.8428E-03**	**1.1923E-04**	**5.7236**	**0.0190**	**80**
Torque range and uncertainty						
99.4	5.7236	T range	0.0218	T%rangemax - T%range		0.213
100.6	5.7236	T midrange	5.713			
99.4	5.7018	T % range	0.381			
100.6	5.7018					

10 ADP						
LS blade	0.16			Rough peak rpm		82
hub	0.32					
SM min	0.02					
max	105					
Mesh check						
SM max%	Cells	Torque (blade) (N)	Torque (hub) (N)	Torque (b - h) (N x10-3)	Final PTS	Rotatn speed (rpm)
99.6	4548208	5.8719E-03	8.2088E-06	5.8637	0.1000	82
100	4549307	5.8696E-03	8.2188E-06	5.8614	0.1000	82
100.2	4556423	5.8741E-03	8.2090E-06	5.8659	0.1000	82
100.4	4558950	5.8674E-03	8.1922E-06	5.8592	0.1000	82
100.1	**4551976**	**5.8938E-03**	**8.1696E-06**	**5.8856**	**0.1000**	**82**
99.8	4555573	5.8654E-03	8.1636E-06	5.8572	0.1000	82
99.9	**4558256**	**5.8620E-03**	**8.1780E-06**	**5.8538**	**0.1000**	**82**
100.3	4549933	5.8670E-03	8.2142E-06	5.8588	0.1000	82
99.7	4550882	5.8622E-03	8.1864E-06	5.8540	0.1000	82
Torque range and uncertainty						
99.4	5.8856	T range	0.0318	T%rangemax - T%range		0.052
100.6	5.8856	T midrange	5.870			
99.4	5.8538	T % range	0.542			
100.6	5.8538					

15 ADP

LS	blade	0.16	Rough peak rpm	82
	hub	0.32		
SM	min	0.02		
	max	105		

Mesh check

SM max%	Cells	Torque (blade) (N)	Torque (hub) (N)	Torque (b - h) (N x10-3)	Final PTS	Rotatn speed (rpm)
99.6	4333518	5.8615E-03	2.5013E-05	5.8365	0.1000	82
99.8	4335859	5.8815E-03	2.5020E-05	5.8565	0.1000	82
100	4333616	5.8835E-03	2.5056E-05	5.8584	0.1000	82
100.2	**4331612**	**5.8602E-03**	**2.4785E-05**	**5.8354**	**0.1000**	**82**
100.4	4334631	5.8750E-03	2.4953E-05	5.8500	0.1000	82
99.9	**4336734**	**5.8867E-03**	**2.4886E-05**	**5.8618**	**0.1000**	**82**
100.1	4332009	5.8620E-03	2.4825E-05	5.8372	0.1000	82

Torque range and uncertainty

99.4	5.8618	T range	0.0264	T%rangemax - T%range	0.143
100.6	5.8618	T midrange	5.849		
99.4	5.8354	T % range	0.451		
100.6	5.8354				

20 ADP

LS	blade	0.16	Rough peak rpm	80
	hub	0.32		
SM	min	0.02		
	max	105		

Mesh check

SM max%	Cells	Torque (blade) (N)	Torque (hub) (N)	Torque (b - h) (N x10^{-3})	Final PTS	Rotatn speed (rpm)
99.6	**4225364**	**5.9301E-03**	**5.7296E-05**	**5.8728**	**0.0065**	**80**
99.8	4229691	5.9527E-03	5.7382E-05	5.8953	0.0045	80
100	**4225106**	**5.9648E-03**	**5.6984E-05**	**5.9078**	**0.0047**	**80**
100.2	4230789	5.9507E-03	5.7083E-05	5.8936	0.0031	80
100.4	4228236	5.9370E-03	5.7138E-05	5.8799	0.0032	80

Torque range and uncertainty

99.4	5.9078	T range	0.0350	T%rangemax - T%range	0.000
100.6	5.9078	T midrange	5.890		
99.4	5.8728	T % range	0.594		
100.6	5.8728				

25 ADP

LS	blade	0.16	Rough peak rpm	80
	hub	0.32		
SM	min	0.02		
	max	105		

Mesh check

SM max%	Cells	Torque (blade) (N)	Torque (hub) (N)	Torque (b - h) (N x10^{-3})	Final PTS	Rotatn speed (rpm)
99.6	4093818	5.8277E-03	1.1794E-04	5.7098	0.0100	80
99.8	**4092014**	**5.8519E-03**	**1.1904E-04**	**5.7329**	**0.1000**	**80**
100	4089884	5.8387E-03	1.1797E-04	5.7207	0.1000	80
100.2	**4093874**	**5.8177E-03**	**1.1819E-04**	**5.6995**	**0.1000**	**80**
100.4	4089836	5.8278E-03	1.1811E-04	5.7097	0.0134	80

Torque range and uncertainty

99.4	5.7329	T range	0.0334	T%rangemax - T%range	0.011
100.6	5.7329	T midrange	5.716		
99.4	5.6995	T % range	0.583		
100.6	5.6995				

Appendix K: Results - 280 mm rotor – Physical testing and calibration

Rotor: 5Rotor5Hub

Resistor (Ω)	Asymptote angular velocity (rpm)						Asymptote angular velocity (rad/s)	*Torque (N.m)	Power (W)
	Run 1	Run 2	Run 3	Run 4	Run 5	Mean			
Rinf	104.294	103.279	103.423	103.266	103.396	103.531	10.842	0.007905	0.08570
R 860	97.690	92.221	98.318	97.978	97.478	96.737	10.130	0.009173	0.09292
R 360	92.599	92.221	91.900	91.375	91.025	91.824	9.616	0.010583	0.10176
R 160	83.833	84.047	82.990	84.448	83.598	83.783	8.774	0.013076	0.11473
R 100	78.870	78.177	78.399	78.373	78.429	78.450	8.215	0.014158	0.11631
R 60	74.204	74.151	72.338	74.287	73.676	73.731	7.721	0.016130	0.12454
R 30	67.416	67.218	68.119	68.073	68.189	67.803	7.100	0.018688	0.13269
R 10	64.088	62.971	63.264	63.347	63.186	63.371	6.636	0.022007	0.14604
R 5	60.928	62.045	61.672	61.972	61.532	61.630	6.454	0.023113	0.14917
R 3	59.233	59.104	58.586	59.511	60.038	59.295	6.209	0.023283	0.14457

*Torque is from calibration equations

Rotor: 5Rotor10Hub

Resistor (Ω)	Asymptote angular velocity (rpm)						Asymptote angular velocity (rad/s)	*Torque (N.m)	Power (W)
	Run 1	Run 2	Run 3	Run 4	Run 5	Mean			
Rinf	101.766	102.086	101.848	103.266	102.368	102.267	10.709	0.007891	0.08451
R 860	96.692	91.935	97.101	96.887	96.841	95.891	10.042	0.009148	0.09187
R 360	91.728	91.935	91.599	92.548	91.025	91.767	9.610	0.010580	0.10167
R 160	84.642	83.922	84.087	83.913	84.113	84.135	8.811	0.013106	0.11547
R 100	79.818	79.298	78.958	79.966	79.928	79.593	8.335	0.014289	0.11910
R 60	73.951	74.405	74.523	74.417	73.764	74.212	7.771	0.016211	0.12598
R 30	67.766	66.264	66.769	67.529	67.660	67.198	7.037	0.018543	0.13049
R 10	62.873	62.797	63.251	62.672	62.601	62.839	6.580	0.021835	0.14369
R 5	62.156	61.431	61.281	61.229	61.284	61.476	6.438	0.023064	0.14848
R 3	59.469	59.058	59.186	57.896	59.030	58.928	6.171	0.023150	0.14286

*Torque is from calibration equations

Rotor: 5Rotor15Hub

Resistor (Ω)	Asymptote angular velocity (rpm)						Asymptote angular velocity (rad/s)	*Torque (N.m)	Power (W)
	Run 1	Run 2	Run 3	Run 4	Run 5	Mean			
Rinf	103.004	102.526	102.617	102.144	102.466	102.551	10.739	0.007894	0.08478
R 860	99.736	93.138	98.698	98.553	98.532	97.731	10.234	0.009201	0.09417
R 360	94.253	93.138	92.316	92.789	92.732	93.046	9.744	0.010637	0.10364
R 160	84.358	85.165	84.714	85.400	84.542	84.836	8.884	0.013165	0.11696
R 100	79.896	79.161	79.218	78.891	78.772	79.188	8.292	0.014242	0.11810
R 60	74.170	74.266	74.500	74.613	74.619	74.433	7.795	0.016248	0.12665
R 30	67.522	67.107	66.861	67.804	68.149	67.489	7.067	0.018613	0.13155
R 10	63.137	63.169	63.049	62.338	62.572	62.853	6.582	0.021840	0.14375
R 5	61.267	61.415	60.571	61.111	61.304	61.134	6.402	0.022953	0.14694
R 3	58.778	58.551	58.491	59.380	58.159	58.672	6.144	0.023056	0.14166

*Torque is from calibration equations

Rotor: 5Rotor20Hub

Resistor (Ω)	Asymptote angular velocity (rpm)						Asymptote angular velocity (rad/s)	*Torque (N.m)	Power (W)
	Run 1	Run 2	Run 3	Run 4	Run 5	Mean			
Rinf	103.717	102.786	102.044	103.079	102.538	102.833	10.769	0.007897	0.08504
R 860	97.397	92.554	97.082	97.340	97.203	96.315	10.086	0.009161	0.09239
R 360	92.837	92.554	92.990	92.683	92.352	92.683	9.706	0.010621	0.10308
R 160	84.133	85.265	83.794	84.379	84.750	84.464	8.845	0.013134	0.11617
R 100	77.992	78.590	78.340	78.180	77.943	78.209	8.190	0.014131	0.11573
R 60	73.344	73.546	73.038	74.025	73.561	73.503	7.697	0.016091	0.12386
R 30	68.291	69.187	68.054	68.682	68.790	68.601	7.184	0.018879	0.13562
R 10	62.802	63.259	62.656	62.583	62.202	62.700	6.566	0.021790	0.14307
R 5	61.078	61.184	60.282	60.990	60.834	60.874	6.375	0.022869	0.14578
R 3	58.824	58.858	58.307	57.465	58.359	58.363	6.112	0.022942	0.14022

*Torque is from calibration equations

Rotor: 5Rotor25Hub

Resistor (Ω)	Asymptote angular velocity (rpm)						Asymptote angular velocity (rad/s)	*Torque (N.m)	Power (W)
	Run 1	Run 2	Run 3	Run 4	Run 5	Mean			
Rinf	100.088	99.853	99.466	99.069	100.120	99.719	10.443	0.007863	0.08211
R 860	94.166	89.657	94.933	95.100	94.089	93.589	9.801	0.009082	0.08901
R 360	90.205	89.657	90.521	89.651	89.190	89.845	9.409	0.010494	0.09873
R 160	83.228	81.975	82.188	83.186	81.950	82.505	8.640	0.012967	0.11204
R 100	77.363	77.156	76.282	76.738	76.901	76.888	8.052	0.013979	0.11256
R 60	72.849	71.411	71.937	71.909	71.502	71.922	7.532	0.015823	0.11917
R 30	66.244	66.548	66.941	66.194	66.286	66.443	6.958	0.018361	0.12776
R 10	61.231	61.581	62.048	61.021	62.105	61.597	6.450	0.021430	0.13823
R 5	58.687	58.802	59.426	59.343	59.696	59.191	6.198	0.022304	0.13825
R 3	54.463	54.763	55.204	54.045	54.336	54.562	5.714	0.021459	0.12261

*Torque is from calibration equations

Rotor: ADP10

Resistor (Ω)	Asymptote angular velocity (rpm)						Asymptote angular velocity (rad/s)	*Torque (N.m)	Power (W)
	Run 1	Run 2	Run 3	Run 4	Run 5	Mean			
Rinf	100.091	100.742	100.714	100.260	99.261	100.214	10.494	0.007869	0.08258
R 860	95.706	91.376	95.057	96.104	96.503	94.949	9.943	0.009121	0.09069
R 360	90.569	91.376	91.168	90.676	91.297	91.017	9.531	0.010546	0.10052
R 160	83.535	84.612	84.711	83.757	84.718	84.267	8.824	0.013117	0.11575
R 100	78.536	78.216	79.611	80.254	78.094	78.942	8.267	0.014214	0.11751
R 60	73.063	73.777	74.143	74.677	73.721	73.876	7.736	0.016154	0.12497
R 30	69.374	68.700	69.193	67.537	68.670	68.695	7.194	0.018901	0.13597
R 10	64.410	64.030	62.713	63.227	65.191	63.914	6.693	0.022180	0.14845
R 5	61.692	61.511	62.562	61.524	61.586	61.775	6.469	0.023160	0.14982
R 3	59.371	59.527	58.990	59.598	59.375	59.372	6.217	0.023311	0.14493

*Torque is from calibration equations

Rotor: ADP15

Resistor (Ω)	Asymptote angular velocity (rpm)						Asymptote angular velocity (rad/s)	*Torque (N.m)	Power (W)
	Run 1	Run 2	Run 3	Run 4	Run 5	Mean			
Rinf	102.534	101.158	101.272	103.512	102.912	102.278	10.710	0.007891	0.08452
R 860	97.348	93.132	97.937	98.563	99.337	97.263	10.185	0.009188	0.09358
R 360	92.903	93.132	92.675	94.136	93.692	93.308	9.771	0.010648	0.10405
R 160	85.245	85.510	86.067	86.377	86.091	85.858	8.991	0.013251	0.11914
R 100	79.900	80.560	80.130	81.237	82.229	80.811	8.463	0.014427	0.12209
R 60	73.969	73.738	74.604	74.194	74.565	74.214	7.772	0.016211	0.12599
R 30	67.550	68.371	68.653	67.896	68.381	68.170	7.139	0.018776	0.13404
R 10	63.427	63.038	62.454	62.536	63.627	63.017	6.599	0.021893	0.14447
R 5	60.437	61.695	61.239	60.918	61.990	61.256	6.415	0.022993	0.14749
R 3	58.784	58.954	58.400	60.116	58.470	58.945	6.173	0.023156	0.14294

*Torque is from calibration equations

Rotor: ADP20

Resistor (Ω)	Asymptote angular velocity (rpm)						Asymptote angular velocity (rad/s)	*Torque (N.m)	Power (W)
	Run 1	Run 2	Run 3	Run 4	Run 5	Mean			
Rinf	99.033	96.902	98.249	98.335	98.173	98.138	10.277	0.007846	0.08063
R 860	94.592	90.245	94.259	93.853	94.029	93.395	9.780	0.009077	0.08877
R 360	89.802	90.245	90.477	89.339	89.668	89.906	9.415	0.010496	0.09882
R 160	82.184	82.462	82.477	82.799	83.596	82.703	8.661	0.012984	0.11245
R 100	77.686	79.849	79.068	78.464	77.886	78.591	8.230	0.014174	0.11665
R 60	73.678	75.372	73.716	72.988	73.800	73.911	7.740	0.016160	0.12508
R 30	69.438	68.485	68.007	69.776	67.996	68.740	7.198	0.018912	0.13614
R 10	62.810	62.722	62.526	63.431	64.160	63.130	6.611	0.021929	0.14497
R 5	60.371	61.126	61.338	61.687	60.064	60.917	6.379	0.022883	0.14598
R 3	58.594	59.093	60.408	59.750	58.931	59.355	6.216	0.023305	0.14485

*Torque is from calibration equations

Rotor: ADP25

Resistor (Ω)	Asymptote angular velocity (rpm)						Asymptote angular velocity (rad/s)	*Torque (N.m)	Power (W)
	Run 1	Run 2	Run 3	Run 4	Run 5	Mean			
Rinf	104.995	103.592	102.901	101.326	102.528	103.068	10.793	0.007900	0.08526
R 860	97.320	92.177	96.711	96.199	96.721	95.826	10.035	0.009147	0.09178
R 360	93.306	92.177	91.971	92.438	91.340	92.247	9.660	0.010601	0.10241
R 160	84.833	84.397	85.656	86.547	85.171	85.321	8.935	0.013206	0.11799
R 100	79.715	79.876	80.200	79.701	79.278	79.754	8.352	0.014307	0.11949
R 60	74.561	75.196	74.874	74.685	75.150	74.893	7.843	0.016325	0.12804
R 30	70.737	70.139	69.790	70.071	69.767	70.101	7.341	0.019234	0.14120
R 10	60.283	59.914	59.721	60.240	60.477	60.127	6.296	0.020940	0.13185
R 5	0.000	0.000	0.000	0.000	0.000	0.000	0.000	-0.015772	0.00000
R 3	0.000	0.000	0.000	0.000	0.000	0.000	0.000	-0.016523	0.00000

*Torque is from calibration equations

Stepper generator R-ω-T calibration

Mass reading data logged at constant time intervals

Moment arm: 23.57 mm

Resistor	Angular velocity	mass readings (g)																									Force	Torque
(Ω)	(rpm)	Initial	1	2	3	4	5	6	7	8	9	10	11	12	13	14	15	16	17	18	19	20	21	22	23	24	Mean	(N)	(N.m)
Rinf	40.91	0.00	30.46	28.26	31.52	30.12	28.48	31.95	27.83	28.71	31.75	28.77	30.92	31.82	28.33	30.95	30.26	29.80	31.54	29.34	31.42	31.98	28.15	30.99	31.84		30.23	0.2965	0.006989
	49.61	0.00	29.29	31.60	31.60	30.84	30.84	32.18	32.18	31.37	29.98	29.98	31.62	31.62	29.12	29.12	31.03	31.88	31.88	30.26	30.41	32.27	32.27	29.15	29.15	32.02	30.90	0.3032	0.007145
	57.96	0.00	30.69	31.45	31.45	30.14	30.14	31.49	30.62	30.62	31.41	31.41	30.37	30.37	31.55	31.55	30.88	30.88	31.82	31.82	30.34	30.34	31.38	31.38	30.51	30.51	30.96	0.3038	0.007159
	66.07	0.00	31.60	31.60	31.60	31.60	32.21	32.21	32.21	32.76	32.76	32.76	32.12	32.12	32.12	32.12	32.81	32.81	32.81	31.97	31.97	31.97	32.11	32.11	32.11	32.11	32.19	0.3158	0.007443
	73.08	0.00	31.81	31.81	31.26	32.45	33.30	31.21	31.98	31.98	31.98	32.00	32.37	30.71	32.85	32.85	31.97	31.97	32.01	32.01	33.05	31.36	32.48	32.48	32.48	32.80	32.13	0.3152	0.007430
	81.62	0.00	33.43	33.10	32.70	33.68	33.10	32.06	33.06	32.06	32.15	33.16	32.15	32.91	32.19	32.13	32.81	32.13	31.28	33.10	31.28	33.10	33.79	32.63	33.79	33.39	32.72	0.3209	0.007565
	92.46	0.00	33.64	33.88	34.41	33.14	34.48	34.48	34.47	34.47	33.73	34.43	33.73	34.16	34.16	33.67	34.42	33.11	34.21	34.21	33.52	34.61	32.93	33.80	34.02	34.02	33.99	0.3334	0.007859
	99.03	0.00	34.31	34.31	34.31	34.66	34.61	34.66	34.01	34.55	34.01	34.55	34.33	34.33	34.33	33.96	34.37	33.96	33.96	33.74	33.45	34.67	35.00	35.07	34.41	35.05	34.36	0.3371	0.007944
	106.66	0.00	34.90	34.26	34.90	34.26	34.96	34.14	34.55	34.55	34.55	34.59	34.55	34.44	34.44	35.07	35.24	35.62	35.24	35.55	34.89	35.11	34.89	35.11	34.63	35.39	34.83	0.3416	0.008053
	115.51	0.00	34.23	33.59	34.23	33.82	34.25	33.82	34.28	33.69	34.25	33.84	34.25	33.84	34.26	33.95	34.26	33.95	34.30	33.91	34.05	33.95	34.05	34.21	34.21	34.14	34.06	0.3341	0.007874
R 860	40.85	0.00	32.00	32.46	32.46	29.54	29.54	30.69	32.71	32.71	30.38	30.38	30.76	33.64	34.40	34.40	29.65	29.65	32.61	33.48	33.52	33.52	30.60	30.60	32.67	33.48	31.91	0.3130	0.007378
	49.60	0.00	34.93	34.93	33.06	33.06	34.11	34.43	34.43	33.22	33.22	34.58	34.58	32.51	32.51	33.51	34.32	34.32	33.69	33.69	34.46	34.46	33.36	33.36	33.93	34.00	33.86	0.3322	0.007829
	57.89	0.00	34.40	35.07	33.48	33.54	33.54	33.35	34.92	33.70	34.80	33.76	35.01	33.77	34.96	33.91	34.71	34.59	35.22	34.59	34.59	34.14	35.14				34.34	0.3369	0.007941
	66.14	0.00	35.56	35.56	36.01	36.01	35.56	35.56	35.56	36.45	36.45	36.35	36.35	36.35	36.39	36.39	35.47	35.47	35.47	35.91	35.91	35.91	35.91	36.47	36.47	36.47	36.00	0.3532	0.008324
	73.05	0.00	35.95	35.00	35.13	35.13	35.13	35.25	35.93	35.25	35.25	36.94	35.54	35.54	35.54	35.51	35.51	36.48	35.13	35.13	35.88	35.88	35.88	36.26	36.26	35.42	35.62	0.3494	0.008237
	81.63	0.00	37.46	36.71	36.99	36.88	36.51	37.78	36.51	36.96	38.11	36.96	37.48	37.70	36.37	37.70	38.46	36.79	38.72	36.79	37.76	37.83	37.04	37.83	38.16	36.24	37.32	0.3661	0.008630
	92.46	0.00	39.92	40.01	38.86	39.92	39.81	39.81	40.11	39.93	40.33	39.13	40.14	40.14	39.71	40.90	39.62	40.25	40.25	40.39	40.79	40.04	40.33	39.90	40.04	39.90	40.01	0.3925	0.009251
	99.07	0.00	39.68	40.28	39.98	39.98	39.98	39.97	39.97	39.97	40.48	39.72	40.50	40.26	40.26	40.26	40.53	40.53	40.53	40.74	40.10	40.86	40.20	40.23	40.23	40.23	40.23	0.3946	0.009302
	106.63	0.00	41.12	40.40	40.92	40.73	40.73	40.73	40.64	41.45	41.08	41.08	41.06	41.07	40.74	41.40	40.84	41.27	40.84	41.27	40.68	41.57	41.31	41.57	41.27	41.83	41.07	0.4029	0.009496
	115.49	0.00	41.40	41.24	41.40	41.24	41.34	41.34	41.34	41.42	41.42	41.42	41.42	41.49	41.49	41.49	41.49	41.49	41.69	41.47	41.69	41.40	41.69	41.34	41.78	41.34	41.45	0.4066	0.009584
R 360	40.87	0.00	37.41	31.61	34.35	35.47	31.97	35.88	36.42	32.49	35.81	32.70	32.94	36.53	33.29	35.65	36.11	32.98	34.95	35.25	32.49	35.19					34.47	0.3382	0.007971
	49.62	0.00	35.96	35.40	36.09	36.78	36.78	35.72	35.72	37.04	37.04	35.37	35.37	35.86	37.41	37.41	35.62	35.62	37.42	37.42	36.25	36.25	36.64	37.21	37.21	35.75	36.39	0.3570	0.008414
	57.88	0.00	37.84	37.40	37.40	38.61	38.61	36.95	36.95	38.61	36.70	36.70	38.84	38.84	37.29	37.29	38.83	38.83	36.74	36.74	38.61	38.61	37.81	37.81	38.85	38.85	37.90	0.3718	0.008764
	66.11	0.00	40.14	40.14	40.14	40.14	40.00	40.00	40.00	41.54	41.54	40.89	40.89	40.89	40.97	40.97	40.97	40.97	40.82	40.82	40.82	41.09	41.09	41.09	40.76	40.76	40.73	0.3995	0.009417
	73.05	0.00	40.60	40.60	40.60	41.64	41.64	40.04	41.34	41.34	41.34	41.51	41.51	40.49	42.10	42.10	41.30	41.87	41.87	41.87	42.30	42.30	40.61	41.14	41.14	41.14	41.35	0.4056	0.009561
	81.66	0.00	43.71	43.30	43.54	43.54	43.14	43.54	43.14	43.14	44.00	42.90	43.11	43.35	42.27	43.11	44.11	41.84	44.16	42.27	43.17	43.81	43.17	43.29	43.82	42.73	43.26	0.4243	0.010002
	92.46	0.00	46.30	48.82	46.64	46.48	46.57	46.57	46.57	46.95	46.71	46.58	47.12	47.12	47.05	47.24	47.02	47.02	46.97	46.97	46.96						46.93	0.4604	0.010851
	99.00	0.00	47.65	47.30	47.65	47.65	47.87	47.87	47.82	47.93	47.78	47.78	47.45	47.45	47.35	47.56	47.56	47.56	47.71	47.57	47.74	47.57	47.57	47.40	47.40	47.64	47.62	0.4671	0.011010
	106.59	0.00	48.10	47.84	48.00	47.86	48.00	47.86	48.14	48.17	47.96	48.12	47.92	48.12	47.92	48.19	48.19	48.18	48.18	48.31	47.99	48.20	48.06	48.06	48.06	48.03	48.06	0.4715	0.011113
	115.52	0.00	49.84	49.67	49.80	49.81	49.68	49.74	49.74	49.71	49.71	49.72	49.72	49.63	49.71	49.77	49.69	49.66	49.62	49.58	49.57	49.57	49.69	49.71			49.70	0.4875	0.011491

Resistor	Angular velocity	mass readings (g)																									Force	Torque
(Ω)	(rpm)	Initial	1	2	3	4	5	6	7	8	9	10	11	12	13	14	15	16	17	18	19	20	21	22	23	24	Mean	(N)	(N.m)
R 160	40.86	0.00	40.47	38.92	37.63	41.23	37.27	37.31	40.35	37.38	41.78	41.73	38.08	41.79	38.82	40.26											39.50	0.3875	0.009134
	48.57	0.00	41.75	40.52	41.86	40.33	41.57	42.68	40.92	42.36	40.76	42.97	41.07	42.45	43.12	41.23	42.82	40.45	42.93	41.80	43.32	42.73	42.47	43.14			41.97	0.4117	0.009703
	55.55	0.00	44.83	43.20	44.44	44.44	45.46	44.31	45.52	44.13	44.12	44.41	45.44	44.33	45.32	44.55	45.19	44.23	45.43	43.68	45.48	44.98					44.67	0.4383	0.010330
	67.73	0.00	48.95	49.06	49.26	49.26	48.69	48.60	49.96	49.96	50.07	50.06	49.96	49.96	49.95	49.99	50.20	50.20	50.80	50.80	49.91	49.70	49.70	50.30			49.79	0.4884	0.011512
	74.23	165.87	112.77	112.63	112.63	111.19	111.37	112.28	111.49	111.41	111.41	111.32	111.18	112.20	111.64	111.59	111.85	111.99	111.48	111.83	111.47	111.28	111.78	111.21			111.73	0.5311	0.012519
	82.12	165.89	107.77	108.87	108.59	108.20	108.81	108.81	108.82	108.44	109.23	109.00	108.76	108.15	108.75	108.73	108.44	108.50	109.08	108.93	108.65	109.65	109.28	109.43			108.77	0.5604	0.013208
	86.73	165.88	109.49	109.91	108.94	109.48	109.13	108.79	108.41	108.59	108.93	108.75	108.79	108.91	108.91	108.86	108.87	109.91	108.91	108.86	108.54	108.55	108.88				108.97	0.5583	0.013158
	91.88	0.00	59.61	59.83	59.20	59.83	59.40	59.83	59.98	59.89	60.31	59.89	59.89	59.77	59.73	59.98	59.73	59.73	59.63	59.81	59.88	59.57	60.06	59.90	60.28	60.39	59.84	0.5870	0.013836
	97.67	0.00	61.61	61.35	61.54	61.28	61.32	61.26	61.25	61.26	61.33	61.48	61.33	61.66	61.36	61.62	61.62	61.62	61.76	61.49	61.66	61.46	61.49	61.49	61.49	61.49	61.47	0.6030	0.014213
	106.59	0.00	63.49	64.36	63.66	64.36	63.66	64.52	63.77	64.11	64.03	64.11	64.11	64.24	63.72	63.76	63.76	63.76	64.24	63.34	63.91	63.61	63.91	63.61	64.37	63.37	63.91	0.6269	0.014777
R 100	40.87	0.00	41.90	38.76	42.01	42.20	40.76	43.96	42.91	40.15	43.29	40.15	41.15	43.50	39.96	43.93	44.16	38.79	42.73	42.73	39.84	43.24	39.41	42.20	42.79		41.76	0.4097	0.009656
	46.61	0.00	43.56	45.92	43.98	45.33	43.71	43.71	45.82	44.47	45.73	44.43	45.31	45.31	45.21	46.20	44.80	46.16	44.76	45.71	45.92	44.49	46.35	44.24			45.05	0.4419	0.010417
	51.46	0.00	46.69	47.80	46.33	47.65	46.43	47.63	46.15	47.75	46.73	47.72	47.72	47.20	48.02	47.18	48.24	47.69	48.19	47.36	48.55	47.28	48.29	47.79			47.47	0.4657	0.010977
	59.13	0.00	50.34	50.16	51.62	50.76	51.10	50.81	51.10	50.77	50.77	51.04	50.61	51.57	50.58	51.24	50.74	50.87	50.60	50.73	50.73	50.90	50.53	50.67			50.83	0.4986	0.011753
	67.06	0.00	55.29	55.29	55.35	55.35	55.47	55.47	55.50	55.50	55.68	55.63	55.63	55.54	55.54	55.34	55.34	55.37	55.37								55.45	0.5440	0.012821
	74.55	0.00	59.31	58.18	58.00	58.24	58.46	58.46	58.90	58.32	58.09	58.59	58.56	58.56	59.22	59.22	58.87	58.91	58.73	58.73	59.08	59.39	58.81	58.73			58.70	0.5758	0.013572
	81.63	0.00	62.09	61.67	62.37	62.09	61.53	62.56	61.53	62.56	62.05	61.73	62.30	62.05	61.55	62.58	61.55	61.66	62.23	61.66	62.23	61.98	61.88	62.46	61.98	61.58	61.99	0.6082	0.014334
	86.72	0.00	64.54	65.01	64.34	64.94	64.34	65.07	65.40	64.17	65.40	65.00	64.88	65.08	64.88	65.92	65.99	65.24	65.74	65.51	65.72	66.57	65.00	66.57	66.00	65.47	65.28	0.6404	0.015095
	95.66	0.00	70.50	70.01	71.48	70.02	70.25	70.00	70.25	70.30	70.30	70.51	70.55	70.51	70.41	70.41	70.41	69.50	70.40	69.90	69.90	69.90	69.90	69.96	69.88	71.18	70.27	0.6893	0.016247
R 60	40.86	0.00	44.77	44.77	41.85	45.06	42.49	43.45	45.32	43.09	45.05	45.52	42.92	45.48	45.73	43.66	45.63	43.70	44.52	46.49	44.13	44.13					44.39	0.4354	0.010263
	45.68	0.00	46.35	47.43	46.46	47.83	46.79	47.43	47.66	46.85	48.84	47.30	47.35	47.31	47.10	48.50	46.77	48.27	47.02	47.02	48.34	47.51	48.41				47.45	0.4655	0.010972
	49.61	0.00	51.18	49.95	51.09	49.82	50.96	50.91	49.74	51.08	50.30	51.47	50.48	51.17	50.51	51.46	51.45	50.67	51.52	50.40	51.33	50.39	51.23	50.92			50.82	0.4985	0.011751
	55.55	0.00	55.00	56.37	55.26	56.04	55.71	56.44	55.72	56.71	55.84	56.61	56.05	56.84	56.13	56.44	55.89	56.84	56.13	57.13	56.30	56.49	56.20	56.62			56.22	0.5515	0.012998
	58.34	0.00	58.47	58.14	58.07	57.86	57.85	57.51	57.88	57.62	57.77	57.56	57.97	57.70	58.08	58.08	58.16	57.63	58.44	58.44	58.49	58.31	58.35				58.02	0.5692	0.013415
	61.43	0.00	58.94	58.94	59.61	59.46	59.46	59.81	59.81	59.89	59.77	60.29	60.13	60.13	59.85	60.19	59.79	59.69	59.64	59.79	60.07	59.89	59.89	59.74	59.74		59.76	0.5863	0.013818
	63.10	0.00	61.43	60.98	61.00	61.19	61.44	61.21	61.36	61.37	61.37	61.27	61.46	61.46	61.53	61.53	61.22	61.71	61.83	61.74	61.46	61.32	61.45	61.04			61.38	0.6021	0.014192
	66.76	0.00	65.37	65.01	65.18	65.18	65.43	64.81	64.88	65.36	65.36	65.17	65.72	65.72	66.13	66.13	65.83	65.77	65.77	65.49	65.49	66.07	66.07	66.07			65.55	0.6430	0.015156
	72.39	0.00	69.34	69.34	69.59	69.69	68.61	69.41	69.48	69.48	69.48	69.60	68.65	69.65	69.92	69.19	69.19	69.39	69.39	69.39	69.69	69.83	69.61	69.61	69.30	69.30	69.42	0.6810	0.016052
	80.85	0.00	74.90	73.86	74.21	74.26	74.15	74.21	74.15	73.57	75.18	73.57	74.07	74.72	73.97	74.07	74.66	74.40	75.61	74.40	74.36	75.50	74.36	74.71	74.90	74.50	74.43	0.7301	0.017210
	86.62	0.00	79.03	78.94	78.45	80.11	78.45	78.54	79.44	77.59	79.44	79.02	79.11	79.94	78.11	79.44	79.44	78.51	79.43	78.07	78.51	79.17	77.92	79.17	77.33	79.19	78.85	0.7735	0.018231

Resistor	Angular velocity	mass readings (g)																										Force	Torque
(Ω)	(rpm)	Initial	1	2	3	4	5	6	7	8	9	10	11	12	13	14	15	16	17	18	19	20	21	22	23	24	Mean	(N)	(N.m)
R 30	40.88	0.00	50.99	48.07	49.36	51.02	48.90	50.70	51.97	50.25	51.50	50.51	49.37	51.37	49.85	50.50	51.20	49.55	50.91	51.20	49.87	51.49	50.47				50.43	0.4947	0.011661
	44.82	0.00	55.73	54.62	54.08	55.33	54.03	55.15	54.45	54.66	56.54	55.63	56.60	55.74	56.04	56.61	55.77	56.42	55.58	56.07	56.52	55.61	56.33	55.60	55.88	56.43	55.64	0.5459	0.012866
	47.89	0.00	57.25	57.71	57.04	57.71	57.30	57.22	58.38	57.68	58.87	57.73	59.31	58.81	58.03	59.18	58.57	59.09	58.41	58.95	58.51	58.44	58.94				58.24	0.5714	0.013467
	52.39	0.00	64.02	63.55	63.70	63.45	63.84	63.48	63.76	63.70	63.68	64.11	63.83	64.41	64.16	64.45	63.91	64.05	63.65	64.26	64.04	64.48	64.18	64.39			63.96	0.6274	0.014789
	54.48	0.00	65.57	65.19	65.36	64.99	64.78	65.42	65.39	65.87	65.51	66.54	66.43	66.72	66.36	66.75	66.53	66.57	66.34	66.58	66.28	66.38	65.95	66.28			65.99	0.6474	0.015258
	56.66	0.00	68.12	68.17	68.01	68.25	68.03	68.48	68.56	69.19	69.06	69.46	69.46	69.46	69.07	69.19	69.19	69.24	69.03	70.15	70.03	70.13	69.75	69.75			69.08	0.6777	0.015973
	57.84	0.00	70.20	70.09	71.11	70.65	70.89	70.54	70.81	70.49	70.58	70.47	70.76	70.40	70.51	70.35	70.54	70.20	70.63	70.37	70.58						70.54	0.6920	0.016309
	60.37	0.00	72.20	71.94	72.28	72.35	71.95	72.47	72.47	72.43	72.43	72.51	72.47	72.50	72.00	72.25	72.37	73.10	73.21	72.97	73.05	72.18					72.46	0.7108	0.016754
	65.46	0.00	78.05	78.05	78.05	78.15	78.15	78.15	78.15	78.46	78.31	78.31	78.31	78.31	78.26	78.26	78.26	78.00	78.00	78.00	78.00	78.21	78.21	78.21	78.24	78.24	78.18	0.7670	0.018077
	72.27	0.00	85.92	84.79	85.93	85.93	85.68	85.68	85.68	85.39	85.39	86.06	85.11	85.80	85.80	85.80	85.80	86.19	85.07	86.46	86.46	85.86	85.86	85.86	85.83	85.83	85.76	0.8413	0.019829
	76.26	0.00	90.25	89.70	89.28	89.70	89.70	89.00	89.89	89.97	89.97	90.24	89.15	89.25	90.19	89.25	89.25	90.27	89.78	89.78	90.40	89.88	89.88	90.50	89.82	90.50	89.82	0.8811	0.020768
	80.99	0.00	93.26	92.96	93.26	93.11	93.36	93.36	93.61	93.74	93.74	93.61	93.47	93.47	93.67	93.87	93.69	93.88	93.76	93.75	93.84	93.84	93.90	94.20	94.15	93.93	93.64	0.9186	0.021652
	86.97	0.00	99.10	99.25	99.94	99.25	99.16	98.95	99.16	98.95	99.06	99.99	98.90	99.09	99.00	99.25	99.25	99.06	99.25	99.06	99.02	99.14	98.68	99.02	99.01	98.97	99.15	0.9726	0.022925
R 10	40.87	0.00	57.12	55.97	57.29	59.47	57.17	59.64	59.31	58.18	59.69	58.42	59.07	59.29	58.32	58.77	59.62	58.31	59.33	59.28	58.45	59.94	59.31	58.36			58.65	0.5754	0.013561
	43.18	0.00	61.20	62.41	61.36	62.52	63.50	62.39	63.51	62.59	62.79	63.71	62.76	64.08	62.85	62.79	63.36	62.85	63.69	62.82	63.13	63.65	62.89	63.24	63.48		62.94	0.6174	0.014553
	44.83	0.00	65.50	64.47	63.73	65.46	64.25	65.61	65.95	65.00	65.82	65.04	65.54	65.18	64.78	65.45	65.09	65.29	65.06	64.89	66.49	65.48	65.78	65.25	65.59		65.25	0.6401	0.015087
	47.09	0.00	68.42	69.13	69.19	68.28	68.90	68.56	69.58	69.08	69.37	69.38	68.96	69.34	68.55	69.44	69.87	69.04	69.43	69.01	69.65	69.10	69.76	69.16			69.15	0.6783	0.015988
	48.07	0.00	71.59	72.30	71.36	71.91	71.58	72.00	71.64	71.14	71.94	71.56	72.14	71.69	72.46	72.34	71.48	72.36	71.73	72.06	71.78	71.63					71.83	0.7047	0.016610
	49.05	0.00	72.62	72.02	72.87	72.06	72.82	72.43	72.47	73.10	72.46	73.34	72.74	73.29	72.82	73.15	72.83	72.82	73.18	72.82	73.24	72.69					72.79	0.7141	0.016830
	49.61	0.00	73.25	73.03	73.90	73.53	73.55	73.96	73.85	74.17	73.75	74.15	73.68	74.35	74.26	74.25	73.95	73.83	73.91	73.64	73.90	73.37					73.81	0.7241	0.017067
	50.67	0.00	75.71	75.03	75.47	74.79	75.15	75.31	75.20	75.15	74.96	77.04	76.67	77.08	76.86	76.98	76.51	76.69	76.30	76.36	76.62	76.39	76.58	76.30			76.05	0.7461	0.017585
	53.42	0.00	80.31	79.41	80.41	79.80	80.47	79.88	80.23	80.23	79.80	80.41	80.01	80.23	79.68	80.29	79.66	80.46	79.91	80.52	80.51	80.84					80.15	0.7863	0.018533
	59.09	0.00	89.81	89.81	89.20	89.20	89.97	89.97	89.27	89.27	90.29	90.29	89.96	89.96	90.24	90.24	89.34	89.34	89.62	89.62	89.62	90.01	90.01	89.93	89.93	89.93	89.78	0.8808	0.020760
	66.12	0.00	98.26	98.26	98.26	98.21	98.21	98.16	98.16	98.16	98.16	98.41	98.41	98.40	98.40	98.40	98.40	98.22	98.22	98.22	98.22	98.36	98.36	98.36	98.45	98.45	98.30	0.9643	0.022728
	69.37	0.00	103.71	103.74	103.28	103.29	103.29	103.30	103.29	103.67	103.63	103.63	103.63	103.63	102.74	103.35	103.35	103.35	103.33	103.83	102.79	102.73	102.83	102.83	102.83	103.28	103.31	1.0134	0.023886
R 5	40.54	0.00	60.69	61.17	61.90	60.99	61.87	62.00	61.09	62.40	60.70	61.05	61.94	60.78	61.90	62.04	61.05	62.06	61.81	60.77	62.42	61.37	61.71	62.56	60.64		61.52	0.6035	0.014224
	44.61	0.00	71.23	69.29	70.36	69.82	69.07	70.05	69.04	69.80	69.24	69.11	69.95	69.10	70.10	69.63	69.40	70.06	69.01	69.93	69.15	69.20	69.88				69.64	0.6832	0.016102
	49.60	0.00	79.95	79.03	79.13	78.98	78.88	79.36	78.68	79.64	78.85	79.78	79.72	80.30	80.16	79.22	80.32	79.64	80.25	79.30	80.29	79.35	80.02				79.56	0.7805	0.018397
	53.40	0.00	87.54	87.54	87.54	87.54	87.93	87.93	87.62	87.62	87.93	87.93	87.58	87.58	87.84	87.84	87.35	87.35	87.93	87.53	87.32	87.22	87.52	87.52			87.62	0.8596	0.020260
	59.07	0.00	96.39	96.39	96.69	96.27	96.27	96.62	96.62	96.49	96.49	96.69	96.69	96.69	96.72	96.72	96.80	96.80	96.77	96.77	97.06	97.06	96.68	96.68	96.83	96.33	96.65	0.9481	0.022347
	66.08	0.00	105.10	105.10	105.10	104.94	104.94	105.27	105.44	105.48	105.48	105.48	105.57	105.57	105.57	105.57	105.57	105.57	105.57	105.57	105.57	105.57	105.65	105.65	105.65	105.68	105.44	1.0344	0.024381
R 3	40.53	0.00	64.40	62.52	64.45	64.00	63.25	64.34	63.31	63.52	64.19	63.21	63.64	64.29	62.85	64.21	63.34	62.50	64.65	62.61	63.14	64.28					63.64	0.6243	0.014714
	44.62	0.00	73.85	73.06	72.02	73.61	72.43	73.34	72.68	72.23	73.48	72.02	74.05	73.22	71.70	73.68	71.94	73.55	72.19	71.93	73.79	72.78	73.11				72.89	0.7150	0.016853
	49.61	0.00	83.28	82.49	82.63	82.13	82.62	82.12	83.03	82.50	82.34	82.86	82.17	83.02	82.52	83.07	82.47	83.22	83.13	82.71	83.07	82.27	82.89	82.15	82.90		82.68	0.8111	0.019117
	53.42	0.00	91.84	91.85	91.85	91.30	91.30	91.49	91.49	91.38	91.26	91.54	91.54	91.29	91.11	91.11	91.73	91.73	91.59	91.59	91.59	91.18	91.18	91.49	91.56	91.25	91.47	0.8973	0.021149
	59.11	0.00	101.25	101.25	100.90	100.90	100.19	100.19	100.78	100.78	100.45	100.45	100.59	100.59	100.11	100.11	100.38	100.10	100.10	100.26	100.26	99.87	99.87	100.32	100.32	100.20	100.43	0.9852	0.023221
	66.09	0.00	110.33	110.33	110.37	110.37	110.20	110.20	110.15	110.15	109.98	109.78	109.78	109.93	109.97	109.38	109.38	109.38	110.20	110.20	110.78	110.76	110.66	110.53	110.53	110.33	110.15	1.0806	0.025470

Appendix L: Overall results - 280 mm rotor – BEMM, CFD and testing

CFD - Relative power		
Hub ratio	Ansys Results: Rotor Set 1 (STD BEMM design)	Ansys Results: Rotor Set 2 (ADP BEMM design)
5	1.0000	1.0000
10	1.0006	1.0035
15	0.9974	1.0018
20	0.9819	0.9860
25	0.9624	0.9618

BEMM - Relative power		
Hub ratio	BEMM Results: Analysis 1	BEMM Results: Analysis 3
5	1.0000	1.0009
10	0.9983	1.0028
15	0.9896	1.0024
20	0.9724	0.9986
25	0.9454	0.9853

Physical Test - Relative power		
Hub ratio	STD BEM	ADP BEM
5	1.0000	1.0000
10	0.9954	1.0044
15	0.9851	0.9888
20	0.9773	0.9786
25	0.9318	0.9466

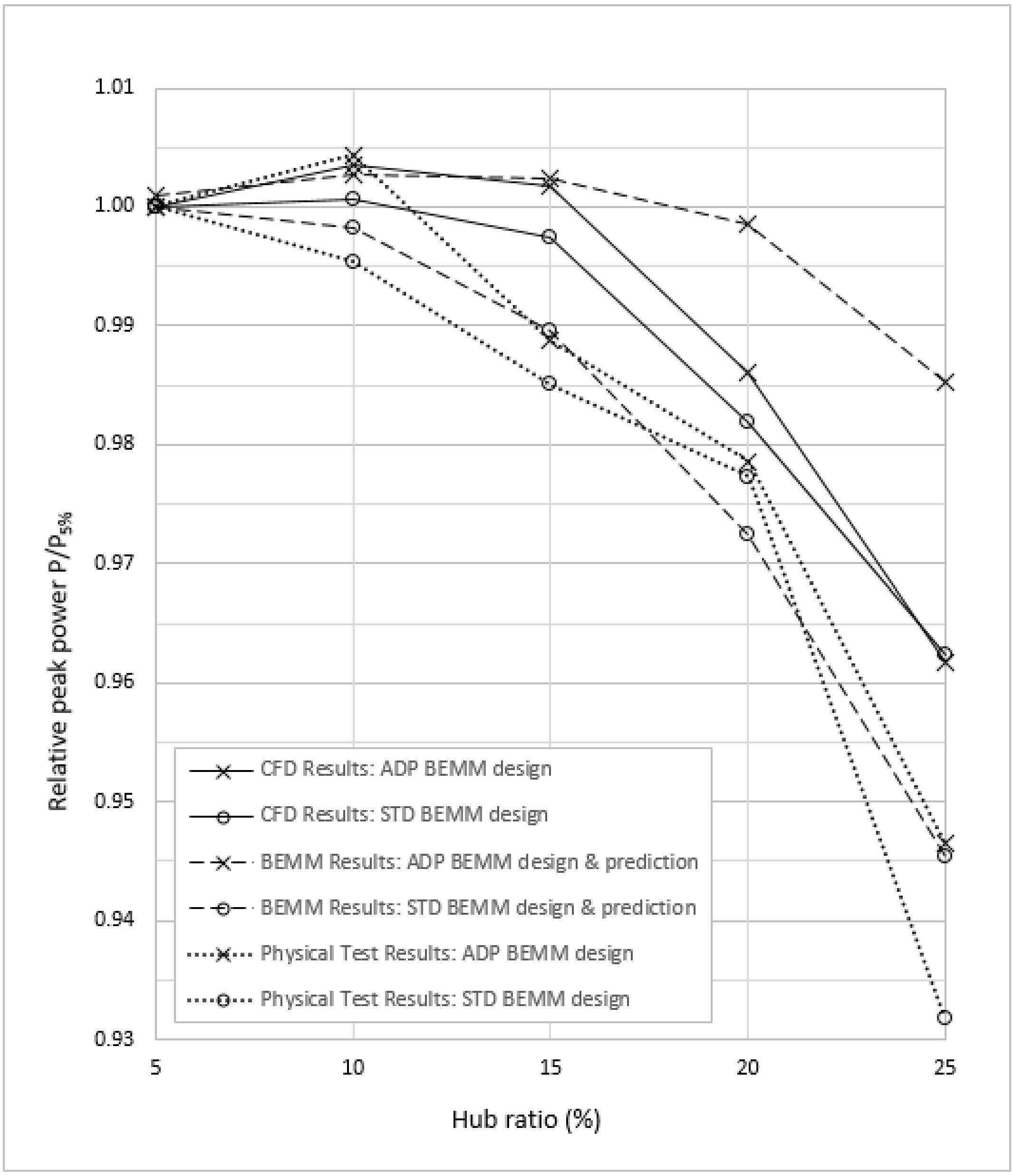

Appendix M: Results – 30 m rotor – BEMM predictions

ADP (Rankine) BEMM Prediction			
BEMM Power (Rankine, Buhl, Trunc, ADP COR) (W)	% Power loss from streamline deflection (%)	Power loss from streamline deflection (W)	Net Power (W)
402149	0	0	402149
402924	0.0394	159	402765
403452	0.2292	925	402527
403105	0.6534	2634	400471
401377	1.4004	5621	395756

STD - STD BEMM Prediction			
BEMM Power (Hansen, Buhl, Trunc, STD STD) (W)	% Power loss from streamline deflection (mean) (%)	Power loss from streamline deflection (mean) (W)	Net Power (W)
401568	0.0025	10	401558
400026	0.0692	277	399749
396554	0.3146	1248	395306
390895	0.8312	3249	387646
382961	1.7082	6542	376419

ADP (Airship) BEMM Prediction			
BEMM Power (Airship, Buhl, Trunc, ADP COR) (W)	% Power loss from streamline deflection (%)	Power loss from streamline deflection (W)	Net Power (W)
402179	0.005	20	402159
402928	0.099	399	402529
403041	0.4	1612	401429
401980	1.009	4056	397924
399194	2.016	8048	391146

Appendix N: Results - 30 m rotor – CFD simulations

	Fluent angular velocity (rpm)	Fluent angular velocity (rad/s)	Torque on blade only (Fluent, one blade, 120° slice) (Nm)	Power (blade only, one blade, 120o slice) (W)	Power (blades only, whole rotor) (W)	Total Torque on Hub only (Fluent, 120° slice) (Nm)	Adjusted Torque on Hub based on fraction of surface area that would be rotating (fraction below) 0.668	Net Torque (Ansys, one blade, 120° slice) (Nm)	Ratio: hub torque / blade torque	Net Power (one blade with hub, 120° slice) (W)	Net Power (whole rotor) (W)
30m 5COR rotor for rough peak (100p)											
	43.85	4.592	26184	120 236	360 708	-0.637	-0.426	26184	-0.00002	120 234	360 702
	44.85	4.697	25608	120 273	360 818	-0.521	-0.348	25608	-0.00001	120 271	360 813
	45.85	4.801	25033	120 193	360 580	-0.574	-0.383	25033	-0.00002	120 192	360 575
Micro-adjustments for 30m 5hub uncertainty estimate											
99.9p	44.85	4.697	25561	120 052	360 156	-0.531	-0.355	25561	-0.00001	120 050	360 151
99.8p	44.85	4.697	25503	119 779	359 338	-0.523	-0.350	25503	-0.00001	119 778	359 333
100.1p	44.85	4.697	25639	120 418	361 255	-0.642	-0.429	25639	-0.00002	120 416	361 249
99.7p	44.85	4.697	25562	120 057	360 170	-0.584	-0.391	25562	-0.00002	120 055	360 164
100.3p	44.85	4.697	25618	120 320	360 959	-0.529	-0.354	25618	-0.00001	120 318	360 954
100.2p	44.85	4.697	25511	119 817	359 451	-0.518	-0.346	25511	-0.00001	119 815	359 446
100p	44.85	4.697	25608	120 273	360 818	-0.521	-0.348	25608	-0.00001	120 271	360 813
Re-graph 30m 5%hub											
99.8p	43.85	4.592	26082	119 768	359 303	-0.581	-0.388	26082	-0.00001	119 766	359 297
99.8p	44.85	4.697	25503	119 779	359 338	-0.523	-0.350	25503	-0.00001	119 778	359 333
99.8p	45.85	4.801	24944	119 766	359 298	-0.497	-0.332	24944	-0.00001	119 765	359 294
Mesh dependence study simulations											
LS135	44.85	4.697	25905	121 668	365 003	-0.551	-0.368	25905	-0.00001	121 666	364 997
LS130	44.85	4.697	25813	121 235	363 706	-0.499	-0.334	25813	-0.00001	121 234	363 702
LS115	44.85	4.697	25600	120 235	360 705	-0.520	-0.347	25600	-0.00001	120 233	360 700
LS90	44.85	4.697	25648	120 460	361 381	-0.547	-0.366	25648	-0.00001	120 459	361 376

30m 10COR rotor for rough peak (100p)

	Fluent angular velocity (rpm)	Fluent angular velocity (rad/s)	Torque on blade only (Fluent, one blade, 120° slice) (Nm)	Power (blade only, one blade, 120o slice) (W)	Power (blades only, whole rotor) (W)	Total Torque on Hub only (Fluent, 120° slice) (Nm)	Adjusted Torque on Hub based on fraction of surface area that would be rotating (fraction below) 0.556	Net Torque (Ansys, one blade, 120° slice) (Nm)	Ratio: hub torque / blade torque	Net Power (one blade with hub, 120° slice) (W)	Net Power (whole rotor) (W)
	39.725	4.160	28717	119 462	358 387	-5.000	-2.779	28714	-0.00010	119 451	358 353
	43.392	4.544	26517	120 493	361 480	-5.100	-2.835	26514	-0.00011	120 480	361 441
	45.17	4.730	25505	120 644	361 931	-5.130	-2.851	25502	-0.00011	120 630	361 890
	47.059	4.928	24448	120 480	361 440	-5.100	-2.835	24445	-0.00012	120 466	361 398
	50.726	5.312	22488	119 457	358 370	-5.200	-2.890	22485	-0.00013	119 441	358 324
Micro-adjustments for 30m 10hub uncertainty estimate											
100p	45.17	4.730	25505	120 644	361 931	-5.130	-2.851	25502	-0.00011	120 630	361 890
99.9p	45.17	4.730	25406	120 175	360 526	-5.129	-2.850	25403	-0.00011	120 162	360 485
100.1p	45.17	4.730	25449	120 379	361 136	-5.119	-2.845	25446	-0.00011	120 365	361 096
100.2p	45.17	4.730	25393	120 114	360 341	-5.120	-2.846	25390	-0.00011	120 100	360 301
99.8p	45.17	4.730	25468	120 469	361 406	-5.119	-2.845	25465	-0.00011	120 455	361 365
99.7p	45.17	4.730	25393	120 114	360 341	-5.081	-2.824	25390	-0.00011	120 100	360 301
100.3p	45.17	4.730	25441	120 341	361 022	-5.089	-2.828	25438	-0.00011	120 327	360 982
Re-graph 30m 10%hub											
100.2p	44.65	4.676	25675	120 050	360 149	-5.111	-2.841	25672	-0.00011	120 036	360 109
100.2p	45.17	4.730	25393	120 114	360 341	-5.120	-2.846	25390	-0.00011	120 100	360 301
100.2p	45.65	4.780	25112	120 047	360 140	-5.146	-2.860	25109	-0.00011	120 033	360 099

30m 15COR rotor for rough peak (100p)

	Fluent angular velocity (rpm)	Fluent angular velocity (rad/s)	Torque on blade only (Fluent, one blade, 120° slice) (Nm)	Power (blade only, one blade, 120o slice) (W)	Power (blades only, whole rotor) (W)	Total Torque on Hub only (Fluent, 120° slice) (Nm)	Adjusted Torque on Hub based on fraction of surface area that would be rotating (fraction below) 0.469	Net Torque (Ansys, one blade, 120° slice) (Nm)	Ratio: hub torque / blade torque	Net Power (one blade with hub, 120° slice) (W)	Net Power (whole rotor) (W)
	39.725	4.160	28605	118 997	356 990	-18.200	-8.528	28596	-0.00030	118 961	356 883
	43.392	4.544	26422	120 062	360 185	-18.830	-8.823	26413	-0.00033	120 021	360 064
	44.6	4.671	25731	120 177	360 530	-19.000	-8.903	25722	-0.00035	120 135	360 405
	45.24	4.738	25370	120 191	360 573	-19.100	-8.949	25361	-0.00035	120 149	360 446
	47.059	4.928	24364	120 066	360 198	-19.400	-9.090	24355	-0.00037	120 021	360 063
	50.726	5.312	22391	118 941	356 824	-19.900	-9.324	22382	-0.00042	118 892	356 675
Micro-adjustments for 30m 15hub uncertainty estimate											
100p	45.24	4.738	25370	120 191	360 573	-19.100	-8.949	25361	-0.00035	120 149	360 446
99.9p	45.24	4.738	25327	119 987	359 962	-19.003	-8.904	25318	-0.00035	119 945	359 835
99.8p	45.24	4.738	25320	119 954	359 862	-18.998	-8.902	25311	-0.00035	119 912	359 736
100.1p	45.24	4.738	25345	120 072	360 217	-19.072	-8.936	25336	-0.00035	120 030	360 090
100.2p	45.24	4.738	25300	119 859	359 578	-18.962	-8.885	25291	-0.00035	119 817	359 452
Re-graph 30m 15%hub											
100.2p	44.74	4.685	25580	119 846	359 539	-18.870	-8.842	25571	-0.00035	119 805	359 415
100.2p	45.24	4.738	25300	119 859	359 578	-18.912	-8.861	25291	-0.00035	119 817	359 452
100.2p	45.74	4.790	25019	119 838	359 514	-19.041	-8.922	25010	-0.00036	119 795	359 386

30m 20COR rotor for rough peak

	Fluent angular velocity (rpm)	Fluent angular velocity (rad/s)	Torque on blade only (Fluent, one blade, 120° slice) (Nm)	Power (blade only, one blade, 120o slice) (W)	Power (blades only, whole rotor) (W)	Total Torque on Hub only (Fluent, 120° slice) (Nm)	Adjusted Torque on Hub based on fraction of surface area that would be rotating (fraction below) 0.471	Net Torque (Ansys, one blade, 120° slice) (Nm)	Ratio: hub torque / blade torque	Net Power (one blade with hub, 120° slice) (W)	Net Power (whole rotor) (W)
	39.725	4.160	28480	118 477	355 430	-48.300	-22.742	28457	-0.00080	118 382	355 146
	43.392	4.544	26322	119 607	358 821	-51.030	-24.028	26298	-0.00091	119 498	358 494
	45.38	4.752	25201	119 760	359 279	-52.780	-24.852	25176	-0.00099	119 642	358 925
	47.059	4.928	24285	119 677	359 030	-54.410	-25.619	24259	-0.00105	119 550	358 651
	50.726	5.312	22366	118 809	356 426	-58.280	-27.442	22339	-0.00123	118 663	355 988
Micro-adjustments for 30m 20hub uncertainty estimate											
99.9p	45.38	4.752	25237	119 931	359 792	-52.739	-24.833	25212	-0.00098	119 813	359 438
100.1p	45.38	4.752	25252	120 002	360 006	-52.677	-24.803	25227	-0.00098	119 884	359 653
99.8p	45.38	4.752	25198	119 745	359 236	-52.541	-24.739	25173	-0.00098	119 628	358 884
100.2p	45.38	4.752	25272	120 097	360 291	-52.707	-24.817	25247	-0.00098	119 979	359 938
Re-graph 30m 20%hub											
99.8p	44.88	4.700	25476	119 733	359 198	-52.077	-24.521	25451	-0.00096	119 617	358 852
99.8p	45.38	4.752	25198	119 745	359 236	-52.541	-24.739	25173	-0.00098	119 628	358 884
99.8p	45.88	4.805	24928	119 768	359 303	-53.006	-24.958	24903	-0.00100	119 648	358 943
99.8p	46.38	4.857	24658	119 761	359 284	-53.470	-25.177	24633	-0.00102	119 639	358 918

30m 25COR rotor for rough peak

	Fluent angular velocity (rpm)	Fluent angular velocity (rad/s)	Torque on blade only (Fluent, one blade, 120° slice) (Nm)	Power (blade only, one blade, 120o slice) (W)	Power (blades only, whole rotor) (W)	Total Torque on Hub only (Fluent, 120° slice) (Nm)	Adjusted Torque on Hub based on fraction of surface area that would be rotating (fraction below) 0.426	Net Torque (Ansys, one blade, 120° slice) (Nm)	Ratio: hub torque / blade torque	Net Power (one blade with hub, 120° slice) (W)	Net Power (whole rotor) (W)
	39.725	4.160	28178	117 220	351 661	-111.550	-47.541	28130	-0.00169	117 022	351 067
	43.392	4.544	26056	118 398	355 195	-121.110	-51.616	26004	-0.00198	118 164	354 492
	45.5	4.765	24921	118 742	356 227	-127.310	-54.258	24867	-0.00218	118 484	355 451
	46.35	4.854	24479	118 815	356 446	-129.930	-55.375	24424	-0.00226	118 546	355 639
	47.059	4.928	24105	118 790	356 369	-132.150	-56.321	24049	-0.00234	118 512	355 536
	49	5.131	23086	118 460	355 381	-138.300	-58.942	23027	-0.00255	118 158	354 474
	50.726	5.312	22195	117 900	353 700	-144.020	-61.380	22134	-0.00277	117 574	352 722
	Micro-adjustments for 30m 25hub uncertainty estimate										
99.9p	46.35	4.854	24478	118 810	356 431	-130.330	-55.545	24422	-0.00227	118 541	355 622
99.8p	46.35	4.854	24401	118 437	355 310	-129.800	-55.319	24346	-0.00227	118 168	354 504
100.1p	46.35	4.854	24503	118 932	356 795	-130.660	-55.686	24447	-0.00227	118 661	355 984
	Re-graph 30m 25%hub										
99.8p	45.35	4.749	24920	118 346	355 038	-126.770	-54.028	24866	-0.00217	118 090	354 269
99.8p	45.85	4.801	24666	118 431	355 294	-128.310	-54.684	24611	-0.00222	118 169	354 506
99.8p	46.35	4.854	24401	118 437	355 310	-129.800	-55.319	24346	-0.00227	118 168	354 504

Appendix O: Overall results - 30 m rotor – BEMM and CFD

CFD Results		
Hub ratio (%)	CFD Rankine corrected rotor (W)	CFD relative power $P/P_{5\%}$
5	359 333	1.0000
10	360 301	1.0027
15	359 452	1.0003
20	358 943	0.9989
25	354 506	0.9866

ADP (Rankine) BEMM Prediction					
BEMM Power (Rankine, Buhl, Trunc, ADP COR) (W)	% Power loss from streamline deflection (%)	Power loss from streamline deflection (W)	Net Power (W)	Adjusted to Ansys 5% result (W)	BEMM Relative power $P/P_{5\%}$
402149	0	0	402149	359333	1.0000
402924	0.0394	159	402765	359884	1.0015
403452	0.2292	925	402527	359671	1.0009
403105	0.6534	2634	400471	357834	0.9958
401377	1.4004	5621	395756	353621	0.9841

STD - STD BEMM Prediction					
BEMM Power (Hansen, Buhl, Trunc, STD STD) (W)	% Power loss from streamline deflection (mean) (%)	Power loss from streamline deflection (mean) (W)	Net Power (W)	Adjusted to Ansys 5% result (W)	BEMM Relative power $P/P_{5\%}$
401568	0.0025	10	401558	359333	1.0000
400026	0.0692	277	399749	357715	0.9955
396554	0.3146	1248	395306	353739	0.9844
390895	0.8312	3249	387646	346884	0.9654
382961	1.7082	6542	376419	336838	0.9374

ADP (Airship) BEMM Prediction					
BEMM Power (Airship, Buhl, Trunc, ADP COR) (W)	% Power loss from streamline deflection (%)	Power loss from streamline deflection (W)	Net Power (W)	Adjusted to Ansys 5% result (W)	BEMM Relative power $P/P_{5\%}$
402179	0.005	20	402159	359333	1.0000
402928	0.099	399	402529	359664	1.0009
403041	0.4	1612	401429	358681	0.9982
401980	1.009	4056	397924	355550	0.9895
399194	2.016	8048	391146	349494	0.9726

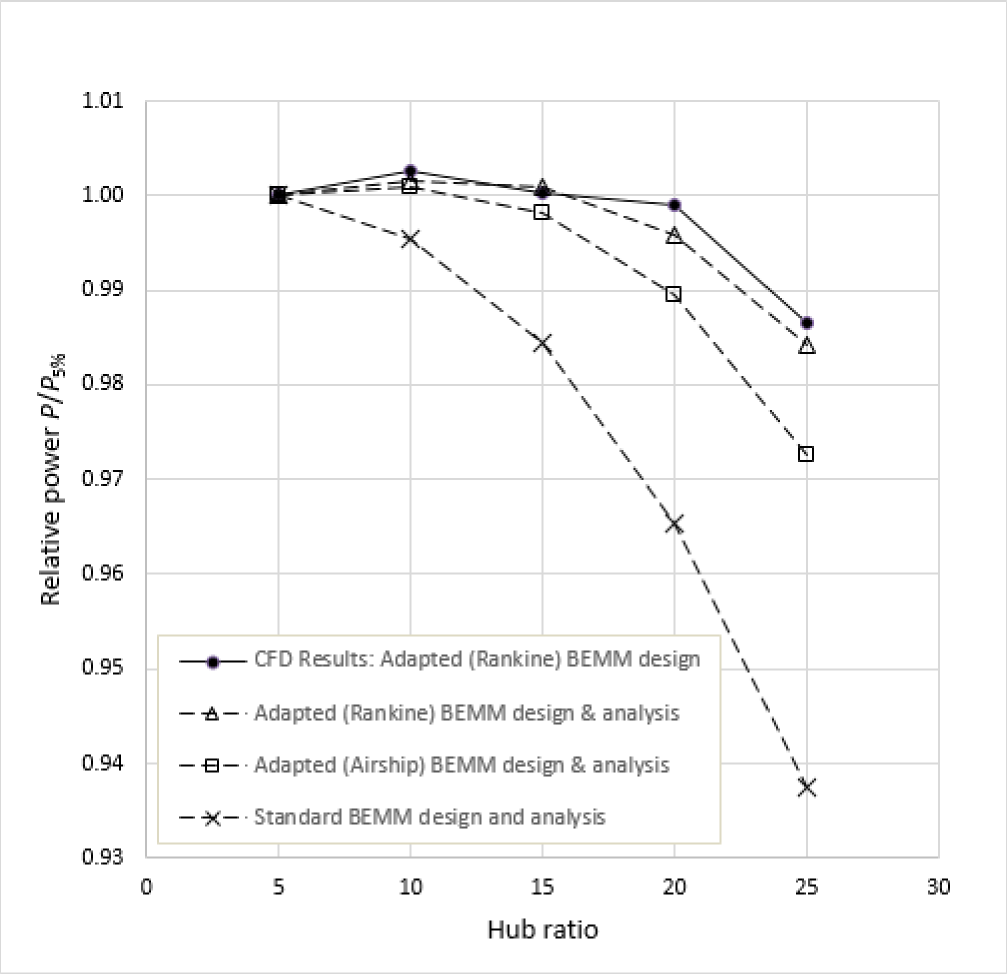

Appendix P: Flow charts of methodology

Flow chart - BEMM, CFD and physical testing of 280 mm rotors

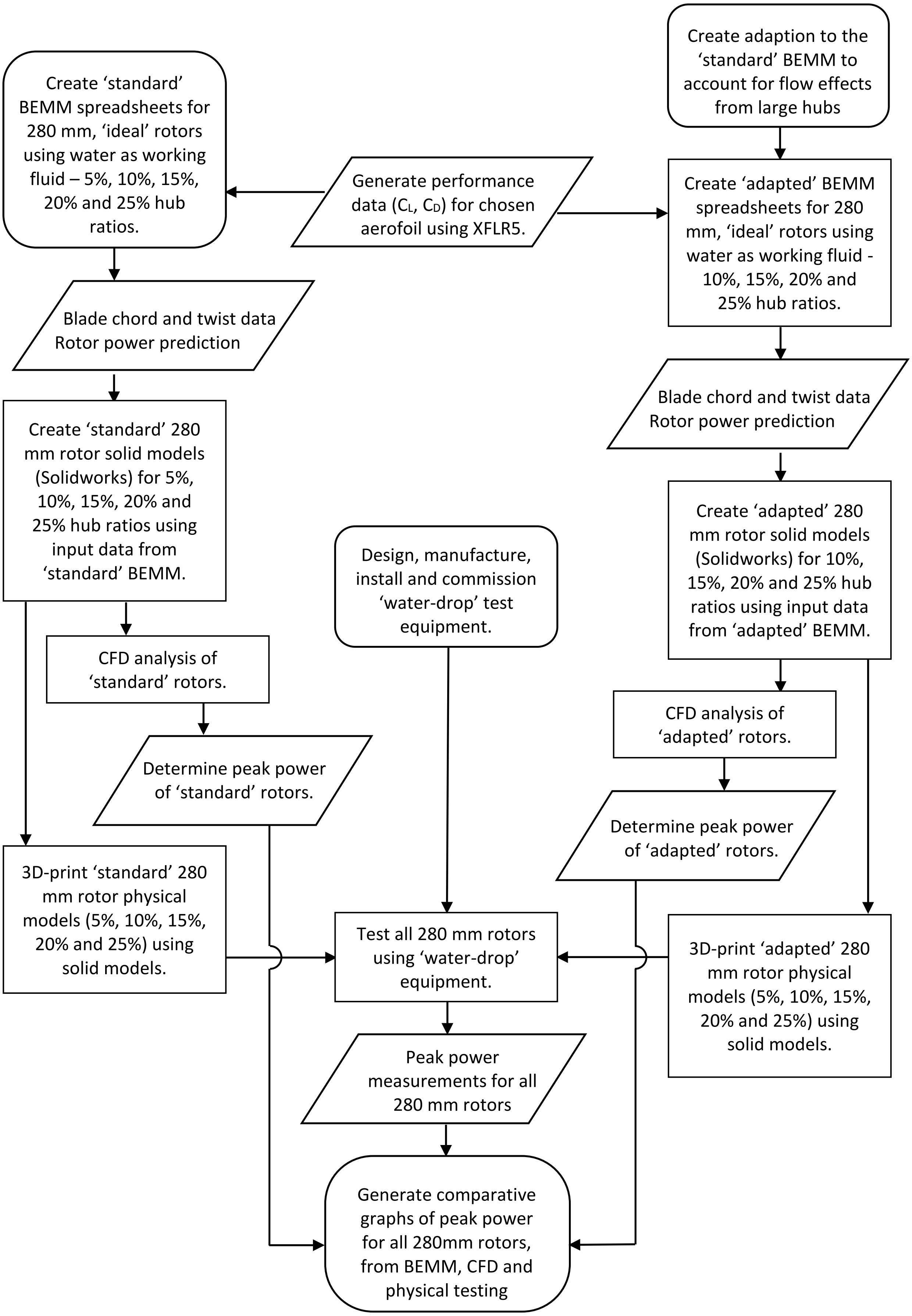

Case Study – Methodology flow chart - BEMM and CFD of 30 m rotors

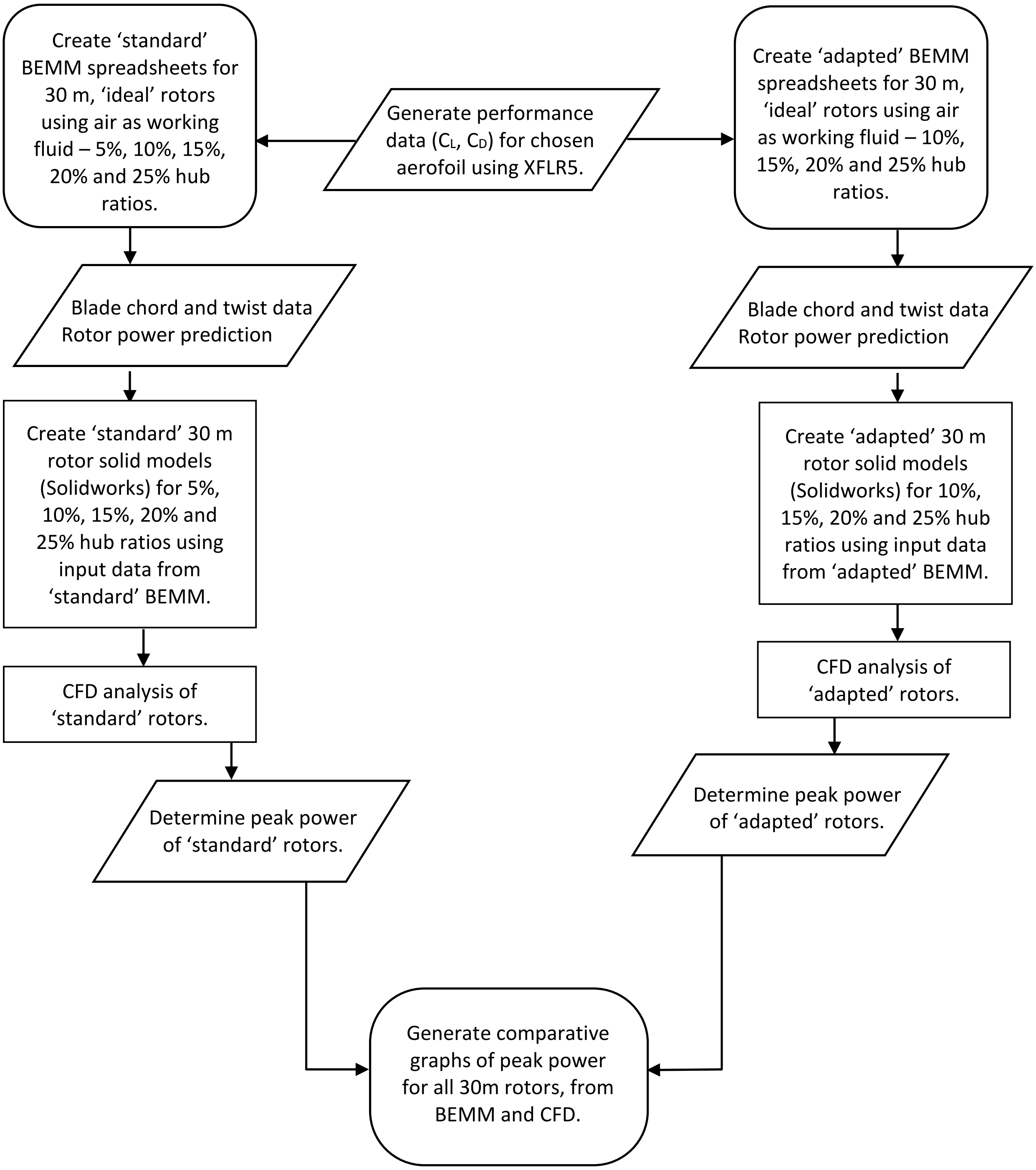

Appendix Q: Flow chart of adapted BEMM

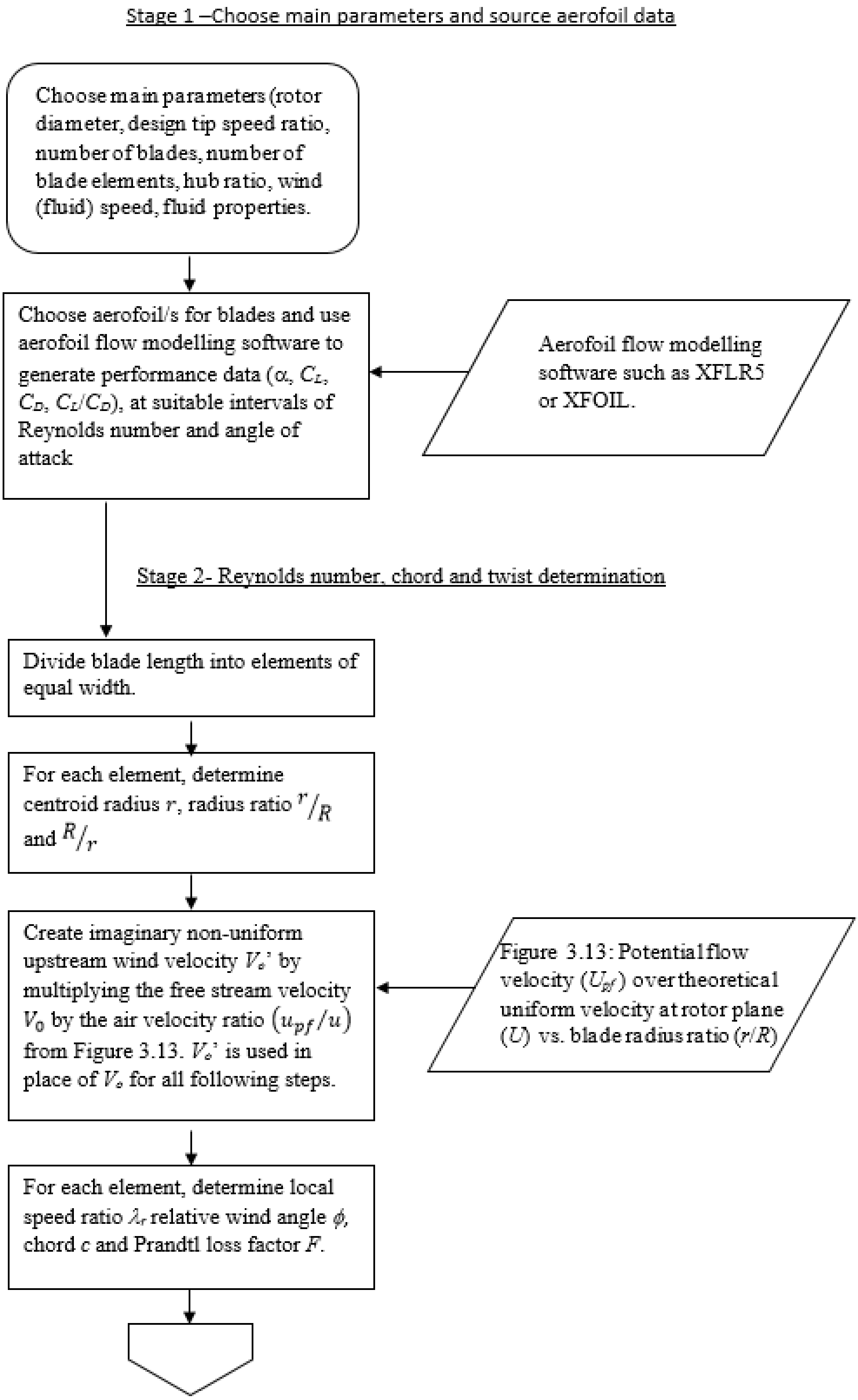

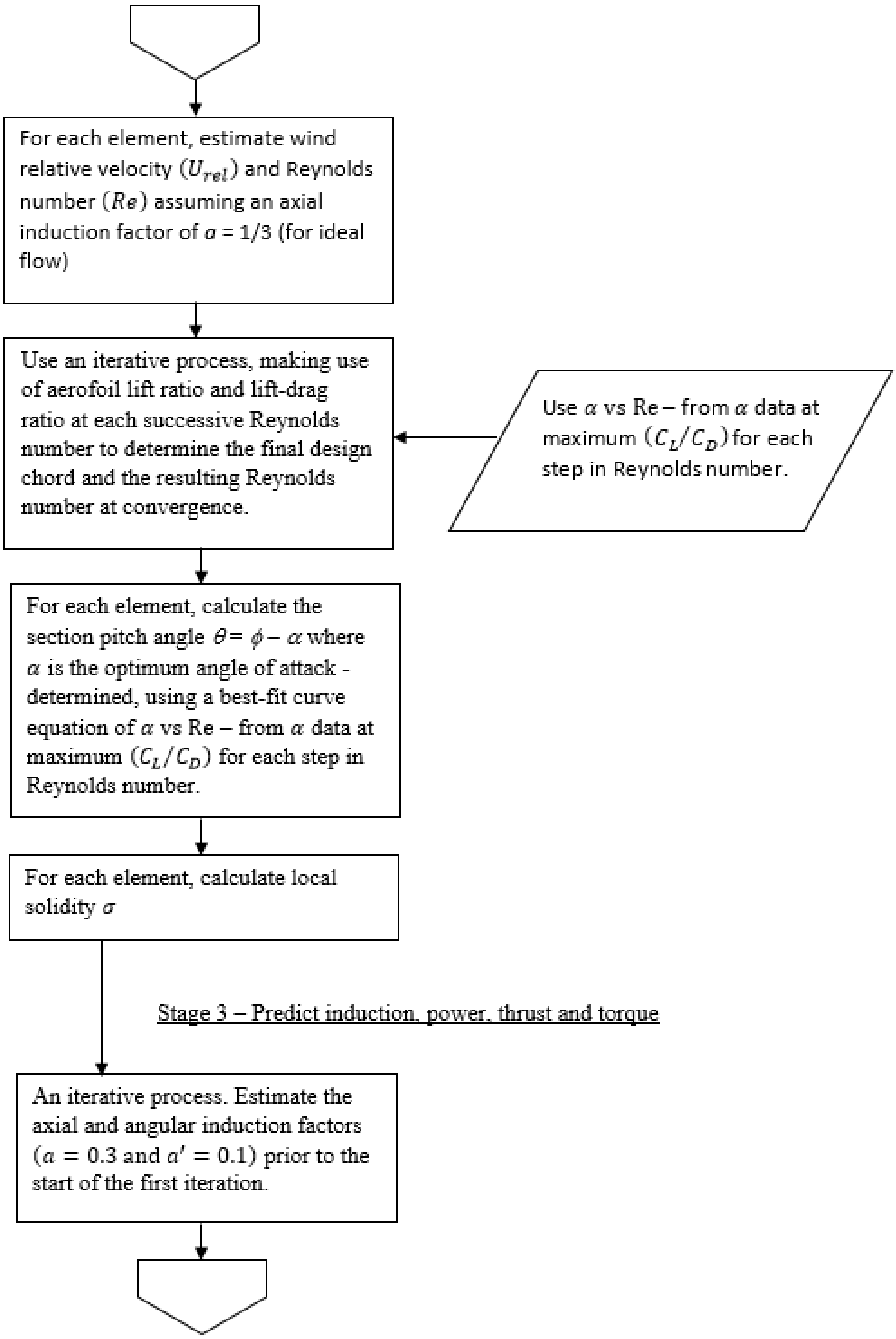
For each element, estimate wind relative velocity (U_{rel}) and Reynolds number (Re) assuming an axial induction factor of a = 1/3 (for ideal flow)
Use an iterative process, making use of aerofoil lift ratio and lift-drag ratio at each successive Reynolds number to determine the final design chord and the resulting Reynolds number at convergence.
Use α vs Re – from α data at maximum (C_L/C_D) for each step in Reynolds number.
For each element, calculate the section pitch angle $\theta = \phi - \alpha$ where α is the optimum angle of attack - determined, using a best-fit curve equation of α vs Re – from α data at maximum (C_L/C_D) for each step in Reynolds number.
For each element, calculate local solidity σ
Stage 3 – Predict induction, power, thrust and torque
An iterative process. Estimate the axial and angular induction factors ($a = 0.3$ and $a' = 0.1$) prior to the start of the first iteration.

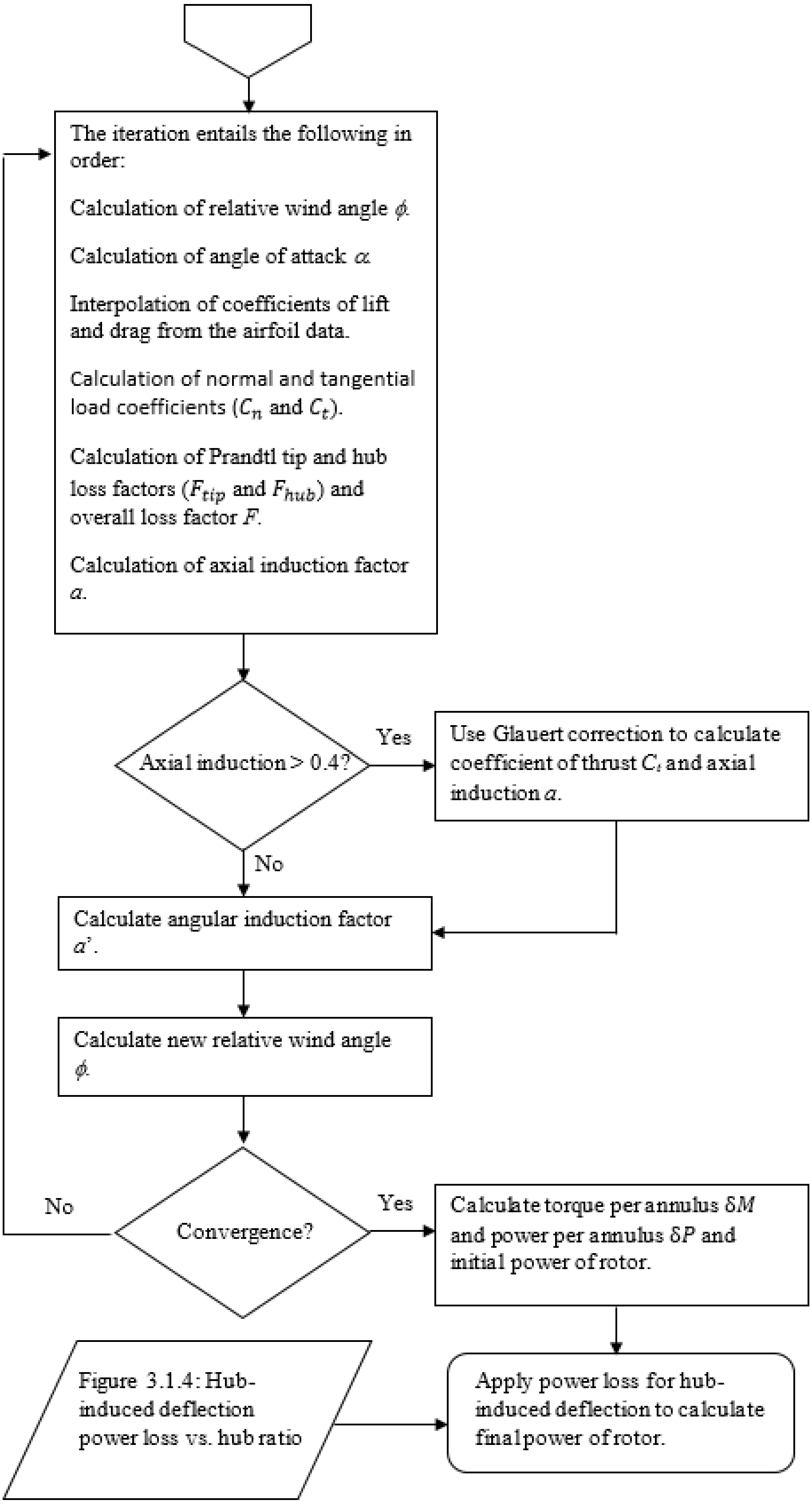

The iteration entails the following in order:
Calculation of relative wind angle ϕ.
Calculation of angle of attack α.
Interpolation of coefficients of lift and drag from the airfoil data.
Calculation of normal and tangential load coefficients (C_n and C_t).
Calculation of Prandtl tip and hub loss factors (F_{tip} and F_{hub}) and overall loss factor F.
Calculation of axial induction factor a.
Axial induction > 0.4?
Yes
Use Glauert correction to calculate coefficient of thrust C_t and axial induction a.
No
Calculate angular induction factor a'.
Calculate new relative wind angle ϕ.
No
Convergence?
Yes
Calculate torque per annulus δM and power per annulus δP and initial power of rotor.
Figure 3.1.4: Hub-induced deflection power loss vs. hub ratio
Apply power loss for hub-induced deflection to calculate final power of rotor.

Appendix R – Meshing the boundary layer

Adequate meshing of the 280 mm and 30 m rotors required knowledge of the expected boundary layer thickness over the width of the blade, and ensuring that sufficient mesh cells were located in this region of high shear stress so that skin friction drag and the boundary layer flow could be reasonably modelled. Owing to the possibility of separation and/or reattachment the choice was made to use cell layers as opposed to a wall function to model all rotors.

For both rotor sizes, an estimate of necessary normal cell and inflation layer height was determined using Excel. Boundary layer and laminar sub-layer thickness for 5% and 25% rotors was determined and graphed – using mid-span element of blade (radius, chord, Reynolds number and relative velocity at element). Height of y+=1 and y+=5 were calculated for the 5% and 25% rotors and graphed over the mid-span chord (treated as flat plate). Computation capacity allowed for a maximum total cell count of about 8 million cells – which limited the number of inflation layers that could be applied.

Effort was made to produce a first inflation layer height approximately equal to y where the y+=1 to capture some part of the viscous sub-layer. Further cell layer heights were designed by using appropriately sized inflation layer growth rate, surface mesh size and volume mesh growth rate. The relationship between y+ and boundary layer is shown in the diagram below.

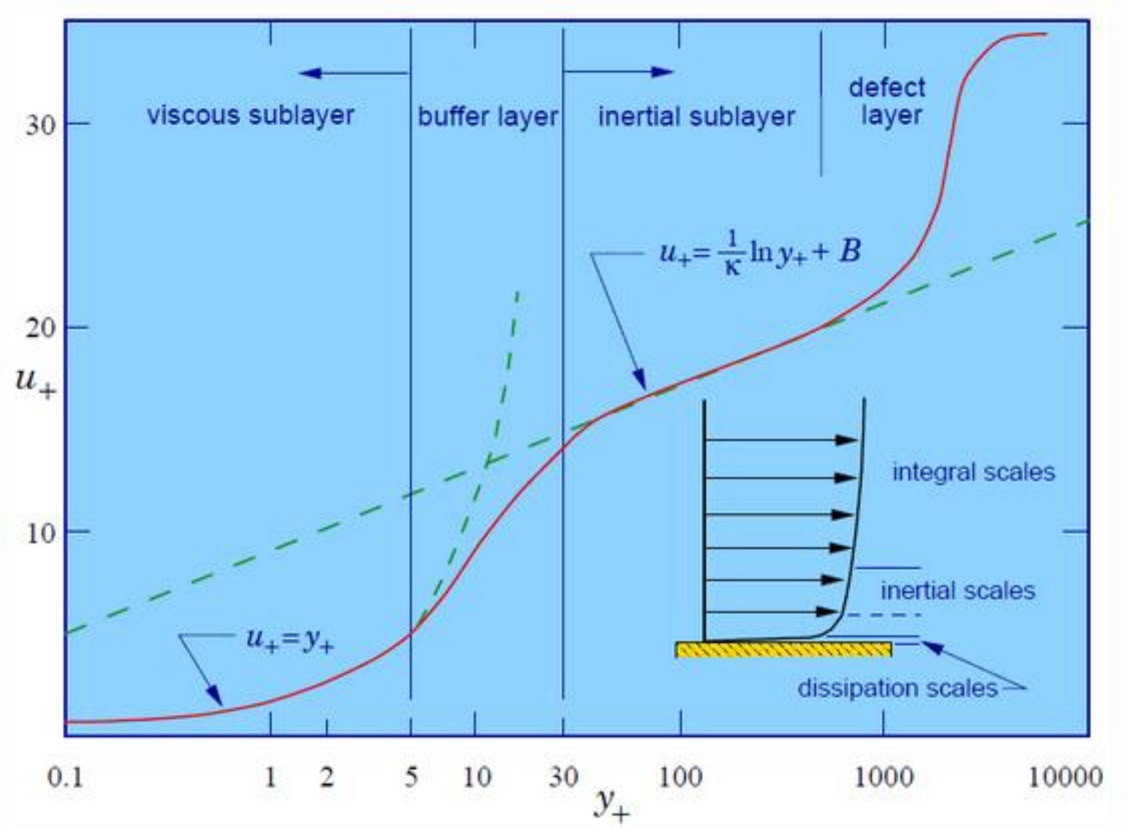

Velocity profiles in turbulent wall flow

Source: www.learncax.com

ϕ280 mm rotors

A laminar boundary layer was expected over 100% of the chord (if treated as flat plate), so this boundary was used to define the height that needed to be filled with cells. The first inflation layer was set at a height where y+ ≈ 1 (within viscous sub-layer). Computing capacity allowed for four inflation layers up to y+ ≈ 5 (all within viscous sub-layer) and surface mesh sizing and a volume growth rate of 1.2 allowed for three further layers within the remaining laminar boundary layer (seven layers in total). Key mesh parameters were: Aspect ratio = 20; Global size min = 0.02 mm; Local size max = 0.32 mm; Local size growth rate = 1.2 and Volume mesh growth rate of 1.2. Graphs of the layers are shown below.

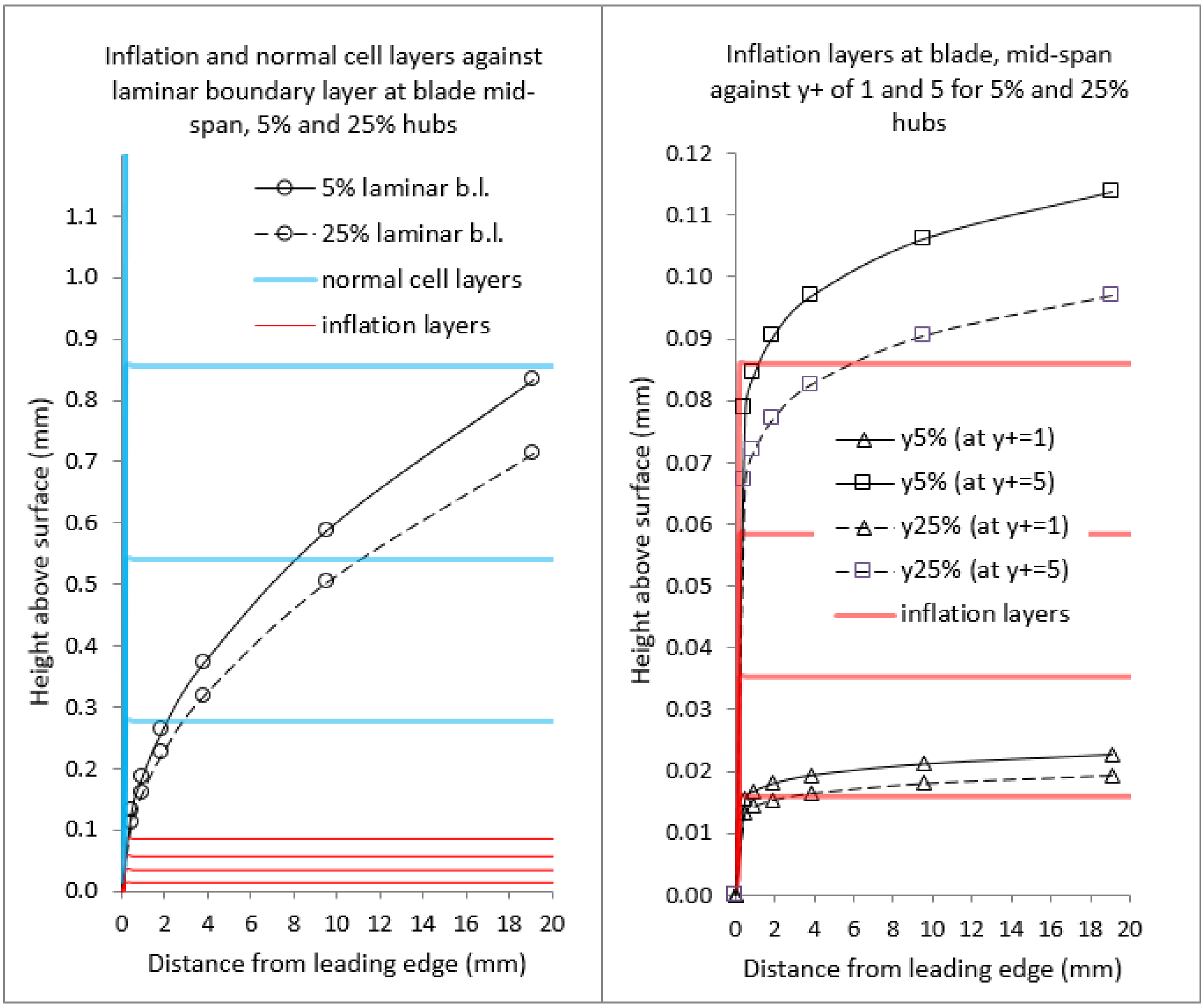

ϕ280 mm rotor boundary layer and sub-layers with mesh height calculation

Key mesh parameters (lengths in millimetres)

Local size blade:	Growth rate 1.2	Target mesh size 0.016	
Local size hub:	Growth rate 1.2	Target mesh size 0.32	
Surface mesh:	Min size 0.02	Max size 105	Growth rate 1.3
Volume mesh:	Inflation layers 4	Aspect ratio 20	Growth rate 1.2

ϕ30 m rotors

A fully turbulent boundary layer was expected over approximately 90% of the chord, so this boundary was used to define the height that needed to be filled with cells. Model size prevented resolution of the laminar sub-layer and the first inflation layer was set at a height where y+≈12 (within buffer layer). Computing capacity allowed for five inflation layers up to y+ ≈ 500 (including viscous sub-layer, buffer layer and inertial sub-layer) and surface mesh sizing and a volume growth rate of 1.2 allowed for two further layers within the remaining turbulent boundary layer (seven layers in total). Graphs of the layers are shown below.

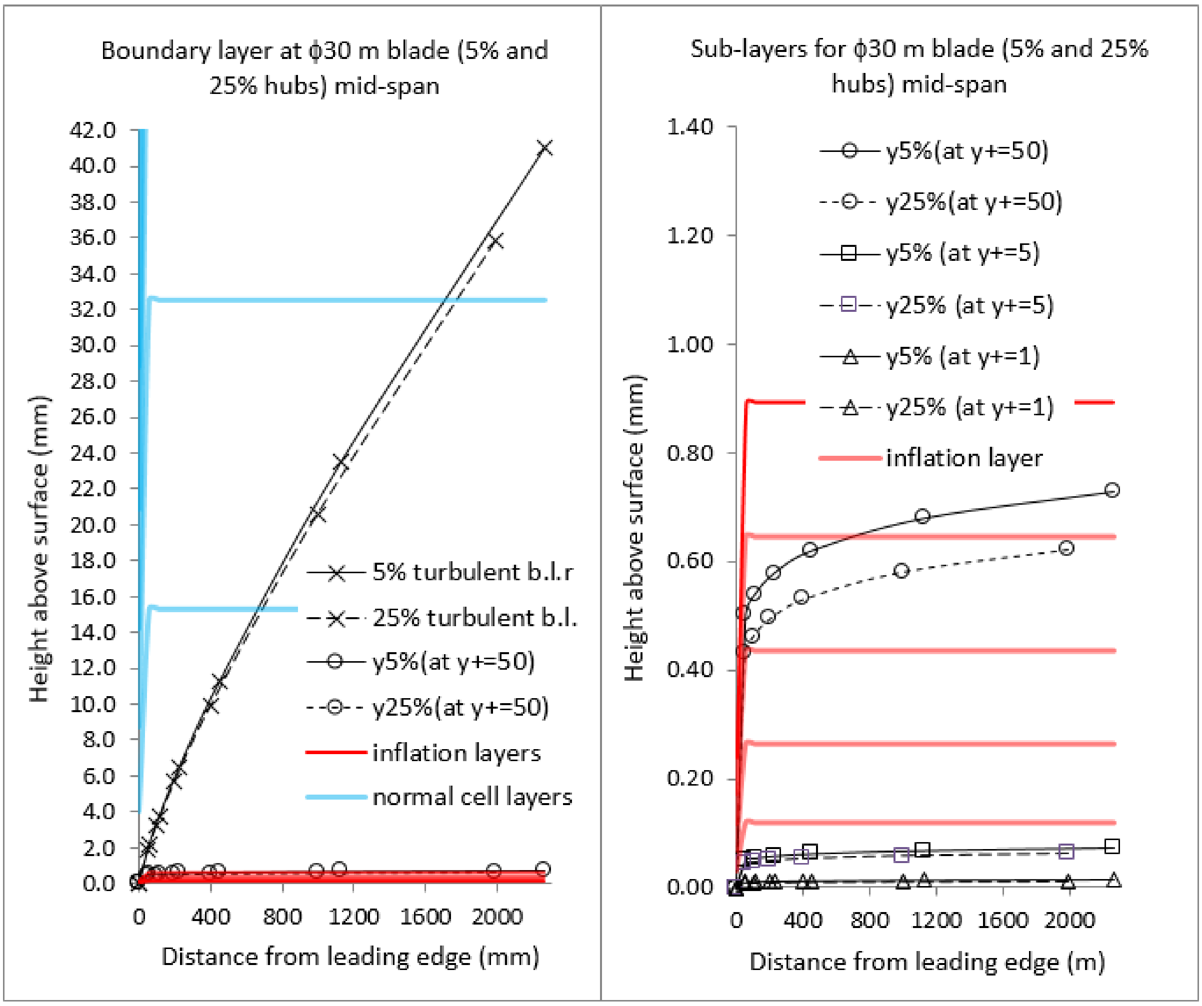

ϕ30 m rotor boundary layer and sub-layers with mesh height calculation

Key mesh parameters (lengths in metres)

Local size blade: Growth rate 1.2 Target mesh size 0.012

Local size hub: Growth rate 1.2 Target mesh size 0.0427

Surface mesh: Min size 0.00192 Max size 22 Growth rate 1.2

Volume mesh: Inflation layers 5 Aspect ratio 100 Growth rate 1.2

Appendix S; Pictures of rotor and domain meshes

<u>ϕ280 mm rotors</u>

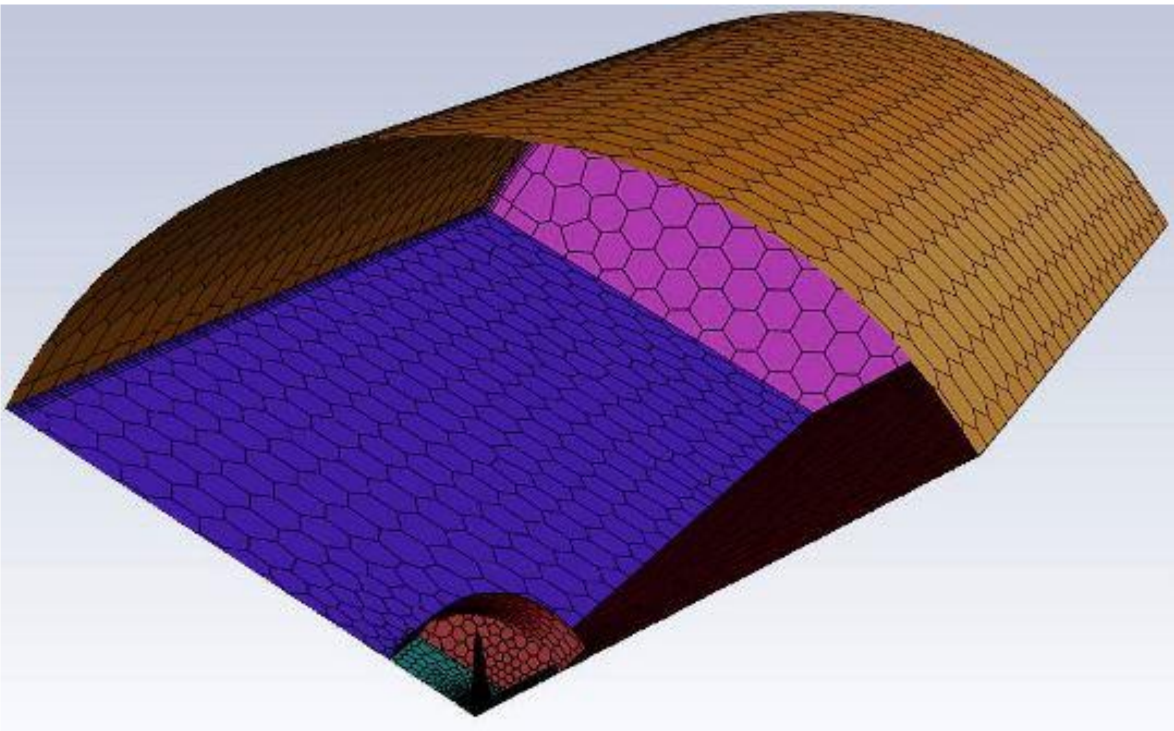

Section through domain showing rotating domain containing hub and blade

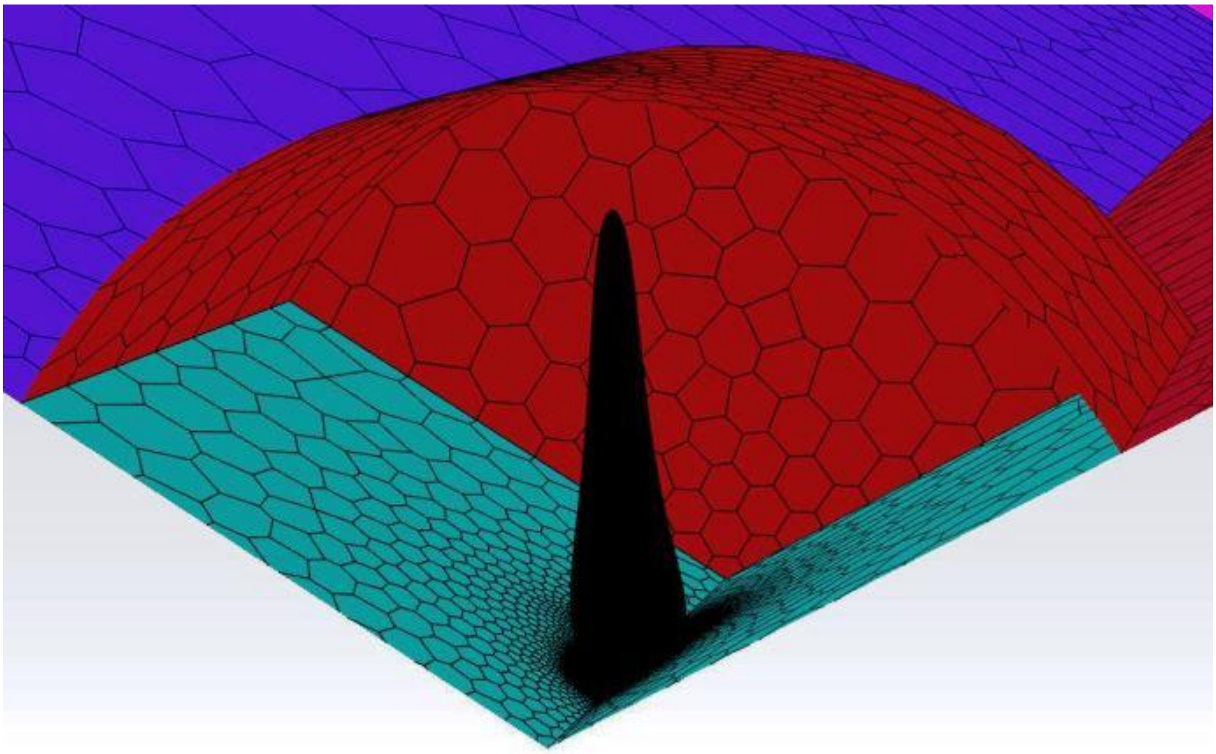

Blade and hub within rotating domain

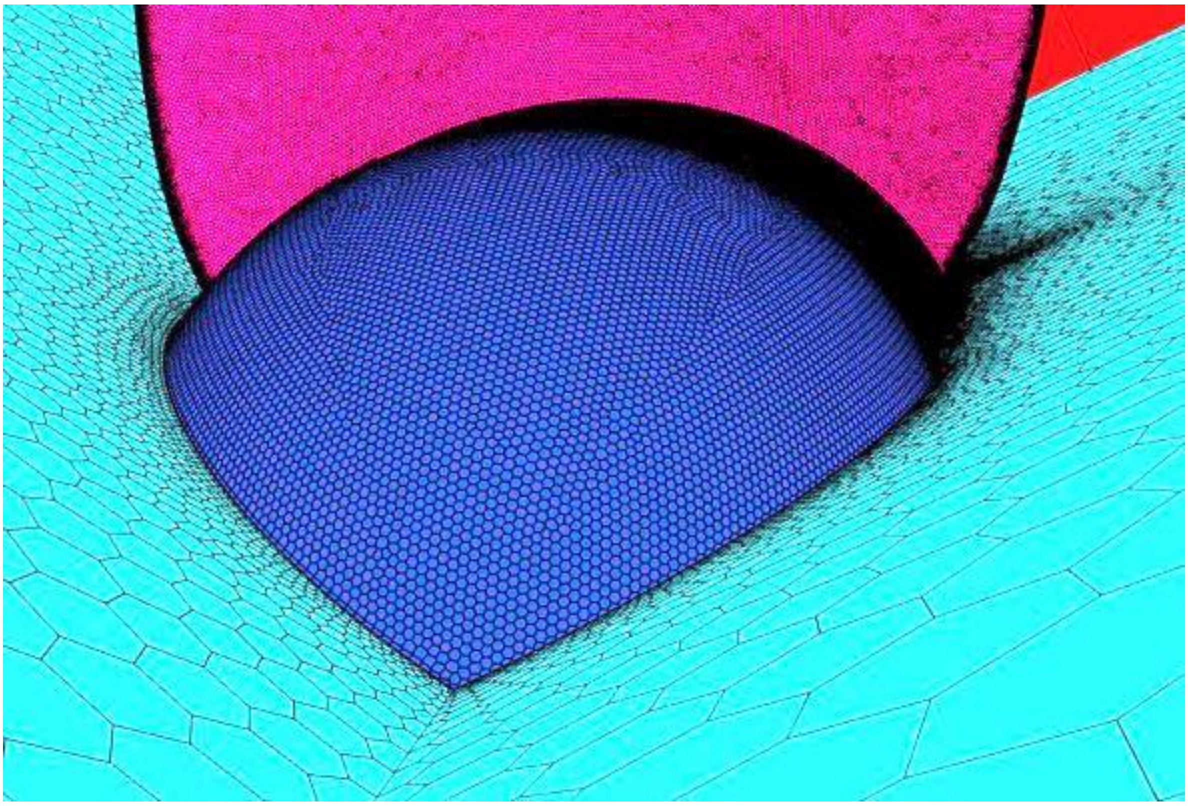

Hub and blade root

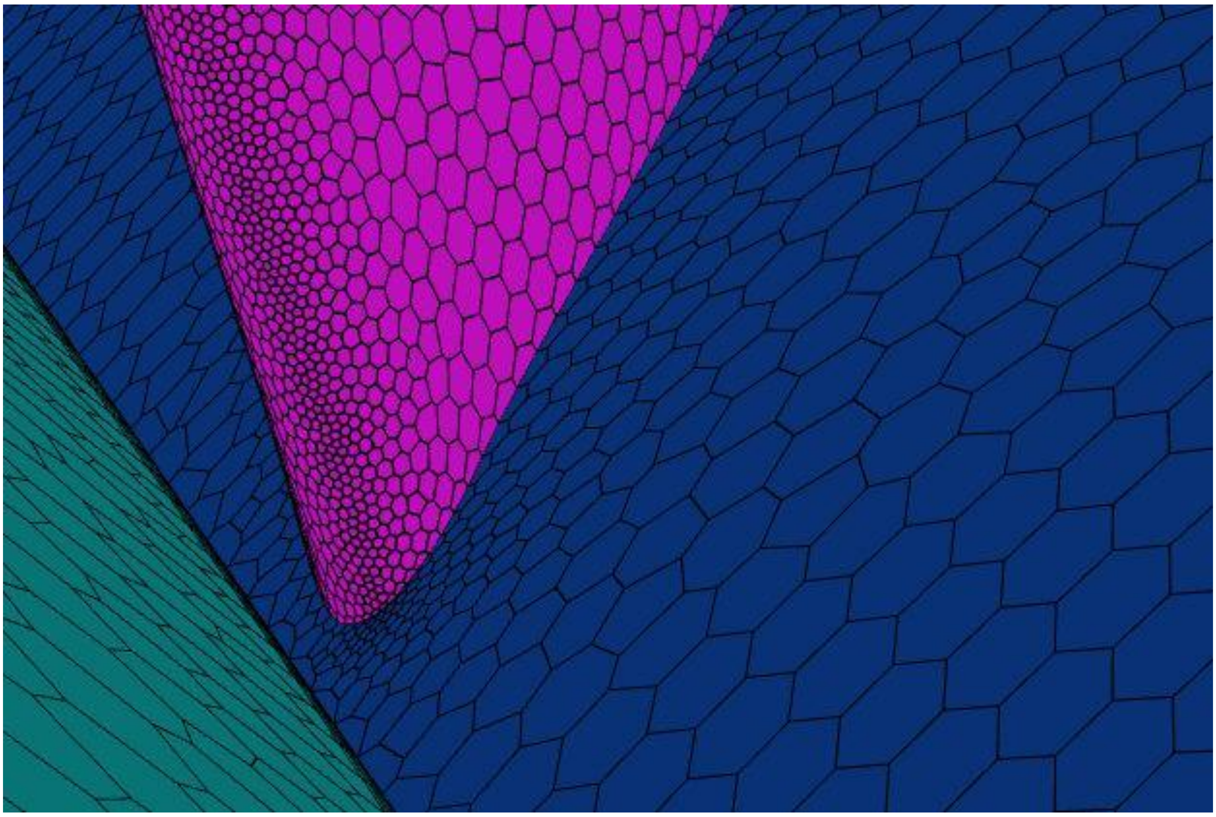

Leading edge of blade root

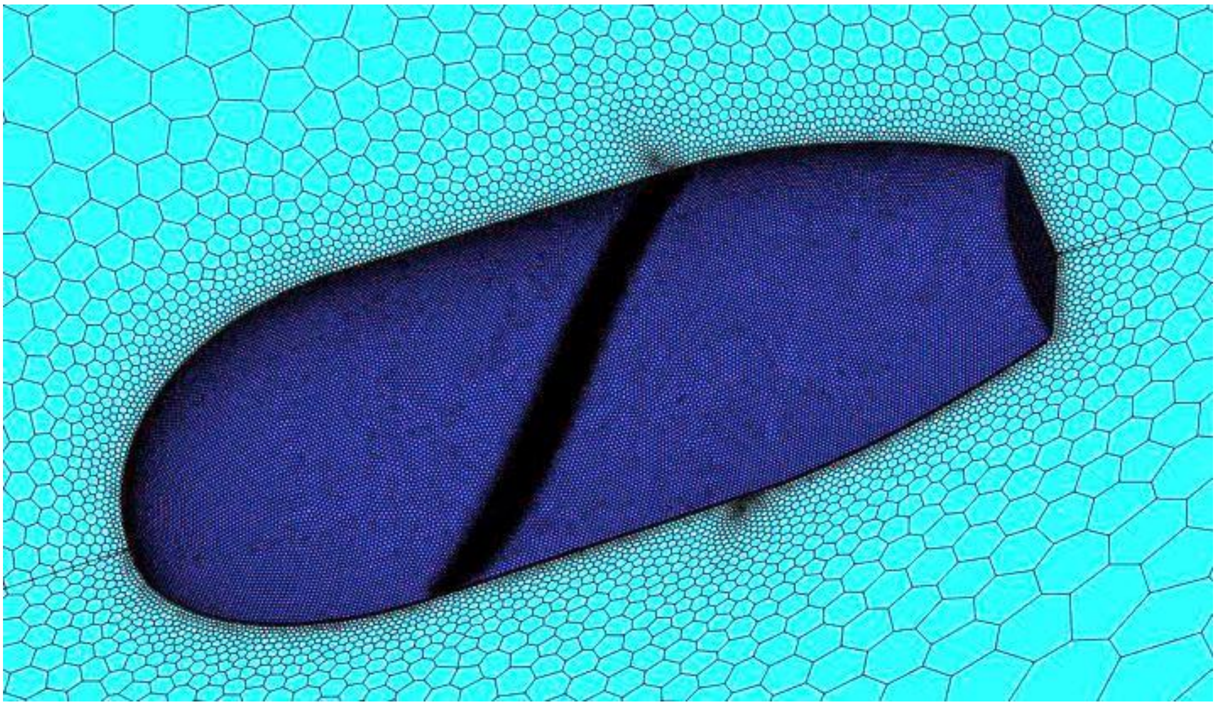

Underside of hub (light blue surfaces are planes of periodicity)

ϕ30 m rotors

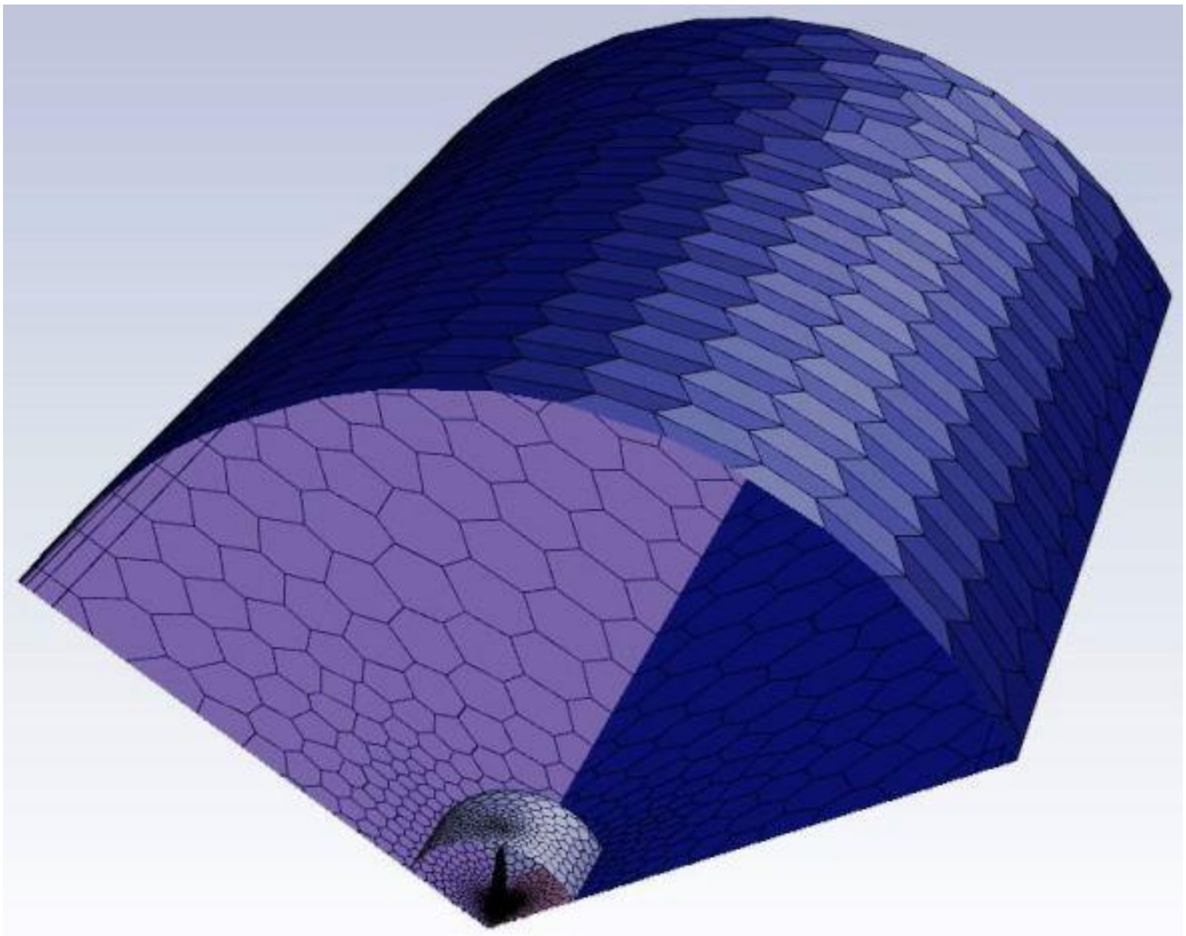

Section through domain showing rotating domain with blade and hub

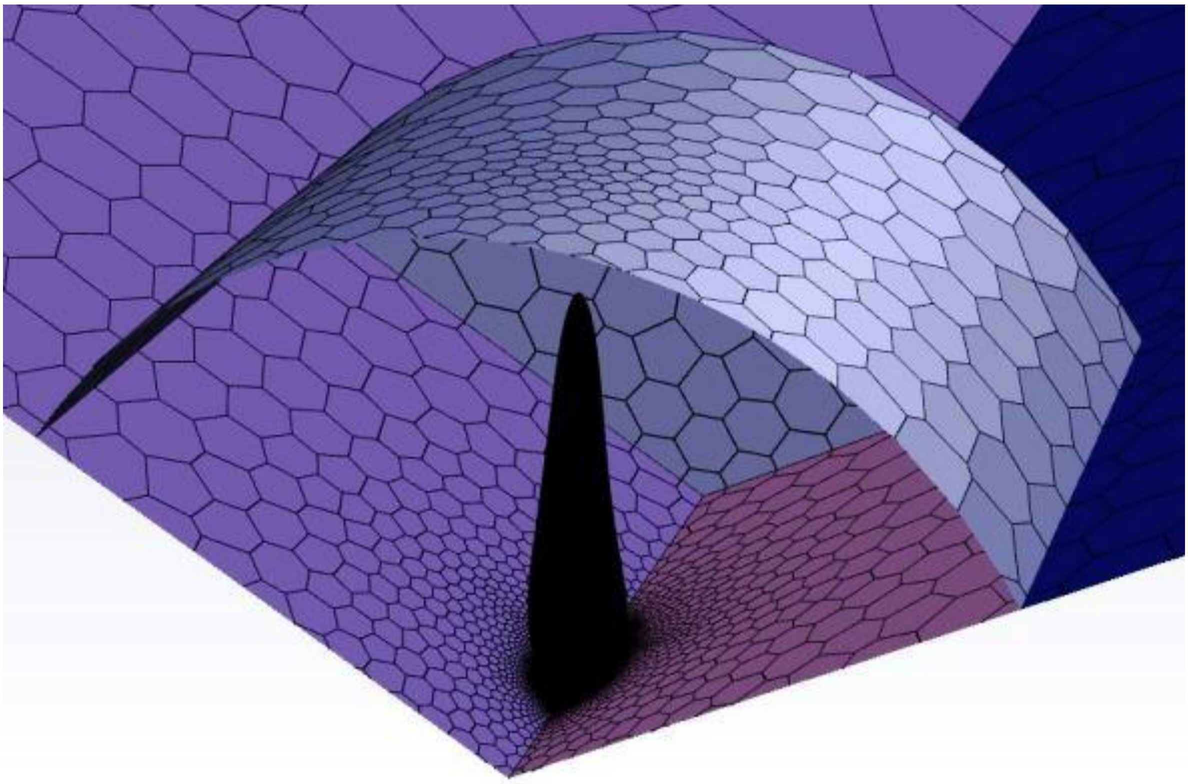

Section through rotating domain showing blade and hub

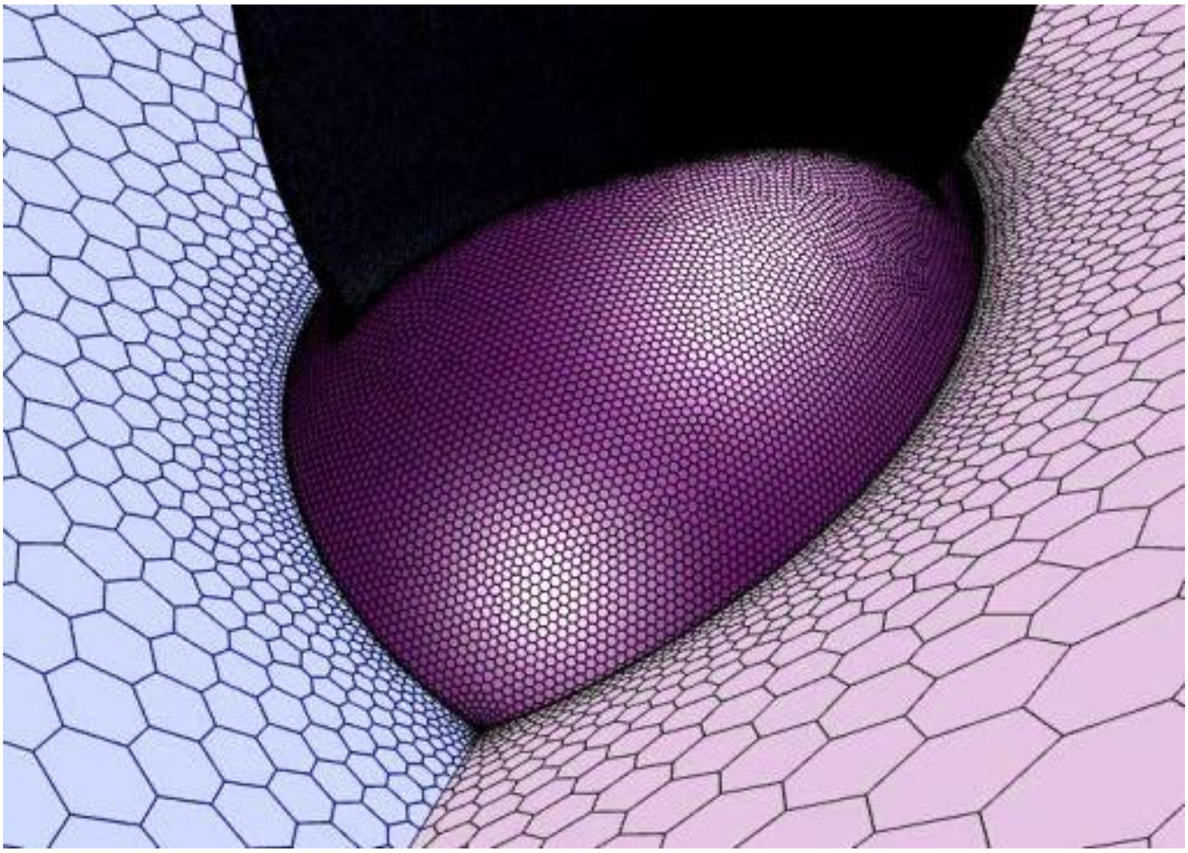

Hub and blade root

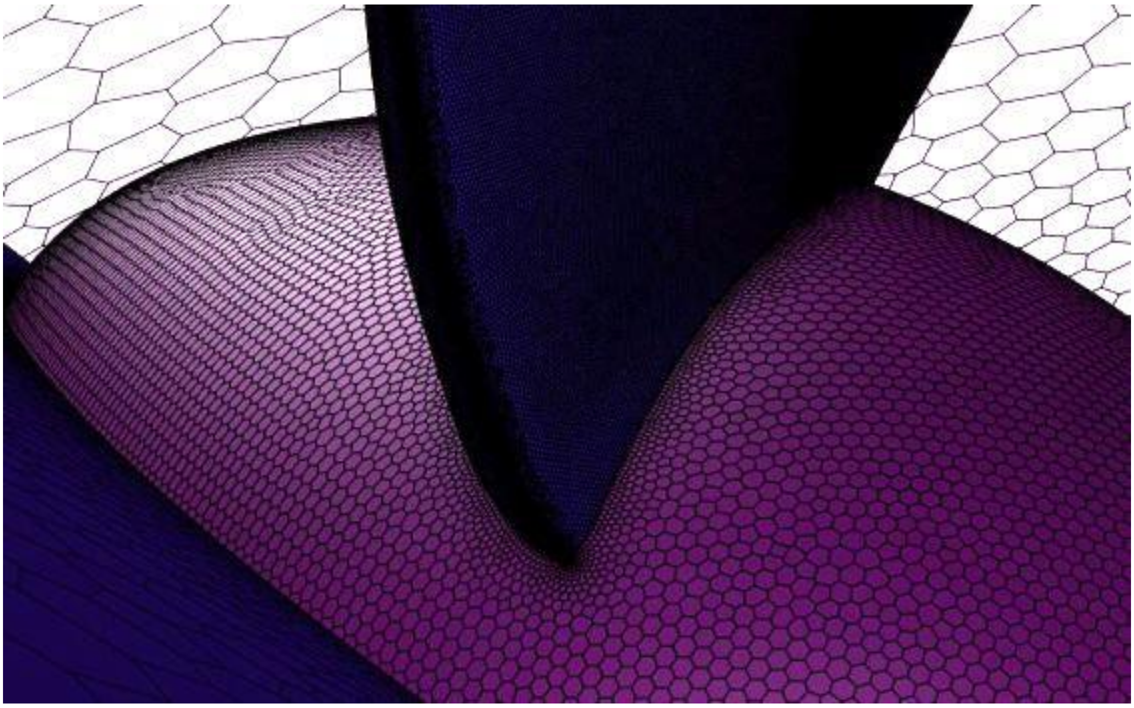

Hub and blade root

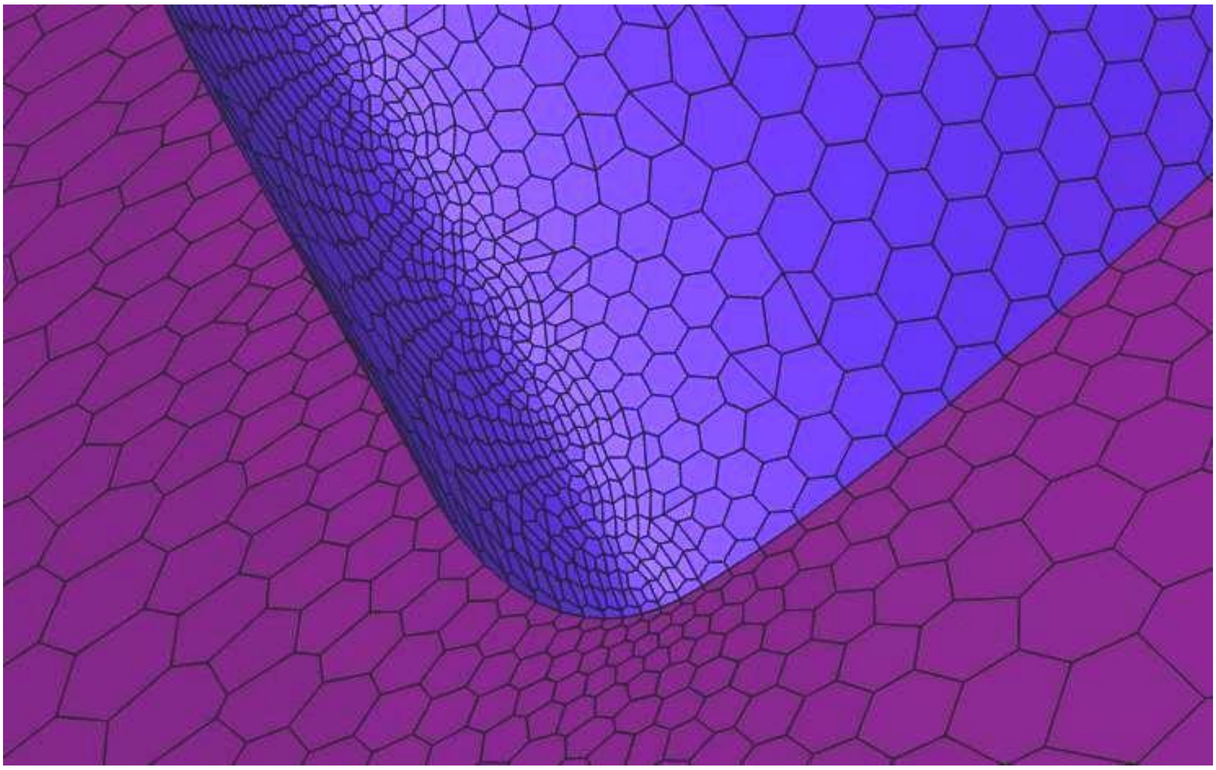

Leading edge of blade root

Appendix T: CFD flow analysis

CFD flow analysis was performed in Ansys Fluent, on the ϕ280 mm rotors, 20% hub. Rotors designed using the standard and adapted BEMM were compared. Water speed used in all tests was 0.25 m/s. Surface contours were created immediately upstream of the rotors to indicate axial, radial and tangential velocities close to the rotor plane. The contour planes were located 2.8 mm (1% of rotor diameter) upstream of blade leading edge. Both rotors were analysed at 81 rpm (rotation speed for peak power for both rotors).

Two analyses were performed. In Analysis 1, range of velocity was minimised to include all velocities within the swept area and rotating domain. This provides a more complete view of the axial, radial and tangential flows, but does not show adequate detail for fine comparison. Analysis 2 attempts to show finer detail of the near-hub region by reducing the velocity ranges to those associated with the near-hub region. In the process, some higher velocity areas, further from the hub, are out of range and show as grey areas.

Analysis 1

Axial velocity – Adapted BEMM design - banded

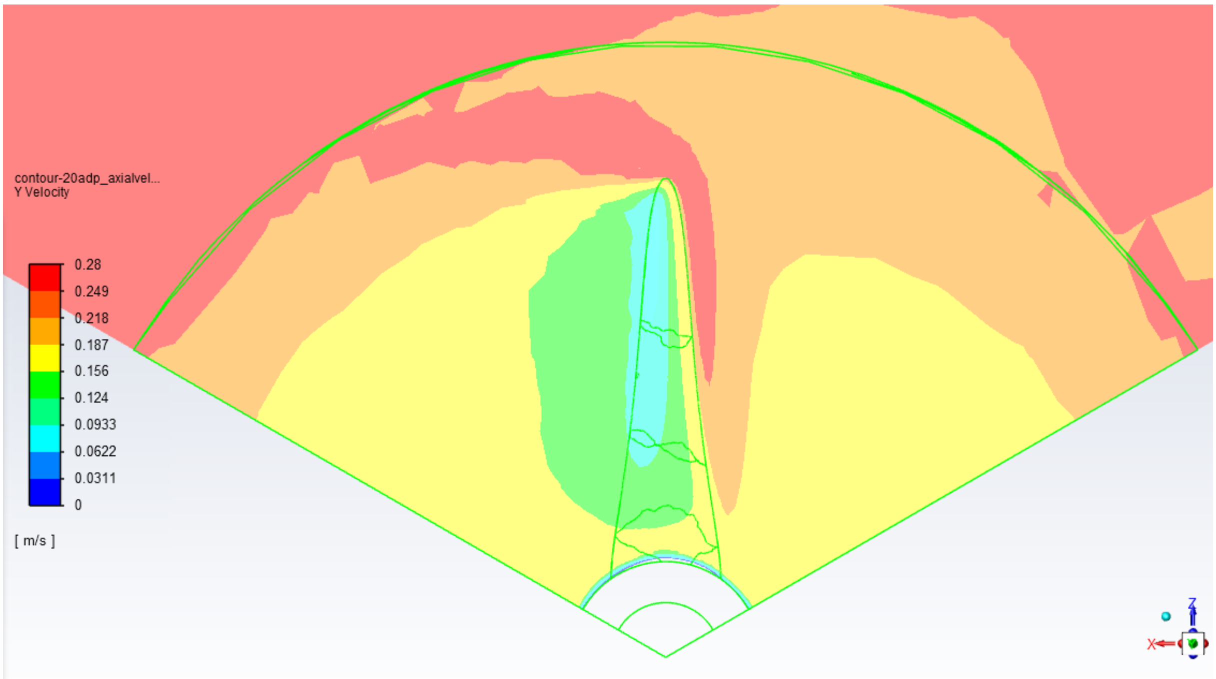

Axial velocity – Standard BEMM design - banded

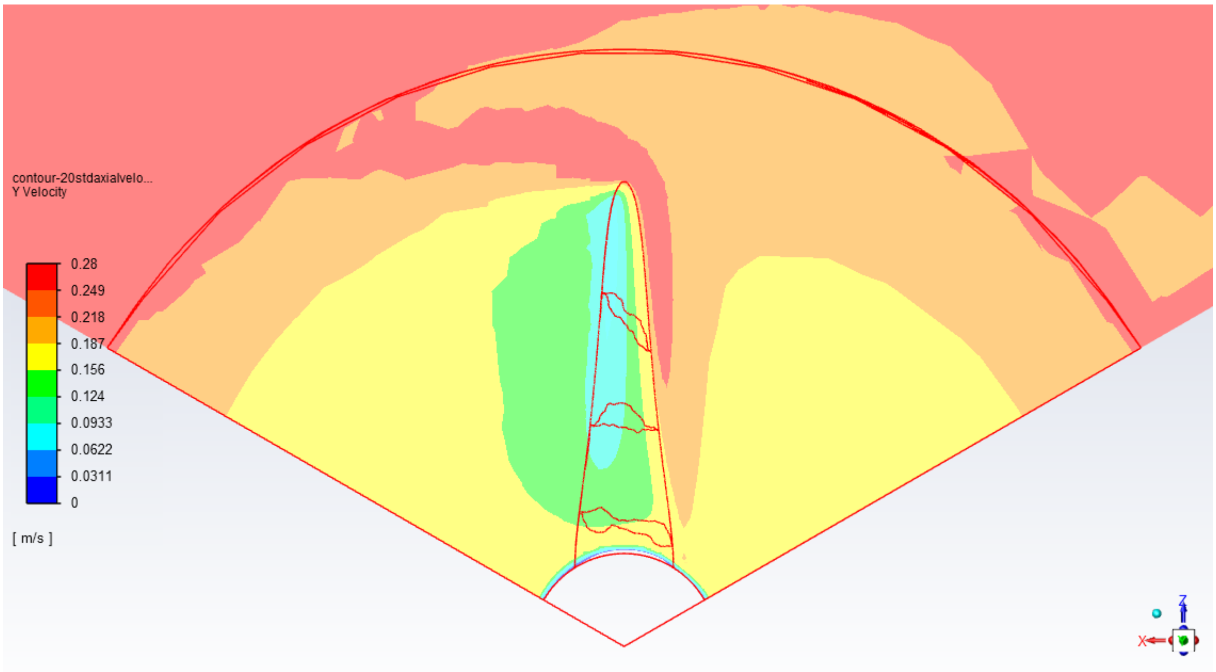

Slightly higher axial velocity (slightly broader yellow area between hub and green area) is visible in the adapted BEMM design rotor.

Axial velocity – Adapted BEMM design - smoothed

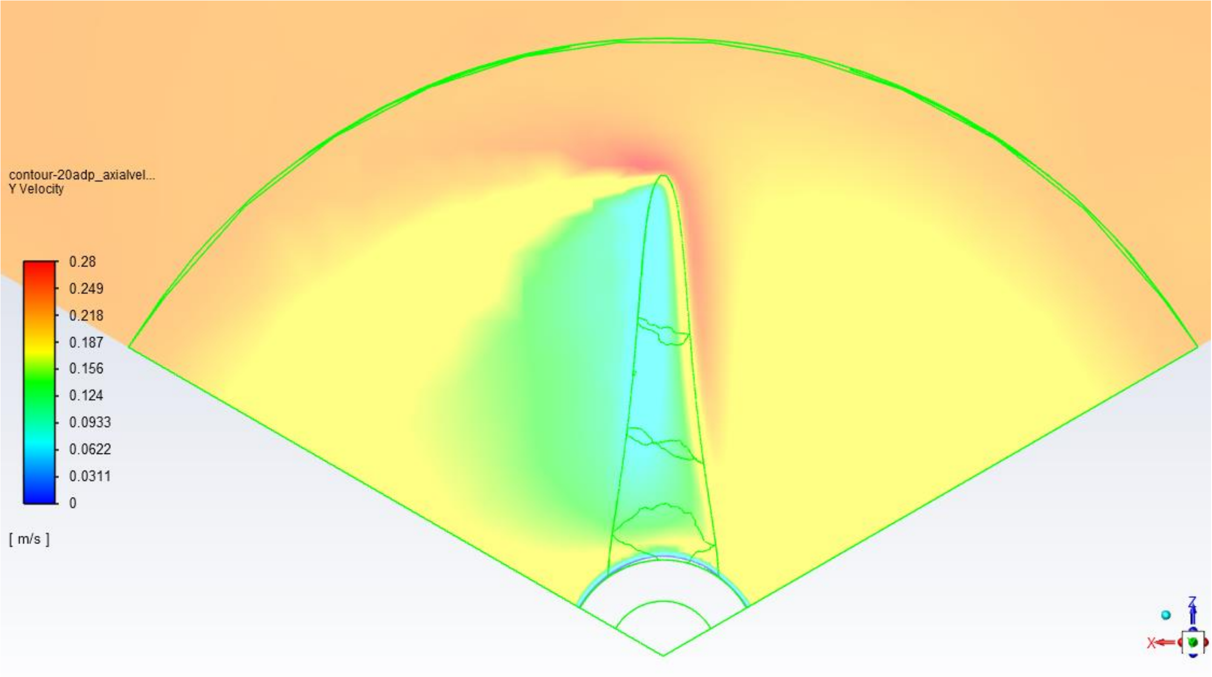

Axial velocity – Standard BEMM design - smoothed

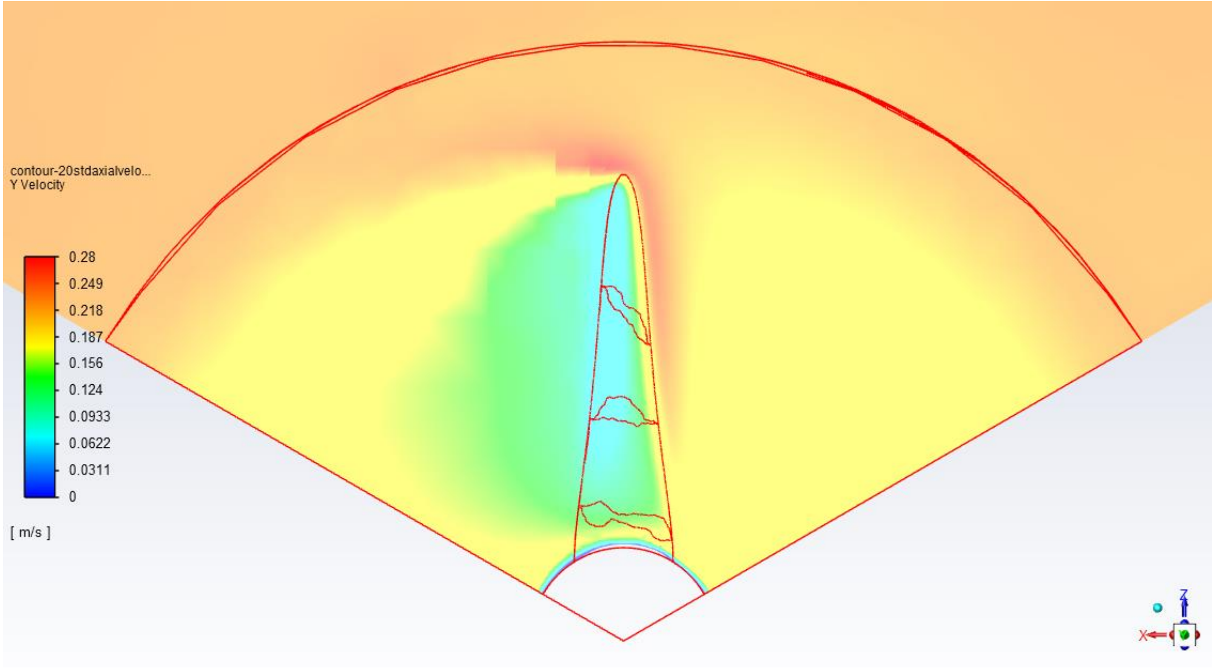

No discernable difference is shown.

Radial velocity – Adapted BEMM design - banded

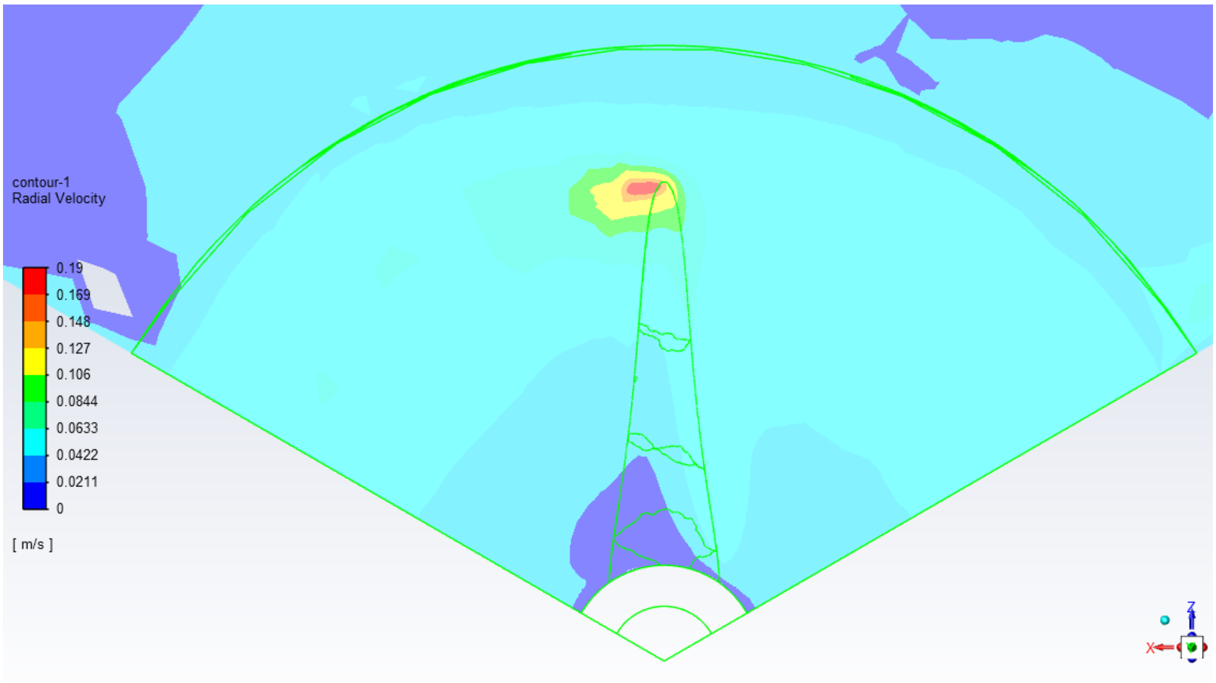

Radial velocity – Standard BEMM design - banded

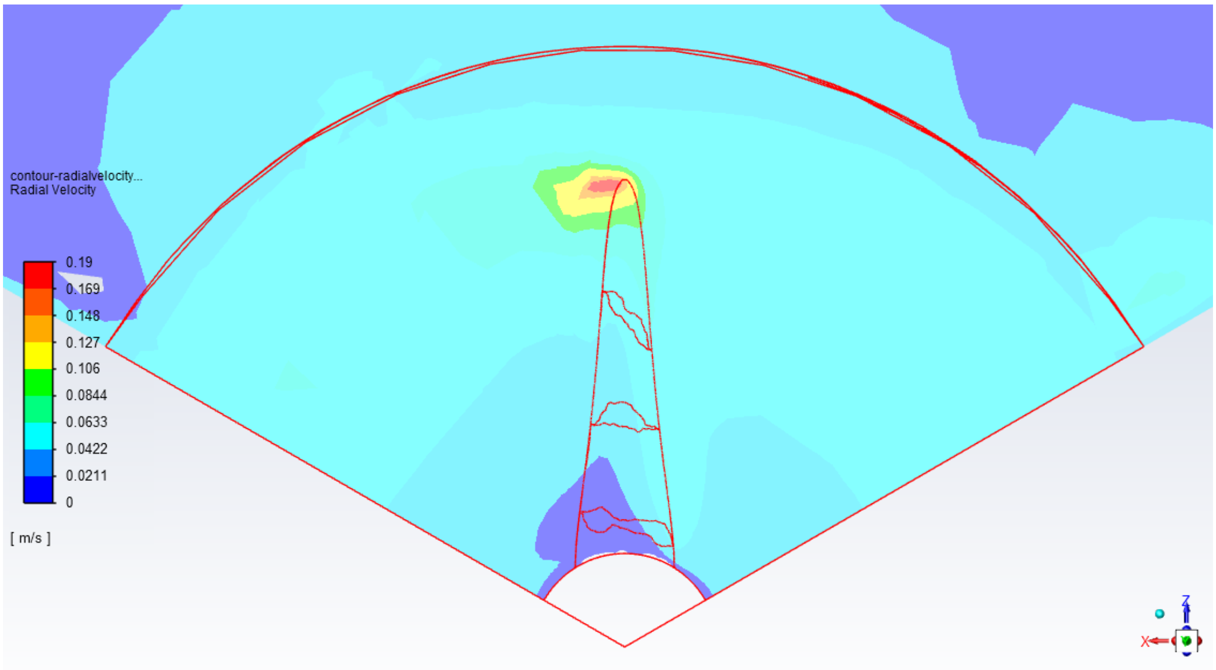

Notice that radial velocity is lower (larger dark blue area) in the near-hub region of the adapted BEMM design. This indicates an efficiency improvement.

Radial velocity – Adapted rotor - smoothed

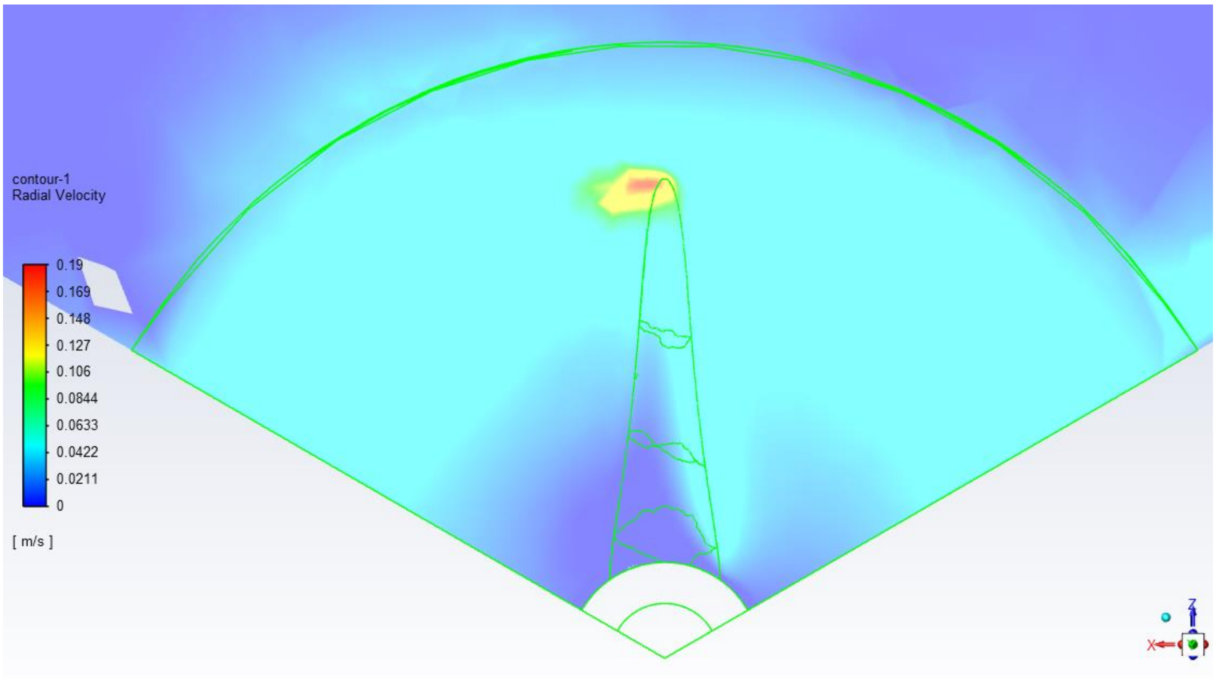

Radial velocity – Standard rotor - smoothed

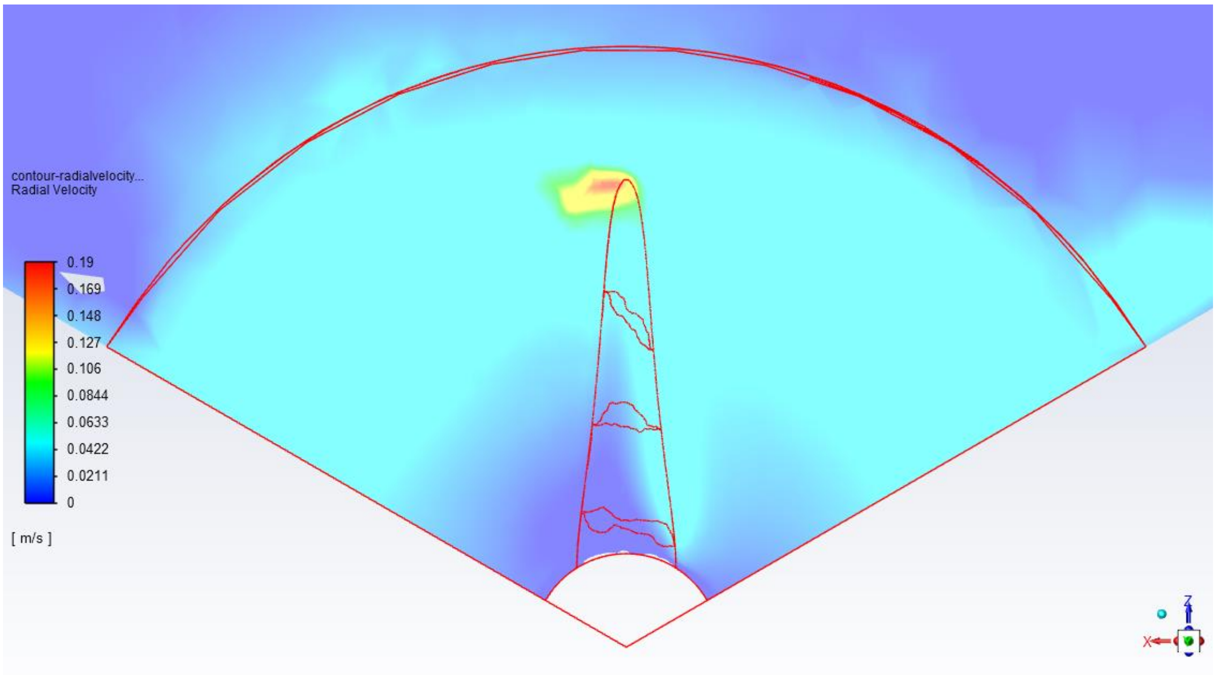

No difference between rotors is discernable.

Tangential velocity – Adapted BEMM design - banded

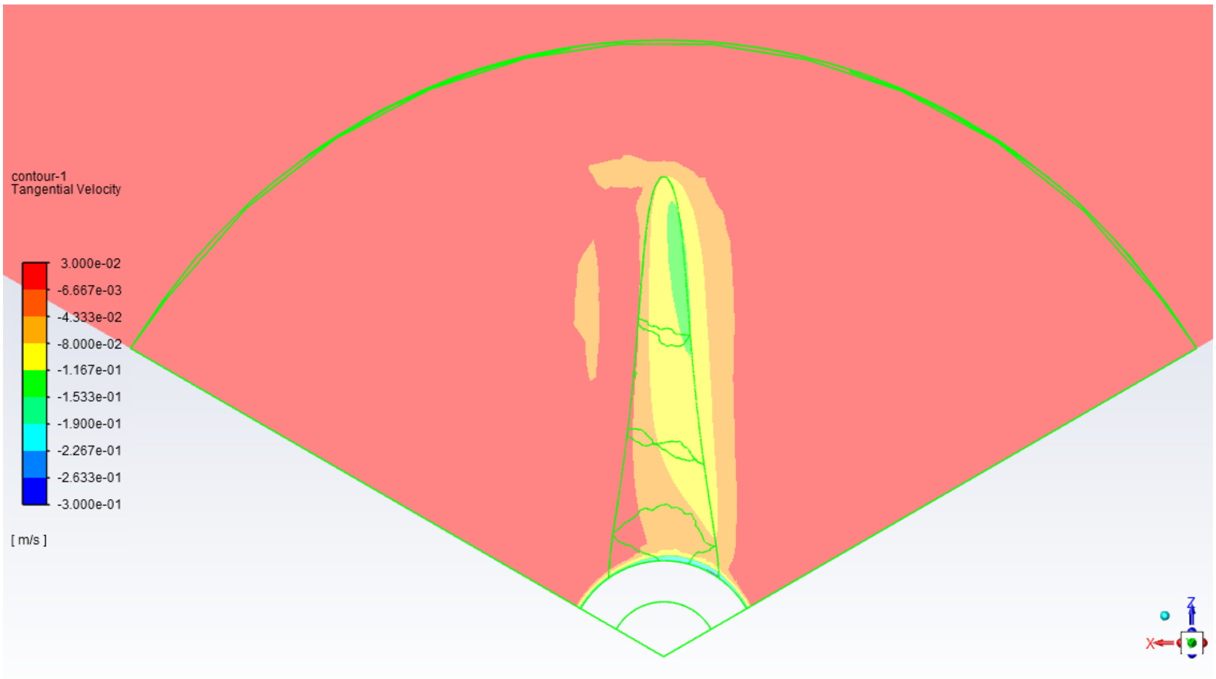

Tangential velocity – Standard BEMM design - banded

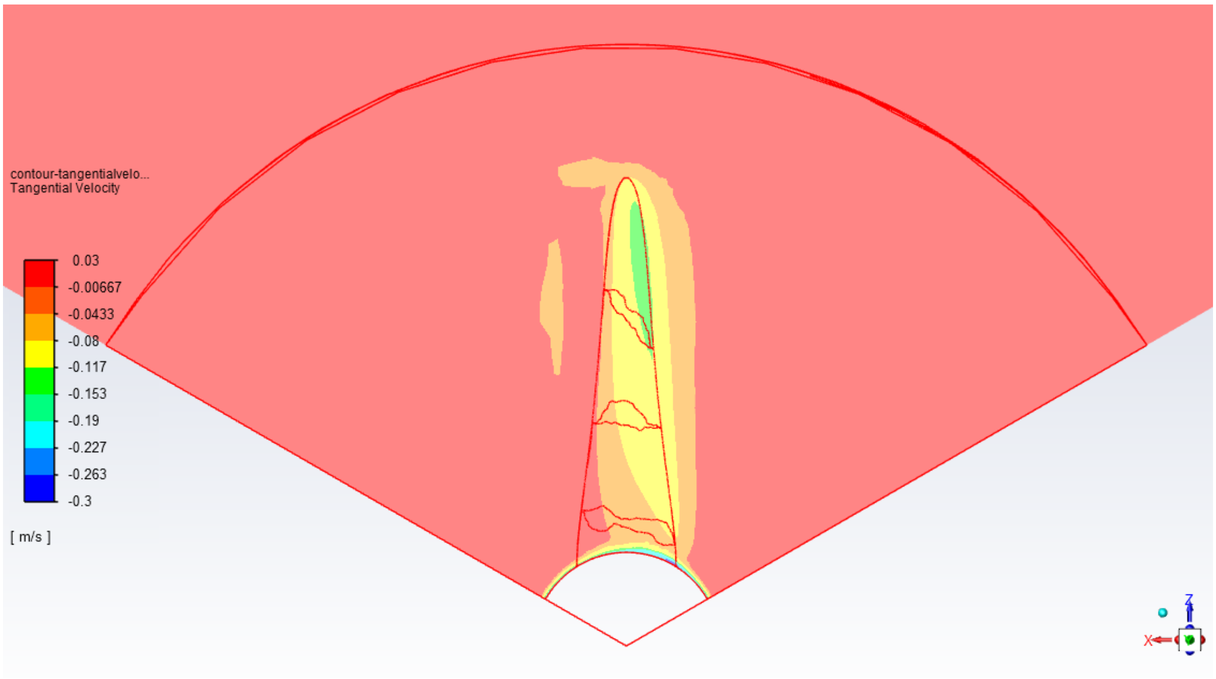

No discernable difference between rotors.

Tangential velocity – Adapted BEMM design - smoothed

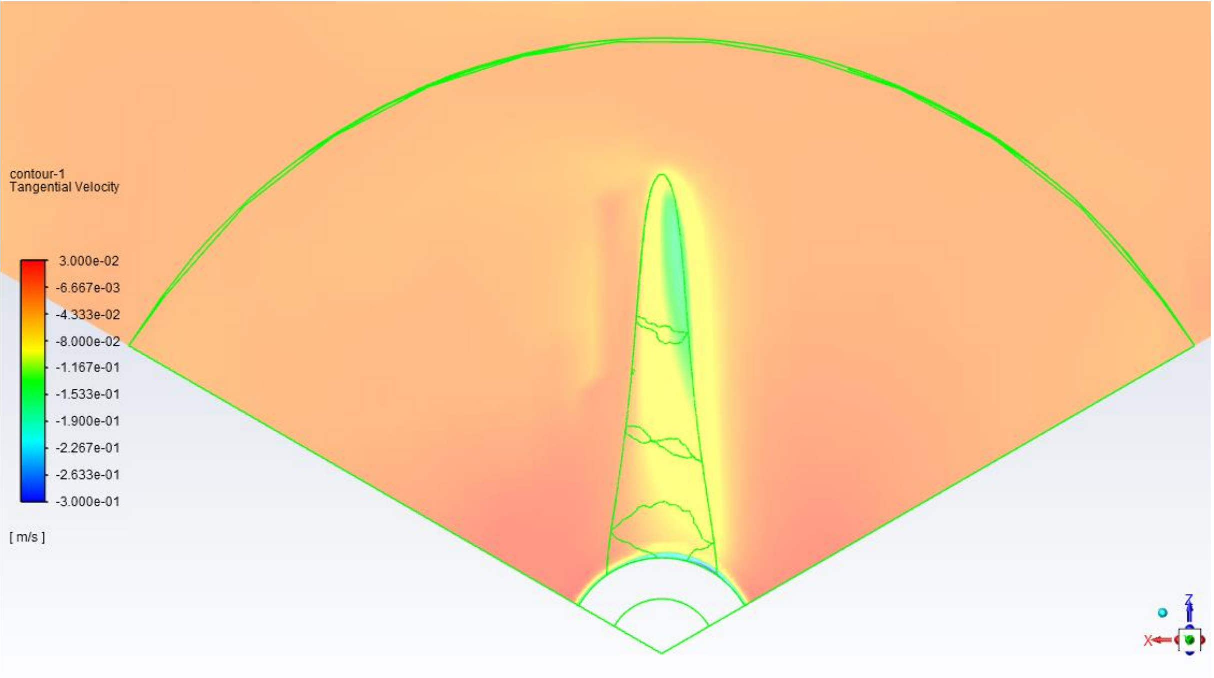

Tangential velocity - Standard BEMM design - smoothed

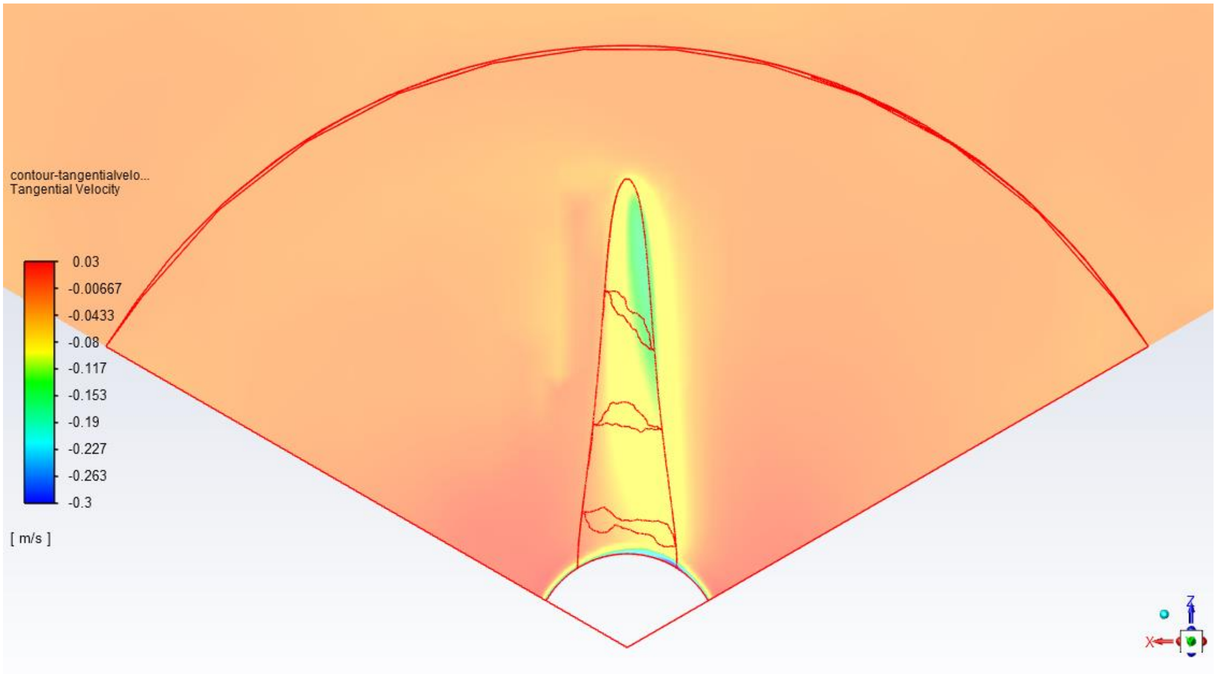

No discernable difference between rotors.

<u>Analysis 2 – (Narrower ranges of velocity to focus on near-hub region)</u>

Axial velocity – Adapted BEMM design - banded – Range (0 to 0.22)

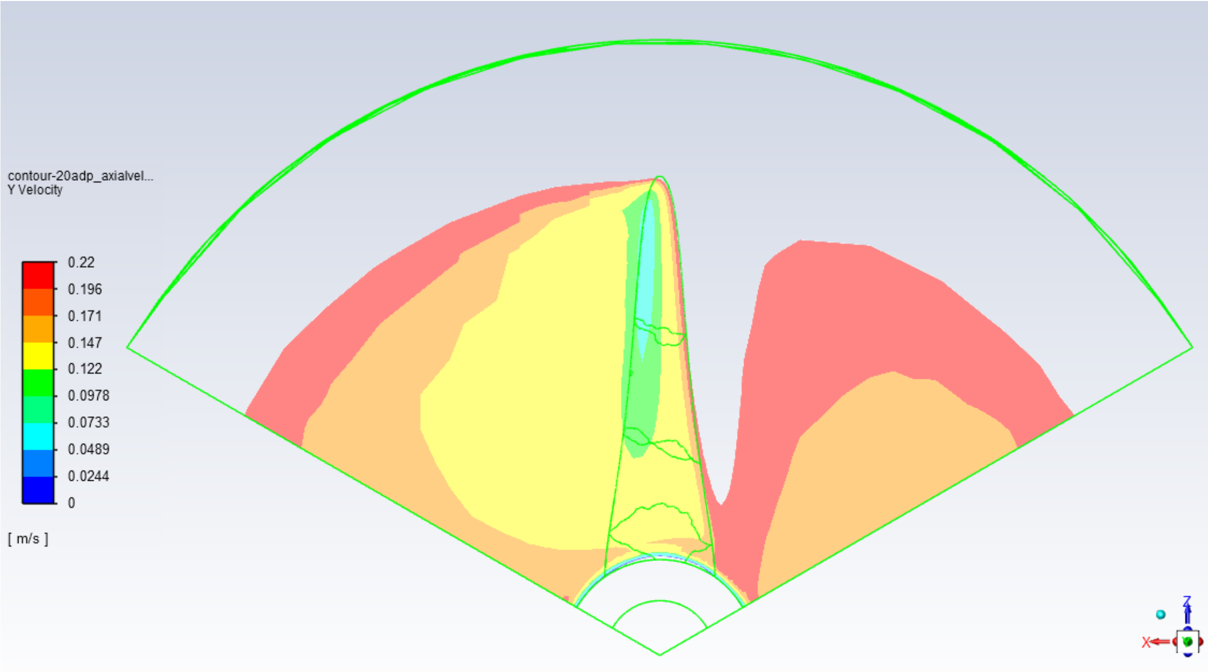

Axial velocity – Standard BEMM design - banded – Range (0 to 0.22)

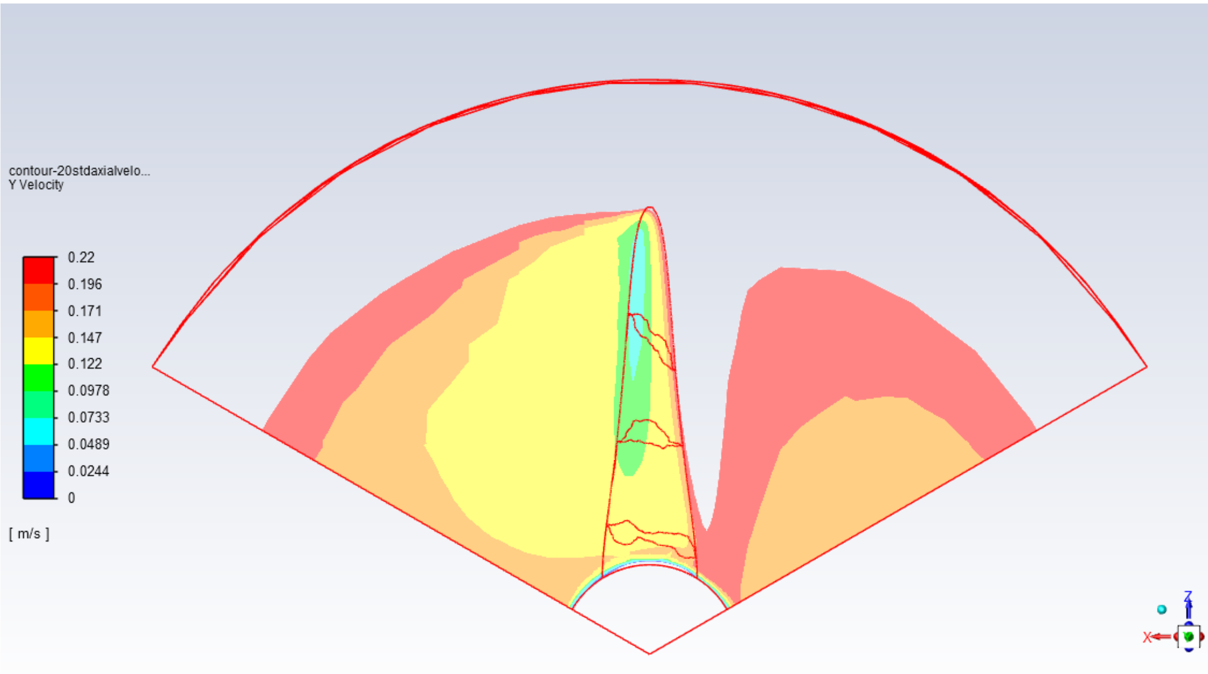

Slightly higher axial velocity at leading edge (narrower red zone and higher velocity (grey) zone near hub) of standard BEMM design.

Radial velocity – Adapted BEMM design - banded – Range (0 to 0.08)

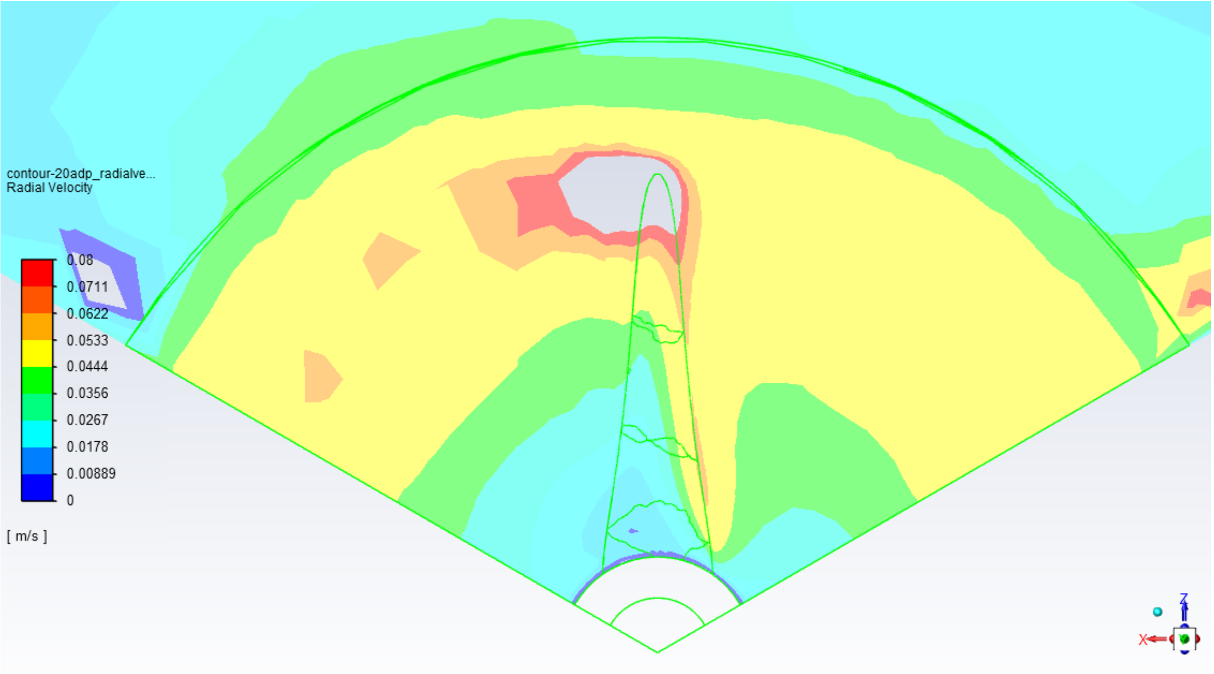

Radial velocity – Standard BEMM design - banded – Range (0 to 0.08)

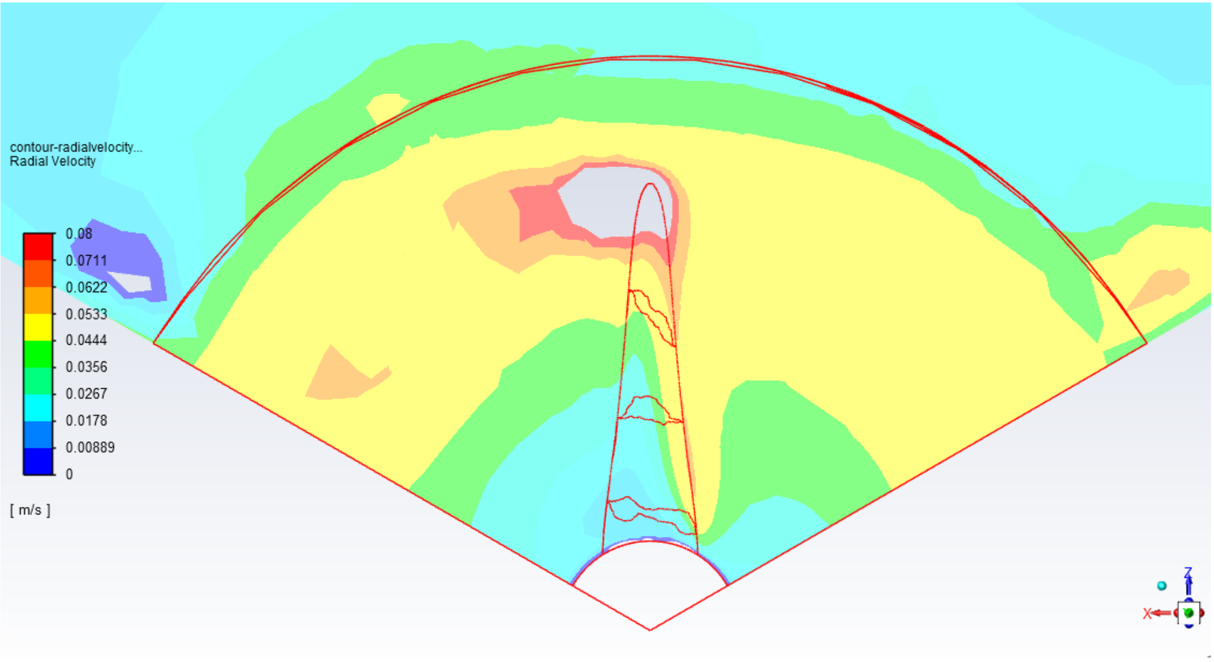

Although the rendering colour is faulty match, the radial velocity is visibly lower (a larger mid-blue zone) in the near-hub region of the adapted BEMM design.

Tangential velocity – Adapted BEMM design - banded – Range (-0.15 to 0.025)

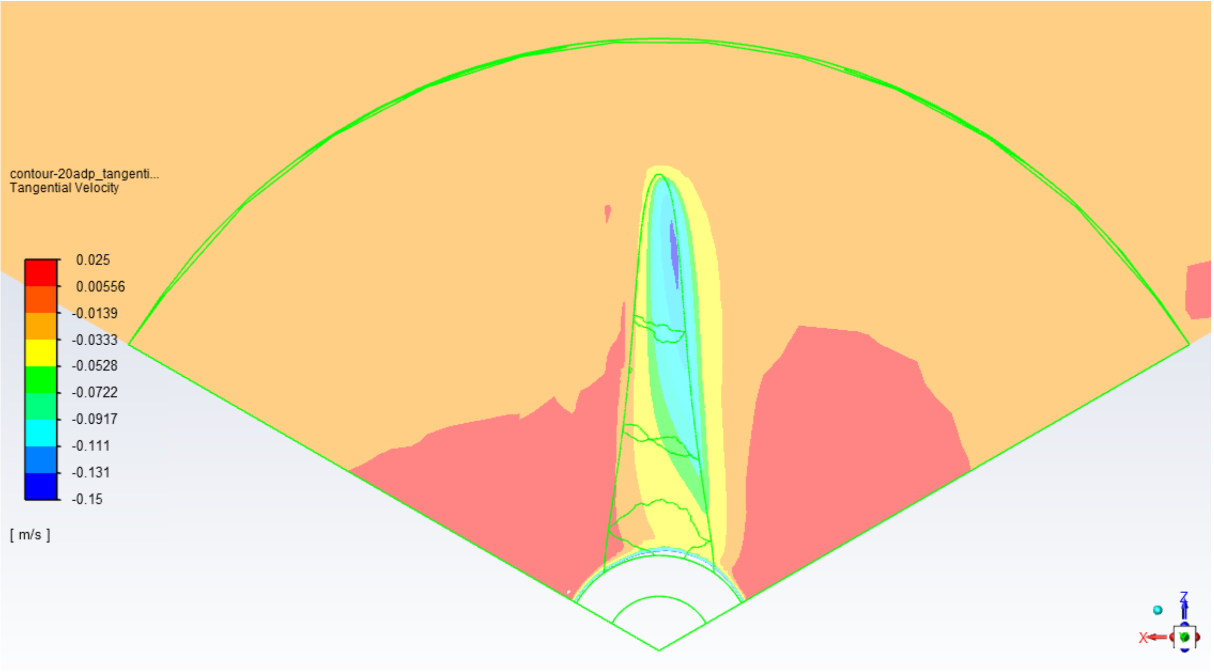

Tangential velocity – Standard BEMM design - banded – Range (-0.15 to 0.025)

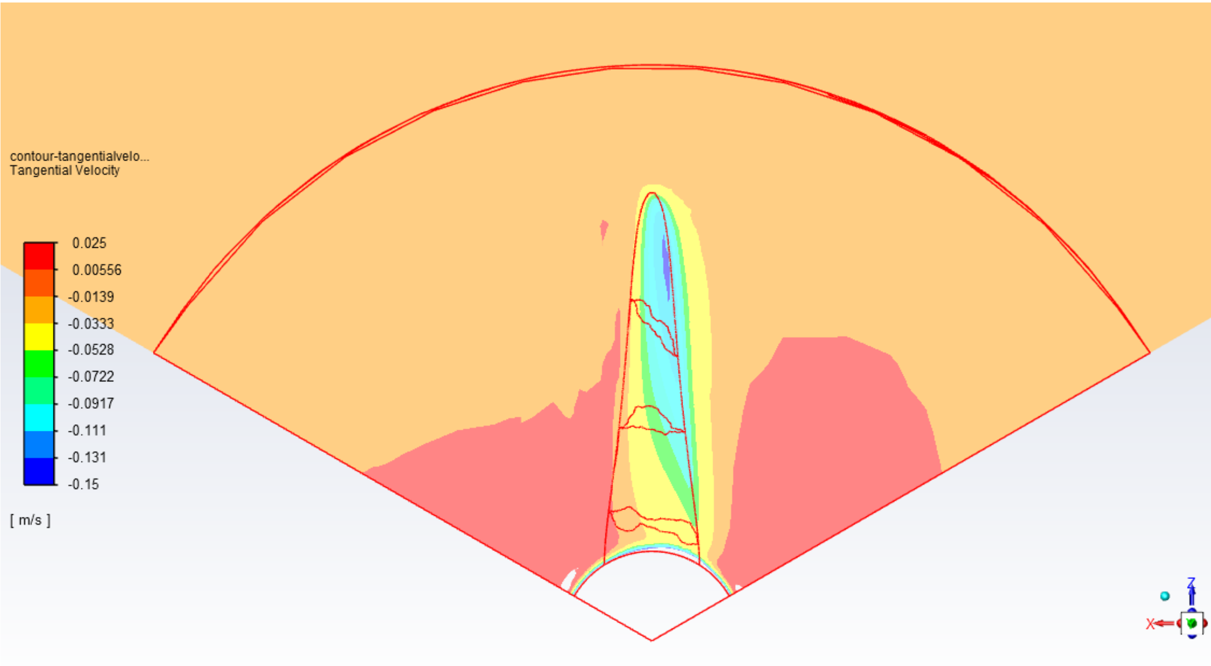

No discernable difference between rotors.

REFERENCES

Astroman Magazine. 2011. ENERCON installs world's most powerful wind energy converter E-126/7.5 MW.
http://www.astroman.com.pl/index.php?mod=magazine&a=read&id=900&printer=true
[1 May 2022]

Benini, E. & Toffolo, A. 2002. Optimal design of horizontal-axis wind turbines using blade-element theory and evolutionary computation. *Journal of Solar Energy Engineering*, 124(4):357-363.

Branlard, E. 2017. *Research Topics in Wind Energy* 7: *Wind Turbine Aerodynamics and Vorticity-Based Methods - Fundamentals and Recent Applications*. Cham. Springer.

Burton, T., Sharpe, D., Jenkins, N. & Bossanyi, E. 2001. *Wind Energy Handbook*. Chichester: John Whiley & Sons.

Carmicheal, B.H. 1981. Low Reynolds number airfoil survey. *NASA* CR 165803.

Chen, T.Y. & Liou, L.R. 2010. Blockage corrections in wind tunnel tests of small horizontal-axis wind turbines. *Experimental Thermal and Fluid Science*, 35(2011):565-569.

Derksen, R.W., Agelinchaab, M. and Tachie, M. 2008. Characteristics of the flow over a NACA 0012 airfoil at low Reynolds numbers. *Advances in Fluid Mechanics*, 7:142–153.

El-Okda, Y.M. 2015. Design methods of horizontal axis wind turbine rotor blades. *International Journal of Industrial Electronics and Drives*, Vol.2, No.3:135-150.

Froude, W. 1878. On the elementary relation between pitch, slip and propulsive efficiency. *Transactions of the Royal Institute of Naval Architects*, 19(47):47–57.

Gasch, R. & Twele, J. 2012. *Wind Power Plants – Fundamentals, Design, Construction and Operation*, 2nd Ed. Heidelberg: Springer.

GE. 2015a. *How Does a Wind Turbine Work? With GE's New ecoROTR, Better than Ever*.
https://www.ge.com/news/reports/how-does-a-wind-turbine-work-with-ges-new
[30 April 2022]

GE. 2015b. The road to ecoROTR: How building a better wind turbine began with an online shopping spree for Styrofoam balls.
https://www.ge.com/news/reports/the-road-to-ecorotr-how-building-a-better-wind-2
[30 April 2022]

Glauert, H. 1983. *The Elements of Aerofoil and Airscrew Theory*. Cambridge Science Classics. Cambridge University Press.

Göçmen, T., van der Laan, P., Réthoré, P., Diaz, A.P., Larsen, G.C. & Ott, S. 2016. Wind turbine wake models developed at the technical university of Denmark: A review. *Renewable and Sustainable Energy Reviews*, 60(2016):752–769.

Hansen, M.O.L. 2008. *Aerodynamics of Wind Turbines*. 2nd ed. London: Earthscan.

Hau, E. 2006. *Wind Turbines – Fundamentals, Technologies, Applications, Economics*, 2nd Ed. Heidelberg: Springer.

Hemami, A. 2012. *Wind Turbine Technology*. New York: Cengage Learning.

Herráez, I.,Stoevesandt, B. & Peinke, J. 2014. Insight into Rotational Effects on a Wind Turbine Blade Using Navier–Stokes Computations. *Energies*, 7(2014): 6798-6822.

Huang, R.F. & Lin, C.L. 1995. Vortex shedding and shear-layer instability of wing at low-Reynolds numbers. *AIAA* J1995:1398–1403.

Jain, P. 2011. *Wind Energy Engineering*. New York: Mc Graw Hill.

Jamieson, P. 2011. *Innovation in wind turbine design*. Chichester: John Wiley & Sons.

Jha, P.K., Duque, E.P.N., Bashioum, J.L. & Schmitz, S. 2015. Unraveling the Mysteries of Turbulence Transport in a Wind Farm. Energies, 8(2015):6468-6496.

Johnson, G.L. 2001. *Wind Energy Systems*, Electronic Edition. Manhattan.

Johnson, N., Bortolotti, P., Dykes, K., Barter, G., Moriarty, P., Carron, S., Wendt, F., Veers, P, Paquette, J, Kelly, C. & Ennis, B. 2019. *Investigation of Innovative Rotor Concepts for the Big Adaptive Rotor Project*. National Renewable Energy Laboratory, Golden, CO. NREL/TP-5000-73605. https://www.nrel.gov/docs/fy19osti/73605.pdf

Juwi AG. n.d. Wind Park Schneebergerhof. https://www.juwi.com/company/references/reference-detail/artikelansicht/wind-park-schneebergerhof [30 April 2022]

Kanya, B.M. & Visser, K.D. 2010. The impact of airfoil selection on the design of small horizontal axis wind turbines. *American Institute of Aeronautics and Astronautics*, AIAA 2010-1583.

Kersale, E. n.d. Chapter 4: Potential flows. Fluid Dynamics lecture notes. Department of Mathematics. University of Leeds.

Koning, W.J.F. 2019. Airfoil Selection for Mars Rotor Applications. NASA Langley Research Center. Hampton, VA. NASA/CR-2019-220236.

Ledoux, J., Riffo, S. & Salomon, J. 2021. Analysis of the Blade Element Momentum Theory. *SIAM Journal on Applied Mathematics*, Society for Industrial and Applied Mathematics, 81(6):2596-2621.

Lee, Y., Jhan, Y. & Chung, C. 2012. Fluid–structure interaction of FRP wind turbine blades under aerodynamic effect. *Composites*, 43:2180-2191.

Libii, J.N. 2013. Comparing the calculated coefficients of performance of a class of wind turbines that produce power between 330 kW and 7,500 kW. *World Transactions on Engineering and Technology Education*, 11(1): 36-40.

Madsen, H.A. 1996. A CFD analysis of the actuator disc flow compared with momentum theory results. IEA Joint Action - *Aerodynamics of Wind Turbines – 10th Symposium*. International Energy Agency. Edinburgh. 109-124.

Manwell, J.F. & McGowan, J.G. 2009. *Wind Energy Explained – Theory, Design and Application*, 2nd Ed. Chichester: John Wiley & Sons.

Mathew, S. 2006. *Wind Energy - Fundamentals, Resource Analysis and Economics*. Heidelberg: Springer.

Moriarty, P.J. & Hansen, A.C. 2005. *AeroDyn Theory Manual*. National Renewable Energy Laboratory. Golden, Colo. Technical Report:NREL/TP-500-36881.

Nava, S., Bot, P., Cater, J. & Norris, S.E. 2016. Modelling the Lift Crisis of a Cambered Plate at 0◦ Angle of Attack. *120th Australasian Fluid Mechanics Conference*, Perth, 2016.

Ohya, Y., Karasudani, T., Sakurai, A., Abe, K. & Inoue, M. 2008. Development of a shrouded wind turbine with a flanged diffuser. *Journal of Wind Engineering and Industrial Aerodynamics*, 96:524–539.

Ohya, Y. & Karasudani, T. 2010. A Shrouded Wind Turbine Generating High Output Power with Wind-lens Technology. *Energies*, 3:634 649.

Okulov, V.L., Naumov, I.V., Mikkelsen, R.F. & Sørensen, J.N. 2015. Wake effect on a uniform flow behind wind-turbine model. *Journal of Physics: Conference Series* 625(2015):1–8.

Patel, M.R. 2006. *Wind and Solar Power Systems – Design, Analysis and Operation*, 2nd Ed. Boca Raton: Taylor & Francis Group.

Porté-Agel, F., Bastankhah, M. & Shamsoddin, S. 2020. Wind-Turbine and Wind-Farm Flows: A Review. *Boundary-Layer Meteorology* 174(2020):1–59.

Rankine, W.J.M. 1865. On the mechanical principles of the action of propellers. *Transactions of the Royal Institute of Naval Architects*, 6:13–30.

Ruiz-Jarabo, J. n.d. *ENERCON 3 MW and 7,5 MW Portfolio E-82 E3 , E-101 and E-126*. Slide presentation of Enercon Director General: ENERCON GmbH. Spain.

Ryi, J., Rhee W., Hwang U.C. and Choi J. 2015. Blockage effect correction for a scaled wind turbine rotor by using wind tunnel test data. *Renewable Energy* 79(2015):227-235.

Sanderse, B., van der Pijl, S.P. & Koren, B. 2011. Review of computational fluid dynamics for wind turbine wake aerodynamics. *Wind Energy*, 14(2011):799–819.

Setoguchi, T., Santhakumar, S., Maeda, H., Takao, M. & Kaneko, K. 2001. A review of impulse turbines for wave energy conversion. *Renewable Energy*, 23:261-292.

Sørensen, J.N., Mikkelsen, R.F., Henningson, D.S., Ivanell, S., Sarmast, S. & Andersen, S.J. 2015 Simulation of wind turbine wakes using the actuator line technique. *Philosophical Transactions. Royal Society*. A 373.
http://dx.doi.org/10.1098/rsta.2014.0071

Spera, D.A. 2009. *Wind Turbine Technology – Fundamental concepts of wind turbine engineering*, 2nd Ed. New York: American Society of Mechanical Engineers.

Tavner, P. 2012. *Offshore Wind Turbines – Reliability, availability and maintenance*. London: The Institution of Engineering and Technology.

Thakker, A., Khaleeq, H.B. & Takao, M. 2003. *KSME International Journal*, 17: 1767-1774.

Tsuchiya, T., Numata, D. & Suwa, T. 2013. Influence of turbulence intensity on aerodynamic characteristics of an NACA 0012 at low Reynolds numbers. *51st AIAA aerospace sciences meeting*.

Van Agt, J. 2011. Estinnes windturbinepark – 11 x Enercon E-126. *OliNo*.
http://www.olino.org/articles/2011/05/17/de-bouw-van-het-estinnes-w
[26 Jan 2018]

Van Kuik, G.A.M. 2007. The Lanchester-Betz-Joukowsky limit. *Wind Energy*, 10(3):289–291.

Weston, D. 2015. GE unveils dome-fronted rotor. *Windpower Monthly*, June 2015. http://www.windpowermonthly.com/article/1351127/ge-unveils-dome-fronted-rotor [6 September 2017]

Wind-turbine-models.com. 2017. *Enercon E-70 E4 2.000*. https://en.wind-turbine-models.com/turbines/827-enercon-e-70-e4-2.000 [30 April 2022]

Wind-turbine-models.com. 2020. *Gamesa G80*. https://en.wind-turbine-models.com/turbines/34-gamesa-g80 [30 April 2022]

Ying, P., Chen, Y.K. & Xu, Y.G. 2015. An aerodynamic analysis of a novel small wind turbine based on impulse turbine principles. *Renewable Energy*, 75:37-43.